Implementation of Window Shading Models into Dynamic Whole-Building Simulation

by

Bartosz Aleksander Lomanowski

A thesis
presented to the University of Waterloo
in fulfilment of the
thesis requirement for the degree of
Master of Applied Science
in
Mechanical Engineering

Waterloo, Ontario, Canada, 2008

I hereby declare that I am the sole author of this thesis. This is a true copy of the thesis, including any required final revisions, as accepted by my examiners.

I understand that my thesis may be made electronically available to the public.

Abstract

An important consideration in energy efficient building design is the management of solar gain, as it is the largest and most variable gain in a building. The design of buildings with highly glazed facades, as well as decreased energy transfer rates through better insulated and tighter envelopes are causing interior spaces to become highly sensitive to solar gain. Shading devices such as operable slat-type louver blinds are very effective in controlling solar gain, yet their impact on peak cooing loads and annual energy consumption is poorly understood. With the ever-increasing role of building energy simulation tools in the design of energy efficient buildings, there is a clear need to model windows with shading devices to assess their impact on building performance.

Recent efforts at the University of Waterloo's Advanced Glazing Systems Laboratory (AGSL) in window shading research have produced a set of flexible shading models. These models were developed with emphasis on generality and computational efficiency, ideally suited for integration into building simulation. The objective of the current research is to develop a complex fenestration facility within a general purpose integrated building simulation software tool, ESP-r, using the AGSL shading models.

The strategy for implementation of the AGSL shading models is the addition of a new multi-layer construction within ESP-r, the Complex Fenestration Construction (CFC). The CFC is based on the standard ESP-r multi-layer nodal structure and finite control volume numerical model, with additional measures for coping with the complexities that arise in the solar, convective and radiant exchanges between glazing/shading layers, the interior zone and exterior surroundings. The CFC algorithms process the solar, convective and radiant properties of the glazing/shading system at each time-step, making it possible to add control (e.g., changing the slat angle of a slat-type blind) at the time-step level. Thermal resistances of sealed cavities between glazing/shading layers are calculated at each time-step for various fill gases and mixtures. In addition to modeling glazing/shading layer combinations, the CFC type also provides an alternate method of modeling unshaded windows without relying on third party software to supply the solar optics and cavity resistances.

To build confidence in the CFC code implementation, two comparison studies were carried out to compare the CFC type against other models. The first study compared the CFC models for unshaded windows with the standard ESP-r transparent multi-layer construction (TMC) models. The second study compared the CFC slat-type blind models with EnergyPlus 2.0. Good agreement was seen in the simulation results in both studies.

The successful implementation of the Complex Fenestration Construction within ESP-r has been demonstrated in the current research. In order for ESP-r users to fully exploit the capabilities of the CFC framework, it is recommended that the current models be extended to include a facility for dynamic shading control as well as the treatment of other types of shading layers. The coupling of daylighting models with the CFC type would provide a useful tool for modeling luminance control in combination with shading control strategies. With these enhancements, it is anticipated that the CFC implementation will be of significant value to practitioners.

Acknowledgments

The work presented in this thesis could not have been completed without the guidance, support and expertise of several people whom I wish to acknowledge here.

I would first like to thank my supervisor, Professor John Wright, for his continuous mentorship, encouragement and direction throughout the daily battles and small victories incurred over the last two and a half years.

I am grateful for the training and support received from Professor Ian Beausoleil-Morrison at Carleton University in guiding me through the steep learning curve of ESP-r development, as well as for reviewing my thesis. In the same vein, many thanks to Alex Ferguson from Natural Resources Canada for providing me with many useful tools required to get the job done and for kindly hosting me during my visits to Ottawa.

I would also like to thank Professor Mike Collins and my colleagues at the Solar Thermal Research Laboratory, Victor Halder and Veronique Delisle for creating an enjoyable atmosphere and many fond memories. A special thanks to Nathan Kotey for his constant guidance and for many interesting discussions and challenging debates.

To Professor John Straube, whose building science class has helped me shape a broader perspective of the built environment and the relevance of my research, thank you for your enthusiasm in conveying, ever so gracefully, your valuable expertise and experience in the field.

Finally, I would like to acknowledge the Solar Buildings Research Network for financial support.

Contents

List of Figures……....ix
List of Tables……...xiii
Nomenclature……..xiv

Chapter 1
Introduction and Background 1
1.1 Motivation 1
1.2 Solar Gain Control and Shading 3
1.3 Energy Flow Through Complex Fenestration 5
1.3.1 Center of Glass Glazing Analysis 6
1.3.2 Solar Analysis 8
1.3.3 Heat Transfer Analysis 9
1.3.4 Addition of Shading Layers to Center of Glass Analysis 10
1.3.5 Relevance to Building Simulation 14
1.4 Building Energy Simulation – The Basics 16
1.5 Objectives, Outline and Scope 19

Chapter 2
Previous Work 21
2.1 Survey of Existing Window Shading Analysis Tools 21
2.1.1 WINDOW 6.2 and THERM 6.2 – Research Version 21
2.1.2 Advanced Window Information System (WIS) 3.0.1 22
2.1.3 Parasol v4.1 24
2.1.4 EnergyPlus 2.2.0 25
2.2 Overview of the AGSL Shading Models 26
2.2.1 Effective Solar-Optical and Longwave Radiative Properties for Slat Blinds 27
2.2.2 Solar Multi-layer Model 28
2.2.3 Longwave Radiation Exchange 29
2.2.4 Convection Models 30

Chapter 3

ESP-r Thermal Model 34

3.1 Formulation of the Finite Volume Heat Balance Method 34

3.1.2 Difference Equation Matrix Formulation Constraints 39

3.2 The Transparent Multilayer Construction (TMC) 41

3.3 Building Domain Simulation Flow 42

Chapter 4

Implementation of the Complex Fenestration Construction (CFC) 44

4.1 The Complex Fenestration Construction 44

4.1.1 Solar Processing 46

4.1.2 Thermal Processing 54

4.2 Front-End 62

4.3 Simulation Performance 64

4.4 Summary of CFC Capabilities 66

Chapter 5

Numerical Comparison Studies 69

5.1 Background 69

5.2 TMC vs. CFC Comparison 71

5.2.1 Simulation Methodology 73

5.2.2 Results 75

5.2.3 Discussion 84

5.2.4 Conclusion 89

5.3 Comparison of CFC and EnergyPlus Slat Blind Models 91

5.3.1 Simulation Methodology 91

5.3.2 Results 93

5.3.3 Discussion 100

5.3.4 Conclusion 106

5.4 CFC Shading Control 107

5.4.1 Slat Control – An Illustrative Example 108

Chapter 6

Conclusions and Recommendations 111

References 113

Appendices

Appendix A:

Convection Heat Transfer Coefficients at Surfaces Exposed to the Environment 118

Appendix B:

Off-Normal Solar Property Adjustment for Glazing Layers 122

Appendix C:

Formulation of the Exchange Factor Method 125

Appendix D:

ESP-r Solar Processing Flow Chart 130

Appendix E:

ESP-r Thermal Simulation Flow Chart 144

Appendix F: CFC User's Reference 164

List of Figures

Figure 1.1: Definition of center-glass, edge-glass and frame areas of fenestration. 6
Figure 1.2: Components of heat gain through center of glass region of a fenestration element. 8
Figure 1.3: Solar fluxes in an array of glazing layers. 9
Figure 1.4: a) One-dimensional heat transfer model of center of glass double glazing. b) Equivalent electrical circuit. Reproduced with permission from (Hollands et al. 2001). 11
Figure 1.5: Expanded spatially averaged set of optical properties and a representative slat enclosure. 12
Figure 1.6: Representative longwave radiation resistance network for glazing/shading layer array in which any or all layers can be diathermanous. 13
Figure 1.7: Representative convective resistance network for three slat-type blind configuration...13
Figure 1.8: Building energy flowpaths. Reproduced with permission from (Clarke 2001). 17
Figure 2.1: Interaction of solar fluxes in a mutli-layer scheme with a scattering shading layer. 28
Figure 3.1: Energy flow-paths in a discretized physical system. Reproduced with permission from (Clarke 2001). 35
Figure 3.2: Nodal scheme of a multi-layer construction. 37
Figure 3.3: Simple nodal scheme of a thermal zone with two stratified air volumes. Reproduced with permission from (Clarke 2001). 38
Figure 3.4: **A** matrix containing future time-row coefficients of the single thermal zone shown in Figure 3.3. Reproduced with permission from (Clarke 2001). 39
Figure 3.5: Air gap thermal resistance network with a) convective and longwave radiative resistances and b) with equivalent total R_{gap} resistance. 40
Figure 3.6: Example of TMC input file defining the optical property set for each control period. .41
Figure 3.7: Simplified ESP-r time-step simulation flow for a thermal zone. 43
Figure 4.1: Simplified ESP-r solar processing flow including CFC implementation. 47

Figure 4.2: Profile angle dependence and slat angle convention for horizontal and vertical slat-type. 48
Figure 4.3: Example of off-normal property adjustment for coated and uncoated glass.....50
Figure 4.4: Curved slat and flat slat input dimensions.....52
Figure 4.5: Simplified ESP-r thermal processing flow including CFC implementation. 56
Figure 4.6: CFC resolution of longwave radiative jump resistors to nodal generation terms.....58
Figure 4.7: CFC resolution of convective jump resistors to nodal generation terms. 61
Figure 4.8: Screen shot of the Glazing and Shading Layer Editor, GSLedit.....63
Figure 4.9: Example of oscillations in simulation results for a CFC glazing with an indoor blind. a) cooling load future time-step data and b) cooling load time-step averaged data. 65
Figure 4.10: Functionality of existing ESP-r constructions (TMC, MLC) and the new CFC type...68
Figure 5.1: X-y scatter plot of the simulated vs. measured SHGC, reproduced from (Kotey et al. 2009).....71
Figure 5.2: Geometry of test cell.....74
Figure 5.3: Hourly incident solar radiation components on south window.....76
Figure 5.4: Hourly cooling load, solar transmission and absorbed solar radiation for Case 1: clear double glazing. Simulation results for Toronto, July 7 CWEC data.....77
Figure 5.5: Hourly cooling load, solar transmission and absorbed solar radiation for Case 2: double glazing with bronze, low-e and argon. Simulation results for Toronto, July 7 CWEC data.....78
Figure 5.6: Hourly cooling load, solar transmission and absorbed solar radiation for Case 3: triple glazing with low-e and argon. Simulation results for Toronto, July 7 CWEC data. 79
Figure 5.7: Hourly convective, longwave radiative, and total gap resistances for triple glazing (Case 3). Simulation results for Toronto, July 7 CWEC data.....80
Figure 5.8: Hourly convective, longwave radiative, and total gap resistances for triple glazing (Case 3) with xenon gas in indoor cavity. Simulation results for Toronto, July 7 CWEC data. 81
Figure 5.9: Comparison of CFC with constant gap for WINTER design condition, and temperature dependant gap resistances. Simulation results for Toronto, July 7 CWEC data..82
Figure 5.10: Comparison of CFC with constant gap for SUMMER design condition, and temperature dependant gap resistances. Simulation results for Toronto, July 7 CWEC data..83

Figure 5.11: a) Hourly incident solar radiation components on south window for EnergyPlus and ESP-r simulations. b) EnergyPlus hourly sky, ground and total diffuse radiation. Simulation results for Toronto, July 7 CWEC data. 95
Figure 5.12: Hourly cooling load for Case 1 (no window). Simulation results for Toronto, July 7 CWEC data. 96
Figure 5.13: Hourly solar transmission and cooling load for Case 2 (clear double glazing). Simulation results for Toronto, July 7 CWEC data. 96
Figure 5.14: Hourly solar transmission and cooling load for OUTDOOR blind (Case 3) with slat angle a) 0° and b) 45°. Simulation results for Toronto, July 7 CWEC data. 97
Figure 5.15: Hourly solar transmission and cooling load for BETWEEN-GLASS blind (Case 4) with slat angle a) 0° and b) 45°. Simulation results for Toronto, July 7 CWEC data. 98
Figure 5.16: Hourly solar transmission and cooling load for INDOOR blind (Case 5) with slat angle a) 0° and b) 45°. Simulation results for Toronto, July 7 CWEC data. 99
Figure 5.17: Hourly cooling load results for comparison of interior surface convection models. Simulation results for Toronto, July 7 CWEC data. 102
Figure 5.18: Effect of slat angle on diffuse transmittance(s) (for flat slat with zero thickness and slat reflectance of 0.5). Reproduced with permission from (Chantrasrisalai & Fisher 2004). 104
Figure 5.19: Hourly cooling load for Case 2 (CDG) and Case 5 (indoor blind). Simulation results for Toronto, July 7 CWEC data. 106
Figure 5.20: Hourly solar transmission and cooling load for outdoor and indoor slat blind with simple control scheme. Simulation results for Toronto, July 7 CWEC data. 110
Figure A.1: Three-resistor network used to model convective heat transfer at surfaces exposed to the environment. 118
Figure A.2: Convective heat transfer coefficients as functions of window/shading layer spacing, b, with $h_c \approx 3.5 \frac{W}{m^2 K}$ 120
Figure B.1: Ratios $R_{\square}$ and $R_{\square}$ used to characterize off-normal solar properties of glazing layers, n=1.526, KL=0.33. 124
Figure C.1: Surface radiosities and irradiances for four surface enclosure with diathermanous layer. 126
Figure F.1: Create material for shade layer. 166
Figure F.2: Construction layers for double glazing with indoor slat blind. 167

Figure F.3: Construction layers for double glazing with between-glass slat blind. 168
Figure F.4: Construction layers for double glazing with outdoor slat blind. 169
Figure F.5: Number of layers in GSLedit does not include gap layers. 171
Figure F.6: Layer type selection. 171
Figure F.7: Main window of GSLedit. Left click on layer or gap to change properties. Right click on layer or gap to display selected properties. 172
Figure F.8: Solar and longwave property display window of glazing layer. 173
Figure F.9: Property display window of venetian blind layer. 174
Figure F.10: Fill gas property display window. 175
Figure F.11: Geometry, composition and boundary conditions of example model. 177
Figure F.12: Slat angle convention for vertical and horizontal slat blinds. 181
Figure F.13: Example simulation results. 182

List of Tables

Table 4.1: Summary of TMC and CFC capabilities in ESP-r 66
Table 5.1: ESP-r simulation parameters for TMC and CFC comparison 74
Table 5.2: Test cases for EnergyPlus/ESP-r comparison study 92
Table 5.3: Total cooling energy, peak cooling load and absolute differences for EnergyPlus and ESP-r results 95
Table 5.4: Cooling energy and peak load reductions of slat-blind cases relative to the reference double glazing 106

Nomenclature

Abbreviation

1-D	One-dimensional
2-D	Two-dimensional
CDG	Clear double glazing
CWEC	Canadian Weather for Energy Calculations
EIA	US Energy Information Association
ESP-r	Environmental Systems Performance – research
GHG	Green house gases
HVAC	Heating, Ventilation and Air-Conditioning
IBPSA	International Building Performance Simulation Association
NFRC	National Fenestration Rating Council
IGDB	International Glazing Database
IR	Infrared
LBNL	Lawrence Berkeley National Laboratory
NSTF	National Solar Test Facility
OPEC	Organization of Petroleum Exporting Countries
SHGC	Solar Heat Gain Coefficient
TDMA	Tri-diagonal matrix algorithm
UV	Ultraviolet
WIS	Window Information System

Symbols

A	Two-dimensional array containing self-coupling coefficients	
A	Absorbed fraction	
B	Two-dimensional array containing cross-coupling coefficients	
C	Column matrix containing known boundary condition excitations and heat flux fluctuations	
c_I	Specific heat of region I	{J/kg K}

C_{ci}	Cross-coupling coefficient	{dimensionless}
C_s	Self-coupling coefficient	{dimensionless}
F	Air volume node	
G	Irradiance	{W/m^2}
h_c	Convective heat transfer coefficient	{W/m^2 K}
h_r	Radiant heat transfer coefficient	{W/m^2 K}
I	Solar flux	{W/m^2}
K	Conductance	{W/K}
N	Inward flowing fraction	{dimensionless}
n*	Cavity spacing modification factor	{dimensionless}
q_{net}	Net heat flow	{W}
q_I	Heat generation within region I	{W}
R	Resistance	{W/m^2 K}$^{-1}$
S	Surface node	
T	Temperature	{K}
U	U-value	{W/K}
W	Weighting factor	{dimensionless}

Subscripts

b	Back
bb	Beam-beam
bd	Beam-diffuse
bld	Building
blind,glass	Blind to glass
blind,out	Blind to outdoor air
cav	Cavity
cg	Center of glass
d	Downward facing
dd	Diffuse-diffuse
e	Equivalent
ext	External surroundings

f	Front
glass,glass	Glass to glass
glass,out	Glass to outdoor air
gl	Glazing
grd	Ground
i	Layer i
in	Indoor air
j	Layer j
n	Normal incidence
out	Outdoor air
rad	Radiant
ref	Reference glass
s	Solar
tot	Total
u	Upward facing

Superscripts

+	Flow towards outdoor side
-	Flow towards indoor side
s	Slat

Greek Symbols

ρ	Reflectance	{dimensionless}
τ	Transmittance	{dimensionless}
ε	Emissivity	{dimensionless}
δV_I	Volume of region I	{m^3}
ρ_I	Density of region I	{kg/m^3}
δt	Discretization time-step	{seconds}
ξ	An independent variable of time	
ψ_{n+1}	Column matrix of nodal temperature and heat injection/extraction terms at the future time-row	

ψ_n	Column matrix of nodal temperature and heat injection/extraction terms at the present time-row	
θ	Solar incidence angle	
α_s	Solar altitude angle	
γ_s	Solar azimuth angle	
γ	Surface azimuth angle	
Ω_v	Vertical profile angle	
Ω_h	Horizontal profile angle	
φ_v	Slat angle for vertical slat blinds	
φ_h	Slat angle for horizontal slat blinds	
σ	Stefan-Boltzmann constant	$\{W/m^2K^4\}$

Chapter 1
Introduction and Background

1.1 Motivation

Today, in 2008, climate change due to increased anthropogenic greenhouse gas emissions is no longer heralded by doomsayer scientists and environmental activists; it is a real, measurable phenomenon stimulating international efforts to reduce the world's energy expenditure. The energy crises of the 1970's were largely attributed to oil supply pressures exerted by the Organization of the Petroleum Exporting Countries (OPEC). This time around the problem is twofold: depleting fossil fuel resources in an energy hungry world, and the real danger of climate change, not only on the long-term economic outlook, but, more fundamentally, because of a growing list of environmental concerns. Although governments are generally slow to act due to economic constraints and political pressures, renewed interest in energy efficiency and investment in renewable resources are moving up the political agenda.

Based on data from the US Energy Information Association (EIA), buildings in the US are responsible for 48% of greenhouse gas (GHG) emissions annually. In 2006, 72% of generated electricity was sold to the residential and commercial building sectors. The building sector clearly accounts for a major portion of the total energy budget in the US and in all industrialized nations. Any real impact on climate change must therefore include an extensive reduction in the global building sector's energy bill. Only after energy conservation efforts are exhausted, can the use of greener, more expensive, alternative energy sources be justified. Historically, especially in North America, emphasis on energy efficiency in building design has been limited. Consequently, there is large potential in the building sector for significant gains in energy efficiency without compromising occupant comfort. Buildings that achieve an annual net-zero energy balance have been demonstrated (e.g., Riverdale Net Zero Project 2008, Plus Energy House in Thening, Austria 2001). Conservation in the built environment can thus be viewed as the most abundant, readily available alternative fuel source.

Architecture 2030, a non-profit organization set up in response to the global-warming crisis, proposed the 2030 challenge, an initiative aimed at reducing GHG emissions by 50% for all new buildings and major renovations by 2010, incrementally decreasing emissions until new buildings become carbon neutral by 2030. These goals are not unrealistic; long-term reduction in energy consumption of the building sector could lie in the 50-75% range for new buildings and 20-40% for the existing stock. Appropriate deployment of on-site renewable energy to meet the remainder of the building sector's energy needs may further result in carbon neutral buildings. These objectives can be met by the systematic application of the following four principles: improved building envelope, changes in occupant behaviour, improved efficiency of energy systems, and the use of renewable energies.

Thus far, the failure to exploit the conservation resource has had little to do with technological challenges. In fact, many approaches to sustainable building design have been available for decades. Access to inexpensive energy has instilled an attitude of conservatism in the building sector, giving energy considerations low priority in building design and construction. The problem also lies in the decision making process and ineffective support for appraising building design decisions, especially at the early design stage (Clarke 2001). The traditional compartmentalized working model between various disciplines involved in building projects limits interdisciplinary engagement and information sharing. A more holistic approach in building design will undoubtedly shift the focus towards integration and optimization of various building disciplines, including increased efforts in linking building science with architecture. Complexity and fine balance of efficient systems necessitates simulation. In this regard, building energy simulation is playing an ever-increasing role in providing researchers, engineers, designers and architects with valuable decision support tools in integrated building design. Test-driving a building through simulation allows for a thorough appraisal of decisions from early on in the design stage, where major decisions have the most impact on a building's performance, to more detailed assessments of energy consumption, comfort and indoor air quality. Using simulation to evaluate alternative design options becomes fast and inexpensive. With a reasonable representation of real-world complexity, simulation offers invaluable insight in the design of high-efficiency buildings.

Despite the advance of building energy simulation software, certain challenges remain, preventing wide-scale adoption of these tools in practice. In particular, the complexity required to adequately represent the real world results in a technically challenging and generally non-intuitive, non user-friendly interface. There is therefore a tradeoff between model accuracy and usability. Furthermore, many modeling approaches exist, with a general lack of agreement on which model is most suitable. This presents a barrier to validation efforts and creates an environment of isolation between research groups (Clarke 2001). In response, organizations like the International Building Performance Simulation Association (IBPSA) serve as an essential vehicle for research collaboration and promotion of the capabilities and potential of simulation in building design.

1.2 Solar Gain Control and Shading

Given the current architectural trend towards highly glazed facades in commercial buildings, the management of solar gain is an important consideration in energy efficient building design. Solar gain through windows represents the most variable and largest gain in a building. As a result, HVAC equipment is often sized to meet the peak cooling demand in response to high solar and internal gains, leading to cooling systems that are over-sized for the majority of environmental conditions. On hot summer days the demand for cooling causes air-conditioner loads to peak simultaneously across large geographic regions, contributing to power grid straining, which can lead to grid bottlenecks and rolling brownouts at a cost to the economy measured in the billions of dollars annually.

The need for better solar gain control strategies is evident in rapidly growing economies in Asia, which are giving rise to a burgeoning, populous middle class that demands air conditioned living and working spaces. Many of the air-conditioners in service there utilize cheap refrigerants that are banned in the west, renewing concerns of ozone depletion.

The case for improved solar gain control can also be made in predominantly heating regions of North America, where the need for improving the thermal resistance of building envelopes to reduce winter heating losses is leading to indoor spaces that are more sensitive to solar gain.

Finally, the implementation of passive solar elements on a large scale, a necessary next step in curtailing GHG emissions in the building sector, will also result in increased building sensitivity to solar gain. For example, the use of large south facing windows with a high insulating value can substantially decrease a building's heating demand. However, given a highly insulated envelope, such a passive solar design would also pose a risk of overheating the indoor space during high solar intensity periods.

Without appropriate solar gain control strategies, building peak cooling loads and increased cooling energy can offset any benefit from thermally benign envelopes. Control of solar gain is thus not only necessary in current highly glazed, poorly insulated buildings, but is critical in the design of new energy efficient residential and commercial green buildings.

Shading devices such as operable slat-type louver blinds, roller blinds, drapes, overhangs, and retractable awnings are simple but effective devices, yet their impact on peak cooling loads and annual energy consumption is poorly understood. Until recently, the impact of shading devices has been generally neglected in envelope design and equipment sizing. Few tools exist that can aid the building designer in quantifying the impact of window shading on building loads. With the renewed impetus towards energy efficiency in building design, the potential benefits of automated switchable shades are significant, and the ability to appraise the impact of such technologies is in demand. There is a clear need for an explicit treatment of window shading layers in building energy simulation. Control schemes for automated shades can be readily integrated with simulation, achieving fine resolution of solar gain control to determine the resulting impact on thermal loads, electrical lighting power and luminance levels.

In order to bridge the gap between research and design practice, such models require practical, straightforward approaches to be successfully deployed, but need to adequately represent real-world complexity. This is the challenge typically encountered in building energy simulation. A realistic representation of building physics ensures that building designers, who may be held liable in the case of poor building performance once built, have confidence in building load assessment tools and may use such tools to maximize energy efficiency.

As a caveat to the previous statements, the reduction of cooling load is not always a good thing, especially in existing buildings. Reducing envelope gains by insulating and/or lowering the SHGC in fenestration, and thus running the air-conditioning system less, can lead to part-load humidity problems (Lstiburek 2008). Air-conditioners cool air, and as a result also dehumidify it. Energy must be removed in order for the moisture to condense. Due to reduced sensible loads the air-conditioner may not operate often enough to attain desirable humidity levels. In other words, if the air conditioner is not cooling the air because of effective passive cooling measures, it can't dehumidify the air. This often leads to a cold environment in which the air conditioning system is kept running to meet the latent load. Effective measures exist to combat this problem. The common approach is to reheat the air after it has been cooled and dehumidified. This requires additional energy input and is much more effective if the sensible and latent loads are separated into two systems with a dedicated dehumidification system. This situation also presents a clear advantage of using operable shades to balance the cooling and dehumidification loads, as solar gain can effectively be turned on when needed and turned off when not needed.

The part-load humidity problem is an example of the complex nature of interactions between building elements, which are not always apparent. Design for energy efficiency must account for such interactions; otherwise efforts to reduce the energy footprint of a building may be offset by compromised occupant comfort, deterioration of construction materials and inefficient operation of energy systems.

1.3 Energy Flow Through Complex Fenestration

Considerable research has been conducted on the topic of glazings over the last 50 years, and the solar and thermal dynamics of glazing systems are well understood. A comprehensive reference on glazing and coating technology can be found in (Hollands et al. 2001).

The energy flowpaths through fenestration can be divided into three sections: center of glass, edge glass and frame, as shown in Figure 1.1. The frame and edge areas require two-dimensional analysis and are not of interest to the current research. The models throughout this thesis are concerned with the center of glass region, traditionally modeled as a one dimensional heat transfer problem for glazing.

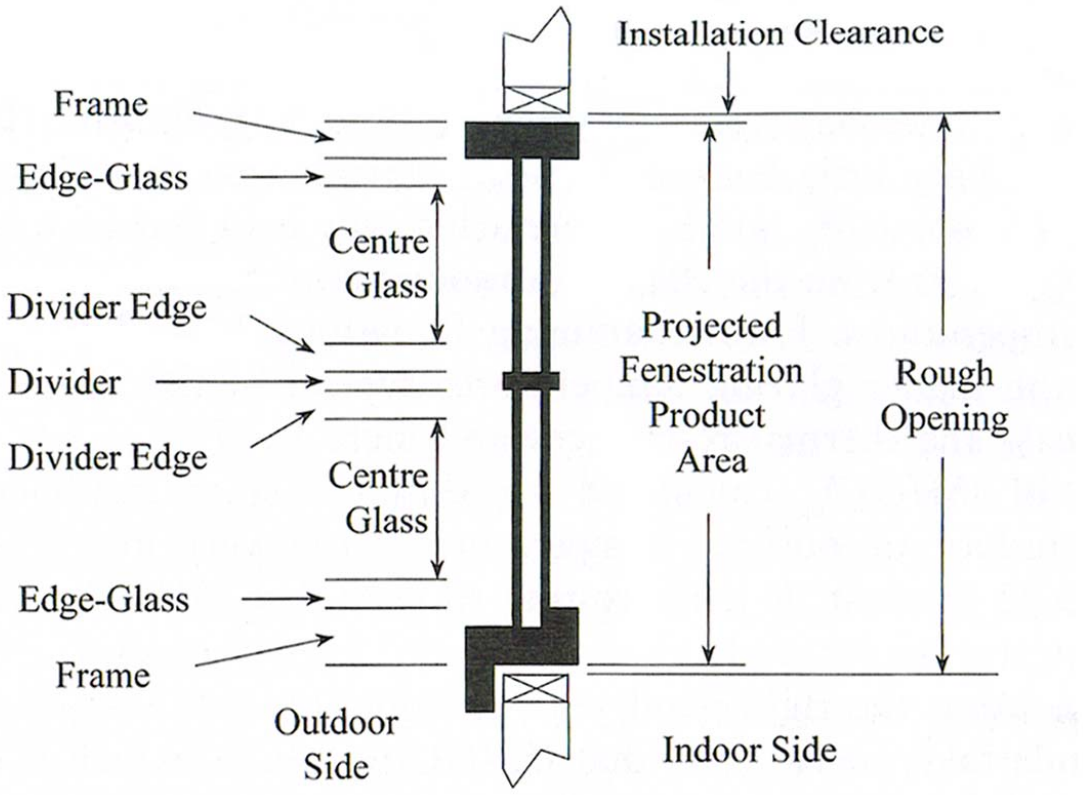

Figure 1.1: Definition of center-glass, edge-glass and frame areas of fenestration.

1.3.1 Center of Glass Glazing Analysis

Prior to introducing shading layers to a window, an analysis of the center of glass glazing region is presented as a baseline. The total gain to the indoor space per unit area of the center of glass region of a glazing system is given by

$$q_{net} = U_{cg}(T_{out} - T_{in}) + SHGC_{cg}G_s \qquad (1.1)$$

where U_{cg} is the center of glass U-value, T_{out} and T_{in} are the outdoor and indoor temperatures respectively, $SHGC_{cg}$ is the center of glass Solar Heat Gain Coefficient and G_s is the solar irradiance. The U-value is defined as the inverse of the total resistance of the glazing system. The total resistance is due to conduction in the glass layers, convection and longwave radiation exchange in-between the glazing layers and on the outdoor/indoor surfaces. The $SHGC_{cg}$ is the ratio of the total solar gain to the solar irradiance and can be written as

$$SHGC_{cg} = \tau_{cg} + \sum_{i=1}^{n} N_i A_i \qquad (1.2)$$

where τ_{cg} is the center of glass solar transmittance, N_i is the inward flowing fraction of glazing layer i, A_i is the solar absorptance of glazing layer i, and n is the total number of glazing layers. The inward flowing fraction N_i is that portion of the absorbed solar flux, $A_i G_s$, in a glazing layer that travels to the indoor side via convection and longwave radiation exchange. The center of glass $SHGC_{cg}$ and τ_{cg} are generally applied to the entire aperature area of the window. The U-value and SHGC fully describe the thermal characteristics of the glazing system.

The flow of solar energy through fenestration elements in a building envelope is non-trivial due to the coupling of the three modes of heat transfer. Solar flux incident on a window is reflected, absorbed and transmitted at each glazing layer, resulting in many inter-reflections of solar rays in the glazing array. Glazing/shading system analysis takes advantage of the fact that there is no appreciable overlap in wavelength between solar (short-wave) and thermal (long-wave) radiation. The analysis can thus be carried out in two steps. First, a solar analysis determines the transmitted, reflected and absorbed solar fluxes at each glazing layer. Second, using the absorbed quantities as source terms, a heat transfer analysis is carried out to establish an energy balance at each layer considering convection and longwave radiation exchange.

Consider a control volume drawn around the fenestration element, treating the entire assembly as a black box. By imposing equal outdoor and indoor temperatures, the resulting energy flow paths to the indoor space are attributed to the incident solar flux only. Illustrated in Figure 1.2, the solar gain is divided into three fluxes: transmitted solar flux, long-wave radiant flux and convective flux. Further imposing a temperature difference across the fenestration element will not change the transmitted solar flux, but will result in a change in the longwave radiant and convective fluxes. The SHGC is not only a function of the solar transmittance, but also depends on the inward flowing fraction of energy due to longwave radiative and convective heat transfer. In turn, the U-value is dependent on the absorbed solar fluxes in each glazing layer due to the coupling of heat transfer modes.

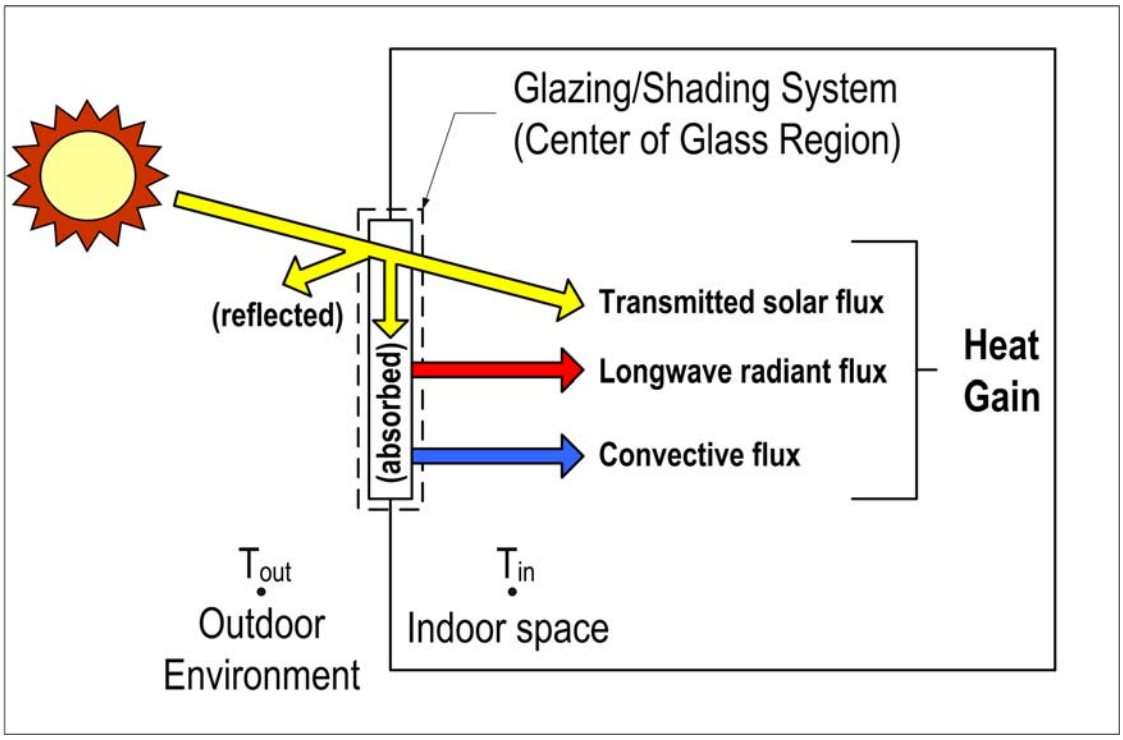

Figure 1.2: Components of heat gain through center of glass region of a fenestration element.

The U-value and SHGC are typically used as performance indicators. Since these indices depend on the outdoor/indoor temperature difference as well as the solar irradiance, standard environmental conditions are usually imposed for purposes of comparison.

1.3.2 Solar Analysis

The distribution of solar fluxes within a center of glass glazing array can be found by carrying out a multi-layer analysis by the net-radiation method (Wright 1998, Wright and Kotey 2006). Figure 1.3 denotes the solar fluxes I^- and I^+, which represent either beam or diffuse fluxes flowing towards the indoor and outdoor sides, respectively. The flux I_1^- is the incident solar radiation, having both beam and diffuse components, which are treated separately. Knowing the optical properties of the smooth specular glass layers, a set of relations describing each solar flux is established. A variety of methods exist for a solution to the solar flux distribution. Details can be found in (Hollands et al. 2001), (Wright 1998) and (Wright and Kotey, 2006). The solution yields all the solar fluxes within the glazing array and the absorbed fractions, A_i, can be determined by performing an energy balance on each layer.

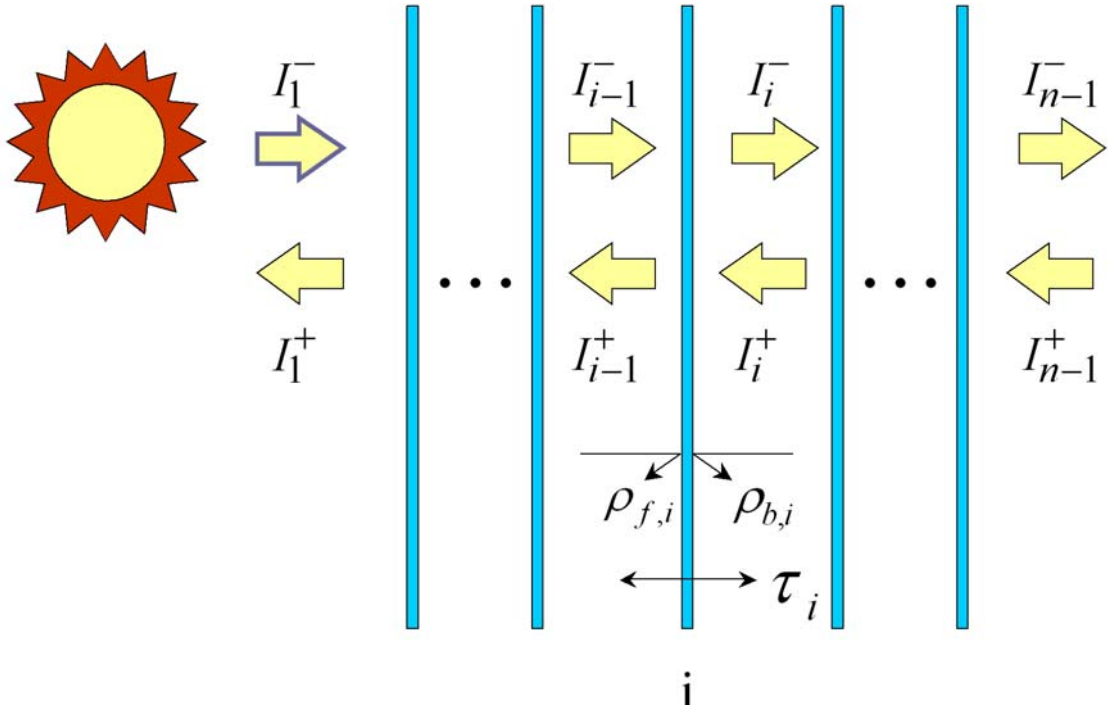

Figure 1.3: Solar fluxes in an array of glazing layers.

1.3.3 Heat Transfer Analysis

The one dimensional heat transfer formulation for a center of glass glazing layer array is shown in Figure 1.4 a). The equivalent resistance network is shown in Figure 1.4 b), where the convective and longwave radiative resistors have been combined for clarity. An energy balance is established at each layer, using the absorbed fluxes taken from the shortwave analysis as source terms. The resistances can be determined by examining the convective and longwave radiative exchanges between each layer and at the outdoor and indoor surfaces. Both convective and longwave radiative resistances are dependent on the glazing layer temperatures, which are initially unknown. Coupling exists between the two modes of heat transfer. Therefore, an iterative procedure is required to solve for the layer temperatures until the fluxes at each layer are balanced. Once the layer temperatures are known, all the fluxes can be determined and the total gain to the indoor space can be established. The resistances can be summed, in series across layers and in parallel within cavities and at exposed surfaces, to determine the total center of glass resistance, and, inversely, the center of glass U-value. The inward flowing fractions required for determination of the SHGC can be obtained from knowledge of the resistances such that

$$N_i = \frac{R_i}{R_{tot}} \qquad (1.3)$$

where R_i is the resistance from layer i to the indoors, and R_{tot} is the total resistance across the glazing system. The series summation of the resistances from the outdoors to the indoors requires that a single temperature be used on the outdoor and indoor sides for convective and longwave radiative exchange at the exposed glass surfaces. To account for the difference between radiant and ambient air temperatures, the radiant resistors can be adjusted so that the resultant flux is equivalent to longwave radiative exchange with the mean radiant temperature of the surroundings, or interior surfaces. Equation 1.3 is only valid for an array of glazing layers which are opaque to longwave radiation. The development of Equation 1.3 can be found in (Wright and McGowan 1999).

1.3.4 Addition of Shading Layers to Center of Glass Analysis

This section provides background material on the complexities associated with the addition of shading layers to the traditional window models.

The conventional one-dimensional center of glass glazing analysis can be extended to include shading layers such as slat blinds, roller blinds, drapes and insect screens. The analysis of shading layers can be simplified by treating the layer as a planar, homogenous layer that is included in the series of layers that make up the glazing/shading system. Although equally applicable to any shading layers, the discussion here will focus on slat-type blinds.

To treat the slat blind as a homogenous layer, a set of effective solar optical and a set of longwave radiative properties are required. Methods exist for determining these properties (e.g., Kotey et al. 2008, Yahoda and Wright 2004, 2005, Rosenfeld et al. 2000, Pfrommer et al. 1996, Parmelee and Aubele 1952) by considering the radiation transport in a single slat enclosure. An expanded set of solar optical properties can thus be established to characterize the entire shading layer for the shortwave calculation, as shown in Figure 1.5. The presence of the slat blind adds significant complexity to the solution of multi-layer solar fluxes due to the scattering of solar beam energy. The surface of the slat material scatters a portion of the incident beam flux when reflected, creating a diffuse source term which goes through subsequent inter-reflections between the slat

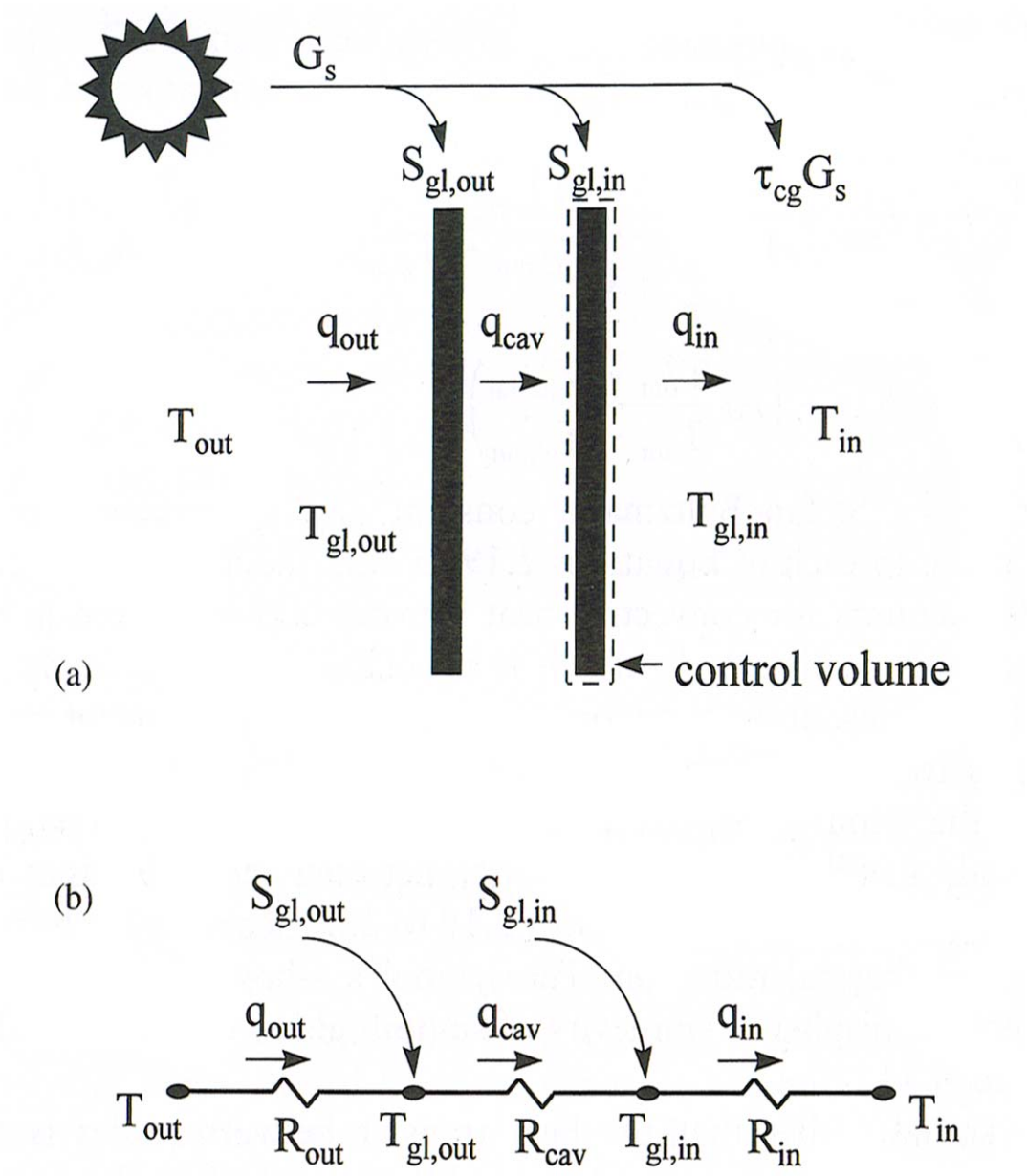

Figure 1.4: a) One-dimensional heat transfer model of center of glass double glazing. b) Equivalent electrical circuit. Reproduced with permission from (Hollands et al. 2001).

enclosure and adjacent glazing layers. The shortwave multi-layer model that copes with such scattering shading layers is discussed in Section 2.2.2.

In contrast to a glazing layer which is completely opaque to longwave radiation, the slat blind layer can be described as diathermanous, or semi-transparent to longwave radiation, as a result of the open gaps between slats. The effective radiative properties therefore include a

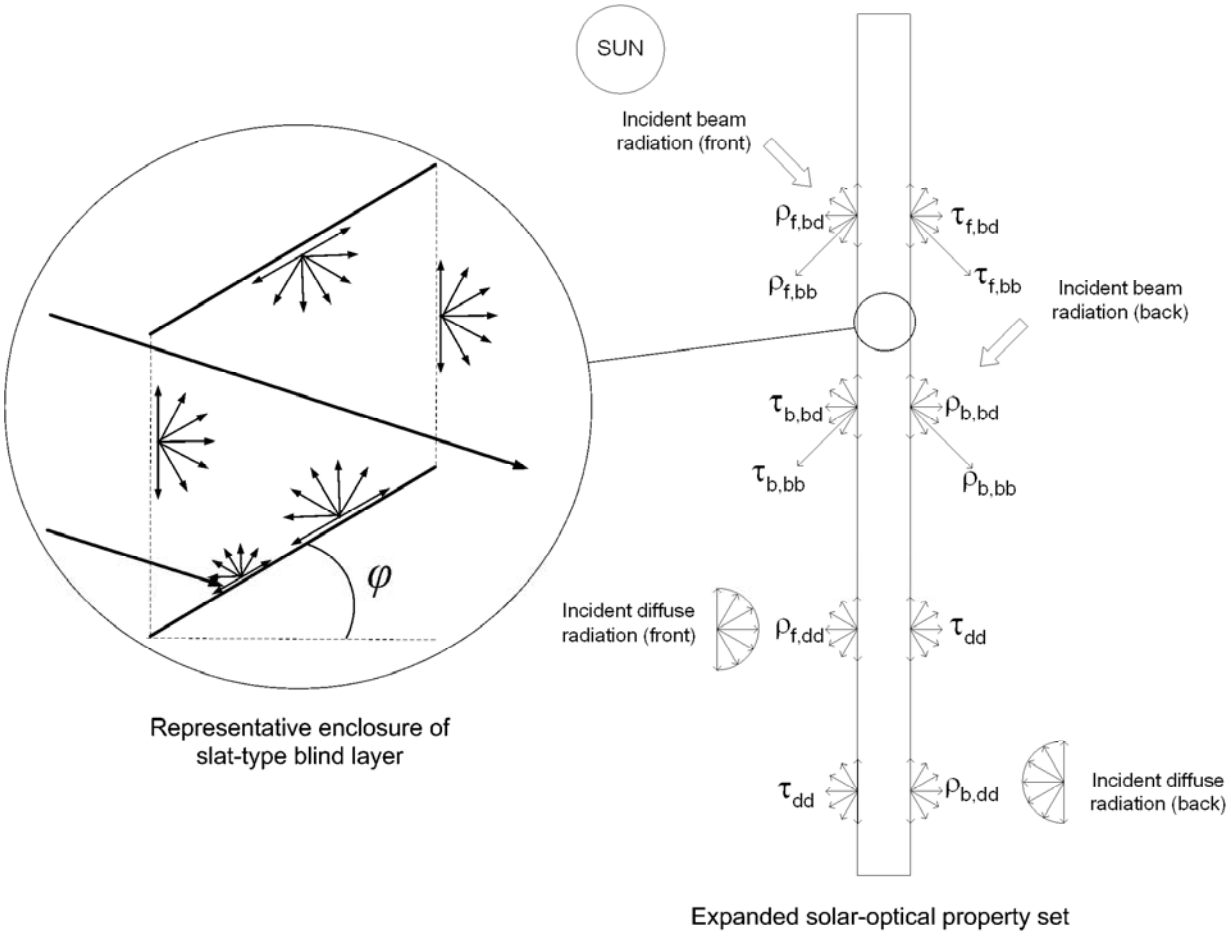

Figure 1.5: Expanded spatially averaged set of optical properties and a representative slat enclosure.

longwave transmittance. The resulting effect on the longwave radiation exchange in the heat transfer analysis is shown in Figure 1.6, where 'jump' resistors need to be established to account for non-adjacent layers in thermal communication with one another. The problem is more complicated when a diathermanous layer is present on the indoor or outdoor side of the glazing/shading system, also shown in Figure 1.6, such that jump resistors extend to the external surroundings and/or the interior enclosure surfaces. To characterize the jump resistors required for the one-dimensional heat transfer analysis, a general procedure for coping with any combination of glazing and diathermanous shading layers is required. Such a procedure is described in Section 2.2.3.

Finally, the presence of a slat blind affects the convective air flow around the blind layer. Figure 1.7 shows three blind configurations (outdoor, between glass, indoor) and the

representative resistances that describe the convective heat transfer situation. The between glass blind configuration results in the possibility of a convective jump resistor to account for air flow that may occur between the two sides of the blind. The outdoor and indoor blind configurations also result in convective jump resistors that account for any convective exchange between the blind surfaces, the glass surface adjacent to the blind and the outdoor ambient air or the indoor

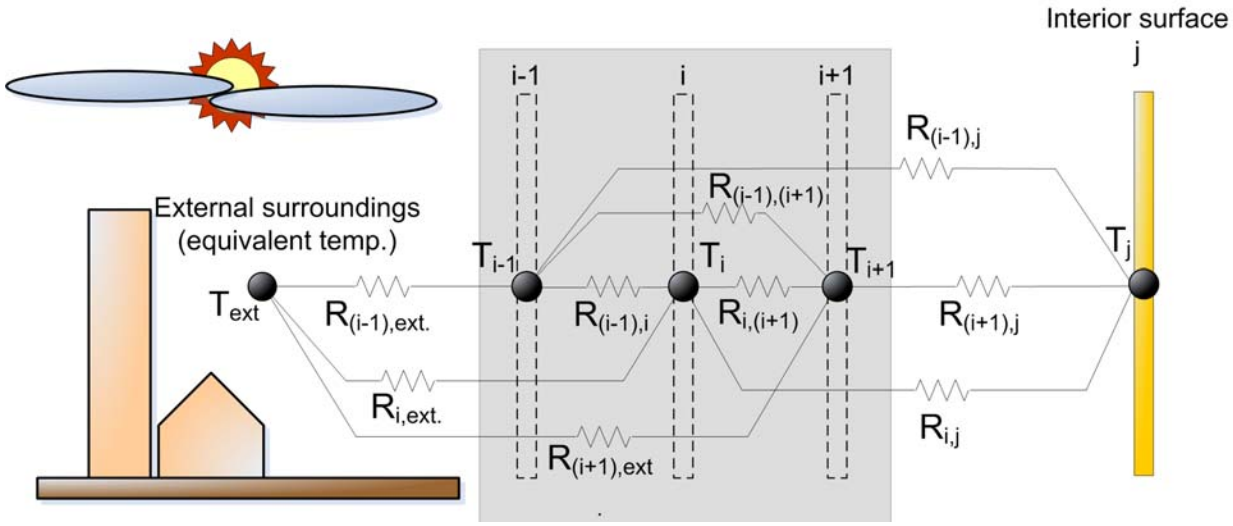

Figure 1.6: Representative longwave radiation resistance network for glazing/shading layer array in which any or all layers can be diathermanous.

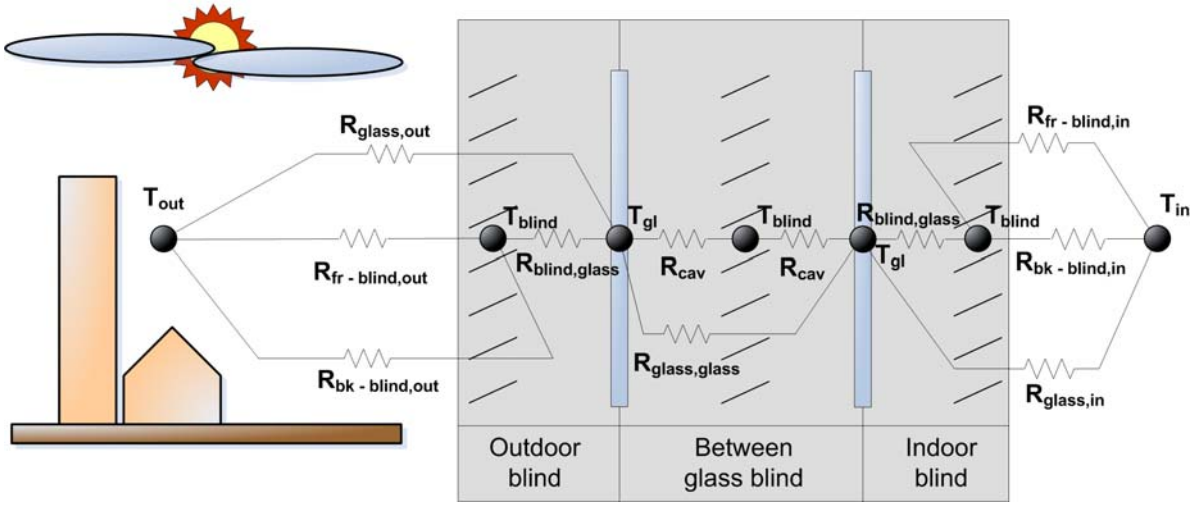

Figure 1.7: Representative convective resistance network for three slat-type blind configuration.

room air, respectively. The problem is complicated by the possibility of boundary layer interaction in free convection flow in the open channel between the outdoor/indoor blind and glass layers. Simplified convection models that attempt to resolve the influence of air flow for outdoor,

between-glass and indoor blind configurations into one-dimensional analysis are presented in Section 2.2.4.

1.3.5 Relevance to Building Simulation

The determination of the U-value and SHGC for a layer array that includes diathermanous shading layers is not straightforward. The standard calculation of U-value and inward flowing fraction depends on the ability to sum the resistors in the glazing array. The presence of jump resistors requires a more involved method for the determination of the U-value and SHGC. The details of one such method are given in (Wright 2008) based on earlier work by Collins and Wright (2006).

Although valuable as performance indicators, it is not necessary to solve for the U-value and SHGC in the context of a time-step building energy simulation. Rather, the determination of the individual components of gain through the glazing/shading system is of interest. The proportions of the three fluxes that constitute the total gain, namely the transmitted solar flux, longwave radiant flux and convective flux, affect the building loads considerably. By definition, the U-value and SHGC do not provide any indication of the convective/radiative split and cannot be used to characterize the fenestration element directly in transient load calculations.

The relative magnitudes of the gain through a glazing/shading system to the indoor space can have significant influence on the design and performance of a building. The convective gain represents immediate cooling load, whereas the radiant fluxes (solar and longwave) impinging on an inner surface become cooling load only when the surface temperature becomes greater than the air temperature, and energy is released to the air via convection. Thermal mass of the construction thus introduces a time lag between impinging radiant fluxes and conversion of this energy to cooling load. In this context, the thermal lag can be used as a load leveling measure to dampen the response of interior surface temperatures to impinging solar fluxes. The thermal storage effect in buildings is presented in many texts (e.g., McQuiston, Parker and Spitler 2005, ASHRAE 2001).

The presence of shading layers can change the composition of the total gain to the indoor space substantially. For example, the use of a dark indoor blind can shift the proportions of the three gain components such that the convective gain becomes dominant due to roughly a three

fold increase in convective heat transfer area (indoor glass surface and front and back of blind). From an energy perspective, this can lead to higher peak cooling loads than by simply permitting the transmitted gain to be absorbed in the mass of the building. However, from a thermal comfort perspective, any shade is better than no shade since, whether outdoors or indoors, shading devices remove glare and improve thermal comfort by decreasing the solar gain directly incident on the occupant's skin and clothing. Both the energy and thermal comfort criteria can be satisfied more easily by shifting the position of the blind towards the outdoors. An investigation of the impact of blind position on the relative proportions of gain components is presented in (Lomanowski and Wright 2007). The ability to resolve the gain components in building simulation for various glazing/shading combinations is critical for an accurate assessment of shading strategies for the appraisal of building loads, energy consumption and thermal comfort.

1.4 Building Energy Simulation – The Basics

This section provides a brief summary of the introductory section of (Clarke 2001), a comprehensive text that covers a broad spectrum of building simulation topics.

Building design tools, such as those found in handbooks, are generally aimed at providing a rough performance estimate, while imposing simplified boundary conditions with a limited number of inputs. Various aspects of building systems are decoupled; each calculation step embodies assumptions that often do not describe real world complexity sufficiently. Such piecemeal tools are intended to provide a rough indication of building performance, and routinely lead to oversized equipment selection due to an inadequate assessment of component interactions. Integrated building simulation programs attempt to combine the energy and mass flowpaths that occur in buildings in order to capture the co-dependency of building systems. Thus, the only independent variables are space and time. Building simulation facilitates an evolutionary design approach, where the designer can receive feedback on the performance of the building at every stage of the design process.

Figure 1.8 shows a representation of the dynamic flowpaths within building systems that dictate building energy performance and comfort levels. A useful analogy is to consider the flowpaths as an electrical network of time-dependent resistors and capacitances, with imposed time dependent potential differences. The nodes of various building system elements are characterized by capacitances, and the nodal connections by conductances. Just as voltage represents the driving potential for current in an electric circuit, state variables such as temperature or pressure impose a potential difference across nodes for energy and mass transfer. The resulting nodal interaction is dynamic, each node responding at a different rate, storing and releasing energy or mass to neighbouring nodes. The complexity of such a dynamic network arises from establishing the flowpaths and network parameters to emulate in a realistic sense the actual building fabric and systems within. The resolution of the nodal network in the simulation is highly dependent on the design task. For example, at the early conceptual design stage, the focus may be on establishing the building envelope elements and optimizing the building construction mass and insulation with glazing elements to balance variable solar loads and skin losses. As the design evolves, plant components may be added to the nodal network to characterize the HVAC system, and control

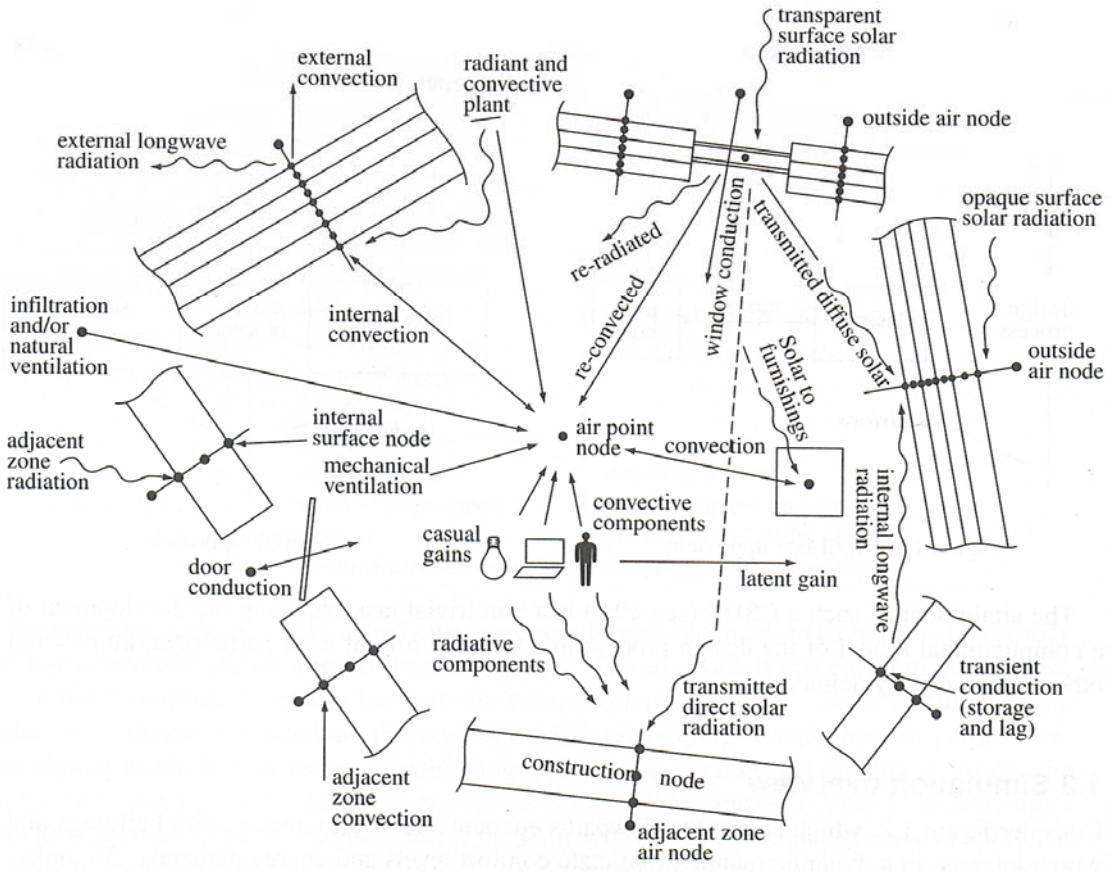

Figure 1.8: Building energy flowpaths. Reproduced with permission from (Clarke 2001).

may be imposed based on the addition of sensors, to analyze the impact of control strategies on building performance. An assessment of thermal comfort levels, indoor air quality, daylighting and luminance may also be added in more detailed simulations. The ultimate aim of integrated building simulation is to apply such a progression in simulation complexity to the entire building design process. Such an approach is inherently more efficient, replacing various piecemeal tools that ignore system interaction and apply simplified assumptions.

Clarke (2001) described the building as being systemic (many parts make the whole), dynamic (the parts respond at different rates), non-linear (the parameters depend on the thermodynamic state) and complex (numerous interactions between building/plant components). The equations describing the fundamental transport paths of energy, mass and momentum must be solved simultaneously to preserve the integrity of the entire building/plant system. Some of the significant energy and mass flowpaths within the building model include:

- Transient conduction
- Surface convection from interior and exterior building surfaces to the zone air and external ambient air, respectively
- Shortwave radiation: distribution of absorbed, reflected and transmitted solar fluxes as nodal excitations, or source terms, for internal and external surfaces
- Longwave radiation exchange between exterior surfaces to the surroundings and internal exchanges between zone surfaces
- Air-flow: mass flow of air due to pressure differences through the building fabric (infiltration and natural ventilation), zones within the buildings, and forced air ventilation
- Internal gains: the sensible convective and radiant fluxes as well as latent fluxes given off from appliances, HVAC components and occupants
- HVAC systems: energy and mass transfer through HVAC components to satisfy the thermal comfort and indoor air quality demands of the interior environment
- Moisture transport through the building fabric and airborne moisture that may lead to condensation and mould growth, as well as cause variations in the building thermophysical properties
- Electric power flow: the dynamic distribution of electric power to building systems such as lighting and equipment, as well as micro scale power generators such as photovoltaics and wind turbines.

The solution methods typically employed in building simulation programs are based on the response function method or on finite difference methods. The response function method will not be discussed here as it is not applicable to the current research, but a detailed overview can be found in Clarke (2001). Finite difference methods, in particular, in the finite volume form, can be used to solve time varying, non-linear systems of differential equations simultaneously at each computational time-step. Chapter 3 introduces ESP-r (Environmental Systems Performance-research), an integrated building energy simulation tool that serves as the platform for the implementation of complex fenestration models. The finite volume method, as applied to the thermal interactions of the building fabric, is described in more detail there. First, in Chapter 2, an overview of existing complex fenestration tools is presented, and complex fenestration models that form the basis of the work are reviewed.

1.5 Objectives, Outline and Scope

The objectives of the research can be summarized in two statements:

- To advance the use of shading in the design of energy efficient buildings through the ability to explore design options
- To implement practical, generalized and accurate window shading models into a sophisticated building energy simulation program, ESP-r, to increase the potency of the software in assessing the impact of window shading on building performance

Ongoing window shading research conducted at the University of Waterloo's Advanced Glazing Systems Laboratory is geared towards bridging the gap between research and building design practice. It is hoped that through the successful implementation of practical shading models into building energy simulation, users of the software, in research as well as professional practice, will adopt window shading assessment as part of the standard design practice for energy efficient building design.

The tasks required to realize the project objectives and the chapters corresponding to these tasks are as follows:

- Carry out an analysis of the underlying theory and source code of ESP-r; a necessary first step to understanding the framework and attaining a level of working knowledge and capability to proficiently modify, add to the source code, compile, run and test the changes made. Chapter 3 outlines some of the basic theory on modeling thermal zones, windows and capacity/insulation systems that make up the building envelope.

- Develop an overall strategy for shading model implementation. The shading models developed at UW have been documented and individually validated in many pieces of previous work (see Section 2.2). The challenge is to design a framework for the implementation of these models in ESP-r as a general complex fenestration facility. Chapter 4 introduces and documents the implementation in ESP-r of the Complex

- Carry out the details of the implementation strategy in ESP-r source code, followed by rigorous testing and debugging. This work is best described in appendix D and E, where detailed flow diagrams document the subroutines and code additions/modifications of the CFC implementation. The appendices are referenced in the thesis body as required.

- Conduct comparison studies that will build confidence in the code implementation. In particular, a study comparing the default ESP-r glazing treatment with the CFC type serves as a baseline prior to examining the shading models. Next, conduct simulation studies comparing shading models in other building energy simulation software. Chapter 5 presents these preliminary studies.

- Commit the code to the distribution branch of ESP-r, making it available to the user base. A guide for using CFCs in ESP-r simulations is provided in appendix F.

The center-of-glass shading models described in Section 2.2 are general enough to allow for specification of glazing/shading configurations in any combination. The implementation of the Complex Fenestration Construction in ESP-r retains such generality, however, the scope of this work only considers slat-type blind layers, although in any combination with glazing layers. Slat-type blinds are well characterized and offer extensive control of solar gain due to their switchable properties. Other shading layers such as drapes, roller blinds and screens may readily be incorporated into the CFC type, but adding these shade models is outside of the scope. The synthesis of algorithms for dynamic slat control at time-step resolution is also beyond the scope of this work, although simple control schemes have been tested as proof of concept (see Section 5.4). The CFC implementation can easily be extended to include shading control, and even glazing optical property control, on a time-step basis. The solar and thermal shading models of the CFC are currently not linked with ESP-r daylighting routines. The main task is to successfully build the simplified shading model framework within ESP-r, providing the foundation for future addition of an expanded set of shading layers, control schemes for operable shades including linking daylight and luminance control and occupancy behaviour models.

Chapter 2
Previous Work

2.1 Survey of Existing Window Shading Analysis Tools

Efforts to characterize glazing systems with shading attachments have recently spurred a number of software tools as the culmination of the research. Most of these tools function as stand-alone programs that determine the flow of energy in glazing/shading combinations bounded by imposed environmental conditions. Most are limited to reporting performance indicators such as U-value, solar transmission and total solar transmission (g-value, SHGC). Such performance rating tools are valuable for the characterization of complex fenestration systems and product comparisons, however, in order to consider the impact of shading in the integrated building design process, an accurate representation of window shading in building simulation is needed. This section provides an overview of four popular programs, WINDOW 6.2 and THERM 6.2, WIS 3.0.1, Parasol v4.1 and EnergyPlus 2.2.0. Only one of these tools, EnergyPlus 2.2.0, can be considered a general purpose building simulation tool.

2.1.1 WINDOW 6.2 and THERM 6.2 – Research Version

WINDOW 6.2 and THERM 6.2 Research Versions are free software programs developed at the Lawrence Berkeley National Laboratory (LBNL) used to characterize the thermal and solar properties of glazing and window systems. The research versions contain significant updates to WINDOW 5 and THERM 5, which are widely used for calculating specular glazing and window thermal and solar-optical performance indices. The combination of WINDOW 6.2 and THERM 6.2 provides a comprehensive toolset for analyzing entire window products with or without shading devices.

Capabilities: General specification of glazing and shading layers including venetian blinds, diffusing shades, and woven shades. Facilities for including bi-directional slat properties are available. Center-of-glass glazing systems can be imported to THERM 6.2 for frame and edge

calculations that can then be then returned to WINDOW 6.2 to generate results for an entire window product. The results include U-value and SHGC for the entire system, plus temperature and solar optical data for the specified window configuration. The software performs steady state calculations, thus the slat angle for slat blinds is fixed, but may be set to any value. Off-normal incidence results for solar transmission and absorption and SHGC are available for glazings without shading layers. THERM 6.2 provides a detailed 2-D heat transfer analysis of the edge of glass and frame regions, including the effect of shading layers on the boundary conditions of frame sections. No load calculations are available. Previous versions (WINDOW 5 and THERM 5) included an interface with DOE-2 and EnergyPlus simulation engines. Currently, no interface is available for the research versions.

Models: Specular glazing solar and thermal models are identical to WINDOW 5 and WINDOW 4 (Finlayson et al. 1993). The calculations of solar optical properties and heat transfer for slat-type blinds are based on ISO 15099 (2003). A detailed description of the ISO 15099 models can be found in (TARCOG 2006). System optical property results can be obtained for normal incidence as well as a detailed set of properties for multiple incident angles using a 'matrix calculation engine' (Mitchell et al. 2008).

Summary: WINDOW 6.2 and THERM 6.2 Research Versions offer extensive capabilities for characterizing an entire window with or without shading layers. In combination, these programs provide performance indices such as U-value and SHGC of the entire window assembly, as well as a detailed set of optical property results at normal and off-normal incidence angles. The software is well suited for performance rating, although the research versions come with a disclaimer stating that the new algorithms should be considered informative, but not definitive. Load calculations are not performed in the software, but future versions may incorporate an interface to building simulation engines such as DOE-2 and EnergyPlus. Extensive documentation, user manuals and model descriptions are available on the product website (WINDOW 6.2 and THERM 6.2 2008).

2.1.2 Advanced Window Information System (WIS) 3.0.1

WIS is a standalone, multi-purpose European software tool used to determine the thermal and solar characteristics of a window, including glazing, frame and shading components. WIS is a product of the WinDat European Thematic Network. The software contains databases describing

the properties of each window component and routines for calculating the thermal/solar interactions of the components based on imposed environmental conditions. Detailed calculation reports can be generated for the entire window assembly or for individual components. The current version is WIS 3.0.1 SP2 (WIS 3.0.1 2006).

Capabilities: The transparent system can be composed of specular glazing layers and scattering shading layers including slat-type blinds, pleated blinds, roller blinds and diffusing shades. A range of frame products with known U-value is available for specifying the frame section of the window. The scattering layer database includes entries for commercially available shading devices and measured slat spectral data. The user can readily modify the slat angle for slat-type blinds. The steady state calculation results include U-value, g-value, solar transmittance (diffuse and direct) for normal and off-normal incidence, visual and UV transmittance. The total U-value, as well as the convective and longwave radiative contributions are reported. The program is designed for performance rating of window products, load analysis is not available.

Models: Two methods are used to calculate the solar optical properties of slat-type blinds: view factor method and ray tracing method. The ray tracing method can be used for slats with partially specular properties, if they are available. Otherwise, the slat is assumed to reflect diffusely. The solar and thermal characteristics of the window components are modeled in accordance with European standards (e.g. ISO 15099 2003, EN 410 1998, EN 673 1997, EN 13363 –2 E 2004, EN ISO 10077-1 2000). Limited documentation can be found on the WIS website (WIS 3.0.1 2006).

Summary: WIS is a comprehensive window performance rating tool with extensive component libraries and calculation reports that detail solar optical and thermal characteristics either on a component level or as an entire window product. The calculations are based on user prescribed, environmental conditions for outdoor and indoor environments. Results include U-value (component and total), g-value, convective/radiative split, normal and off-normal incidence solar optics for specular and scattering layers. A building load analysis is not performed as the software is intended only for evaluating the relative performance of window products.

2.1.3 Parasol v4.1

Parasol is a tool for assessing the performance of various glazings and shading attachments by considering the solar transmittance values and cooling/heating demands for a single room with a window. The software is under continuous development at the division of Energy and Building Design, LTH, Lund University, Sweden. The core of the program is an hour-by-hour energy simulation engine DEROB-LTH, originally developed at the University of Texas, Austin, Texas (Hellstrom et al. 2007). Parasol performs annual hour-by-hour energy simulations to compute integrated heating and cooling demands, peak loads for a prescribed room and window geometry with glazing and shading attachments selected from provided databases. In addition, monthly average values of solar transmittance and g-value (or total solar transmittance) can be obtained. Output is generated in graphical form with a report generation facility. Post processing of thermal comfort and daylight analysis for the room with window is available. The software is available for free download on the product website (Parasol v4.1 2008).

Capabilities: The room walls, floor and ceiling are assigned an adiabatic boundary condition in order to simulate an office located within a larger building. Variables for describing the room and window arrangement include room and window dimensions, room orientation, wall U-value and light, medium or heavy walls to vary the mass. Shading options for external, between glass and internal shades include awnings, brise-soleil, venetian blinds, shutters, screens, roller blinds and pleated curtains. User input for venetian blinds includes slat type and slat angle. New entries in databases can be created for glazings and shading layers. Simulations for solar transmittance, g-value, and cooling/heating demand are performed for cases with and without shading. Internal gains, ventilation rate, heating/cooling set-points, inlet air temperature and ventilation heat recovery are input parameters for the simulation. Simple shade up/down control is available, based on the insolation on the window.

Models: Solar optical models for specular glazings are based on Fresnel and Snell's law relations, the details of which can be found in the literature (e.g., Duffie and Beckman 1980). For coated glass, the angle dependent optical properties are normalized to a grey absorbing uncoated pane with a high extinction coefficient (Hellstrom et al. 2007). Some spectral data are available in the glass library, but shading layers are described with total band-averaged properties. Curtains and roller blinds (screens) are not modeled with incidence angle dependency. Venetian blinds are

modeled with averaged layer properties based on geometry and optical properties of the slats. Properties for venetian blinds are calculated separately for ground reflected and sky components of diffuse insolation. A constant convective heat transfer coefficient is applied to the outdoors, while the indoor coefficient is calculated from the temperature difference in the room. Simplified convective heat transfer correlations for indoor shades, and between-glass shades are used. Outdoor shades are assumed to be fully ventilated. Details can be found in (Hellstrom et al. 2007).

Summary: Parasol is a unique software tool for the analysis of shading attachments in three configurations relative to glazing layers. Load calculations via an hour-by-hour energy simulation engine provide valuable information for assessing the energy savings potential of using various shading devices. The simulation engine used for load calculations, although limited to a prescribed geometry and boundary conditions, provides valuable information for assessing the energy savings potential of using various shading devices. The program is available for free download. A description of the models and references to more detailed documentation is provided in (Hellstrom et al. 2007).

2.1.4 EnergyPlus 2.2.0

EnergyPlus is a standalone building energy simulation tool developed by the US Department of Energy. It is based on the most popular features of its predecessors, DOE-2 and BLAST. The reader is referred to the product website for details on these programs (EnergyPlus 2.2.0 2008). EnergyPlus is an integrated simulation tool with simultaneous solution of the building, system and plant domains of a building. EnergyPlus does not have a graphical user-friendly interface; it is a simulation engine that reads text input files and writes text output files. Several free and commercial graphical interfaces are available to aid the user in the creation of the input files and graphical post-processing of the output data.

Capabilities: Complex fenestration capabilities include models for glazing, frame, divider and shading devices. Fenestration models are integrated into the time-step simulation engine, allowing for impact assessment of complex glazing/shading systems. Four categories of shading devices may be specified: perfectly diffusing shades, venetian blinds, insect screens and switchable glazings. The window models are coupled to zone solar gains calculation and daylighting. Slat angle control for venetian blinds is possible at single time-step resolution. Three possible slat controls are

available: (1) slat angle adjusted to block beam solar, (2) slat angle schedule (3) fixed angle. Venetian blind layers may be specified for indoor, between the glass and outdoor configurations.

Models: Glazing models are based on WINDOW 5 algorithms (Finlayson et al. 1993). The solar-optical model of a venetian blind is based on (Simmler, Fischer and Winkelmann 1996). Venetian blind optical properties are sensitive to profile angle geometry. Spectral dependence of inter-reflections between blind slats and adjacent glass layers is ignored. Total (i.e., band-averaged) solar properties are used. Models for natural convection airflow between shades and glazing layers are based on ISO 15099 (2003). Longwave radiation effects are considered for outdoor, between the glass and indoor blind positions. The solar-optical and thermal models used in EnergyPlus are system specific. That is, the equation sets describing layer solar-optical properties as well as heat balances are generated based on a specific model for each glazing/shading configuration. Models are described in the EnergyPlus Engineering Reference (2008).

Summary: EnergyPlus is a popular simulation engine used in many third party commercial software programs geared towards graphical input generation and output results analysis for building energy performance. Recently, in version 2.0, complex fenestration models have been coupled with the zone solar gains calculation and daylight routines. Solar-optical and thermal models are specific to glazing/shading system configuration. Control of blinds is possible on a time-step basis. Documentation, including detailed user guides and a comprehensive engineering reference, is available from the product website (EnergyPlus 2.2.0 2008).

2.2 Overview of the AGSL Shading Models

Recent efforts in window shading research at the University of Waterloo's Advanced Glazing Systems Laboratory (AGSL) have produced a set of practical and flexible models that characterize shading layer properties and the interaction of such shading layers within a glazing system. The strategy is to separate the solar and thermal analysis, as in conventional glazing analysis, and to treat the shading layer as an equivalent homogeneous layer, suitable for one-dimensional analysis. Improved solar multi-layer methods for coping with scattering shading layers, a general treatment of longwave radiation exchange with diathermanous layers, and the development of between glass slat blind convection models have been completed. The models have been developed with emphasis on generality and computational efficiency, while retaining

accuracy. These models are applied to the development of the complex fenestration facility in ESP-r. A description of the solar and heat transfer models is provided in this section. It is worth noting that the only model component that relies heavily on empirical information is the convective heat exchange between glazing/shading layers. Solar and longwave radiation models that characterize glazing/shading layer interaction are based on fundamental heat transfer relations valid for any combination of glazing/shading layers. The applicability of the AGSL shading models is thus limited to:

- Center of glass analysis
- Availability of convection correlations. A correlation has been developed for a between-glass shade and an approximate treatment of outdoor/indoor shades exists. These models do not cope with more than one contiguous shading layer
- Convection models only consider natural convection in sealed window cavities (no ventilated cavities)

2.2.1 Effective Solar-Optical and Longwave Radiative Properties for Slat Blinds

Kotey et al. (2008) have developed simplified effective solar optical property models for slat-type blinds intended for building energy simulation, where computational efficiency is a strong requirement. Based on previous work by Yahoda and Wright (2005) the simplified models eliminate computationally intensive ray tracing techniques required in the original formulation to account for the slat beam-diffuse split with respect to solar radiation. Kotey at al. (2008) assume the slats are perfect diffusers and therefore reflect and transmit beam radiation diffusely. Slat material properties are assumed to be independent of the angle of incidence. A four or six surface radiosity enclosure flat slat model is used to account for beam-diffuse reflectance and transmittance, depending on slat illumination. Diffuse-diffuse solar properties are calculated using a four surface flat slat model. The four-surface model can also be applied to determine effective longwave radiative properties. The flat slat model over-predicts blind transmission when the solar profile and slat angles are aligned. Thus, a curvature correction was applied to the flat slat model. A correction for slat thickness was not considered. The flat slat model and the curvature slat model are in excellent agreement with experiments. However, for cases where the slat and profile angles

are closely aligned, the curved slat model falls more closely in line with experiments (Kotey et al. 2008).

2.2.2 Solar Multi-layer Model

Wright and Kotey (2006) have developed a method by which existing solar optical models for systems of 1-D center-of-glass specular glazing layers can be extended to include the effect of scattering shading layers. The model is based on the assumption that only specular and/or isotropically diffuse components of solar radiation result from the interaction of insolation with any item in a glazing/shading layer array. An expanded set of solar optical properties is assigned to each layer accordingly to account for beam-beam, diffuse-diffuse and beam-diffuse solar fluxes (see Figure 1.4). Beam-diffuse properties are needed to account for the presence of non-specular layers that scatter solar radiation. Spatially averaged effective properties are used to characterize shading layers. The model establishes a balance of solar flux components for each layer, including beam-beam fluxes, diffuse-diffuse fluxes and beam-diffuse fluxes (Figure 2.1). A sequential three-step solution is then used to solve for all solar fluxes. First, beam-beam fluxes are solved using a tri-diagonal matrix algorithm (TDMA). Second, beam-diffuse source terms are calculated using known beam-beam fluxes and beam-diffuse layer properties. Third, the beam-diffuse source terms along with diffuse-diffuse properties are used to solve for diffuse-diffuse fluxes using the TDMA

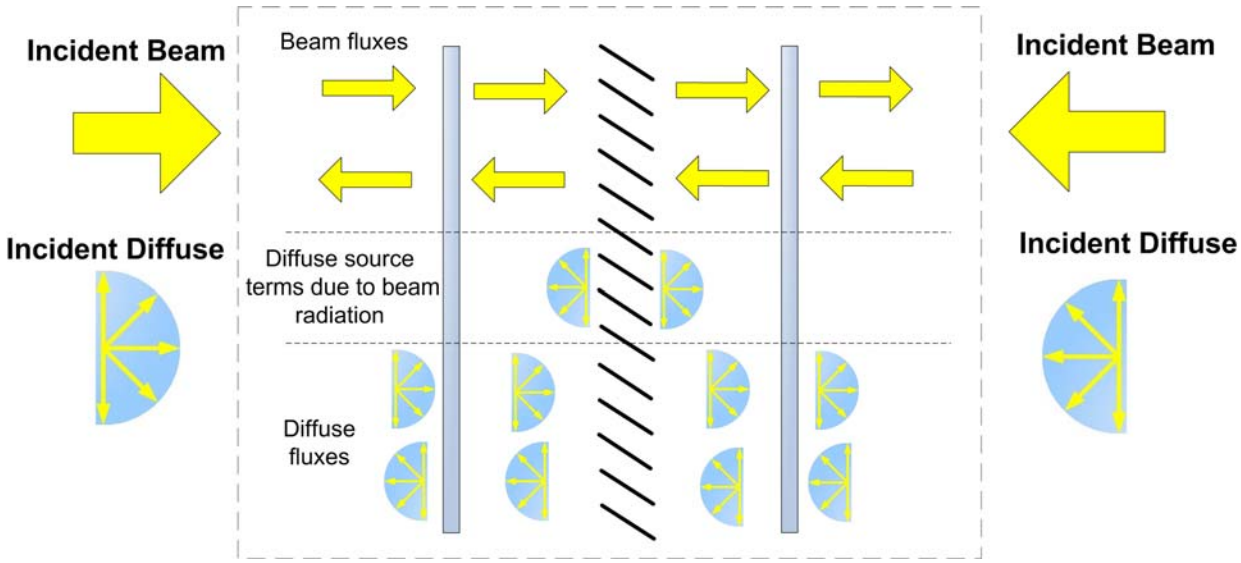

Figure 2.1: Interaction of solar fluxes in a mutli-layer scheme with a scattering shading layer.

method. Thus, the model provides full detail concerning the quantities of reflected, transmitted and absorbed solar radiation. The method is general enough to allow for introduction of incident solar radiation both on the outdoor side and indoor side of the window. The resulting computer code is well suited for use within an time-step building energy simulation (Wright and Kotey 2006).

2.2.3 Longwave Radiation Exchange

The presence of diathermanous shading layers adds complexity to the thermal resistance network of the 1-D glazing/shading array. Standard methods for determining the radiant exchange, such as the net radiation method, are general enough to cope with jump resistors, and the temperature solution can still be resolved accurately. However, methods for calculating glazing system U-value and SHGC (e.g., Wright 1998, Hollands et al. 2001) can be in error when a jump resistor is present. A new method for calculating the indices of merit of multi-layer systems has been developed by Wright (2008) based on earlier work by Collins and Wright (2006). This method is sufficiently general to handle any combination of diathermanous and opaque layers in the glazing/shading system.

Although the U-value and SHGC are not required to characterize complex fenestration elements for time-step building simulation, Wright's (2008) method is useful, particularly in determining the longwave radiant exchange. The method is similar to Gebhart's analysis of diffuse, grey enclosures (Gebhart 1959), with an extension for specific treatment of diathermanous layers. The method, referred to here and throughout this thesis as the "exchange factor method", is based on knowledge of a set of exchange factors. Similar to the concept of a view factor (also referred to as form factor or shape factor), defined as the "fraction of the radiation leaving surface i that is directly intercepted by surface j", an exchange factor also accounts for all of the inter-reflections in an enclosure. An exchange factor can therefore be defined as:

"The fraction of the radiant energy emitted by surface i that reaches surface j via both direct radiation and by all possible reflections."

The basic procedure for determining exchange factors is to 'turn on' one surface at a time and determine the irradiation at each surface via a radiosity balance. In other words, allowing only one surface to emit radiation while 'turning off' all other surfaces, the flux absorbed by any surface j, as

a result of emission from surface i, can be resolved. Wright (2008) does not specifically refer to exchange factors, but instead uses a modified radiosity notation with superscripts to denote the surface of origin, or the 'turned on' surface. The concept is the same. More information on the exchange factor concept can be found in literature (e.g., Wright 2008, Hollands 2004, Gebhart 1959).

The main benefit of the exchange factor method is the ability to determine individual radiant heat transfer coefficients between any pair of surfaces in an enclosure containing any combination of diathermanous and opaque surfaces. This is useful for tracking longwave radiant exchange between indoor diathermanous layers and zone interior surfaces, which also exchange longwave radiation with each other. The ability to track individual surface exchanges in a room enclosure containing diathermanous surfaces makes book keeping of radiant fluxes manageable. In addition, using this method allows for determination of the U-value and SHGC, useful for documentation purposes as performance indicators, although not necessary for the temperature solution of the thermal zone in time-step simulation.

2.2.4 Convection Models

Convective heat transfer in a sealed cavity with a large aspect ratio between two glass panes has been well characterized. Standard correlations exist (e.g., Shewen et al. 1996) and can be used for different fill gas types and mixtures. With the addition of a shading attachment, the nature of convective heat transfer is highly dependent on the position of the blind. Fill gas flow in a sealed cavity with an integral, or between-glass, slat-type blind behaves in a predictable manner. Placing a shading layer on the outdoor or indoor side roughly triples the area of convective heat transfer to the ambient or indoor air, respectively. Air flow around an outdoor blind is dictated by the outdoor conditions whereas for indoor blinds, ventilation and temperature conditions influence the flow. Air flow at the indoor surface of a window may be affected by the presence of a ventilation system, position of vent inlets, the presence of a baseboard heater or the influence of natural convection currents. In the simplest case, isolated buoyancy flow is driven by indoor temperature differences. The prediction of convective heat transfer coefficients for outdoor and indoor blinds is non-trivial, however, even with approximate values for the coefficients, the sheer increase in convective heat transfer area results in large convective fluxes to the ambient and indoor air in the presence of outdoor and indoor blinds, respectively.

The following one-dimensional models attempt to characterize the convective heat transfer in glazings with adjacent slat-type blinds for three different blind configurations.

Between Glass Slat Blind

The effect of a slat-type blind on the convective exchange within a glazing cavity is well understood. Huang, Wright and Collins (2006) conducted an experimental investigation into the effects of a slat-type blind on convective and radiative heat transfer inside a vertical window cavity. A simplified convective heat transfer model was developed that compared well with experimental results. The model essentially modifies any vertical cavity correlation (e.g., Shewen et al. 1996) to account for the presence of the blind by applying a modification factor, n*, to the slat width which results in a wider cavity spacing. It was found that a constant value of n*=0.70 produced excellent results irrespective of cavity temperatures and blind slat angle, except when the cavity spacing is wide. Collins, Tasnim and Wright (2008) further examined the problem using a numerical model to describe the steady laminar natural convection within the cavity. The results suggest that flow across the louvers between the two sides of the blind is negligible and that essentially the convective heat transfer can be represented as exchange between glass-blind and blind-glass, without including a glass-glass term. The modified cavity correlation with n* factor was re-examined, giving a slightly different value of n*=0.61, due to the approximation of the experimental set up in the numerical model. It is suggested that Huang's (2006) value of n*=0.70 be used in practice, with confidence, up to a cavity glass-to-glass width of 40 mm (Collins, Tasnim and Wright 2008).

Indoor Blind

As discussed in Section 1.3.4, the thermal resistance network for convective heat transfer of an indoor shading layer includes jump resistors from the indoor glass and blind surfaces to the interior air. As already mentioned, this results in roughly tripling the convective heat transfer area. The nature of natural convection flow around an indoor slat-type blind is a subject of ongoing research (e.g. Collins 2004, Shahid and Naylor 2005, Oosthuizen et al. 2005, Naylor et al. 2006). To date, a general correlation describing convective exchanges with an indoor slat-type blind does not exist. The problem is further complicated by the various flow and mixing conditions that may exist in practice and deviate from the steady laminar buoyancy flow assumption.

Shahid and Naylor (2004) have shown that the tip of the slat to glass spacing can significantly affect the energy performance of a window with an indoor venetian blind. As the blind is positioned closer to the window, the convective exchanges between the inner glass and blind surfaces to the indoor air are diminished, while convective exchange between the inner glass and blind surface is increased. Given such a dependence on blind to glass spacing, an approximate convection model has been developed by Wright et al. (2008). The model predicts heat transfer coefficients for a shading layer that is exposed to an indoor environment, as a function of the distance from the tip of the blind slats to the glass surface. Two limiting conditions exist:

- Blind is well away from the window. There is no interaction between the blind and glass surfaces. Convective exchange between the blind and glass surfaces approaches zero. Convective heat transfer to the room air occurs at the three indoor surfaces (glass, blind front and blind back).
- Blind is in physical contact with (or very close to) the glass surface. Convective exchanges between the outdoor facing blind surface and indoor air, as well as the glass surface and indoor air, approach zero.

If the blind is positioned at some spacing that is in-between the two extremes, convective heat transfer coefficients are approximated by an exponential decay. The procedure is ideally suited for building simulation, where an indoor convective heat transfer coefficient is determined for each surface according to type of flow within the thermal zone and surface orientation. This heat transfer coefficient is therefore used for the indoor surfaces (glass and both sides of the blind) when the blind is well away from the window, adjusting the glass surface convective coefficient for the glass temperature. The exponential function applies a smooth transition between the two position extremes, adjusting the convective heat transfer coefficients based on blind to glass distance. Thus, the flow type in the thermal zone and the glass to blind spacing characterize the convective exchanges for an indoor blind configuration. Further adjustment to the slat-blind heat transfer coefficients is made based on the slat angle. A slat angle 'penalty' is applied for cases where the blind angle is not fully open or fully closed and cross flow between the louvers is known to occur, increasing convective exchange with the indoor air. Details of the model are presented in appendix A.

The above model is an approximate method and does not account for various frame and window sill designs that may impede the flow. Further study of the general problem is recommended; specifically in regard to effects of imposed air flow types and window geometry, to provide insight on the validity of using this simplified model.

Outdoor Blind

Figure 1.7 in Chapter 1 shows the convective resistors on the outdoor side when an outdoor blind is present. Convection heat transfer takes place on both sides of the blind slats as well as the outdoor glass surface. An approximate convection model for an outdoor blind consists of applying the external convective heat transfer coefficient to the front and back of the blind as well as the outdoor glass surface. The convective heat transfer area is thus tripled. The outdoor convection coefficient may be supplied by the user or may be determined within a building energy simulation based on wind speed and direction, surface orientation and temperature conditions. Since the outdoor blind is exposed to forced convection, the interaction between the blind and outermost glass surface is ignored. Essentially, the blind is assumed to have no influence on the air flow at the outdoor glass surface and the outermost cavity is considered fully vented. This assumption may not hold during relatively calm sunny conditions when the solar radiation absorbed in the outdoor blind is not readily rejected back to the ambient due to low convective heat transfer rates, thus creating a hot zone adjacent to the window. This effect may not be significant but further study is needed to establish the relative impact, if any, of outdoor blind to glass spacing for various ambient conditions.

Chapter 3
ESP-r Thermal Model

ESP-r is a general purpose integrated building simulation software environment encompassing the modeling of multi-zone building thermal domains, inter-zone air flow, intra-zone air movement, HVAC systems and electrical power flow. The software has been in development since the 1970s and is made available at no cost under an open source license. ESP-r is based on a design approach in which additional complexity and technical domain solvers are applied as the building description evolves. Although ESP-r has strong research roots, it is being used as a consulting tool by engineers, architects and designers (Crawley et al. 2005). The software is supported by extensive publications, examples and tutorials, listed on its website (ESP-r v11.5 2008). A support network of active users and developers provides timely response to inquiries. The software serves as a comprehensive platform for development and collaboration in building simulation efforts. This section presents the approach used in ESP-r used to solve the transient thermal building domain, and the constraints of the solver as related to the complex fenestration models. The current treatment of glazing elements in ESP-r is discussed. Simplified simulation flow of a thermal zone is also presented.

3.1 Formulation of the Finite Volume Heat Balance Method

The formulation described in this section is presented in more detail in (Clarke 2001) and (Beausoleil-Morrison 2000).

The finite volume heat balance method is used in ESP-r to establish an equation set describing the thermal state of discretized building systems, for which a simultaneous numerical solution can be generated. The approach is based on applying conservation principles to small control volumes, which are in thermodynamic communication with one another. Figure 3.1 shows a simple representation of a discretized physical system with element I communicating with its

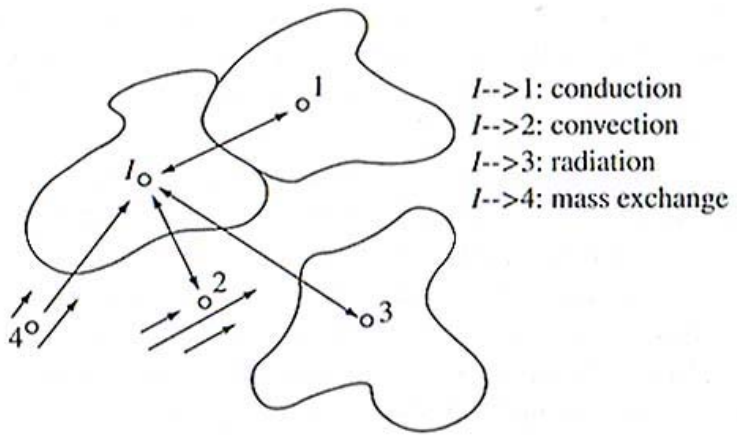

Figure 3.1: Energy flow-paths in a discretized physical system. Reproduced with permission from (Clarke 2001).

surrounding regions. The energy balance for control volume I equates the rate of heat being stored in element I to the net rate of heat flow to element I, which yields

$$\frac{\rho_I(\xi)c_I(\xi)\delta V_I(\xi)}{\delta t}\left[T(I,t+\delta t)-T(I,t)\right] = \sum_{i=1}^{N} K_{i,I}\left[T(i,\xi)-T(I,\xi)\right]+q_I(\xi)+\varepsilon \quad (3.1)$$

where $\rho_I(\xi)$ is the representative density (kg/m^3) of region I at some time ξ, $c_I(\xi)$ the representative specific heat (J/kg K) of region I, $\delta V_I(\xi)$ the region volume (m^3), δt the discretization time step (s), $T(I, \xi)$ the representative temperature (K) of region at time ξ, $K_{i,I}$ the heat flow conductance (W/K) between region i and I, $q_I(\xi)$ the heat generation (W) within region I, N the number of energy flowpaths between region I and surrounding regions, t the present time-row, $t+\delta t$ the future time-row and ε the discretization error.

Evaluating the heat flows and generation terms on the right side of the equation at the present time-row $\xi=t$ gives the fully explicit formulation. This implies that the future time-row temperature of node I is a weighted average of the present time-row temperature of I, temperatures of the adjacent regions in thermal contact with I, plus any heat generation terms. All nodal equations in the fully explicit scheme are independent and can be solved directly, as they

only contain present values of temperature from all coupled nodes. The fully explicit scheme is relatively easy to formulate, but can become unstable. In contrast, the fully implicit scheme, obtained by evaluating the heat flows and generation terms at $\zeta=t+\delta t$, is unconditionally stable. In this formulation, the system is represented by a series of nodal equations that are linked to one another by the unknown future temperature term of all coupled nodes. The set of equations must be solved simultaneously for each time-step.

Multiplying the implicit equation by weighting factor W and the explicit equation by (1-W) and adding the two resulting equations yields a generalized formulation. By changing the value of W, one can vary the implicitness of the scheme where, at the extremes, setting W to 1 yields the fully implicit scheme and setting W to 0 yields the fully explicit scheme. Setting W=0.5 results in the Crank-Nicolson formulation, a commonly used method due to its stability and accuracy in numerical analysis. Although the method is unconditionally stable, the solutions can still contain oscillations if the time-step is too large.

The Crank-Nicolson energy balance can be applied to any discretized physical system within a building such as building envelope and interior fabric, HVAC components and air flow networks. A building thermal zone can be described with three types of characteristic nodes:

- Intra-constructional nodes that represent capacity/insulation systems within building components such as walls, floors and ceilings
- Nodes at exposed surfaces (e.g. interior/exterior of wall, ceiling, floor surfaces)
- Nodes that represent fluid volumes in enclosed indoor spaces

A standard ESP-r nodal scheme characteristic of a building multi-layer construction (MLC) is shown in Figure 3.2. Resistors represent the energy flowpaths between nodes and capacitors represent the energy storage capacity of each node. The inside surface node S_i is coupled with other inside surface nodes (S_j) in the thermal zone through longwave radiation exchange. F_j represents the air volume in the thermal zone, to which S_i is coupled to by convective heat transfer. Each construction node is also connected with adjacent nodes through conduction heat transfer. The outside surface node, if exposed to the environment, exchanges heat by long-wave

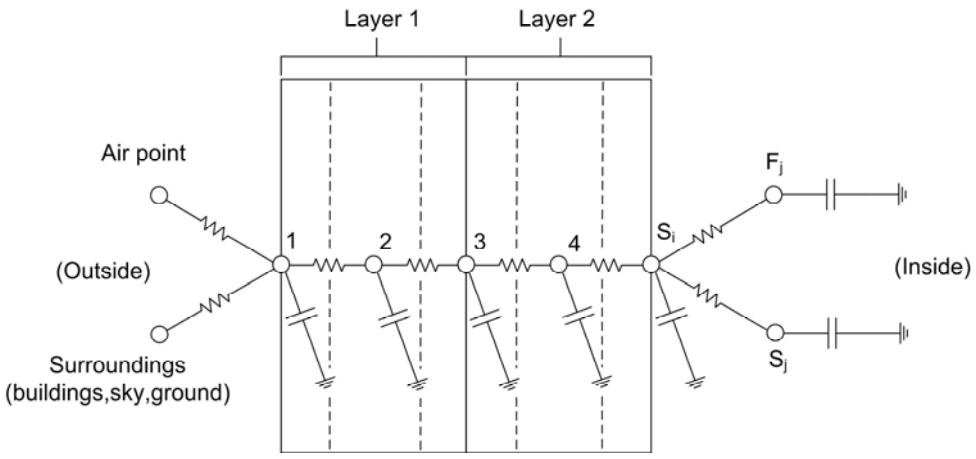

Figure 3.2: Nodal scheme of a multi-layer construction.

radiation to the surroundings and convection to the ambient air. If exposed to an adjacent thermal zone, the outside surface node is coupled to other inside surfaces of the adjacent zone as well as the adjacent zone air node. In addition to balancing heat fluxes and energy storage at each node, generation terms may be added to represent plant interactions (e.g., radiant heating), or solar radiation absorption. The resulting nodal difference equations are of the form of Equation 3.1.

Figure 3.3 illustrates the basic nodal scheme of a single thermal zone with two air volumes, reproduced from (Clarke 2001). Further complexity may be added to the nodal scheme by, for example, introducing plant components or internal gains such as appliances. The Crank-Nicolson difference equation formulation for each node can be expressed, after algebraic manipulation, as

$$\begin{aligned} &C_s(t+\delta t)T(I,t+\delta t)-\sum_{i=1}^{N}C_{ci}(t+\delta t)T(i,t+\delta t)-\frac{\delta t q_I(t+\delta t)}{\delta V_I} \\ &\quad = C_s(t)T(I,t)-\sum_{i=1}^{N}C_{ci}(t)T(i,t)-\frac{\delta t q_I(t)}{\delta V_I}+\varepsilon \end{aligned} \tag{3.2}$$

where C_s is the self-coupling coefficient of node I, and C_{ci} are the cross-coupling coefficients for all nodes in thermal contact with node I. The left side of the equation contains future time-row terms, the right side contains present time-row terms. Each nodal equation contains one self-coupling coefficient and several cross-coupling coefficients relating to the present time-row and

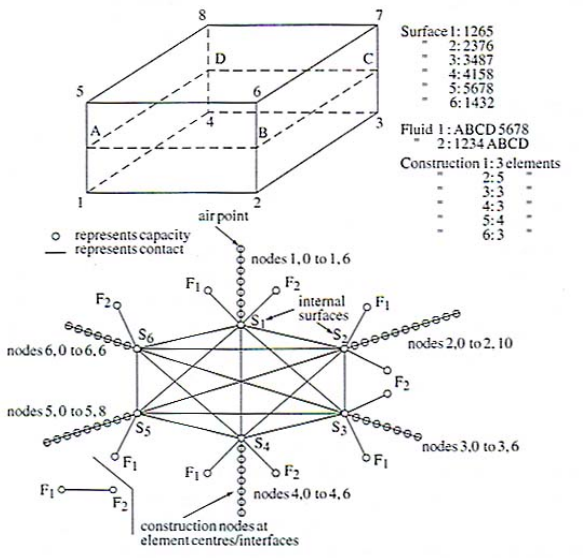

Figure 3.3: Simple nodal scheme of a thermal zone with two stratified air volumes. Reproduced with permission from (Clarke 2001).

the future time-row of the computational time-step. The overall equation set can be rewritten in matrix form,

$$\mathbf{A}\Psi_{n+1} = \mathbf{B}\Psi_{n} + \mathbf{C} \qquad (3.3)$$

where **A** and **B** are two-dimensional arrays containing self-coupling and cross-coupling coefficients at the future and present time-row respectively. ψ_{n+1} and ψ_n are column matrices that contain the nodal temperature terms and heat injection/extractions at the future and present time-row respectively. Column matrix **C** contains known boundary condition excitations due to temperature and heat flux fluctuations imposed on boundary nodes. The future time-row coefficient **A** matrix of the single zone is shown in Figure 3.4. The **A** matrix is sparse, containing mostly zeros, except for equation coefficients, represented by 'X'. Since the right side of Eqn. 3.3 contains known present time-row terms and known boundary terms, a column matrix combining these terms can be generated such that

$$\mathbf{Z} = \mathbf{B}\Psi_{n} + \mathbf{C} \qquad (3.4)$$

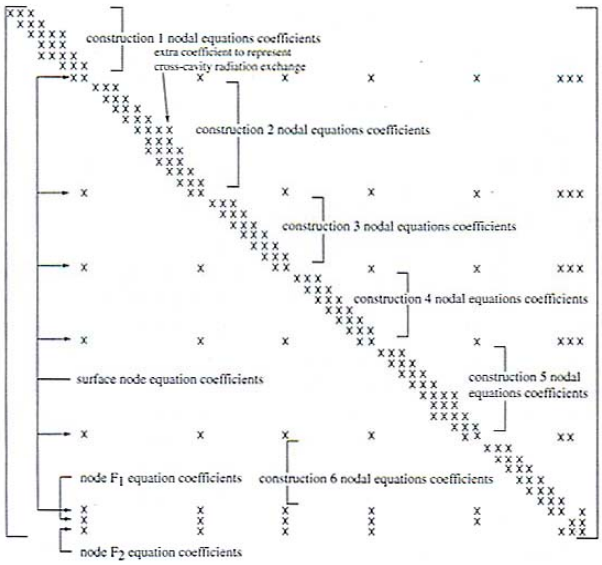

Figure 3.4: **A** matrix containing future time-row coefficients of the single thermal zone shown in Figure 3.3. Reproduced with permission from (Clarke 2001).

Now Eqn. 3.3 can be rewritten as

$$\mathbf{A}\Psi_{n+1} = \mathbf{Z} \qquad (3.5)$$

One possible solution of the future terms is to invert the future coefficients matrix **A**, such that

$$\Psi_{n+1} = \mathbf{A}^{-1}\mathbf{Z} \qquad (3.6)$$

The above technique is a general formulation of the Crank-Nicolson difference method for an equation set that describes a transient physical system. Layers of complexity can be added to the system and various solution techniques exist. The details of the solution techniques can be found in (Clarke 2001). For the purposes of the thesis objectives it is relevant to outline the constraints and assumptions made in establishing the future coefficients matrix in ESP-r.

3.1.2 Difference Equation Matrix Formulation Constraints

Obtaining the future term solution by inversion of a sparse matrix at every time-step is computationally inefficient. Instead, ESP-r employs a semi-direct approach by partitioning the matrix into smaller elemental sub-matrices, each of which can be processed independently (details

in (Clarke 2001)). The key constraint of the method is that the sparse matrix does not actually exist in computer memory. The partitioned matrix solution technique relies on matrix reduction algorithms based on a specific matrix structure. For intra-constructional nodes this structure constrains each node to be in thermal contact with only adjacent nodes. In other words, a node can only communicate with its near-neighbours, preventing the presence of any jump resistors. The implications of such a matrix structure for an air-gap within a multi-layer construction are illustrated in Figure 3.5. The heat transfer processes within an air-gap include convective heat transfer and longwave radiation exchange between the two interfacial nodes (Figure 3.5 a). To simplify the matrix processing requirements of multi-layer constructions, a total resistance (R_{gap}) that combines the convective and radiant processes is used in ESP-r to represent heat transfer across an air-gap. This ensures that the cross-coupling coefficients throughout the intra-constructional nodes remain the same in the presence of an air gap. As discussed later in Chapter 5, section 5.2.3, the use of a constant air gap resistance is a good trade-off between accuracy and reducing matrix processing complexity. However, for complex fenestration, which may include diathermanous layers, and in turn jump resistors, this constraint complicates shading model implementation. Ideally, a flexible sparse matrix formulation would allow any node to be in thermal contact with any other node. However, the solution technique required for such a general matrix formulation would carry a heavy computational burden. Reworking the ESP-r matrix processing routines in any capacity would be a difficult undertaking, far beyond the scope of the current research.

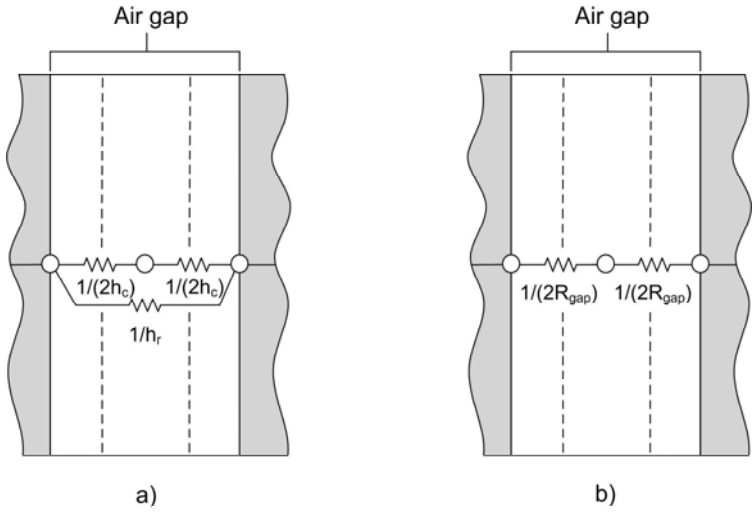

Figure 3.5: Air gap thermal resistance network with a) convective and longwave radiative resistances and b) with equivalent total R_{gap} resistance.

3.2 The Transparent Multilayer Construction (TMC)

The distribution of solar radiation within a building envelope and interior surfaces is resolved in ESP-r by introducing generation terms to appropriate nodes. The processing of solar fluxes through transparent elements is handled in ESP-r by the transparent multi-layer construction (TMC). The TMC is an extension of the multi-layer nodal scheme used to model opaque constructions, or MLCs. Nodal solar absorption sources for TMC transparent layers as well as overall system transmission are determined on a time-step basis based on the sun's position.

In ESP-r a set of optical data is associated with each TMC. This set consists of system solar transmission for the entire window and absorption at each glazing layer. The properties are given for normal incidence and 5 off-normal incidence angles. The TMC off-normal properties corresponding to the solar incidence angle at each time step are determined by interpolating the given optical data. Standard optical property sets are included in the ESP-r optical database. The user can also define a custom property set or import data from third party software such as WINDOW 5. Solar gain control may be achieved by manipulating the optical property sets of a TMC for prescribed control periods. For example, Figure 3.6 shows the optical property set input file for a double glazing with prescribed control periods, defined prior to the simulation. The first set represents the default glazing optical properties associated with the TMC, the second set for control period 1 represents a shaded window with roller blind. At run-time, the default optical set is used until control period 1, for which the replacement optical set is then invoked. This strategy

```
# transparent properties of zone1 defined in
../zones/zone1.tmc
   6    # surfaces
# tmc index for each surface
1,0,0,0,0,0
   3  DCF7671_06nb # layers in tmc type 1
# Transmission @ 5 angles & visible tr.
   0.611   0.583   0.534   0.384   0.170   0.760
# For each layer absorption @ 5 angles
   0.157   0.172   0.185   0.201   0.202
   0.001   0.002   0.003   0.004   0.005
   0.117   0.124   0.127   0.112   0.077
   1  # optical control flag
   1   1  # no control periods & sensor loc
# Replacement properties for each control period
  12  18   # period start and end
 -99   0.0  # sensing time @ actuation point
# Alt solar & vis trans followed by absorp for each layer
   0.060   0.045   0.033   0.019   0.006   0.070
   0.893   0.892   0.890   0.803   0.600
   0.001   0.002   0.003   0.004   0.005
   0.004   0.003   0.002   0.002   0.001
```

Default optical property set

Control period 1 optical property set

Figure 3.6: Example of TMC input file defining the optical property set for each control period.

relies on prior knowledge of the optical properties for a specific window/blind configuration, and therefore relies on third party software or manual input of the properties by the user.

As previously mentioned, convective and longwave radiative heat transfer across a sealed glazing cavity is lumped into a single resistor (R_{gap}) to minimize complexity in matrix processing algorithms. This gap resistance can be tuned to represent various fill gases and glazing coatings but this approach relies heavily on specific knowledge of the window U-value. In the ESP-r multi-layer construction database, the user is able to construct a multi-layer construction (MLC) or a TMC. A calculator predicts the U-value of the assembly based on the ISO 6946 (1996) standard. In order to account for the presence of a low emissivity coating or a fill gas the gap resistance must be tuned until the U-value calculated by ESP-r is matched with third party software. Edge and frame effects can also be modeled by adjusting the gap resistances. In reality, the total resistance in a window cavity is temperature dependent. The convective heat transfer coefficient is dependent on the glazing temperatures. Longwave heat fluxes have a fourth order temperature dependency. The degree of temperature dependency of window cavity resistances is investigated in Chapter 5, Section 5.2.

3.3 Building Domain Simulation Flow

Figure 3.7 illustrates the simplified flow of a thermal zone simulation time-step in ESP-r. It is assumed here that the building is essentially free floating with respect to weather excitations, without additional simulation domains such as a plant or air-flow network, or any thermostatic control. To establish the necessary future and present time-row coefficients for the nodal difference equations, thermophysical properties of the building construction and heat-flow conductance values between each node connection must be determined. Material properties such as density, specific heat capacity and conductivity are typically treated as time-independent properties. Heat flow conductance values for convection and long-wave radiation processes are temperature dependent, thus time dependent. Convection regimes may also change during the simulation upon actuation of plant components which impact flow distribution within the zone. Time dependent properties as well as solar gains impinging on all exposed outdoor and indoor surfaces are computed at each time-step. However, since the future-time row time dependent properties rely on temperature information that is unknown until simultaneous solution has been

achieved, these properties are evaluated one time-step in arrears. Specifically, the future time-row convective heat transfer coefficients and linearized longwave radiation coefficients are evaluated at the present time-row temperatures. This lagging method has acceptable consequences in loss of accuracy and approaches the exact formulation (i.e., where future time-row coefficients are not lagged) as the time-step is reduced, such that the temperature variations between each time-step are diminished.

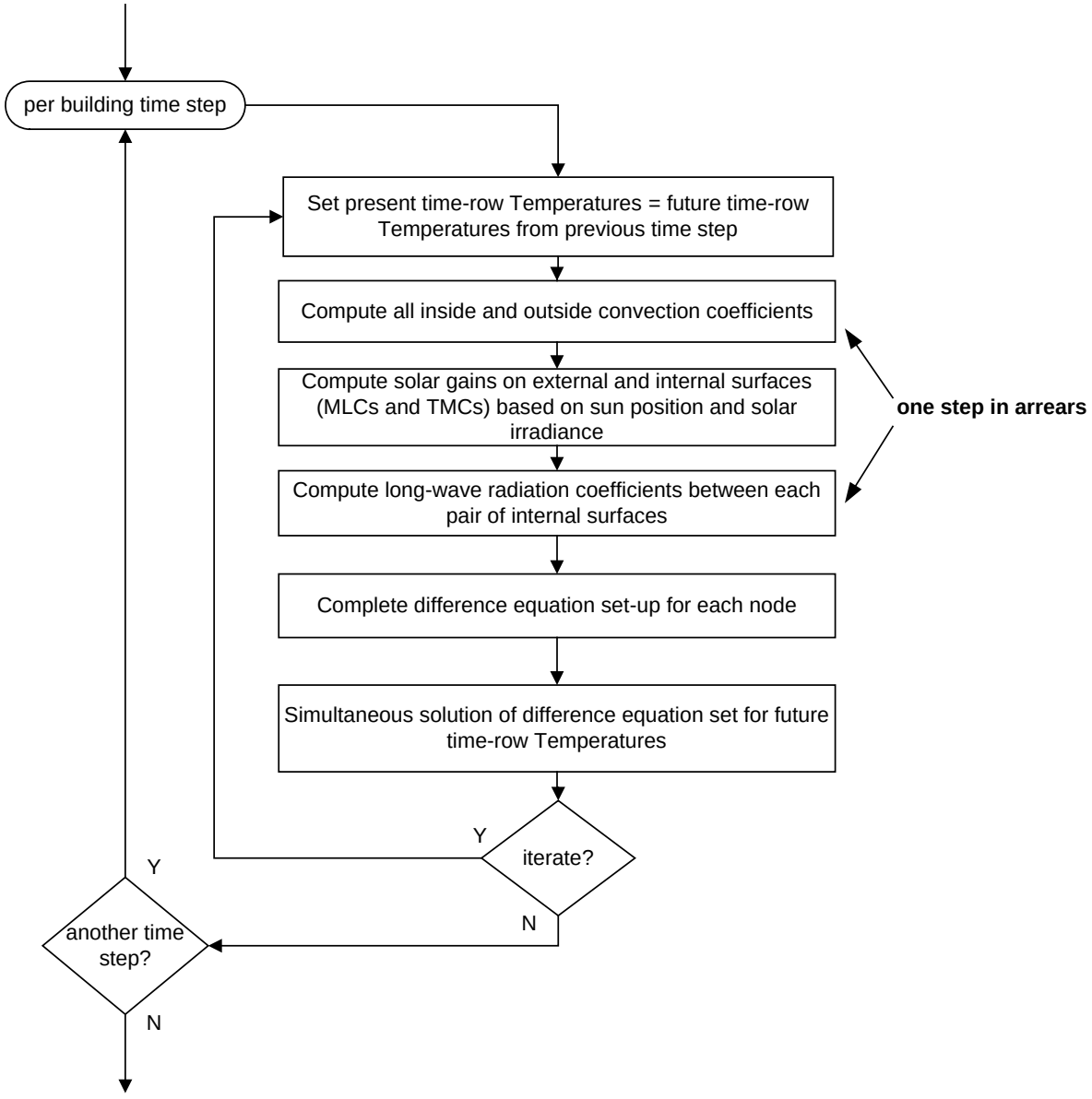

Figure 3.7: Simplified ESP-r time-step simulation flow for a thermal zone.

Chapter 4
Implementation of the Complex Fenestration Construction (CFC)

In Chapter 1, Section 1.3 discussed general theory of the complexities inherent in the addition of shading layers to glazing systems. Chapter 3 outlined the constraints in representing multi-layer constructions (MLCs) and transparent multi-layer constructions (TMCs) in ESP-r, including the limitations in the nodal structure, matrix processing, and existing solar gain control methods. This chapter deals with the practicality of implementing solar and thermal shading models within the framework of ESP-r.

The continuous development of the ESP-r system by different groups necessitates each additional model to be self-contained, to preserve functionality and limit complexity within the source code. The framework presented in this chapter for implementation of the AGSL shading models is designed with the intent of creating a self-contained module. However, linking these models with ESP-r simulation structure requires modifications and additions to existing sub-routines. Hence, sub-modules that contain specific shading models (e.g., calculation of solar-optical properties, convection model for indoor blinds, long-wave exchange through a diathermanous layer) are general enough to allow for utilization in any building simulation program, but the processing and invocation of these models within the construct of ESP-r simulation flow is specific to the ESP-r system.

4.1 The Complex Fenestration Construction

The fundamental strategy for the implementation of the AGSL shading models is the design of a new multi-layer construction within ESP-r, the Complex Fenestration Construction (CFC). Its design is an attempt to contain the glazing/shading system in a separate facility while

preserving current ESP-r functionality of MLCs and TMCs. The CFC type utilizes the same multi-layer nodal scheme as the MLC and TMC type, with provisions to cope with shading layer complexities.

Alternatively, it is possible to fully contain the glazing/shading system external of the ESP-r solution domain. This approach relies on ESP-r run-time information such as temperatures, solar irradiance, and convection coefficients, to serve as boundary conditions for a separate solution of the glazing/shading system. The fenestration system would then be treated as a black box accepting ESP-r data as boundary conditions, computing resultant temperatures and fluxes, and outputting this information to the ESP-r building domain in the form of energy generation terms. The main advantage of this method is computational efficiency, as the window solution is external to the nodal difference equation set and does not add to the size of the future term coefficient matrix.

Explicit treatment of the multi-layer glazing/shading system has a distinct advantage over the 'black-box' approach. Characterizing the complex fenestration system within the ESP-r nodal structure allows for linking of nodes across technical domains. The possible integration of a mass-flow network with window cavity ventilation for double-facades or plant system radiant heating flux injections on the inside surface of a glazing/shading layer are two examples. The structure is general enough to facilitate further model integration and support cross-connectivity with other building systems.

As outlined in the scope in Section 1.5, only slat-type blind models are currently considered in the ESP-r implementation of the CFC type, however, the framework is general enough for the addition of other types of shading layers. The CFC type can be applied to ESP-r simulation with the following geometric constraints:

- Center of glass region
- Surfaces with 'exterior' boundary condition
- Vertical surfaces

4.1.1 Solar Processing

The CFC type is intended to provide a general facility for the analysis of complex glazing/shading systems. Operable shading devices such as slat-type blinds offer the means for active control of solar gain. Dynamic control of shading devices imposes changes in optical properties of the glazing/shading system on the order of a single time-step. As such, CFC solar optical data is calculated during the simulation at each time-step, based on individual layer properties. Total system optical property sets used for TMCs are not required for CFCs. Instead, each CFC layer can be characterized by determining a set of 12 solar optical properties as discussed in Section 1.3.4 (Figure 1.4). Before going into more detail, Figure 4.1 illustrates the overall procedure for CFC solar processing within ESP-r. The sections that follow describe each step (highlighted in Figure 4.1) of the solar processing procedure for a CFC at any given time-step when incident solar radiation is greater than zero.

Appendix D presents more detailed flow charts of solar processing routines in ESP-r, highlighting the CFC implementation subroutines.

Determine Angle Symmetry

The 12 optical properties that describe each layer depend on the sun's position. For specular glass layers, optical properties are a function of incidence angle. That is, a specular layer is considered rotationally symmetric. Optical properties of a slat-type blind layer are dependent on the profile angle. The profile angle is typically used in calculating shading as it represents the projected shadow length on a surface. Slat blinds are typically composed of horizontal or vertical slats. The orientation of the slats determines the type of profile angle dependence. Figure 4.2 shows the horizontal and vertical slat profile angle dependence and the sign convention for the blind slat angle.

The vertical profile angle, Ω_v, is defined as

$$\tan \Omega_v = \frac{\tan \alpha_s}{\cos(\gamma_s - \gamma)} \qquad (4.1)$$

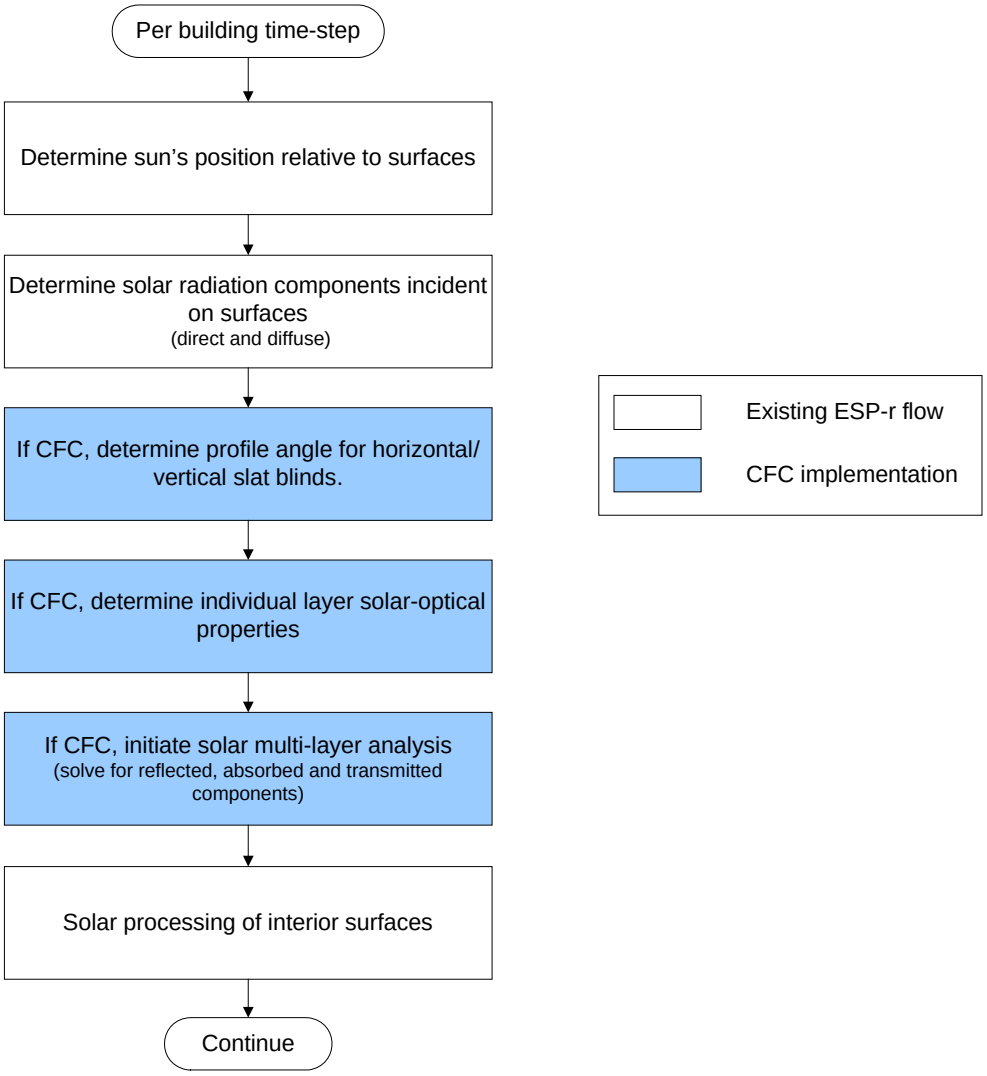

Figure 4.1: Simplified ESP-r solar processing flow including CFC implementation.

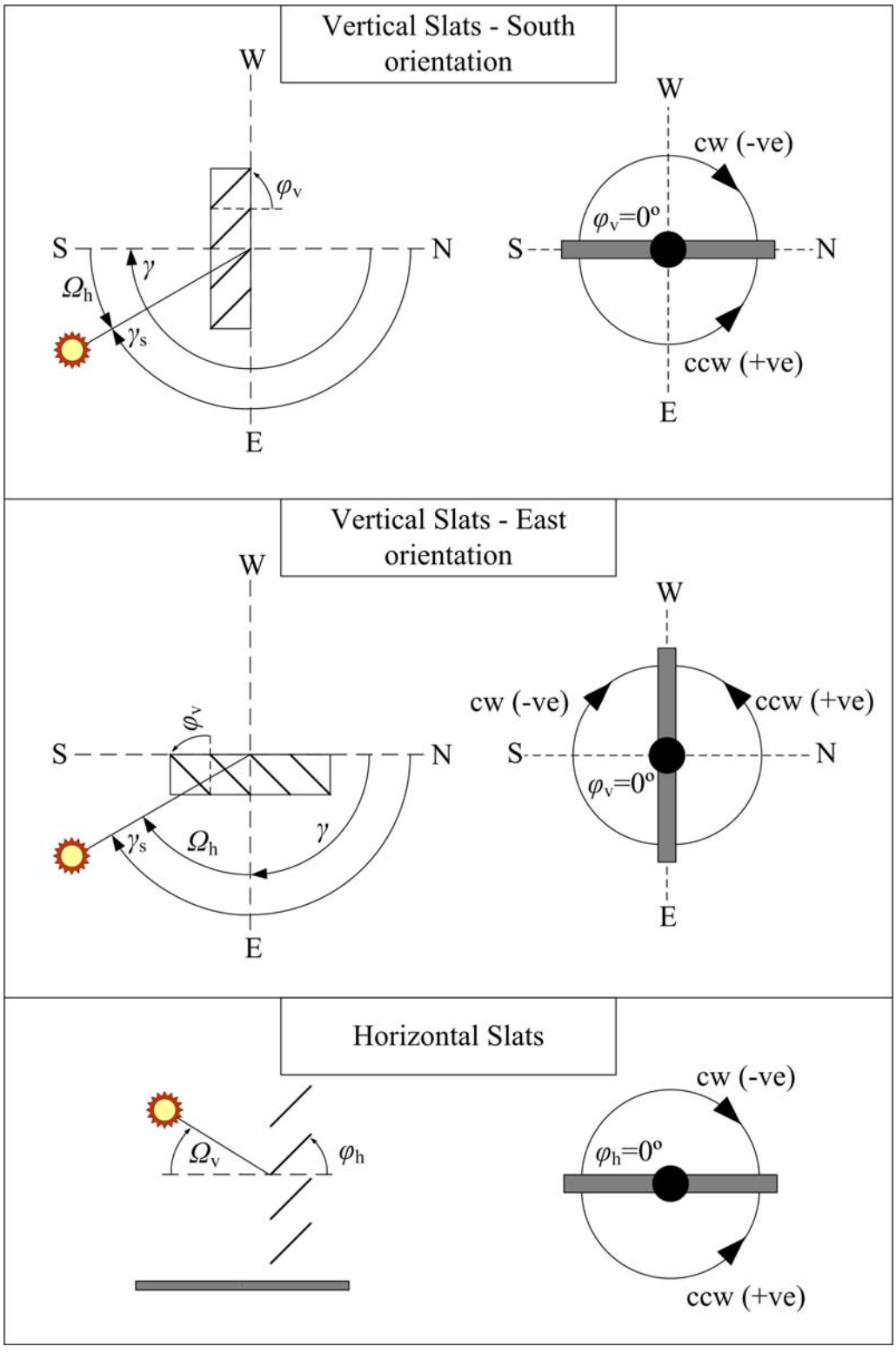

Figure 4.2: Profile angle dependence and slat angle convention for horizontal and vertical slat-type.

where α_s is the solar altitude angle, γ_s is the solar azimuth angle (degrees from north, cw) and γ is the surface azimuth angle (degrees from north, cw). The horizontal profile angle Ω_h is simply the difference of the solar azimuth and surface azimuth angles:

$$\Omega_h = \gamma_s - \gamma \qquad (4.2)$$

Determine Individual Layer Solar-Optical Properties

The method for determining the 12 optical properties that characterize a homogenous layer in the glazing/shading system depends on the type of layer. Here, glazing layers and slat-type blinds are considered.

Glazing Layers:

Inputs required for the solar-optical property characterization of glazings consist of front and back solar reflectance and solar transmittance of the glazing layer at normal incidence angle; ρ_f, ρ_b and τ, respectively. A comprehensive database of various glazing manufacturers and products containing measurements of solar optical properties at normal incidence is available in the International Glazing Database (LBNL 2008). For glass that has not been rated, spectro-photometer measurements may be performed to obtain the required properties at normal incidence. Glass (clean glass) panes reflect light specularly, therefore beam-diffuse properties $\rho_{f,bd}$, $\rho_{b,bd}$ $\tau_{f,bd,}$ and $\tau_{b,bd}$ are set to zero. Adjusting the normal incidence properties of a glazing layer, for both coated and uncoated glass, to off normal incidence angles is achieved by normalizing the optical property angle dependency to a reference glass type and thickness, constituting a glass 'template'. Knowing the refractive index, the extinction coefficient and thickness of the reference glass, its optical properties can be calculated from theory using a combination of Fresnel equations, Snell's Law and the Stokes equations (e.g. Duffie and Beckman 1980). Figure 4.3 illustrates the principle for adjustment of optical properties to off normal incidence. Knowing the optical property curve for off-normal incidence of the reference glass, and knowing the normal incidence optical property (reflectance or transmittance) of any coated or uncoated glass, the off-normal property may be determined. Details of this method are presented in appendix B. This reference glass method is known to be very accurate for uncoated glass (Furler 1991, Milburn 1994). An accurate treatment of coated glass requires knowledge of exact physical properties of the coatings,

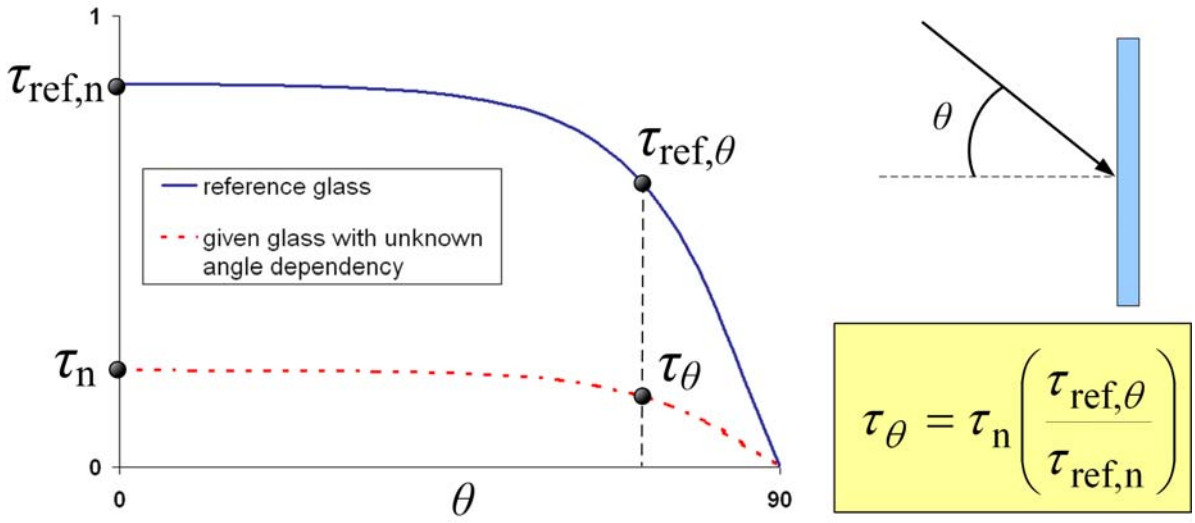

Figure 4.3: Example of off-normal property adjustment for coated and uncoated glass.

such as thickness, refractive index and extinction coefficient. If such properties are available, fundamentals of electromagnetic wave theory could then be used to determine the layer overall optical properties. However, the properties of coatings are difficult to measure and generally not available. The reference glass method is not only simple but surprisingly accurate for coated glass, with maximum errors of 5% compared to the more exact Fresnel data calculated with knowledge of coating properties (Karlsson, Rubin and Roos 2001). To increase the accuracy of the off-normal property adjustment for coated and tinted glass, a reference uncoated bronze glass is used with a higher extinction coefficient and therefore higher solar absorption. The appropriate reference glass is selected for off-normal property adjustment by examining the normal solar transmission value of the glass layer of interest. If the normal solar transmittance of the glazing layer is greater than 0.645, a clear reference glass is used. Otherwise, the bronze reference glass is selected. This approach is similar to the off-normal optical property adjustment model in WINDOW 4 and WINDOW 5 (Finlayson et al. 1993).

The reference glass method allows for the determination of off-normal beam-beam properties $\rho_{f,bb}(\theta)$, $\rho_{b,bb}(\theta)$ $\tau_{f,bb}(\theta)$, $\tau_{b,bb}(\theta)$. Diffuse radiation incident on a vertical glazing consists of scattered radiation from the sky and reflected solar radiation from the ground. To obtain total diffuse optical properties, in principle, one could integrate the diffuse radiation over all incidence angles. However, the angular distribution of diffuse radiation is generally unknown. A common

approach is to define an equivalent beam incidence angle representing the average approach angle for diffuse radiation of combined sky and ground components. Diffuse-diffuse optical properties thus correspond to beam-beam properties at the equivalent incidence angle. Different values for the equivalent angle of incidence are quoted in literature, depending on assumptions made about the distribution of diffuse radiation. For the case of isotropic sky and ground radiation, an incidence angle of 59° is used for vertical surfaces (Duffie and Beckman 1980). A fully anisotropic sky model was shown to give best overall performance when applied to a wide range of locations (Clarke 2001). The corresponding equivalent incidence angle for anisotropic sky conditions is 51° (Clarke 2001). This value is used in ESP-r for interpolating beam-beam solar optical properties of TMCs to determine equivalent diffuse-diffuse properties. Likewise, the anisotropic sky model is used in determining CFC glazing diffuse-diffuse properties.

Slat-type Blinds:

Two types of slat-type blind models are implemented into the CFC type: curved slats and flat slats. The effective, spatially averaged, solar-optical and longwave radiative properties are determined using the simplified model by Kotey et al. (2008), described in Section 2.2.1. The model includes a curvature correction, but not a slat thickness correction. For treatment of flat slats in the CFC type, the model by Kotey et al. (2008) has been modified to correct for slat thickness using the thickness correction factor method in EnergyPlus (EnergyPlus Engineering Reference 2008).

The dimensional inputs for the two slat types are shown in Figure 4.4. Based on the dimensional input provided by the user, either the curved or flat slat model is automatically chosen to represent the slat geometry. For example, if the crown, c, is close to zero, the flat slat model is used. Other slat profiles (e.g., an extrusion with curvature on both sides) can be approximated by determining the maximum thickness and specifying the crown as zero. The double sided curvature of the slat geometry is then approximated by the flat slat model with thickness correction.

In the model by Kotey et al. (2008) slats are treated with the following assumptions:

- Incident diffuse radiation is isotropic

- The slats reflect beam radiation diffusely
- The slats transmit beam radiation diffusely, if at all
- Slat reflectance and transmittance is independent of the angle of incidence

Consequently, the only solar-optical properties required as input to the blind model are reflectance of the upward-facing and downward-facing slat surfaces and slat transmittance; $\rho^{s}_{u,bd}$, $\rho^{s}_{d,bd}$ and τ^{s}_{bd}, respectively.

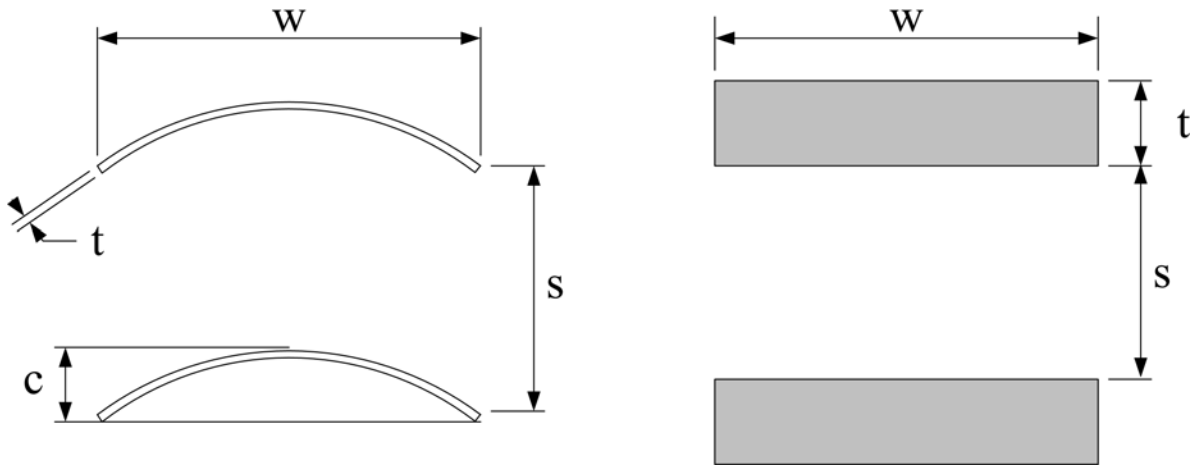

Figure 4.4: Curved slat and flat slat input dimensions.

Solar Multi-Layer Analysis

Once each layer in the glazing/shading system of the CFC has been characterized by the set of 12 total solar-optical properties and adjusted for the incidence/profile angle, a multilayer accounting technique is used to determine how much of the incident solar flux is absorbed at each layer, reflected or transmitted. Details of the multi-layer model are given in Section 2.2.2 and Appendix D. The multi-layer model accounts for scattering of beam solar fluxes due to the presence of shading layers by introducing beam-to-diffuse source fluxes.

Spectral vs. Band-Averaged (Total) Solar-Optics:

The solar-optics procedure for CFC types determines total solar optical properties for each layer of the CFC glazing/shading system, at each simulation time-step. Neglecting spectral selectivity of solar radiation between glazing/shading layers provides great flexibility in modeling

complex fenestrations, with acceptable loss of accuracy for most glazing combinations. User input is greatly reduced, requiring only total properties at normal incidence for each layer. Dynamic control of operable shading-devices on a time-step basis is also possible without a heavy computational burden. Although spectral data are available for many glazing products through the IGDB (LBNL 2008), data for shading layer materials (e.g., painted aluminum slats, wood slats, fabrics) are generally not available. Thus, characterizing the system at the spectral level is typically not practical and may require extensive optical property measurements. Total optical property models are therefore ideally suited for building simulation as they are computationally efficient, do not rely heavily on user expertise and de-emphasize user input. The reader is referred to (Wright 1995) for a discussion on the impact of spectral and total optical property models on indices of merit (U-value, SHGC) results for a variety of glazing combinations.

Interior Solar Processing

Solar fluxes transmitted through external windows continue onward impinging on internal surfaces of the thermal zone. These internal beam and diffuse fluxes are then absorbed, reflected at opaque and transparent surfaces and are re-transmitted to other zones through internal windows or back out to the environment through external windows. This process is modeled in ESP-r by an iteration scheme whereby the aggregate internal solar reflections of the entire zone are iteratively reduced due to absorption and re-transmission at the internal zone surfaces.

ESP-r's shading/insolation module determines the percentage of direct flux that is incident on interior surfaces through external windows. The solar distribution is based on the sun's position and zone geometry relative to placement of external transparent constructions. The absorbed portions in opaque and transparent elements are then added to appropriate nodes as shortwave flux injections at each time-step. Thus, the causal effects of solar fluxes are represented in the nodal conservation equations as flux injections, with appropriate accounting for direct and diffuse solar radiation distribution. More details on the theory are presented in (Clarke 2001).

Typically, the solar fluxes incident on an interior glazing surface represent a small portion of the initial incoming external radiation. However, for buildings with highly glazed facades, sunlight escaping back to the environment through corner sections may be significant. The treatment of re-transmission of solar fluxes through internal or adjacent corner glazings may

influence the interior loads for highly glazed facades. The multi-layer scheme for processing external solar fluxes incident on CFC types is also used for calculating internal solar flux re-transmission and re-absorption. The advantage of the multi-layer model by Wright and Kotey (2006) is the generality in the placement of incident solar fluxes. Beam and diffuse fluxes may in theory be introduced in any position within the glazing/shading array. CFC solar processing takes advantage of this fact by executing the multi-layer algorithm for beam and diffuse fluxes incident on the inside surface of an external CFC, such as at a corner of a curtain wall façade. By default, an interior beam flux incident on the inner surface of an external CFC is treated as diffuse. The multi-layer routine then calculates the solar fluxes due to this internal radiation source, and adds the absorbed quantities to the original values. The internal beam flux may readily be treated as an internal beam source in the multi-layer routine, but a calculation for the incidence angle and profile angle (for blinds) on the inside surface would be required. The accuracy gained in such an exact treatment, compared to the default internal diffuse source assumption, is expected to be marginal; hence this exact treatment has not been implemented. The flow chart in appendix D, containing the ESP-r solar processing routine, provides a more visual representation of the iterative procedure for internal solar processing.

4.1.2 Thermal Processing

Solar processing of CFC types with scattering shading layers is handled using effective total solar optical properties and a multi-layer scheme that accounts for the reflected, transmitted and absorbed solar fluxes of the system and copes with beam-to-diffuse scattering layers. The resulting absorbed fluxes in each layer of the CFC are used as input to the nodal difference equations in the thermal calculation, causing temperature elevations in glazing/shading layer nodes. The absorbed solar energy is then transmitted via conduction, convection and long-wave radiation inward and outward. The placement of the shading layer (e.g., indoor/outdoor/between glass) has a significant impact on the distribution of absorbed solar fluxes, and thus affects considerably the portion of solar energy flowing inward to the thermal zone. In extreme cases (e.g., dark indoor blinds) the placement of the shading layer can have adverse effects on the building cooling load (Lomanowski and Wright 2007).

The convective and radiant jump resistors to non-adjacent nodes must be added to the difference equation formulation to account for diathermanous shading layers, which may be placed

in any configuration within the multi-layer array. Given the matrix structuring constraints discussed in Section 3.1.2, the approach taken for implementation of CFC jump-resistors in ESP-r is to resolve these into nodal generation terms. This method applies to the transmission of longwave radiation through a diathermanous layer with possible interaction with interior zone surfaces or external surroundings. It also applies to the convective interaction of zone air or ambient air with indoor/outdoor blinds.

Figure 4.5 illustrates the processing of the thermal zone in ESP-r with CFC implementation routines highlighted. Routines for processing of air node ventilation loads and casual gains are not shown for clarity. The subsequent sections provide more detail on each of the highlighted CFC routines. Appendix E provides more detail of CFC implementation into ESP-r thermal processing sub-routines.

CFC Time-Step Shading Control

Prior to solar and thermal processing of a CFC type at a given time-step, operable shading layer control may impose a change in the blind's control variable. Currently, the only variable available for dynamic control of a CFC shading layer is the slat angle of a slat-type blind. Specific control schemes are outside the scope of this thesis, however, the general facility for future implementation of time-step control is provided and initial testing of shading control is explored in Chapter 5, Section 5.4. Of note is the fact that, although the framework of CFC solar and thermal processing is complex, the shading control algorithms may be implemented without knowledge of the inner-workings of the CFC type. Appendix E shows the placement of the control sub-routine within the thermal processing simulation flow.

Long-wave Radiation Exchange

In ESP-r, the radiant exchange within an air cavity of a multi-layer construction is currently lumped with the convective exchange into a constant gap resistance (R_{gap}). Interior surface longwave radiation exchange is determined by an analytical method that generates a linearized longwave radiation coefficient between each pair of indoor surfaces. Details on this method are presented in (Clarke 2001). Exterior surface longwave radiation exchange is determined by considering the difference between emitted and received fluxes from each surface node exposed to

sky, ground and surrounding buildings portions of the exterior hemispherical envelope. The representative

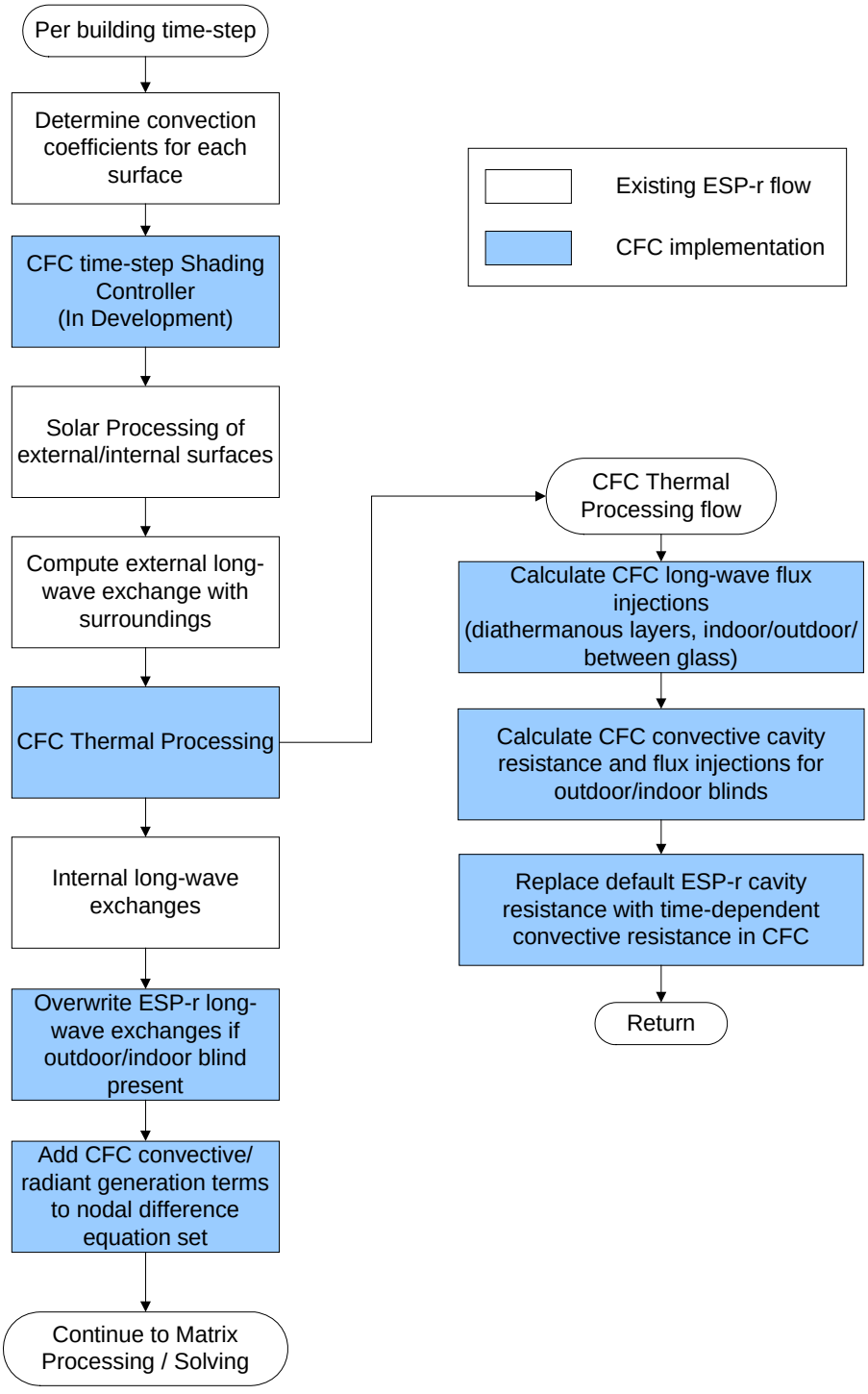

Figure 4.5: Simplified ESP-r thermal processing flow including CFC implementation.

values for the sky, ground and surroundings view factors are selected for appropriate site exposure, or can be user-defined. Temperatures for each portion of the environment are predicted and an overall longwave radiant flux injection/extraction term is calculated for addition to the nodal difference equation of the outdoor surface node.

Longwave radiation exchange in a CFC type is represented by nodal flux injection/extraction terms. The method is generalized to allow for any number of diathermanous layers in any configuration, to communicate with intra-construction nodes as well as external surroundings and surface nodes of the conditioned space. The method yields the heat flux between each pair of surfaces by determining an exchange factor that accounts for the direct view (shape) factor as well as all reflected fluxes in the enclosure. Here, due to the presence of diathermanous layers, the enclosure that bounds the radiation exchange may be a combination of external surrounds, intra-constructional CFC layers and zone interior surfaces, depending on the glazing/shading configuration. The details of the model are found in (Wright 2008) and a general description is given in Chapter 2, Section 2.2.3. The model has been extended to include the longwave radiation exchange between multiple interior zone surfaces, rather than treating the interior space as a single equivalent surface. Appendix C presents the details of this extended radiation model.

Figure 4.6 illustrates the principle of resolving individual flux exchanges into a total generation term for each glazing/shading layer. For simplicity, each CFC layer is represented by a single node in the illustration. Gas gap nodes are not shown. The scheme allows any or all of the layers to be diathermanous, however, direct longwave exchange between an indoor zone surface and the outdoors (e.g., a single diathermanous layer) is not considered. The longwave exchange factors, like view (shape) factors, are a function of enclosure geometry but also depend on surface radiative properties. Thus, they are determined at the beginning of the simulation, and every time a change in the CFC geometry occurs during the simulation. For example, a change in the slat angle of a blind results in a new set of optical and longwave radiative properties. Thus, given a set of exchange factors, long-wave exchange fluxes are computed at each time step. Interaction of diathermanous layers with interior surfaces requires that a longwave flux generation term also be added to the intrior surface nodes (as shown in Figure 4.6). In the case that two CFC constructions 'see' each other inside the thermal zone, the 'other' CFC inside surface is treated as an opaque

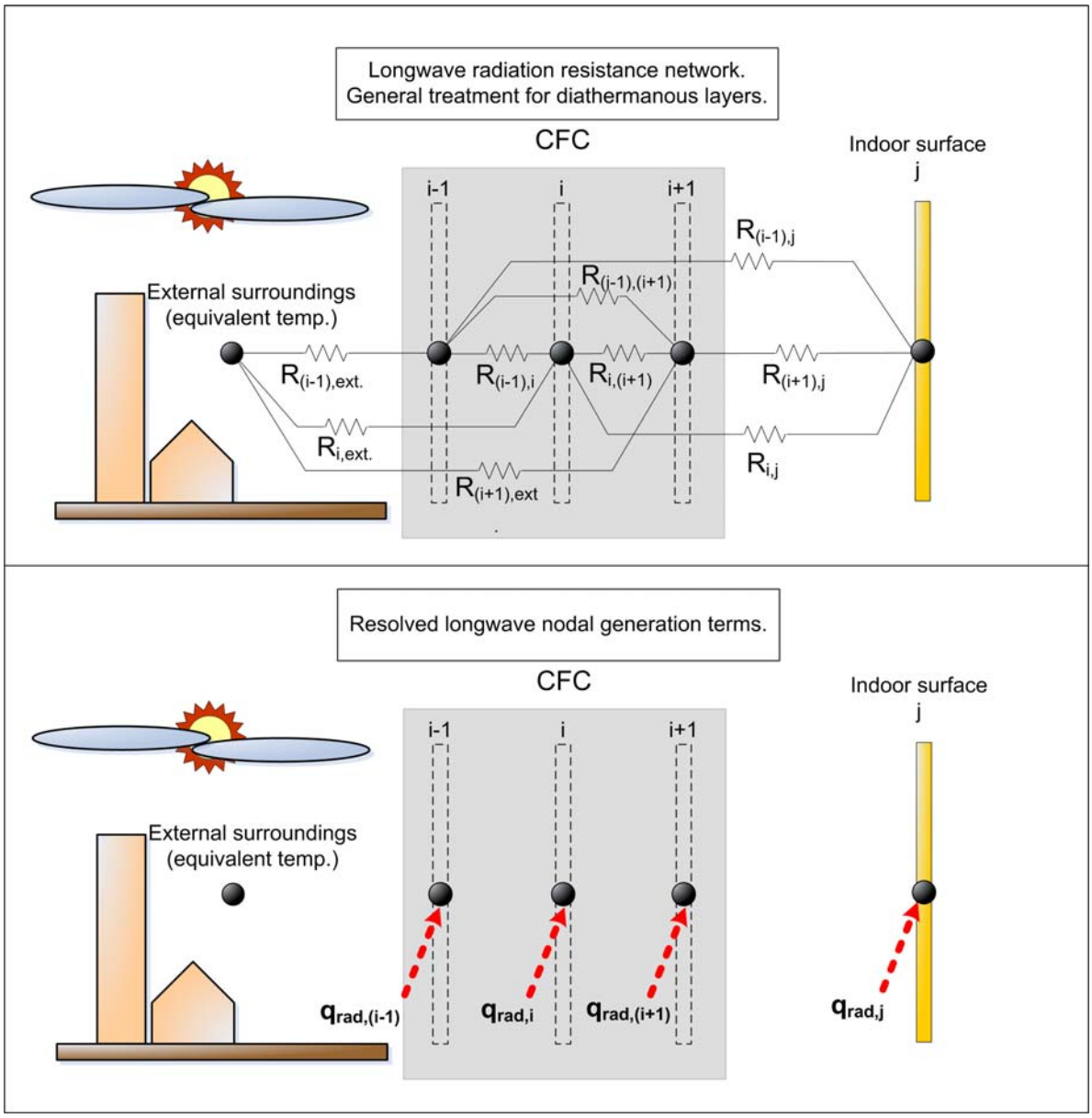

Figure 4.6: CFC resolution of longwave radiative jump resistors to nodal generation terms.

surface like the rest of the interior surfaces. For example, if two corner CFC constructions with indoor blinds are present, the innermost glass layers of the two CFCs are not in radiant contact with one another. This introduces a small error in some cases, but simplifies the long-wave exchange computation significantly.

Long-wave exchange between CFC layers and the outdoor environment is determined by introducing an equivalent surroundings temperature. This equivalent temperature, T_e, is approximated by

$$T_e^4 = f_{sky} T_{sky}^4 + f_{grd} T_{grd}^4 + f_{bld} T_{bld}^4 \qquad (4.3)$$

where T_{sky}, T_{grd} and T_{bld} are the temperatures of the sky, ground and surrounding buildings respectively; f_{sky}, f_{grd} and f_{bld} are the view factors to the sky, ground and surrounding buildings respectively.

The ESP-r routines for the computation of interior and exterior surface longwave exchanges are carried out separately from the CFC longwave exchange algorithm (see Figure 4.5). The default ESP-r routines for longwave exchange only consider opaque interior and exterior surfaces and do not account for any jump resistors. To ensure that double accounting of longwave radiative exchanges does not occur for CFC types with indoor/outdoor blinds, the linearized longwave radiative heat transfer coefficients and external radiant fluxes are set to zero in the default ESP-r routines. Therefore, if an indoor diathermanous layer is present in a CFC, the default ESP-r internal longwave radiative coefficients are set to zero for any internal zone surface that exchanges longwave radiation with that CFC surface. Similarly, the calculated ESP-r external surface flux, due to the longwave radiative exchange with the surroundings, is set to zero for a CFC type with an outdoor diathermanous layer. If the CFC indoor and outdoor layers are opaque to long-wave radiation (such as a glazing), the default ESP-r long-wave exchange routines apply.

Convective Exchange

The longwave exchange factor method outlined above retains generality for all types of layers, as long as they are characterized by appropriate spatially averaged, effective longwave radiative properties. Models characterizing the convective interaction of shading/glazing layers are, on the other hand, very specific to the type of shading layer and its position within the glazing/shading array. Since the scope of this thesis only deals with slat-type blinds, only convective models for this type of shading device have been investigated and implemented. Section 2.2.4 describes the models used in CFC implementation for three possible slat-type blind

configurations: indoor blind, outdoor blind and between glass blind. Whereas the behaviour of natural convection flow around a slat-type blind in between glass panes is well known (e.g., Huang, Wright and Collins 2006, Collins, Tasnim and Wright 2008), the outdoor and indoor models are approximate, as research in this area is at an early stage (see Section 2.2.4). Furthermore, the interaction of convective heat transfer for two consecutive blind layers has not been explored. As such, the lack of generality in the convective models restricts the CFC type to cope with only one slat-type blind layer albeit in any position within the glazing/shading layer array. It is deemed unlikely that the need to model two consecutive slat-type blinds per window will arise. It is important to note that this restriction is solely due to the availability of convection correlations, and in general the solar multi-layer scheme and the long-wave radiation exchange scheme can readily cope with any number and type of glazing/shading layers.

Future implementation of other types of shading layers, such as roller blinds, drapes and insect screens, will present challenges in characterizing the convective exchange between multiple types of shading layers. For example, a common occurrence that may arise is a window with an insect screen and a blind next to the screen.

The strategy for resolving convective exchange between CFC layers is to calculate gas gap resistances on a time-step basis and replace the existing constant gap resistances within ESP-r with these temperature-dependent resistances. For between glass blinds, these resistances are calculated based on the model developed by Huang, Wright and Collins (2006) using a modified gap spacing (see Section 2.2.4). For convective jump resistors, the strategy is the same as for longwave exchange, namely to resolve these by using convective flux nodal generation terms. Figure 4.7 illustrates this resolution for the three configurations of slat-type blind placement.

For the indoor blind case, the air node flux injection represents the additional convective exchange between the inner-most glass surface and the back of the blind. The front of the blind surface is treated as a standard interior surface, for which an appropriate convective coefficient is supplied by ESP-r. This coefficient is multiplied by the slat penalty function as explained in Section 2.2.4. Appendix A presents the details of the indoor blind convection model.

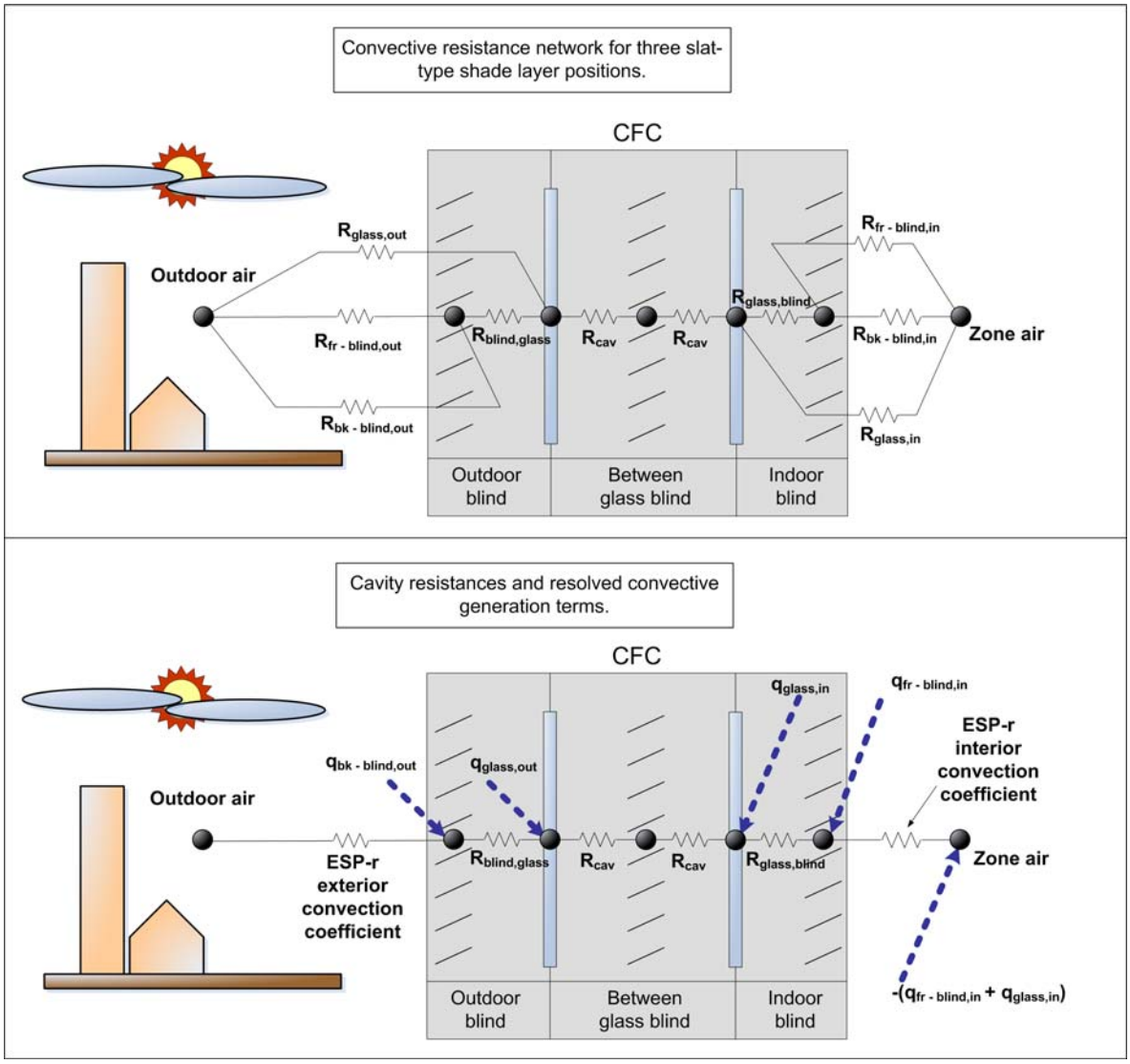

Figure 4.7: CFC resolution of convective jump resistors to nodal generation terms.

In the case of an outdoor blind, the fully ventilated condition is imposed, thus the blind and outdoor glazing surfaces are thermally isolated from each other. The convective gap resistance is set to infinity for this condition. The jump resistor from the back of the blind to the ambient is accounted for by simply doubling the blind front side convective heat transfer coefficient supplied by ESP-r. The jump resistor from the glass surface to the ambient is accounted for by adding a convective flux generation term to the outdoor glass layer, as shown in Figure 4.7. The outdoor convective heat transfer coefficient supplied by ESP-r is used to calculate this convective flux.

In summary, the combination of convective resistances and convective generation terms account for the presence of indoor and outdoor blinds and thus the resultant increase in convective heat transfer area. The interior zone air node is linked with the indoor blind and glazing layer nodes through the convective generation terms. Similarly, the outdoor blind and glazing nodes are linked with the outdoor air. A flow chart of the convective exchange subroutine for CFCs is given in Appendix E.

Once the CFC temperature-dependent (and hence time-dependent) convective resistances have been computed, the default ESP-r constant air-gap resistances are replaced. Finally, the shortwave absorptions, long-wave and convective exchange generation terms are applied to the difference equations of appropriate nodes, completing the thermal processing of the CFC type.

4.2 Front-End

Instructions on using CFC types in ESP-r are presented in Appendix F. This section describes the GLSedit tool (Wright et al. 2008) developed at UW's AGSL for creation of CFC input files.

A CFC is assembled much like a TMC or MLC in ESP-r. Material layers with thermal capacity are constructed from databases to produce an overall assembly, or multi-layer construction. Cavity resistances for TMC and MLC types are specified during the construction assembly process but these can be ignored for CFC types since the resistances are calculated at run-time. In addition to thermo-physical properties of the solid material layers, a CFC, much like a TMC, requires additional inputs for solar processing. Unlike a TMC however, a CFC also requires fill gas information for the gas gap temperature dependent resistance calculation.

The Glazing Shading Layer Editor, GSLedit, is a simple graphical user interface tool for constructing complex fenestrations. It was designed for quick synthesis of a glazing product with or without shading components. The editor compiles system information into an organized output file. The output information can then be read by another program such as ESP-r. The main advantage of the editor is access to glazing and shading layer databases that allow for quick manipulation of the system components. Glazing databases are based on the International Glazing

Database (LBNL 2008) which contains an extensive glazing product selection for many manufacturers. Shading layer entries currently include venetian (slat-type) blinds, roller blinds, drapes/curtains, and insect screens. Gas mixtures for cavities include any combination of air, argon, krypton, xenon and SF6 gas. Figure 4.8 shows a screenshot of GSLedit.

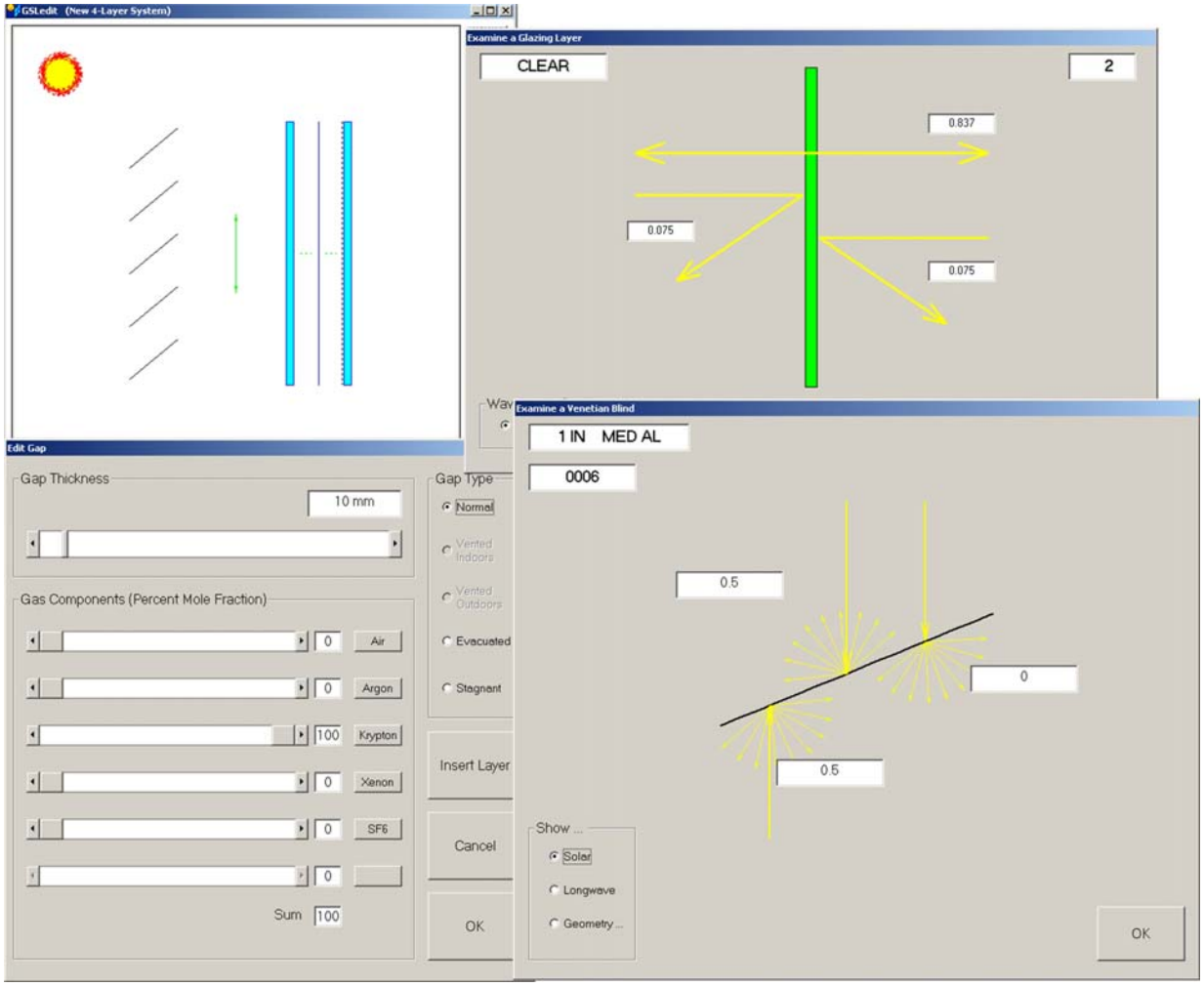

Figure 4.8: Screen shot of the Glazing and Shading Layer Editor, GSLedit.

The output file generated by GSLedit consists of:

- Construction information – types of layers and layer position
- Total normal solar optical and longwave radiative properties for glazing layers
- Glazing thickness and conductivity
- Total normal solar optical, visible and longwave radiant properties for venetian blind slats, roller blinds, drapes/curtains and insect screens
- Venetian (slat-type) blind slat geometry

- Gas mixture coefficients for determining specific heat, conductivity and viscosity based on a linear temperature curve fit

Appendix F provides instructions on using GSLedit and importing GSLedit output files into ESP-r to generate CFC input files. It is worth noting that the procedure is simple and automated, and does not require any user manipulation of text files.

4.3 Simulation Performance

As discussed in Section 3.1.2, the structure of the difference equation matrix in ESP-r is constrained such that intra-constructional nodes may only be linked with their neighbouring nodes. The sparse difference equation matrix does not actually exist in computer memory; rather, the partitioning and reduction techniques rely on a predetermined matrix structure. The resolution of longwave and convective exchange jump resistors into generation source terms in CFC types provides one method of bypassing this restriction. The generation terms are determined using past time-step temperatures and are thus lagged one time-step.

The Crank-Nicolson formulation of the difference equations is equivalent to a weighted average of the fully explicit scheme, where heat fluxes/rates are estimated using present temperature values, and the fully implicit scheme, where all terms are expressed in terms of future temperatures. The source terms, when added to the difference equations, are explicit since they rely on past information. As a consequence of adding the lagged source terms to the Crank-Nicolson difference equations, the solution is shifted in the direction of the fully explicit scheme.

Due to the increased degree of explicitness, in order for the solution to converge consistently, measures must be taken when setting up simulations to 1) reduce the simulation time-steps per hour and 2) provide sufficient thermal capacity for the shading layer. These measures ensure that temperature fluctuations between each simulation time-step are dampened sufficiently. A time-step reduction from 1 time-step per hour to 6 time-steps per hour was found to work well, in combination with a shading layer thermal capacity (product of density, specific heat and thickness) set to an equivalent of a 6mm glass pane. Given these settings, it was found that the solution converged consistently, however, oscillations were observed in the simulation results for some CFC glazing/shading combinations, especially for the indoor slat-blind configurations. The

oscillations were observed in zone/surface flux results and temperature results when a thermostatic control law was imposed to heat and/or cool the interior space and only when time-step averaging was turned off.

The oscillations are present in the results when either the future, or present temperature or fluxes are plotted through the H3K reporting facility in ESP-r. If time-step averaging is turned on (i.e. the future and present time-step temperatures and fluxes are averaged), the oscillations are smoothed out. For example, Figure 4.9 illustrates cooling load results for a simple room with a south facing window and a closed indoor slat-type blind (80º slats). Basic cooling control is imposed to maintain the air temperature at 25ºC. Figure 4.9 a) shows the future time-step data for a time step of 10 minutes, with clearly visible oscillations. Figure 4.9 b) shows the smooth cooling load curve for time-step averaged results for the same simulation. Thus, to avoid oscillations showing up in the simulation results, time-step averaging is always recommended.

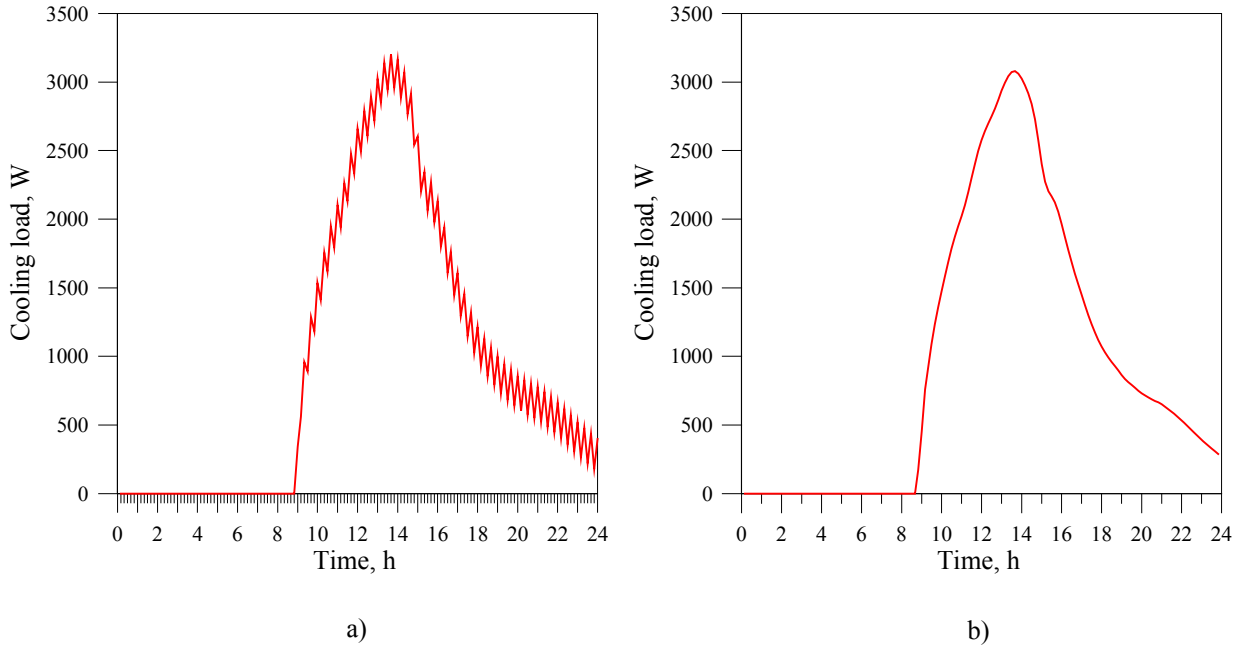

Figure 4.9: Example of oscillations in simulation results for a CFC glazing with an indoor blind. a) cooling load future time-step data and b) cooling load time-step averaged data.

4.4 Summary of CFC Capabilities

Table 4.1 summarizes the capabilities of a CFC type in comparison to the ESP-r TMC type. Figure 4.10 illustrates the functionality and features of the current ESP-r construction types (MLC and TMC) in contrast with the CFC type.

Table 4.1: Summary of TMC and CFC capabilities in ESP-r

	TMC	CFC
Solar Optics	Described by overall system properties from optical database. Properties given for normal incidence and 5 off-normal angles. WINDOW 5 typically used to get set of optical data.	Described by individual layer total properties for normal incidence. Slat-type shading layers described by total normal slat properties. Off normal properties and effective shading layer properties calculated at every time-step during simulation.
Shading treatment	Achieved by manipulating the optical property sets of a TMC for prescribed control periods. Up to 3 control periods. Various sensors are linked with optical property control (see Fig. 4.10) Incidence angle symmetry (flat shades such as roller blinds only).	Currently only slat-type shading layers available. Modeled explicitly by manipulating the slat angle. Effective optical properties of shading layer calculated at each time step. Profile angle symmetry (vertical or horizontal slats). Shading layer may be placed anywhere within the assembly (indoors, outdoor, between glass)
Solar processing	Transmitted, absorbed fluxes calculated by interpolating the optical property set. Approximate treatment of back transmission and absorption. Cannot handle scattering shading layers.	Multi-layer model computes transmitted, reflected and absorbed fluxes based on individual layer data. General treatment of any combination of glazing/shading layers. Treatment of scattering shading layers. More exact treatment of indoor incident beam and diffuse fluxes for internal solar processing.

Spectral selectivity	Solar optical property sets based on spectral analysis of glazing layers if WINDOW 5 data used.	Transmitted, reflected, absorbed fluxes based on total solar optical properties of individual layers.
Convection treatment	Fixed total cavity resistance that combines convective and longwave radiative exchange. Can be modified by user to account for fill gases, low-e coatings, edge and frame losses. Requires third party software to establish the gap resistances. Does not account for temperature dependency of convective/radiant exchange.	Exact treatment of cavity convection based on fill gas properties and cavity thickness. Cavity convective resistances calculated per time-step, accounting for presence of a slat-type shading layer. Exact treatment of between glass slat-type blind. Approximate treatment of outdoor/indoor slat-type blinds
Long-wave radiation treatment.	See Convection treatment	Advanced model: Copes with jump resistors due to presence of diathermanous (semi-transparent to longwave radiation) layers. Copes with outdoor/indoor diathermanous layer exchange with interior zone surfaces and external surroundings. Calculates longwave fluxes per time-step, based on individual layer longwave radiative properties.
Input	Thermal capacity layers assembled from materials databases. Manual input of cavity resistances by user. System optical properties selected by user from optical database, or manually input.	Thermal capacity layers assembled from materials databases. Glazing/Shading Layer editor – GSLedit – used to assemble optical, longwave radiative, fill gas properties of glazing/shading layers based on supplied databases or user-defined entries. GSLedit output imported to ESP-r to generate CFC input file.
Simulation time step	No additional measures necessary to ensure convergence.	Requires time-step reduction to ensure solution convergence. Recommended 6 time steps per hour.

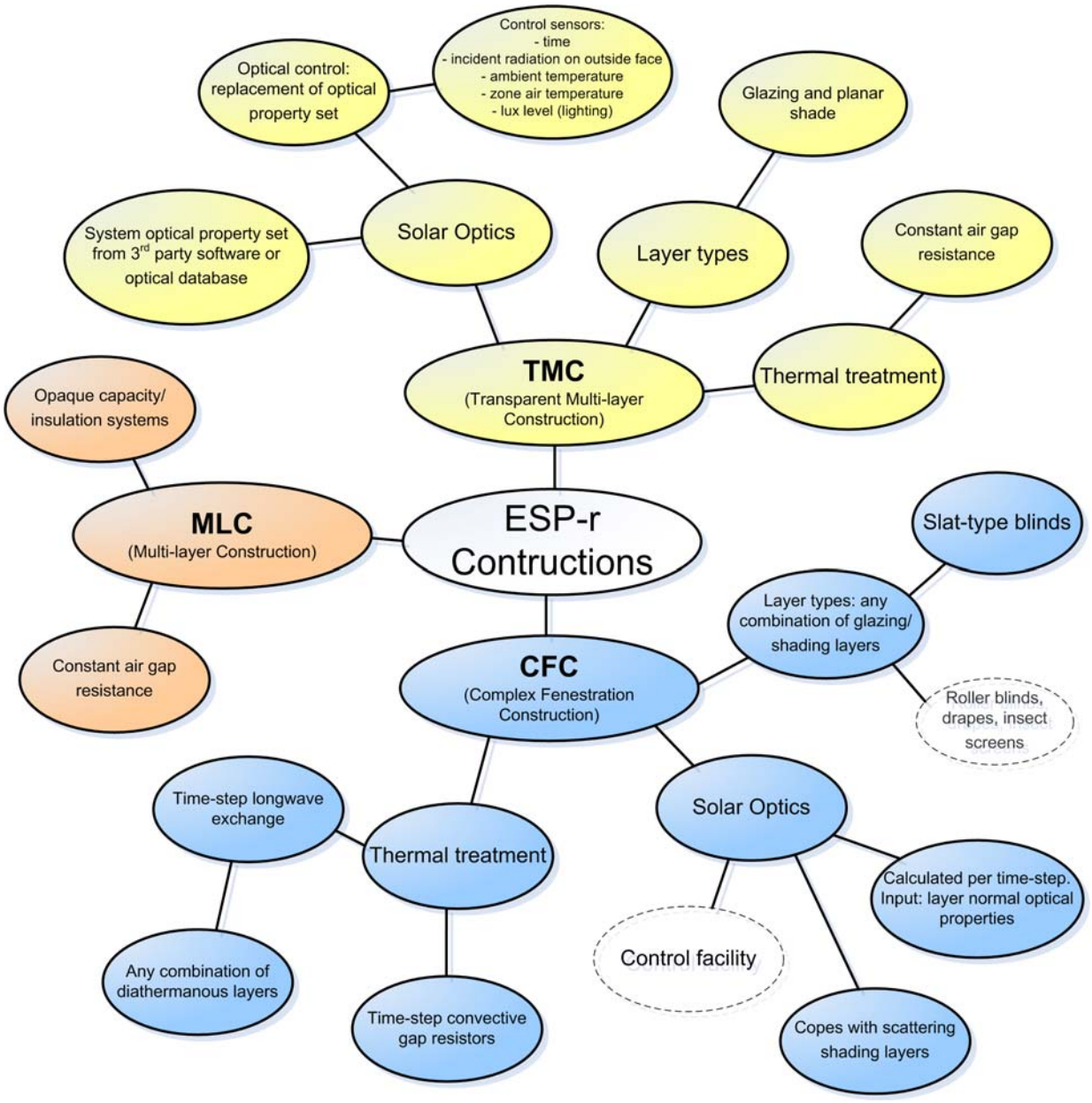

Figure 4.10: Functionality of existing ESP-r constructions (TMC, MLC) and the new CFC type.

Chapter 5
Numerical Comparison Studies

Chapter 4 described the details of implementing the window shading models in the ESP-r program via a new type of multi-layer construction, the CFC. Various parametric studies may be performed to demonstrate the impact of window shading on building energy simulation results using the added capability of the CFC. Of particular interest is the impact of shading components on peak cooling loads and aggregate cooling energy consumption. Before undertaking any such analyses, it is first essential to build confidence in the CFC code implementation. Two comparison studies were carried out to compare the CFC type against other models.

5.1 Background

Combining various modeling aspects into an integrated building energy simulation program certainly results in a high level of numerical complexity. Numerous validation efforts must be undertaken to ensure that numerical model predictions approximate the real world with acceptable accuracy. Measurement, although relatively expensive, is the most effective method of validation. A controlled environment provides the most useful comparison as the boundary conditions may be precisely controlled while retaining a reasonable level of realism. The next level of validation is the comparison of different building energy simulation codes. Such an approach offers a more practical comparison at a fraction of the time and investment required to perform measurements.

Recently, a series of experiments conducted by Loutzenhiser et al. (2006, 2007, 2008) and Manz et al. (2006) examined the impact of glazing/shading systems on solar gain in an attempt to compare with building energy simulation codes. An outdoor controlled test cell located at the Swiss Federal Laboratories for Materials Testing and Research (EMPA) was used. First, a glazing unit was analyzed (Loutzenhiser et al. 2006) and four building energy simulation codes, including ESP-r, were compared to the experimental results. All four codes yielded a mean absolute percentage difference in predicted cooling power between 1.9% and 6.2% compared to the

experiment. In particular, the mean absolute percentage difference in predicted cooling power for ESP-r was 3.1%. Following these tests, a glazing unit with outdoor and indoor venetian blind assemblies was analyzed (Loutzenhiser et al. 2008) and two building energy simulation codes were used to simulate the experiment. The mean percentages of the absolute mean differences in predicted cooling power between the two codes were within 6.1% and 7.1%, as compared to the experimental data. Both of these studies yielded good results, considering the challenges associated with modeling glazing systems in building energy simulation, especially the complexities associated with slat-type blind modeling. Although these tests represent only a small subset of possible glazing/shading configurations, the results are encouraging.

The AGSL window shading models used as the basis for the ESP-r CFC implementation have been concurrently incorporated in the ASHRAE Toolkit, under the designation ASHWAT (Wright et al. 2009). The ASHRAE Toolkit allows heat balance loads to be calculated for buildings with complex fenestration. Work on integrating the ASHWAT models in the software is ongoing, but preliminary results comparing ASHWAT calculations and measured data have been reported in (Kotey et al. 2009). Measurements of solar transmission and SHGC for a conventional double glazing with various internal shading layers (venetian blind at four slat angles, roller blind, pleated drape and insect screen) were taken at the National Solar Test Facility (NSTF) located in Mississauga, Ontario, Canada. Figure 5.1 shows an x-y scatter plot of the measured vs. calculated SHGC, reproduced from (Kotey et al. 2009). The calculated results compared well with experiments, with absolute difference in solar transmission and SHGC values in most cases below 0.05. These preliminary results reinforce the applicability of the AGSL shading models for the accurate determination of building loads.

Empirical validation of the CFC capabilities within ESP-r was not possible within the time constraints and scope of this work. However, two studies were conducted to compare the CFC models against codes, which have been evaluated in the experiments by Loutzenhiser et al. (2006 & 2008). First, the CFC center glass models were compared to the current ESP-r center glass window models for glazing systems without shading elements. Subsequently, CFC center of glass slat-type blind models were compared with EnergyPlus 2.0, which was recently upgraded with shading models for slat blinds, planar diffusing shades and insect screens.

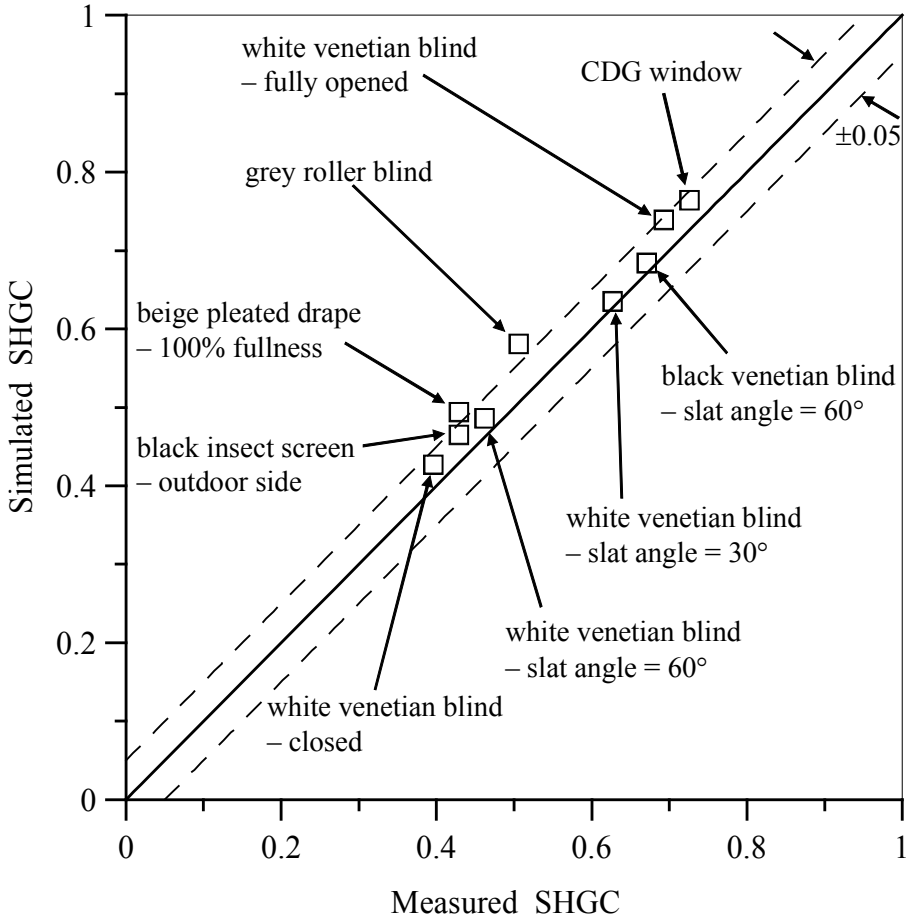

Figure 5.1: X-y scatter plot of the simulated vs. measured SHGC, reproduced from (Kotey et al. 2009).

5.2 TMC vs. CFC Comparison

The implementation of the Complex Fenestration Construction in ESP-r adds capabilities for modeling glazing/shading systems, currently limited to slat-type blinds. Although the CFC models are primarily intended as a framework for modeling shading elements within a glazing array, the CFC type also introduces an alternative method to process unshaded windows in ESP-r. Both the solar optical property determination and the heat transfer model used in the CFC type differ significantly from the TMC approach. As such, before examining the shading models, it is worthwhile to compare the two ways of representing glazings in ESP-r. Of particular interest are the effects of using CFC temperature dependent glazing cavity convective and longwave radiative

resistances versus the current TMC fixed gap resistance approach. Comparisons of solar transmission, absorbed solar flux distribution and cooling load results are presented for ESP-r simulations using the two construction types.

TMC description

Solar optics of a Transparent Multilayer Construction are based on a set of data stored in ESP-r's optical database. Each entry in the optical database contains solar optical properties for center of glass system transmission, reflection and layer absorption. The window is characterized by properties at normal incidence as well as 5 off-normal incidence angles. Standard entries exist for a variety of single, double and triple glazing configurations and new entries can be user defined based on third party software. Solar optical properties for the windows considered in this analysis were imported from the WINDOW 5 software, which is based on models described by Finlayson et al. (1993). WINDOW 5 calculates optical properties of glazing systems using either a multi-band spectral model, or a single band solar averaged model, depending on availability of spectral data. The calculation of angular properties of uncoated glass is based on first principles of electro-magnetic wave theory. For coated glass, a regression fit is used to calculate the angular dependence of optical properties. This method is less exact than the model for uncoated glass. If the normal incidence solar transmittance of a glazing layer is greater than 0.645, the angular dependence is determined through a regression fit to a reference clear glass. If the transmittance is less than or equal to 0.645, the coated glass angular properties are modeled using a bronze reference glass. Details can be found in Finlayson et al. (1993). Given the angular properties for a glazing system at 5 incidence angles, ESP-r interpolates to determine the optical properties at each time-step based on the sun's position relative to the surface receiving solar radiation. Diffuse properties are based on an equivalent incidence angle. A value of 51° is used based on a fully anisotropic sky model, shown to give best overall performance for a wide range of locations (Clarke 2001).

Heat transfer through a gas cavity between glazing layers of a TMC is treated by applying a constant gap resistance, which can be modified by the user to achieve a specific system U-value. The user can tune the gap resistance to account for different fill gases and low-e coatings.

CFC description

Although the CFC type was developed primarily for modeling window shading devices, it also provides an alternate way of modeling unshaded glazing, without relying on angular optical property data from third party sources. Using the GSLedit glazing/shading editor (Wright et al. 2008) to assemble a center of glass glazing system, the user can choose glazing layers from an extensive database, similar to the WINDOW 5 program. Fill gas mixtures can also be specified. Input data from GSLedit can then be imported to ESP-r to define a CFC composition. Solar optical properties are calculated at run-time, based on the normal incidence values supplied by the glazing libraries. The angular dependency of optical properties is calculated in similar fashion to the WINDOW 5 program, based on clear or bronze reference glass. The calculation method for determining the solar flux distribution in the glazing system is based on a multi-layer model (Wright and Kotey 2006) that copes with scattering layers. The glazing system is described with band-averaged solar optical properties. A more exact treatment of convective and longwave heat transfer through a gas cavity is used for the CFC type. Based on fill gas properties imported from GSLedit, a temperature dependent convective heat transfer coefficient is determined at each timestep. Longwave fluxes between layers are calculated at each time-step and added to glazing nodes as source terms. More details on the underlying models of the CFC are given in Chapter 2, Section 2.2.

Both WINDOW 5 glazing solar optical properties, used for the TMC type, and CFC solar optical properties depend on the glass normal transmittance to categorize the glazing as either uncoated or coated.

5.2.1 Simulation Methodology

A window/room configuration was chosen such that solar gain through the window represents the largest heat gain to the interior. An insulated envelope ensures that absorbed solar radiation on opaque sections is mostly rejected to the environment. The combination of an insulated envelope and a large south-facing window causes the cooling load to be driven primarily by the selection of glazing system. Figure 5.2 shows the simulation domain for the study. Table 5.1 summarizes the model parameters.

Table 5.1: ESP-r simulation parameters for TMC and CFC comparison

Model Parameters	**Description**
Walls, floor, roof construction	Exterior layer: Brown brick – 10 cm Mid layer: Glasswool – 7.5 cm Interior layer: Breeze block – 10 cm
Climate data	CWEC Toronto, Canada
Simulation period	July 7, 0-24 h
Site exposure	Rural/country
Ground reflectivity	0.2
Ground temperature	22.3˚C
Thermostatic control	Basic ideal thermostatic control with cooling setpoint at 25˚C
Ventilation and infiltration	No ventilation / no infiltration Default ESP-r interior convection correlations.
Warm up days	4
Time steps per hour	6

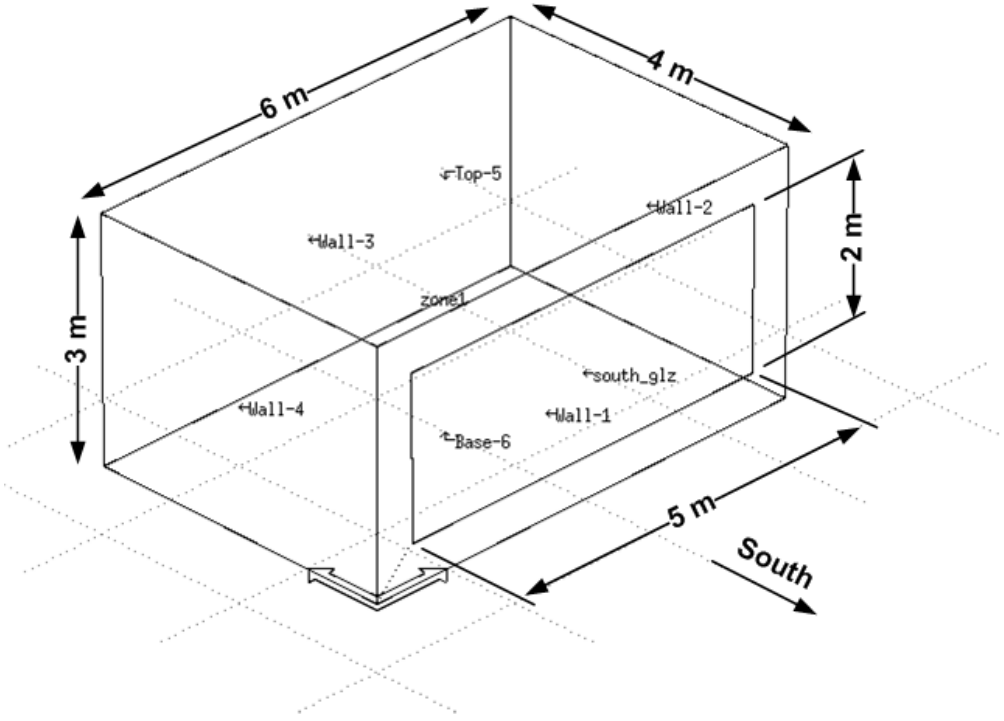

Figure 5.2: Geometry of test cell.

The thermal zone walls, window and roof were modeled with an exterior boundary condition, which includes exposure to wind, shortwave and longwave radiation. The floor was modeled with a ground boundary condition using a default monthly temperature profile. A ground temperature of 22.3˚C was used. Weather input for the chosen simulation period (July 7) was based

on CWEC (Canadian Weather for Energy Calculations) data for Toronto, Ontario. The data set contains hourly weather observations representing an artificial one-year period specifically designed for building energy calculations.

The internal loads of the test cell are largely driven by the value of incident solar radiation on the south facing window. Given global solar radiation data (direct normal and diffuse horizontal) from the climate file, the Perez et al. (1990) model was used in ESP-r to resolve the solar irradiance. The internal solar distribution scheme assumed that all directly transmitted beam radiation was incident on the floor, while transmitted diffuse radiation was distributed evenly to all interior surfaces excluding the south wall and window. Edge and frame effects of the window were not considered.

Test Cases

Three glazing systems were used in simulations to compare TMC and CFC models in ESP-r:

- Case 1: Double glazing - clear 6mm glass panes with 12.7 mm air cavity
- Case 2: Double glazing - bronze 6mm outdoor glass pane, low-e on clear 6mm indoor glass pane, 12.7 mm cavity with argon
- Case 3: Triple glazing - clear 6mm outdoor glass and mid panes, low-e on clear 6mm indoor glass pane, 12.7 mm cavities with argon

5.2.2 Results

Hourly simulations were carried out in ESP-r to compare the three glazing systems as modeled by a TMC type and CFC type. To demonstrate that the CFC models have been correctly implemented into ESP-r's zone matrix algorithms, simulations were first performed on a triple glazing CFC and TMC with equivalent constant gap resistances and with the solar processing turned off to render the optical property calculations irrelevant. The resulting average percentage differences between the pane temperatures were 0.07%, 0.06%, and 0.03% for the outdoor, mid and indoor glazing layer temperatures respectively. The maximum percentage differences in temperatures were 0.11%, 0.07%, and 0.06% for the outdoor, mid and indoor glazing layer respectively. The excellent agreement in these results gives confidence to the code implementation.

Results for Cases 1 to 3 include the cooling load, solar transmission and solar absorbed flux at each layer. The cooling load represents the theoretical instantaneous heat extraction required to maintain the indoor air temperature at 25°C. Ventilation and infiltration was set to zero, thus, the cooling power is the sum of interior surface convective fluxes based on buoyant flow convection models.

ESP-r hourly beam and diffuse solar radiation fluxes incident on the south window for the simulations are shown in Figure 5.3.

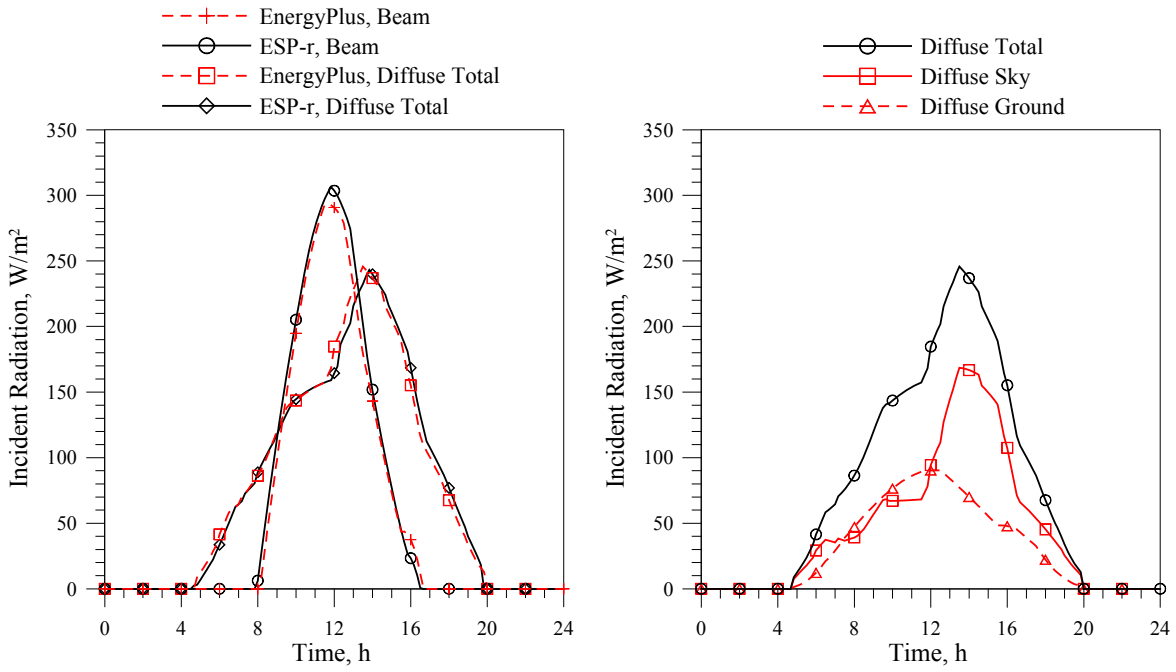

a) b)

Figure 5.3: Hourly incident solar radiation components on south window.

Figures 5.4, 5.5, and 5.6 show hourly results for cooling load, solar transmission and layer solar absorbed gain for simulation Case 1, 2, and 3, respectively.

Cavity Resistance Results

The temperature dependency of gap resistances for CFC types was analyzed for the triple glazing (Case 3). Glazing cavity resistances for both cavities in the triple glazing were examined.

The resulting hourly convective, longwave radiative and total resistances are plotted in Figure 5.7, each versus time of day for the 24 h July 7 simulation period. In Figure 5.8, cavity resistances are plotted for a case in which argon is replaced with xenon in the indoor side cavity. Figures 5.9 and 5.10 show the cooling load and layer temperatures for simulations comparing constant and dynamic gap resistances, where the constant resistances are determined from WINDOW 5 using either a winter or summer design condition. These constant resistances are then hard coded into the CFC convection routine. Therefore, a direct comparison using the CFC type is made for constant and variable resistances, retaining everything else equal.

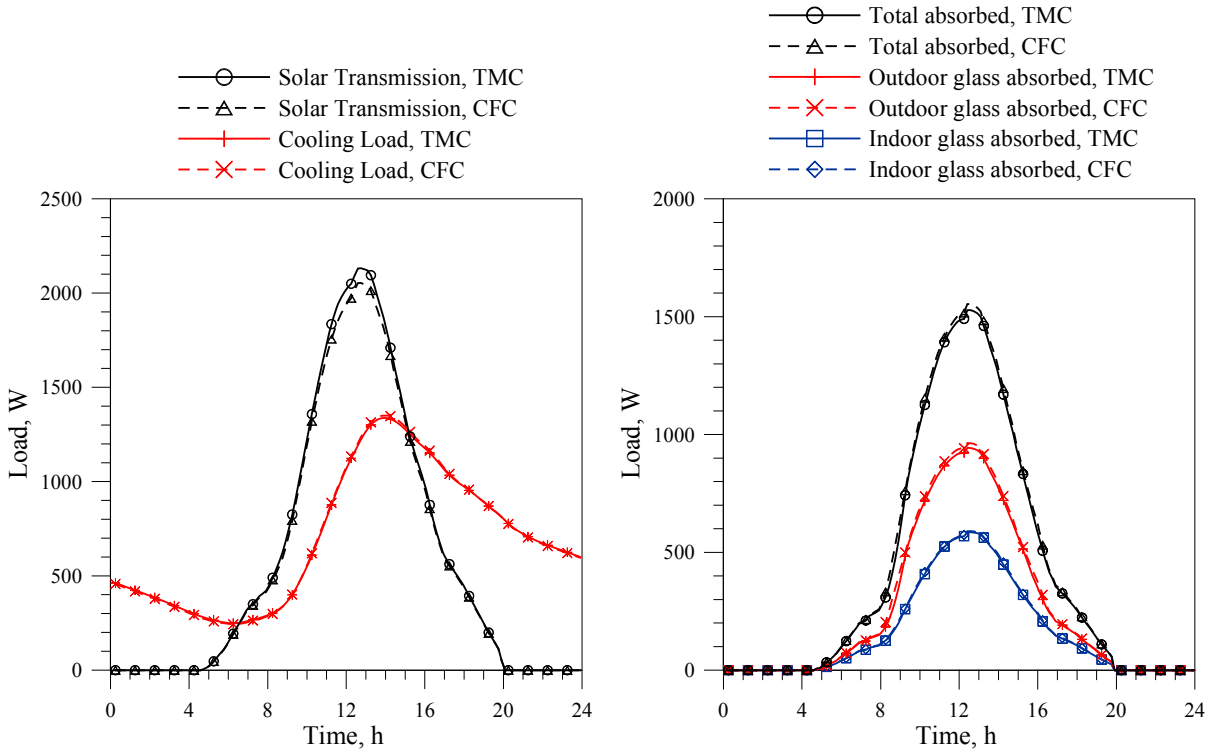

Figure 5.4: Hourly cooling load, solar transmission and absorbed solar radiation for Case 1: clear double glazing. Simulation results for Toronto, July 7 CWEC data.

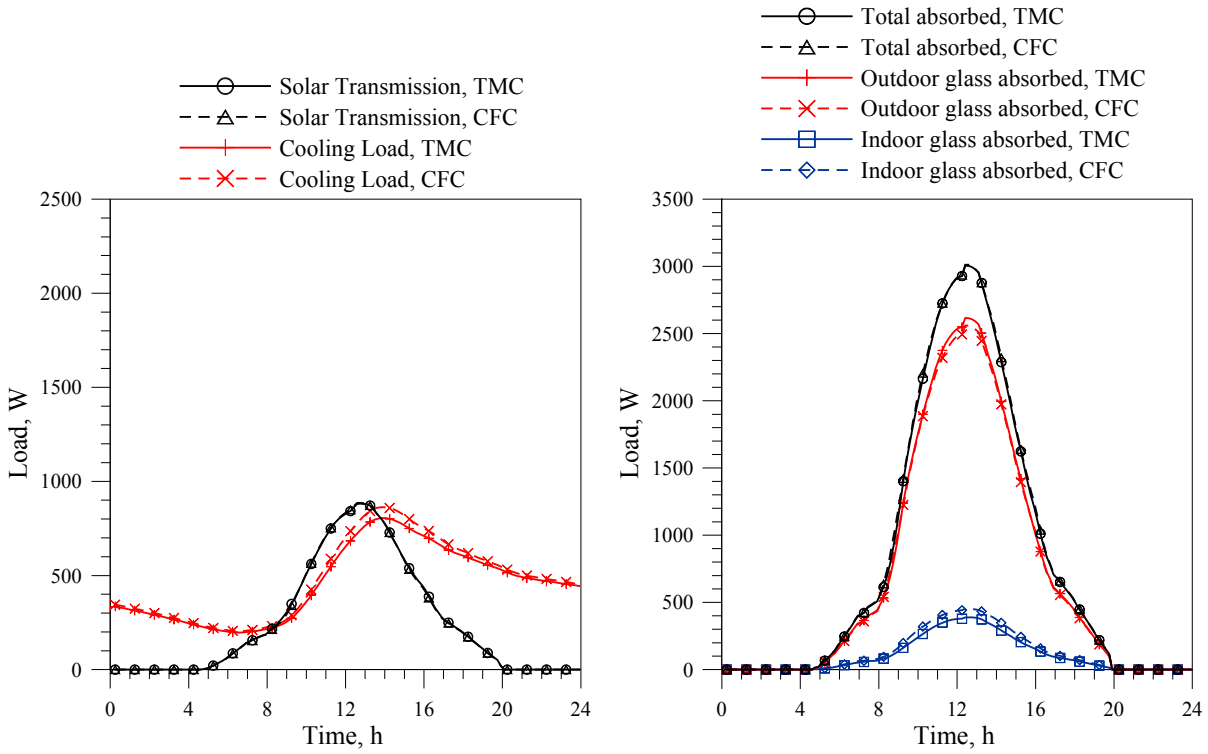

Figure 5.5: Hourly cooling load, solar transmission and absorbed solar radiation for Case 2: double glazing with bronze, low-e and argon. Simulation results for Toronto, July 7 CWEC data.

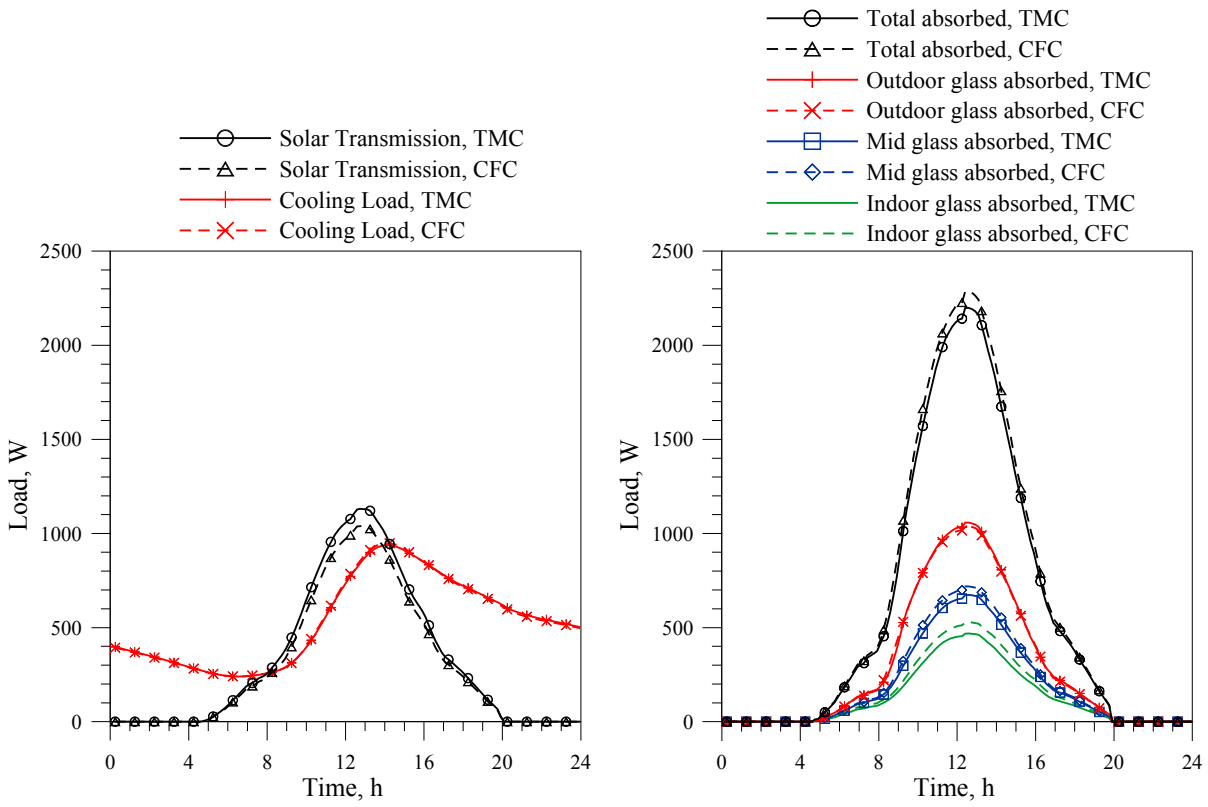

Figure 5.6: Hourly cooling load, solar transmission and absorbed solar radiation for Case 3: triple glazing with low-e and argon. Simulation results for Toronto, July 7 CWEC data.

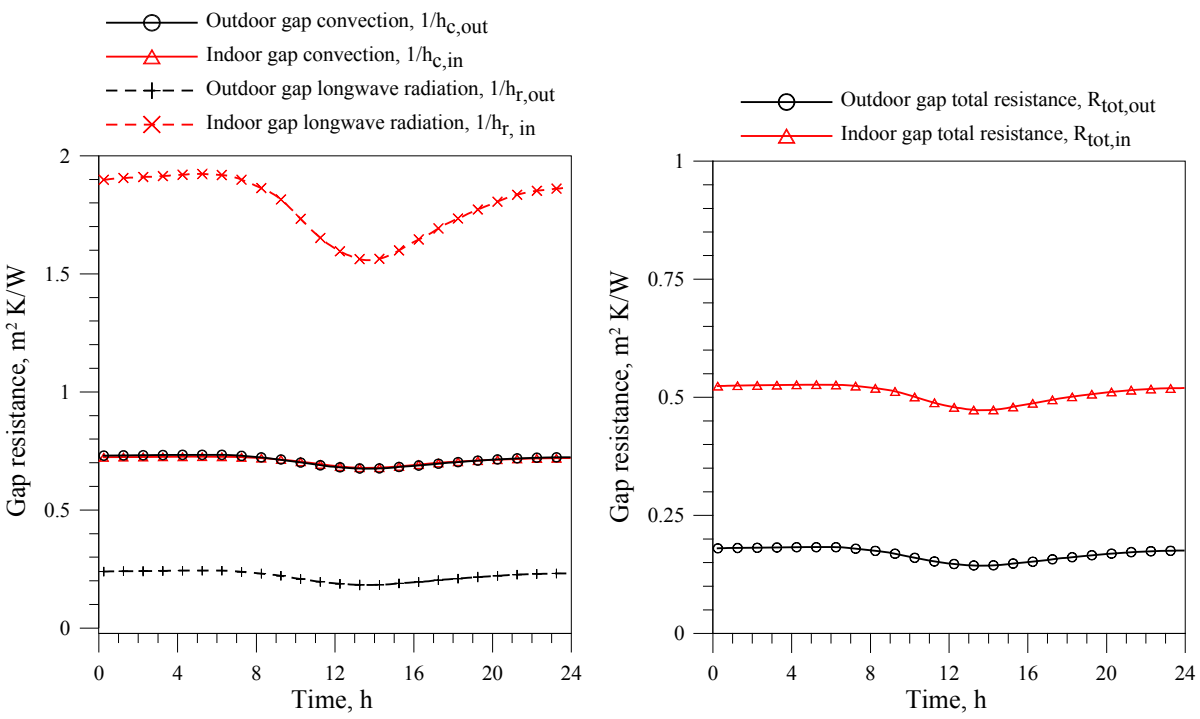

Figure 5.7: Hourly convective, longwave radiative, and total gap resistances for triple glazing (Case 3). Simulation results for Toronto, July 7 CWEC data.

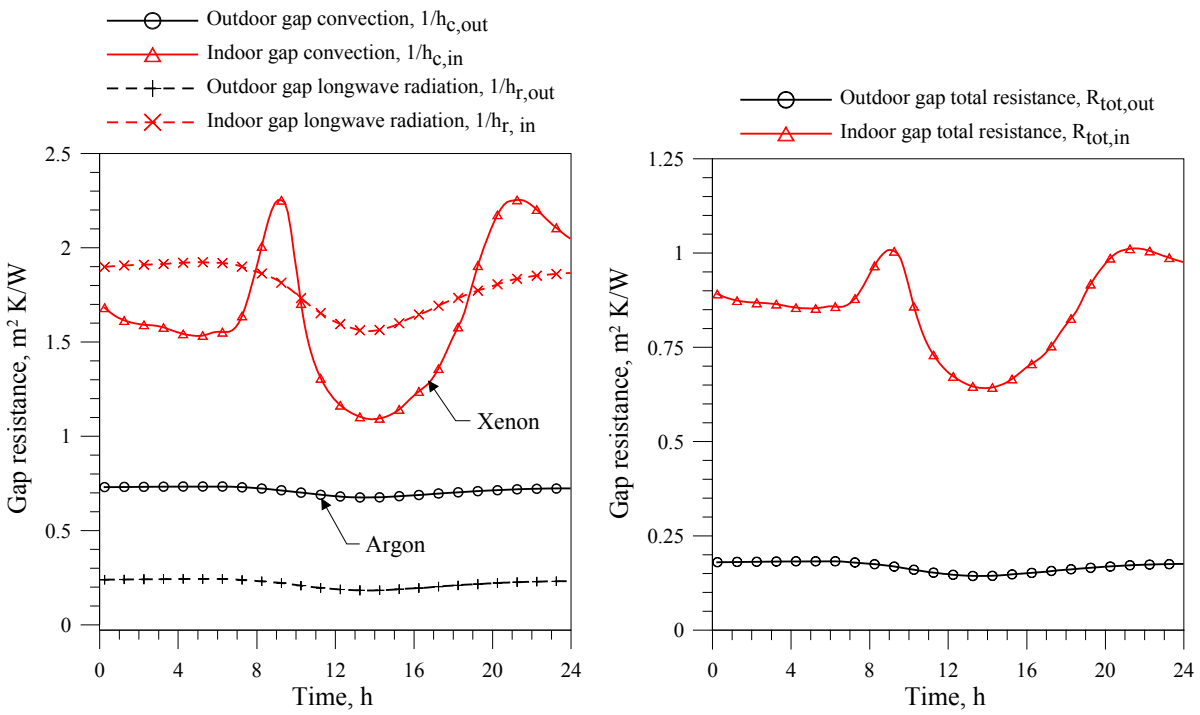

Figure 5.8: Hourly convective, longwave radiative, and total gap resistances for triple glazing (Case 3) with xenon gas in indoor cavity. Simulation results for Toronto, July 7 CWEC data.

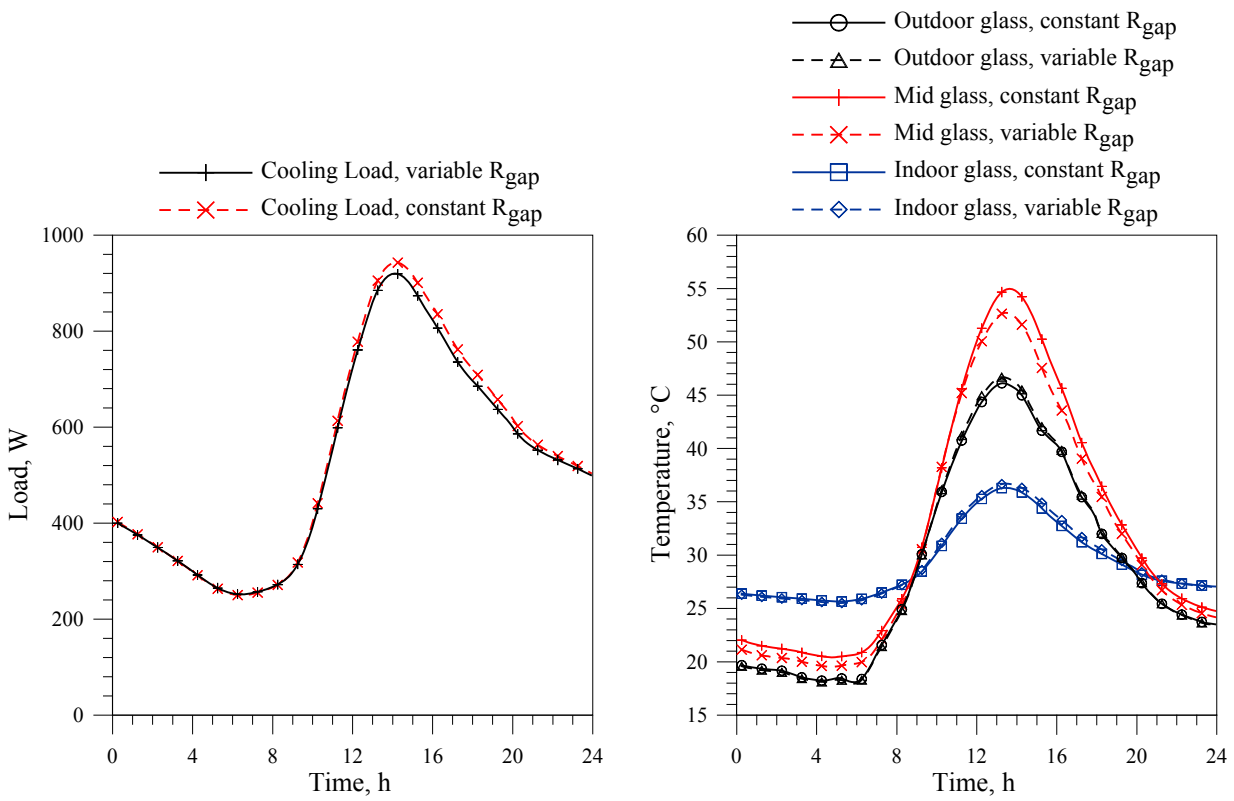

Figure 5.9: Comparison of CFC with constant gap for WINTER design condition, and temperature dependant gap resistances. Simulation results for Toronto, July 7 CWEC data.

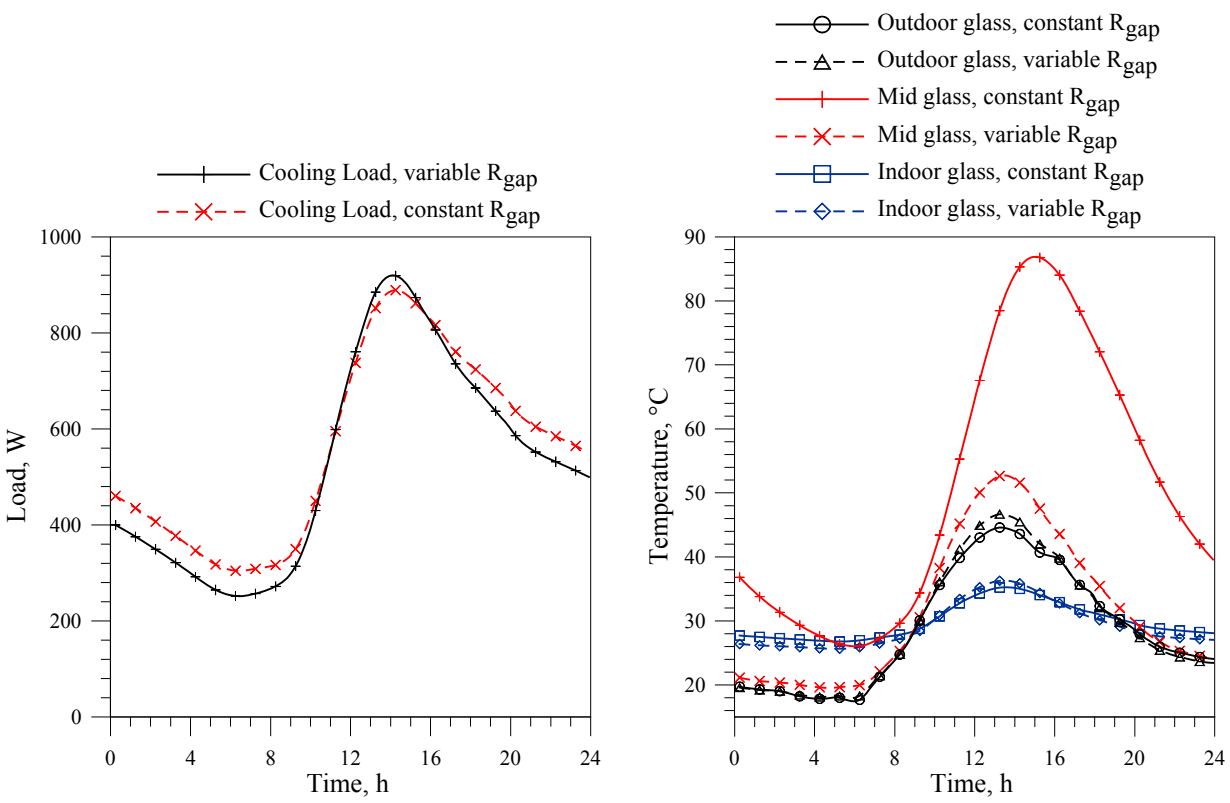

Figure 5.10: Comparison of CFC with constant gap for SUMMER design condition, and temperature dependant gap resistances. Simulation results for Toronto, July 7 CWEC data.

5.2.3 Discussion

On July 7 in Toronto (latitude 43.67°), the incidence angle on the south glazing varies between 69° and 90° as a result of the high sun elevation angle for that time of year. Therefore the comparisons of TMC and CFC window models rely on determining solar optical properties at high off-normal angles of incidence, where off-normal property adjustment models are most likely to differ. The bronze glazing in Case 2 as well as the low-e coated glass in Case 2 and Case 3 are both treated as coated glass due to their respective normal transmittance values, which fall below 0.645. Hence, glazings chosen for the analysis capture both coated and uncoated glass off-normal property adjustment models. The TMC solar optical property set represents the off-normal property adjustment models described by Finlayson et al. (1993), since the angular optical properties are imported from WINDOW 5.

The solar gain through the south window accounts for most of the cooling load variation throughout the 24 hour period. The large window area and high level of insulation of the opaque wall sections result in high sensitivity to solar gain. This pronounced effect creates suitable conditions for assessing the impact of solar thermal characteristics of windows such that differences in results can be mostly attributed to the window models.

The results for hourly cooling load, solar transmitted and absorbed fluxes are generally in very good agreement for all three simulation cases. Results for Case 1 (Figure 5.4) show that although there is a slight difference in the peak solar transmission, the cooling load is essentially identical at all times. Absorbed solar radiation values for both outdoor and indoor glazing layers show little difference.

Case 2 consists of an outdoor bronze tinted glazing and an indoor low-e on clear glazing, with argon in the cavity. The low-e coating is spectrally selective in the solar band, with high transmittance and low reflectance in the visible band, and low transmittance and high reflectance in the near IR band. This spectral selectivity is ignored in the CFC model, where solar band-averaged optical properties are used. Compared to Case 1, the results (Figure 5.5) show a significantly lower peak for solar transmission and a higher peak for absorbed flux. The outdoor tinted glass absorbs most of the incident solar radiation. There is a small discrepancy in the peak cooling load between the TMC and CFC values, corresponding to the difference in absorbed flux for the indoor glass

layer. The hourly total absorbed flux for the TMC and CFC is identical, however, the individual layer absorbed gains differ slightly. The difference may be attributed to the spectral selectivity of the low-e coating or assumptions regarding off-normal property adjustment models but it is difficult to draw any conclusions because the difference is so small.

The TMC and CFC cooling load curves for Case 3 triple glazing are closely aligned (Figure 5.6), although the solar transmitted and absorbed fluxes differ somewhat. In this case, the higher TMC solar transmission peak is offset by the lower TMC absorbed fluxes at the indoor and mid glass layers.

The mean absolute difference of cooling loads and solar transmissions in the entire result set is below 30 W. The maximum absolute difference, occurring at the peaks, is below 95 W for all cases. Mean percent difference in cooling load for Case 1, Case 2 and Case 3 are 1.1%, 4.5% and 0.9%, respectively. Maximum percent difference in cooling load for Case 1, Case 2 and Case 3 are 2.5%, 7.9% and 1.8%, respectively.

The CFC results compare well with the TMC results, given that the TMC is characterized by optical properties imported from WINDOW 5. The CFC model, which determines solar optical properties and temperature dependent gap resistances on a time-step basis, yields expected results within the scope of the three windows chosen for the comparison study. The observed differences between TMC and CFC results may be attributed to interpolation error in establishing off-normal optical properties in the TMC model and neglecting spectral selectivity of coatings in the CFC model, but it is difficult to draw any conclusions since the differences are so small.

The use of dynamic temperature dependent gap resistances in the CFC type, as opposed to constant gap resistances used in the TMC type, is the main difference between the two glazing models. The coupling of convective and radiative heat transfer is taken into account by calculating the gap resistances at each time step in the CFC model, however, the impact of this more exact treatment on simulation results is not clear. A comparison of the two approaches is thus warranted.

Cavity Resistance

In order to isolate the effect of temperature dependent convective and longwave radiant gap resistances, simulations were carried out for the triple glazing (Case 3) CFC with either constant or variable resistances. Using only the CFC type for this analysis ensured that any differences in solar processing between the TMC and CFC would not be present. The triple glazing was used to study the impact of fill gases and low-e coatings on gap resistances.

First, gap resistances were analyzed for the case of argon fill gas in both cavities with the low-e coating on the outdoor-facing side surface of the indoor glass pane. Figure 5.7 shows the convective and longwave radiative hourly resistances, as well as the total hourly resistances for the outdoor side and indoor side gaps, for the July 7 simulation period. The total hourly resistances are obtained by combining the convective and longwave radiative resistances in parallel. The results show that the longwave radiative resistance in the outdoor clear glass cavity is lower; therefore most of the energy transfer in the outdoor cavity is due to longwave radiation exchange. The convective resistances for argon in both gaps, as well as the radiant resistor in the outdoor gap, show very little variation over the course of the simulation period. Significant variation is observed in the longwave radiant resistance corresponding to the indoor cavity with low-e coating. The trough of the radiant resistance corresponds approximately to the peak in cooling load, as shown in Figure 5.7.

Any variation in convective gap resistances is driven by temperature difference across the glazing cavity. A higher temperature difference results in a higher convective flux across the gap, and a lower resistance. Variation in longwave radiative gap resistance is due to a third order temperature dependency of the radiant heat transfer coefficient,

$$h_r = \frac{\sigma}{\frac{1}{\varepsilon_1} + \frac{1}{\varepsilon_2} - 1} \cdot \frac{(T_1^4 - T_2^4)}{(T_1 - T_2)} \qquad (5.1)$$

where T_1 and T_2 are the bounding temperatures, ε_1 and ε_2 are the emissivities of the two surfaces and σ is the Stefan-Boltzmann constant. The radiant heat transfer coefficient increases with an increase of the glass temperatures across the cavity. Thus, taking the inverse of the radiant

coefficient, the radiant resistance is expected to go down during sunlit periods when glass pane temperatures are high and approach each other. Overall, the low emissivity coating on the indoor glass surface drives down the radiant coefficient, resulting in a relatively high resistance to longwave radiation exchange.

Combining the convective and radiant resistors in parallel such that $R_{gap}= 1/(h_c+h_r)$, both total gap resistances show little variation. This case suggests that as long as the constant gap resistances are determined accurately, temperature variations have only a small effect on the total gap resistance for this glazing system.

To examine the effect of using a heavier fill gas, argon was replaced with xenon in the indoor cavity of the window. Xenon can drive down the convective heat transfer coefficient in the glazing cavity primarily due to its lower conductivity relative to argon, thus it can increase the resistance to convective heat transfer across the glazing cavity. This increase in resistance depends on the pane spacing of the sealed cavity. Given a winter nighttime condition, the optimum spacing for xenon is 5.3 mm (Hollands, Wright and Granqvist 2001). This optimum spacing varies depending on the glass pane temperatures, which fluctuate with outdoor and indoor temperatures, wind speed and solar irradiance. For the purpose of this study, the cavity spacing was not changed from 12.7 mm when argon was replaced with xenon. The larger cavity spacing actually increases the resistance for the summer day simulation period and amplifies the sensitivity in resistance value to changes in the bounding pane temperatures, relative to the optimum 5.3 mm spacing. Strong sensitivity of the gap resistance was preferred for demonstrating the relative impact of using constant or dynamic resistances on simulation results, although in reality a window with xenon in a 12.7 mm cavity would not make sense.

Figure 5.8 shows results for individual convective and radiant resistances as well as total resistances for the outdoor argon/clear gap and the indoor xenon/low-e gap. As before, the convective and radiant resistances for the outdoor gap are much lower and less variable than the indoor gap resistances. The convective resistance for xenon fluctuates strongly throughout the simulation period. The effect of the fluctuating convective and radiant resistances in the indoor gap, when combined in parallel, result in a total resistance that is highly variable in comparison to

the outdoor gap. The results indicate that heavier fill gases and low-e coatings, which offer higher gap resistances, are also much more sensitive to temperature variations across the gap.

Although the temperature dependence in gap resistance is clearly significant for the indoor gap with xenon/low-e coating, the question remains as to what extent the cooling load is affected by this variability. Simulations were performed to illustrate the impact of temperature dependent resistances on the cooling load of the test cell.

In the first case, constant gap resistances were used based on information from WINDOW 5 for the winter design condition. In WINDOW 5, the NFRC 100-2001 Winter condition (NFRC 2001) was applied to calculate the U-value of the triple glazing. Based on these results, the outdoor argon/clear gap was assigned a total resistance of 0.24 m^2K/W, the indoor xenon/low-e gap was assigned a total resistance of 0.62 m^2K/W. This constant gap resistance case was compared to the CFC variable resistance model. The resultant cooling load and glazing layer temperatures are shown in Figure 5.9. Hourly cooling load results show only a slight difference between the winter condition constant resistances and variable resistance cases. The temperature results for the mid glass layer show a 3°C difference at the peak.

The temperature profiles of the three glass layers in Figure 5.9 can be used to explain the rapid fluctuations observed for xenon convective resistance in Figure 5.8. The first xenon convective resistance peak, which occurs at 9:00 h corresponds to a point on the temperature plot where the curves cross one another, when all three layers are at the same temperature. The xenon convective resistance reaches a low point at 14:00 h, when the temperature difference is greatest. Another peak occurs at 21:00 h, when once again the temperature profiles cross. The xenon convective resistance fluctuations are thus clearly the result of the fluctuating temperature difference across the gas gap. The outdoor gap resistance variations are much smaller in magnitude and thus are not clearly visible.

In the second case, the Summer NFRC 100-2001 design condition (NFRC 2001) was imposed to establish the U-value in WINDOW 5 and the corresponding gap resistances. Based on these results, the outdoor argon/clear gap was assigned a total resistance of 1.79 m^2K/W, the indoor xenon/low-e gap was assigned a total resistance of 2.82 m^2K/W. These resistances differ

significantly from the winter design condition values. This constant gap resistance case was compared to the CFC variable resistance model. The resultant cooling load and glazing layer temperatures are shown in Figure 5.10. Hourly cooling load results show significant differences throughout the simulation period, more so during nighttime hours. Large variations between constant and variable resistance cases are seen in the mid glass temperature results. Looking at Figure 5.8, the variable resistance corresponding to the xenon/low-e gap fluctuates between 0.65 and 1.05 m^2K/W, compared to a constant of 2.82 m^2K/W gap resistance specified by WINDOW 5 for the summer condition. The argon/clear gap resistance, with an average value of 0.17 m^2K/W is an order of magnitude smaller than the WINDOW 5 constant resistance of 1.79 m^2K/W.

Although the analysis was conducted with climate data for a summer day in July, the results suggest that using the winter design condition gap resistances from WINDOW 5 is a better choice. The NFRC 100-2001 Summer condition imposes a normal incident solar radiation value of 783 W/m^2 (NFRC 2001). However, for a south facing window on a July day, the incidence angle is high and the resolved incident solar radiation is expected to be much lower. Therefore, the simulated hourly temperature distribution of the glazing layers in ESP-r is expected to differ considerably from the WINDOW 5 results where the solar irradiance is fixed at normal incidence. This will undoubtedly result in large discrepancies between design condition gap resistances and variable temperature dependent gap resistances.

The CFC variable resistance model plays a more significant role when a shading layer is placed within the glazing. For example, a between the glass blind absorbs most of the solar radiation, depending on the slat angle and colour. The resulting temperature differences between the blind and glass could be very high, driving down the convective resistance in the cavity substantially. With the variable resistance model, the guess work in establishing a correct gap resistance is eliminated. Technical expertise required to properly assemble a glazing using the TMC type is not needed if instead the CFC type is used to model glazings.

5.2.4 Conclusion

Hourly simulations comparing solar transmission, solar absorbed fluxes and cooling load, using TMC types and CFC types in ESP-r for three different glazing systems, showed good agreement in all cases. It was shown that gas gap resistances are sensitive to glazing layer

temperature, more so when the convective heat transfer is attenuated by a heavy fill gas and the longwave radiative exchange by a low-e coating. The effects of modeling gas gap resistances as either constant or variable temperature dependent were analyzed. The appropriate selection of constant gas gap resistances for a simulation is highly dependent on the environmental conditions chosen for the U-value calculation in programs such as WINDOW 5. The results showed that using WINDOW 5 gap resistances for a winter condition matched well with the variable temperature dependent resistances and little difference in cooling load was observed, even though the simulation was carried out for a summer day. Using a summer condition in WINDOW 5 resulted in gap resistances that differed significantly from the temperature dependent variable resistances. Large differences in temperatures and cooling load were observed for this case. These results suggest that using constant gas gap resistances for glazing systems in time-step simulation does not result in a significant loss in accuracy, as long as the values are determined by selecting the right environmental conditions for the U-value calculation.

Although the impact of dynamic gap resistances on cooling load for the three glazing cases was not significant, the benefit of using the CFC type to model glazings is the ability to easily select glazing products from a database such as the International Glazing Database using the GSLedit tool, while foregoing the need to select a design condition to evaluate fixed resistances. Fill gases and fill gas mixtures can also be selected through the GSLedit tool. Finally, since shading devices are typically more absorbing to solar radiation than glazings, temperature differences across gaps in glazing/shading systems may become high when exposed to solar radiation, thus causing more variability in gap resistance.

5.3 Comparison of CFC and EnergyPlus Slat Blind Models

A preliminary study was conducted to compare slat-type blind models featured in EnergyPlus 2.0 with the Complex Fenestration Construction slat-type blind models in ESP-r. EnergyPlus shading models serve as a useful comparison, as they have been compared to experiments carried out by Loutzenhiser et al. (2008) with encouraging results. The impact of window shading on simulation results is emphasized by specifying a test cell geometry with a large south facing window and insulated envelope. Different blind configurations were examined and results for solar transmission and cooling load compared.

5.3.1 Simulation Methodology

The simulation methodology is similar to the methodology in the TMC/CFC comparison study of Section 5.2. The test cell from that study was modeled in EnergyPlus and ESP-r for the present study. Details of the model geometry, boundary conditions, and simulation parameters can be found in Section 5.2.1.

The internal loads of the test cell are largely driven by the value of incident solar radiation on the south facing window, thus to reduce discrepancies in the results, emphasis was placed on selecting the same sky radiance distribution model for the two codes. Given global solar radiation data (direct normal and diffuse horizontal) from the climate file, the Perez et al. (1990) model was used in both simulation programs to resolve the solar irradiance incident on external surfaces.

Test Cases

In comparing the shading models of the two simulation codes, of particular interest is the impact of the blind position relative to the glazing, and the impact of a shaded window compared to an unshaded window. Table 5.2 summarizes the test cases examined in the study.

Table 5.2: Test cases for EnergyPlus/ESP-r comparison study

Test case	Details
Case 1: no window	Fully enclosed test cell.
Case 2: CDG	Unshaded window – reference case. Clear double glazing (CDG), 6mm clear glass with 12.7mm air gap.
Case 3: CDG with OUTDOOR slat blind.	Slat orientation: horizontal Slat angles: 0° (horizontal) and 45° Slat width: 0.0127 m Slat spacing: 0.01058 m Slat thickness: 0.00033 m, flat slats Distance to glass (Case 3 & 5): 0.04 m Between-glass gap space (Case 4): 0.0254 m Slat reflectivity: 0.5 Slat emissivity: 0.85 Slat transmittance: 0 Opening multipliers for Case 5 (EnergyPlus only): 1
Case 4: CDG with BETWEEN-GLASS slat blind	
Case 5: CDG with INDOOR slat blind	

EnergyPlus Description

Solar optical property calculations in EnergyPlus 2.0 are based on WINDOW 5 algorithms (Finlayson et al. 1993). The double glazed window with clear glass was modeled with spectrally averaged solar optical properties. The flat horizontal slats are considered to be perfect diffusers in the EnergyPlus 2.0 blind model. The solar-optical model of slat-type blinds, which is dependent on the slat geometry (width, spacing, angle) and slat material optical properties, is based on (Simmler, Fischer and Winkelmann 1996). Ground and sky diffuse radiation components are treated separately for blind optical property calculations. Heat transfer between the window and shading device is calculated using ISO 15099 (2003). A detailed interior convection algorithm was used to compute the natural convection coefficients of interior surfaces. The algorithm, taken from (Walton 1983), correlates the coefficients to surface orientation and the temperature difference between the surface and zone air. The thermal capacity of glazing/shading layers is neglected. The glass/blind temperatures are solved at each time step iteratively. The shade thermal model accounts for convection from an indoor blind and glass surfaces to the zone air, and from outdoor blind and glass surfaces to the ambient. Longwave radiation exchange accounts for indoor/outdoor blind transmission to the interior surfaces and external surroundings, respectively.

More detail on EnergyPlus window shading models is provided in EnergyPlus documentation (EnergyPlus Engineering Reference 2008).

CFC Description

The Complex Fenestration Construction (CFC) type was used in ESP-r to model the glazing/shading center-of-glass system. An overview of solar optical and thermal models used in the CFC type can be found in Chapter 2, Section 2.2. Glazing/shading layers in the CFC type are treated explicitly within the nodal scheme of the thermal building domain. The difference equations describing the glazing/shading nodes are linked to other zone surface nodes and the zone air node via convection and radiation processes. The entire set of equations is solved simultaneously for nodal temperatures. Thermal mass of the glazing/shading layers is not neglected and is assigned in the same manner as opaque envelope constructions. Interior surface convection for vertical and horizontal surfaces was treated as buoyancy driven flow, using correlations developed by Alamdari and Hammond (1983). The calculation of the slat blind solar optical properties for incident diffuse radiation does not differentiate between sky-diffuse and ground-diffuse components.

In both EnergyPlus and ESP-r models, edge and frame effects of the window were not considered. Conceptually, the edge and frame regions of a window modeled with a CFC can be modeled as a separate construction if the U-Value and frame and edge areas are known.

5.3.2 Results

Several comparisons were made to quantify the effect of shaded glazings on the test cell cooling load. The cooling load represents the instantaneous heat extraction required to maintain the indoor air temperature at 25°C. Ventilation and infiltration were set to zero in the model, thus, the cooling load is the sum of interior surface convective fluxes based on the buoyant flow convection models. In addition to the cooling load, the solar transmission was compared in all cases. All hourly simulation results are based on a 24 h simulation period for July 7 CWEC data for Toronto, Canada.

Solar Irradiance

Figure 5.11 a) shows the hourly solar radiation components incident on the south window as predicted by both EnergyPlus and ESP-r simulations. Figure 5.11 b) shows EnergyPlus results for hourly sky diffuse and ground diffuse components of solar radiation on the south window.

Fully Enclosed Test Cell

Figure 5.12 shows the hourly cooling load results for a fully opaque test cell (Case 1).

Double Glazing

The reference case for all subsequent shading comparisons is the conventional double glazed window (Case 2) with clear glass and an air filled cavity. Solar transmission and cooling load results for this case are shown in Figure 5.13.

Double Glazing with Slat Blind

Plots were generated to compare solar transmission and cooling load for outdoor, between-glass, and indoor blinds (Case 3, 4, and 5, respectively). For each blind configuration, two slat angles, 0° and 45° were simulated. Figures 5.14, 5.15, and 5.16 present the hourly results for Case 3, 4 and 5, respectively.

Total Cooling Energy and Peak Cooling Load

Although the result plots are more informative, the cooling energy for the 24 hour simulation period as well as the peak cooling load were also tabulated for comparison. The data are presented in Table 5.3. Since the magnitudes of the peaks vary significantly between the simulated cases, absolute differences are used for comparison. Using percentage difference as an indicator of agreement inflates the reported differences for cases where the solar gain is small.

Table 5.3: Total cooling energy, peak cooling load and absolute differences for EnergyPlus and ESP-r results

Case	Slat angle (°)	Total Cooling Energy (kWh)		Absolute Difference (kWh)	Peak Cooling Load (W)		Absolute Difference (W)
		EnergyPlus	ESP-r		EnergyPlus	ESP-r	
Double-glazing (Case 2)	N/A	15.9	16.5	0.6	1259.5	1303.7	44.2
Outdoor blind (Case 3)	0	8.6	8.0	0.6	566.6	555.8	10.8
	45	6.7	6.3	0.4	399.1	436.7	37.6
Between-glass blind (Case 4)	0	12.4	12.9	0.6	1012.4	1073.6	61.2
	45	10.9	11.6	0.6	911.9	948.1	36.2
Indoor blind (Case 5)	0	15.2	14.0	1.2	1492.9	1392.8	100.1
	45	14.2	13.1	1.1	1456.1	1373.3	82.8

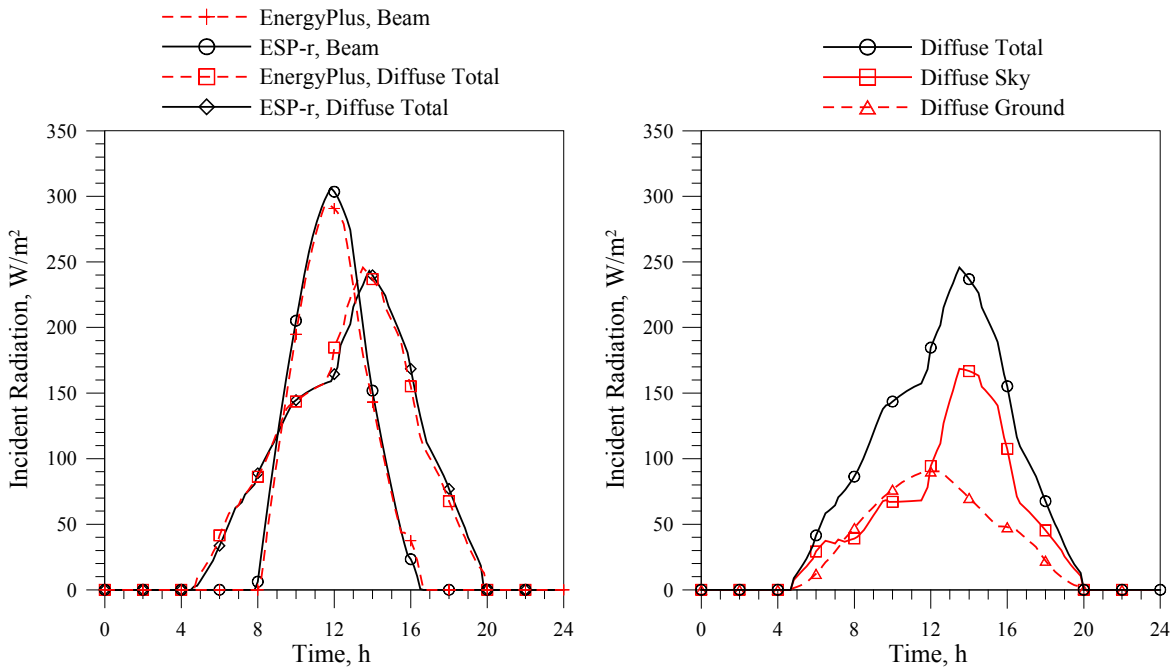

a) b)

Figure 5.11: a) Hourly incident solar radiation components on south window for EnergyPlus and ESP-r simulations. b) EnergyPlus hourly sky, ground and total diffuse radiation. Simulation results for Toronto, July 7 CWEC data.

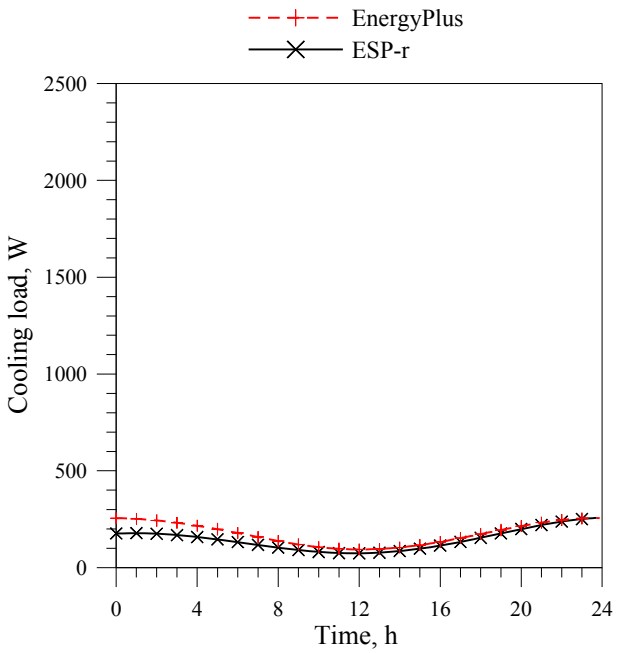

Figure 5.12: Hourly cooling load for Case 1 (no window). Simulation results for Toronto, July 7 CWEC data.

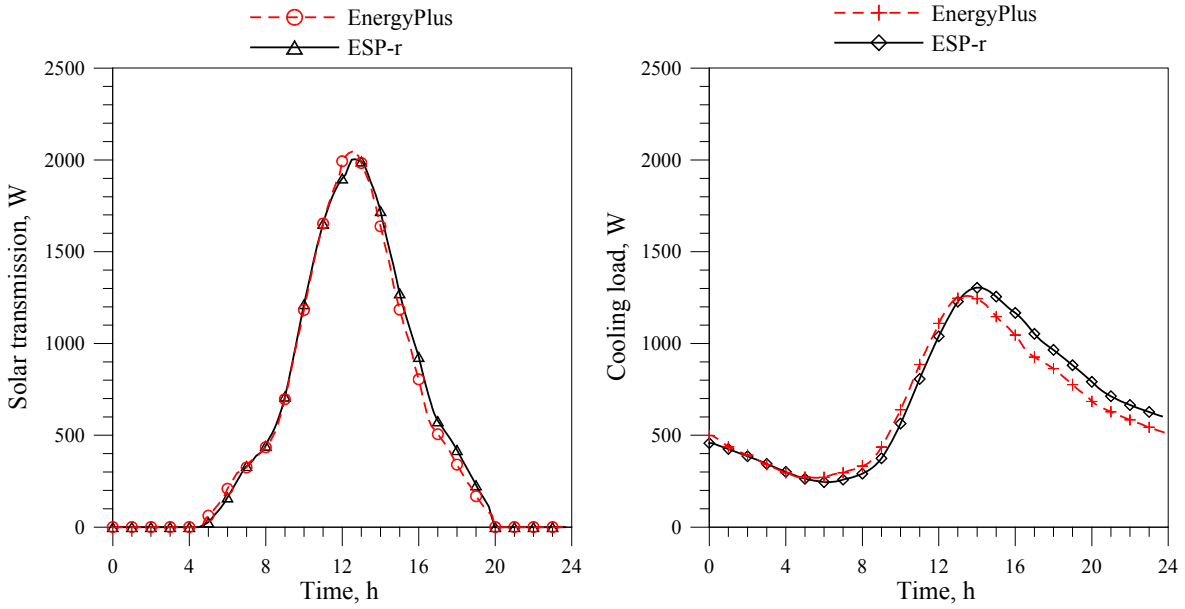

Figure 5.13: Hourly solar transmission and cooling load for Case 2 (clear double glazing). Simulation results for Toronto, July 7 CWEC data.

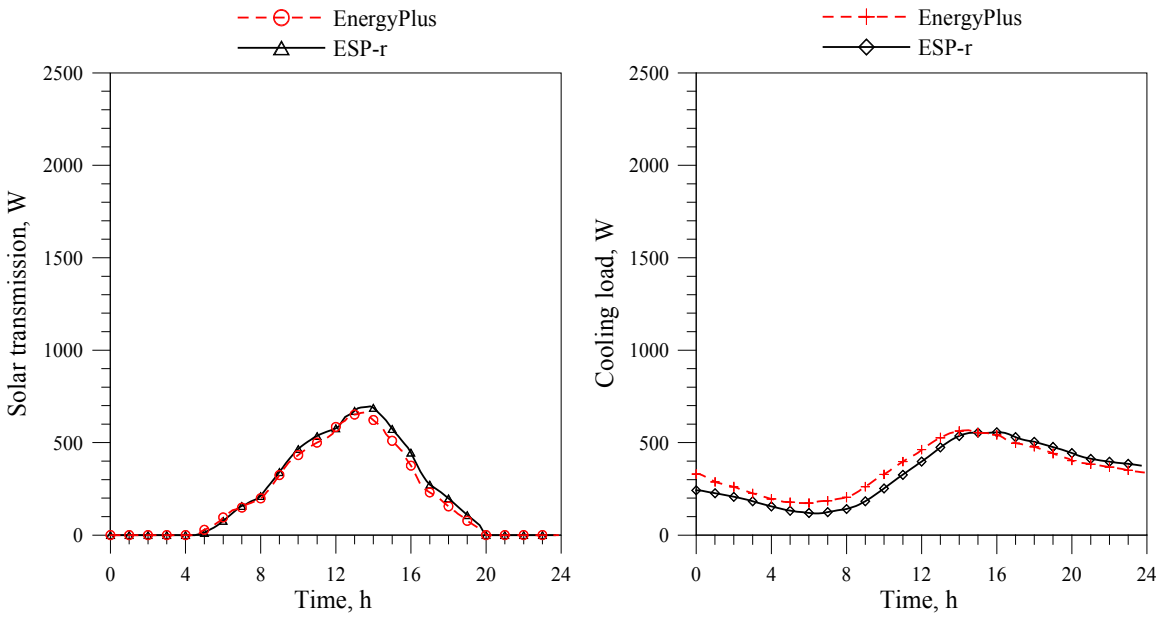

a)

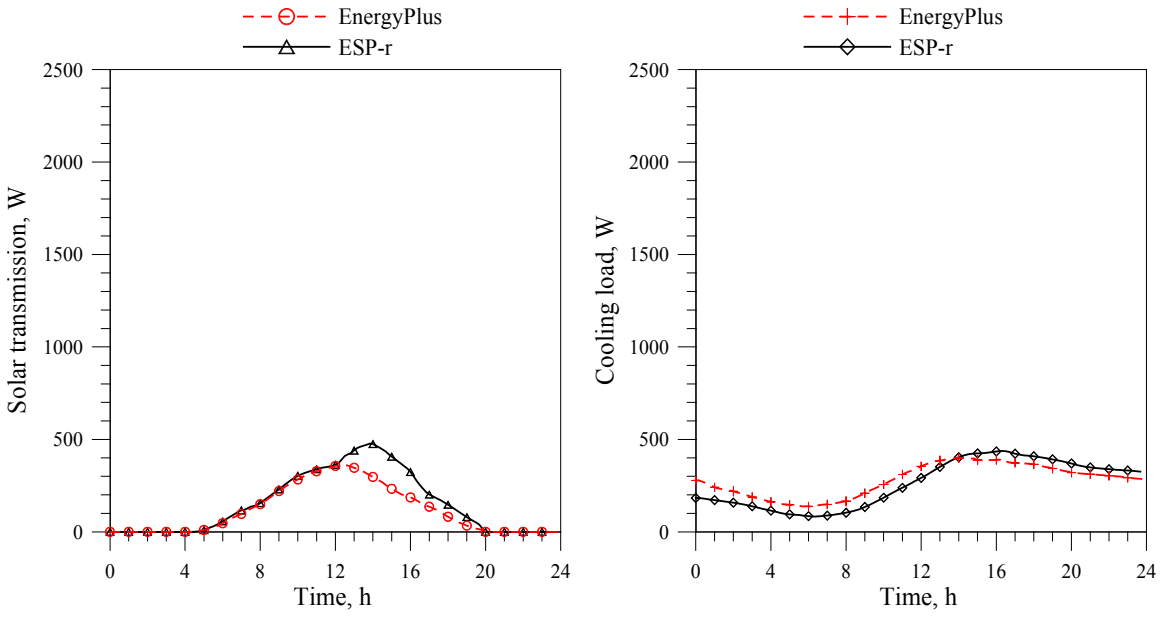

b)

Figure 5.14: Hourly solar transmission and cooling load for OUTDOOR blind (Case 3) with slat angle a) 0° and b) 45°. Simulation results for Toronto, July 7 CWEC data.

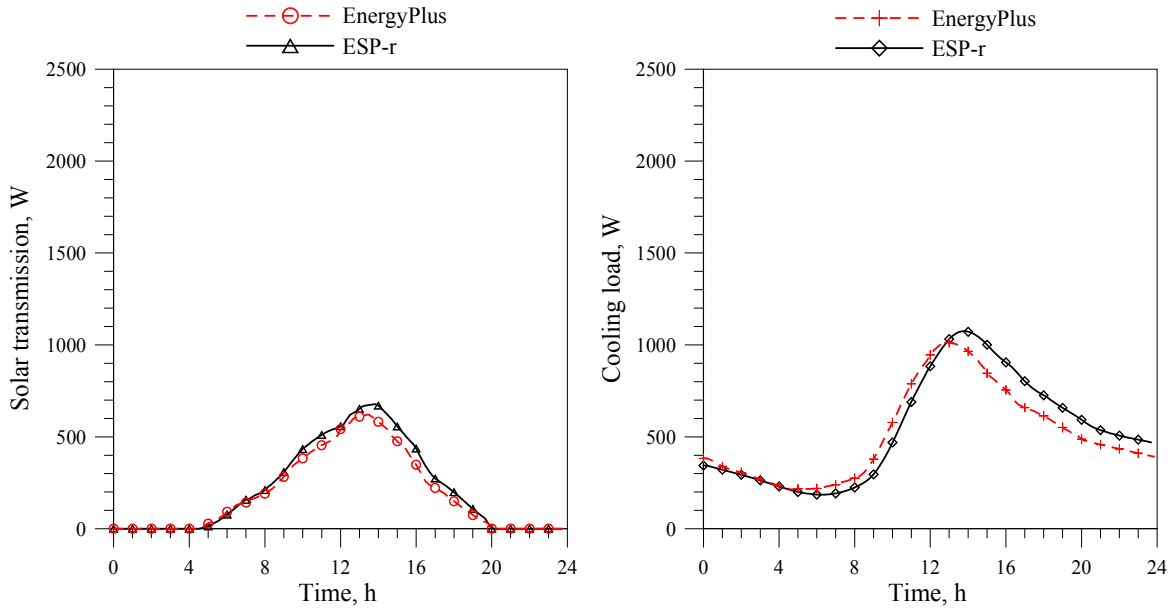

a)

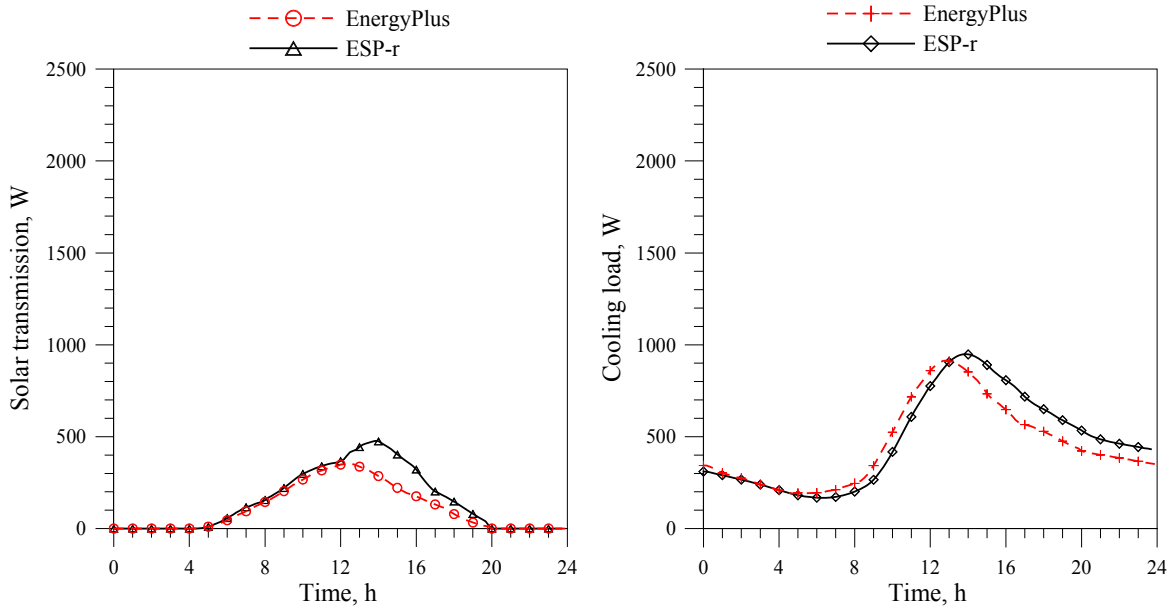

b)

Figure 5.15: Hourly solar transmission and cooling load for BETWEEN-GLASS blind (Case 4) with slat angle a) 0° and b) 45°. Simulation results for Toronto, July 7 CWEC data.

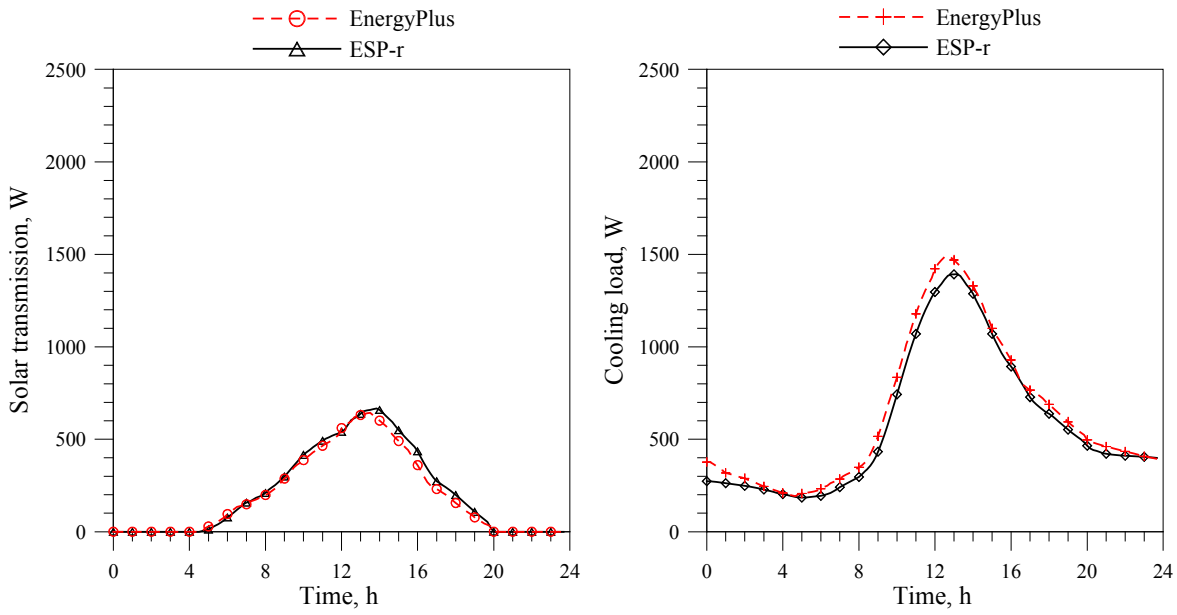

a)

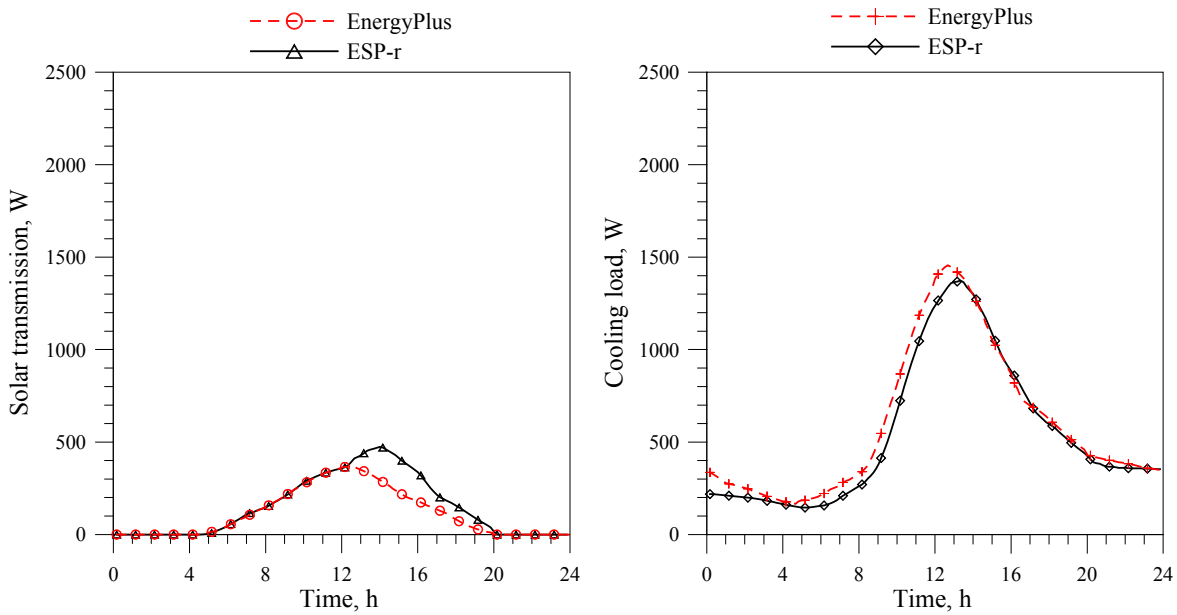

b)

Figure 5.16: Hourly solar transmission and cooling load for INDOOR blind (Case 5) with slat angle a) 0° and b) 45°. Simulation results for Toronto, July 7 CWEC data.

5.3.3 Discussion

On July 7 in Toronto (latitude 43.67deg), the sun's position relative to the south window is such that the blind with horizontal slats at 0° or 45° blocks any direct beam radiation from entering the interior zone. Since both EnergyPlus and ESP-r CFC models treat slats as perfectly diffusing, the transmitted solar gain is composed of scattered beam radiation resulting from slat inter-reflections, as well as transmitted and reflected diffuse radiation. In both models the transmitted beam-diffuse and diffuse-diffuse flux is uniformly distributed to all internal surfaces, excluding the south wall and window surfaces. In the unshaded double glazed window case, both EnergyPlus and ESP-r were set to treat the transmitted beam flux as incident on the floor surface. Any reflected radiation by the floor is assumed to be diffuse. Potential discrepancies associated with interior solar processing of beam fluxes were eliminated for the slat-blind cases as the slats blocked the beam radiation in all cases.

Figure 5.11 shows a plot of the hourly beam and diffuse radiation values incident on the south window. The results from the two codes are in very good agreement. Given the good agreement in establishing the solar irradiance in EnergyPlus and ESP-r, the resolution of global solar radiation data from the climate file into vertical surface solar irradiance input may be ruled out as a significant source of discrepancy between the two models.

Fully Enclosed Test Cell

To quantify the relative impact of solar gain through the window and walls, Figure 5.12 shows the cooling load curves for a fully enclosed test cell without a window. These results clearly indicate the marginal effect of solar gain through the opaque wall sections on the interior conditions. The insulated envelope prevents the absorbed solar radiation on external opaque surfaces from reaching the interior via conduction and then to the indoor air via convection.

Conventional Double Glazing

The double glazing (Case 2) serves as a reference for the rest of the slat-blind model comparisons. The transmitted solar fluxes (Figure 5.13) peak at about 2000 W at 12:30 h solar time. The substantial glazing area of 10 m^2 results in a large cooling load which peaks at about 1300 W. The thermal mass of the interior walls causes the cooling load peak to lag the solar transmission

peak. The impact of the window on the loads can be seen by comparing the cooling load curve for the double glazing (Case2, Figure 5.13) and the case with no window (Case 1, Figure 5.12). It is evident that the addition of the south window accounts for most of the cooling load during sunlit hours. Even at night time the thermal lag resulting from the absorbed solar energy in the walls results in significant cooling demand. Some discrepancy in the cooling results is observed, most visible in the afternoon hours after the peak cooling load occurs. Since the solar irradiance and window solar transmission results are closely aligned for both codes, the interior heat balance in the thermal zone requires further scrutiny to account for the discrepancy.

Beausoleil-Morrison and Strachan (1999) conducted an investigation into the impact of convection model selection in building energy simulation codes and concluded that simulated building loads are especially sensitive to the convection algorithm when the convection regime is natural buoyancy driven flow, as is the case in the current study. The lag observed between the cooling load curves in Case 2 (Figure 5.13) may be attributed to the application of different interior surface convection algorithms in EnergyPlus and ESP-r. The different treatment of glass thermal capacity in the respective codes may also contribute to the lag.

Simulations were carried out to examine the sensitivity of the results with respect to changes in the interior surface convective algorithm and glass thermal capacity. To isolate the effect of convection model selection, the default ESP-r convection correlation, Alamdari & Hammond (1983), was replaced with the model by Walton (1983) used in EnergyPlus. To isolate the effect of thermal capacity, the glass thermal capacity in ESP-r was set to a very small number to correspond to the EnergyPlus treatment of glass layers. Four cases were considered for this analysis:

1) EnergyPlus Walton (1983)
    - The reference EnergyPlus case with the default Walton (1983) interior convection correlation
2) ESP-r Alamdari & Hammond (1983)
    - The reference ESP-r case with the default Alamdari & Hammond (1983) interior convection correlation

3) ESP-r Walton (1983)
    - The Walton (1983) interior convection correlation was hard coded into ESP-r to replace the default Alamdari & Hammond (1983) correlation
4) ESP-r Walton (1983), no capacity
    - In addition to replacing the interior convection model, thermal capacity of the glass was removed

A snapshot of the simulation results for the above four cases is presented in Figure 5.17, where the result set is clipped in order to magnify the differences. Replacing the Alamdari and Hammond (1983) model with the Walton (1983) model in ESP-r results in a significant reduction in the peak cooling load, and falls more closely in line with the EnergyPlus curve. The removal of thermal mass from glass layers in ESP-r results in a slight horizontal shift to the left in cooling load since the thermal lag is reduced.

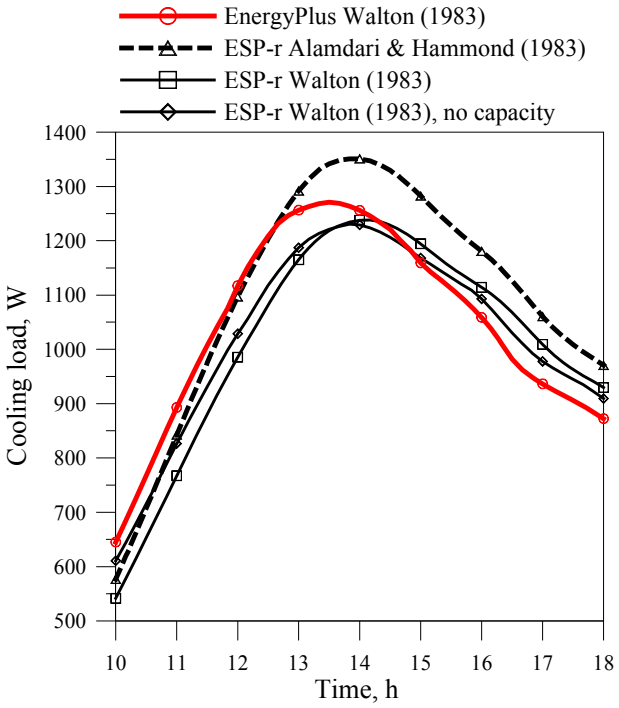

Figure 5.17: Hourly cooling load results for comparison of interior surface convection models. Simulation results for Toronto, July 7 CWEC data.

Although the selection of the interior convection model is shown to have a significant impact on the results, a lag between ESP-r and EnergyPlus cooling loads is still present. A more thorough investigation into the heat balance approach of both codes could unearth more reasons

for the observed differences in results, however, that investigation was not warranted within the scope of this preliminary study.

Double Glazing with Blind

The solar optics of a window with a slat blind are highly dependent on the profile angle of the sun with respect to the blind as well as the blind slat angle. For the case of a blind in combination with a clear double glazing, the overall solar transmission is primarily dependent on the slat angle and not so much on the position of the blind within the glazing layers. However, since total solar gain consists of not only transmitted solar flux, but also convective and longwave radiative flux, the position of the blind has large implications on the resulting cooling load. The blind layer absorbs most of the solar radiation, therefore to obtain maximum benefit from shading, the blind should be placed on the outdoor side of the window. The absorbed solar energy can then be rejected to the environment instead of the indoor space.

The overall effect of adding a slat-type blind within a window can be observed by comparing Figures 5.14, 5.15, and 5.16 for outdoor, between-glass and indoor blind cases, respectively. The first thing to notice is that irrespective of blind position, the solar transmission does not change much for a given slat angle. However, a clear discrepancy between EnergyPlus and ESP-r results is visible for solar transmission for all blind configruations after 12:00 h when slats are at 45°. This discrepancy is the result of two different treatments of diffuse radiation incident on the window. EnergyPlus considers sky-diffuse and ground-diffuse components separately in the calculation of diffuse optical properties of the blind. ESP-r lumps the two components and considers incident diffuse radiation to be uniform across the hemisphere as seen by the vertical surface.

Chantrasrisalai and Fisher (2004) have compared the effect of diffuse radiation treatment on horizontal slat blind transmission. At the time of publication of their study, EnergyPlus treated incident solar diffuse radiation as uniform. In their study, comparisons were made between EnergyPlus and other models by Parmalee and Aubelle (1952) and Pfrommer et al. (1996), which considered the sky and ground components separately. The results, reproduced from (Chantrasrisalai and Fisher 2004), are summarized in Figure 5.18. Transmission for slats in the horizontal position (0° slat angle) is equal for all three models. As the slats are tilted towards the

sky (slats pointing upward), transmission for the sky component increases and decreases for the ground component. The two treatments yield considerably different transmittance values reaching a maximum difference at 30° slat angle.

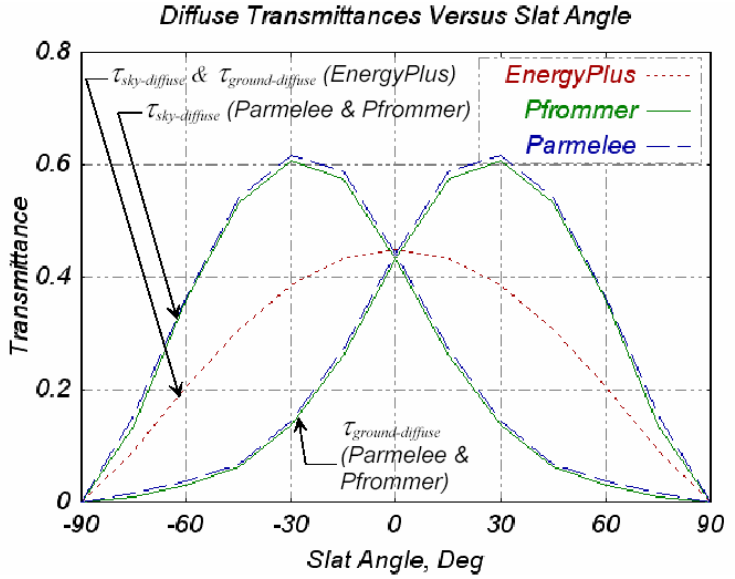

Figure 5.18: Effect of slat angle on diffuse transmittance(s) (for flat slat with zero thickness and slat reflectance of 0.5). Reproduced with permission from (Chantrasrisalai & Fisher 2004).

In the current analysis, the sky component of incident diffuse radiation (Figure 5.11 b) is seen to peak in mid afternoon. If the slats are tilted 45°, pointing towards the ground, the ground transmission is expected to be higher than the sky transmission. However, if the sky and ground components are lumped together, as they are in ESP-r, the sky component dominates the total incident diffuse radiation, resulting in a higher blind diffuse transmittance in mid afternoon, as seen in the ESP-r results. Thus, the treatment of incident diffuse radiation in the CFC implementation in ESP-r over-predicts the solar transmission for a 45° tilt compared to the EnergyPlus results. For a slat angle of –45°, ESP-r results would instead under-predict solar transmission.

The between-glass blind cooling load curves (Case 4, Figure 5.15) show a shift in the peak between EnergyPlus and ESP-r results, similar to the double glazing case (Case 2, Figure 5.13). The hemispherically uniform incident diffuse radiation treatment in ESP-r causes a slight increase in cooling load in mid-afternoon for the 45° slat tilt. In the indoor blind configuration (Case 5), convection occurs on both blind surfaces and the indoor glazing surface. Two different natural buoyancy convection models are used for the indoor blind treatment. EnergyPlus applies the ISO

15099 (2003) model based on a pressure balance approach, whereas the ESP-r CFC model is based on an approximate method developed by Wright et al. (2008), also described in appendix A. The EnergyPlus cooling load results for the indoor blind case are slightly higher compared to ESP-r (Figure 5.16), but compare well to each other.

Cooling Energy and Peak Load

Absolute differences in total cooling energy between the two codes for the outdoor and between-glass and indoor blind configurations (Table 5.3) are consistent with the reference double glazing case. Absolute differences in peak cooling load results (Table 5.3) show the same trend. The highest discrepancy is observed for the indoor blind (Case 5), although the magnitude of absolute differences for all cases is small relative to the peak values.

Of note are the relative cooling energy and peak load reductions due to the presence of a slat blind when compared to the reference double glazing case. Table 5.4 summarizes the findings. The reduction values are based on the percent difference between the reference double glazing case and each blind configuration. Both total cooling energy and peak loads are significantly reduced as the blind is placed towards the outdoors. The presence of an outdoor blind is seen to reduce the total cooling energy by up to about 60% and peak cooling load by more than 65%. The between-glass blind case shows a reduction up to 30% in total cooling energy and about 27% in peak cooling load. Although the cooling load plots (Figure 5.16) for the indoor blind case are closely aligned with respect to each other, with respect to the double glazing results the difference between EnergyPlus and ESP-r cooling energy and peak load reductions are as much as 11%. Figure 5.18 shows the double glazing and indoor blind results plotted on the same graph, where differences relative to the double glazing case can be seen more clearly. The relative impact of adding the indoor blind on the peak cooling load is higher for EnergyPlus results. For both result sets, the indoor blind decreases the total cooling energy over the 24 h period, but increases the cooling peak. The indoor blind effectively acts as a solar absorber and readily converts much of the absorbed energy into convective cooling load. The peak cooling load for an indoor blind also occurs at the peak solar transmission, as the blind has little or no thermal capacity. The presence of an indoor blind can therefore cause the cooling peak to coincide with the solar peak, placing even more demand on the cooling system than in the double glazing case.

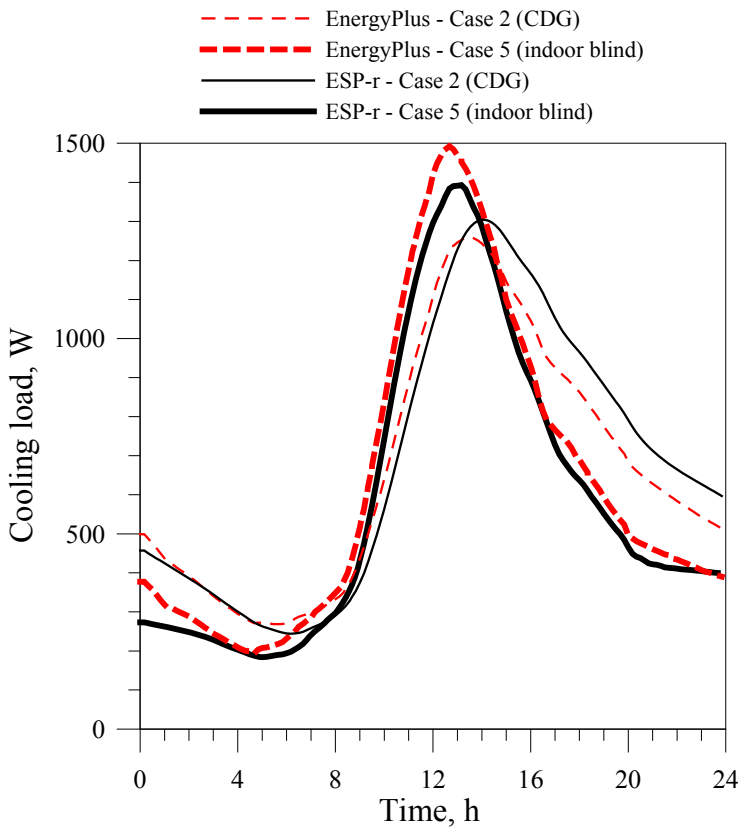

Figure 5.19: Hourly cooling load for Case 2 (CDG) and Case 5 (indoor blind). Simulation results for Toronto, July 7 CWEC data.

Table 5.4: Cooling energy and peak load reductions of slat-blind cases relative to the reference double glazing

		% Total Cooling Energy Reduction		% Peak Cooling Load Reduction	
Case	Slat angle (°)	EnergyPlus	ESP-r	EnergyPlus	ESP-r
Outdoor blind	0	45.9	51.3	55.0	57.4
	45	57.9	61.9	68.3	66.5
Between-glass blind	0	22.2	21.3	19.6	17.6
	45	31.2	29.7	27.6	27.3
Indoor blind	0	4.7	15.0	-18.5	-6.8
	45	10.8	20.6	-15.6	-5.3

5.3.4 Conclusion

Overall, the comparison of EnergyPlus 2.0 and ESP-r CFC slat blind model results are encouraging. Hourly cooling loads for the outdoor, between-glass and indoor blind cases are in good agreement, showing absolute differences in the same range as the reference double glazing

case. The indoor blind results showed slightly higher discrepancies, an expected result given the approximate nature of the respective indoor blind convection models of the two codes.

Differences in solar transmission are attributed to the treatment of incident diffuse radiation. EnergPlus 2.0 considers both ground and sky components, whereas the CFC model treats incident diffuse radiation as uniform across the hemisphere as seen by the vertical surface.

The trends in cooling energy and peak cooling load reduction clearly underline the importance of blind position within the multi-layer array. It was shown that an outdoor blind reduced the total cooling energy by 60% and peak cooling load by more than 65%, relative to a conventional double glazing. A between glass blind showed a reduction of 30% in total cooling energy and 27% in peak cooling load. The indoor blind actually increased the peak cooling load in both EnergyPlus and ESP-r results. In all simulation cases, variations in the results between the two codes may be attributed primarily to the interior surface convection models and to a lesser degree, the thermal capacity treatment of glazings/shades and the incident diffuse radiation treatment. Some discrepancy still remained and could not be explained for cases where the differences in interior surface convection treatment and thermal capacity were accounted for. A more thorough investigation in deconstructing the solar/thermal models of the two codes is recommended.

5.4 CFC Shading Control

The Complex Fenestration Construction is ideally suited for dynamic control of glazing/shading system properties. It is designed with solar and thermal algorithms based on glazing/shading layer and gas gap properties that are determined at each time step. These include:

- Off-normal solar optical properties of glazing layers based on their normal incidence input values
- Spatially averaged solar optical and longwave radiative properties of slat-type blind layers based on slat geometry and slat material properties
- Temperature dependent fill gas properties such as density, conductivity, heat capacity and viscosity

Longwave radiation exchange for intra-constructional layers, and layers that 'see' the outdoors or indoors, is determined at each time step, and is a function of glazing/shading layer temperatures, blind layer geometry, interior surface temperatures and exterior mean radiant temperature. Convective resistance, or, inversely, convective heat transfer coefficients in gas gaps are determined at each time-step based on fill gas properties, and temperature difference across the gap.

Manipulation of individual glazing/shading layer solar optical properties can be achieved easily by changing the normal optical properties of the glazing, or changing the slat angle of the blind for some prescribed condition. The ability to resolve convective resistances on a time-step basis within the CFC opens the possibility for integrating an air-flow network for vented window cavities.

Although control strategies have not been explored in the scope of the work, a facility for further implementation of dynamic slat control has been created in the source code (see Appendix E). A simple subroutine determines a 'new' slat angle at each time step based on some prescribed condition.

Currently, one of the limitations of the CFC type is that it is not linked to the daylighting algorithms within ESP-r. One of the underlying assumptions in the treatment of slat-type blinds in the CFC model is that the slat reflects diffusely. Based on this assumption, the implication for slat-blind daylight control is that if the blind is positioned such that it blocks beam radiation, any radiation entering the indoor space is considered uniformly diffuse. This is a good assumption for solar energy distribution and load calculations, but may be insufficient for detailed daylight simulations in programs such as Radiance. If the slats are positioned such that direct beam transmission exists, the directionality is not lost. The daylight factor method (see Clarke 2001) used in ESP-r could easily be extended to interact with the CFC type based on the direct and diffuse visible transmittance of the glazing/shading system.

5.4.1 Slat Control – An Illustrative Example

As an illustrative example, this section describes a simple slat control scheme and the resulting implications for cooling load when controlling solar gain with an indoor or outdoor blind.

Two simulations were carried out, employing the CFC type within the test cell used in Sections 5.2 and 5.3. To emphasize the effect of slat angle on transmission and cooling load, the test cell was rotated 90° clockwise, positioning the window toward the west. During the simulation period (July 7 in Toronto) incidence angles in the afternoon hours on the vertical west façade are much smaller than incidence angles on the vertical south façade near solar noon. The solar altitude angle falls below 30° after 4:30 h solar time on July 7. Direct beam radiation is thus closer to the normal of the window in late afternoon on the west façade, posing a much greater risk of summertime overheating and emphasizing the usefulness of a slat-type shading device.

Two CFC configurations were simulated, a clear double glazing with outdoor blind and a clear double glazing with an indoor blind, Case 3 and Case 5 from Section 5.3, respectively. The slat control strategy consisted of a simple schedule to close the blinds at 17:00 h until 19:00 h. During this period, the slat angle was set to 80°. At any other time outside this period, the slat angle was set to –30° (slats pointing up to the sky). The control algorithm was hard coded into the CFC shading control subroutine (see Appendix E).

The results for cooling load and solar transmission for the outdoor and indoor blind simulations with the imposed control scheme are shown in Figure 5.20. The two hour period during which the blinds are closed is clearly visible in the solar transmission profile. During this period, the impact of the shade on the cooling load is quite different for the two configurations. At 17:00 h, the cooling load for the outdoor blind case drops immediately and falls until the blinds are opened again at 19:00 h, where a slight peak can be seen. For the indoor blind case, the cooling load continues to rise after 17:00 h, and peaks around 2700 W, more than three times that of the corresponding outdoor blind cooling load during the closed blind control period. The indoor blind in this case does not reduce the peak gain, as most of the absorbed energy is released through convection to the room air.

This simple example provides insight into the possible applications of the CFC type to analyze peak cooling load reduction for a prescribed glazing/shading configuration. The development of control schemes for the CFC and the implementation of these into the graphical

user interface is a crucial next step to providing the user community with a valuable tool for dynamic shading analysis within ESP-r.

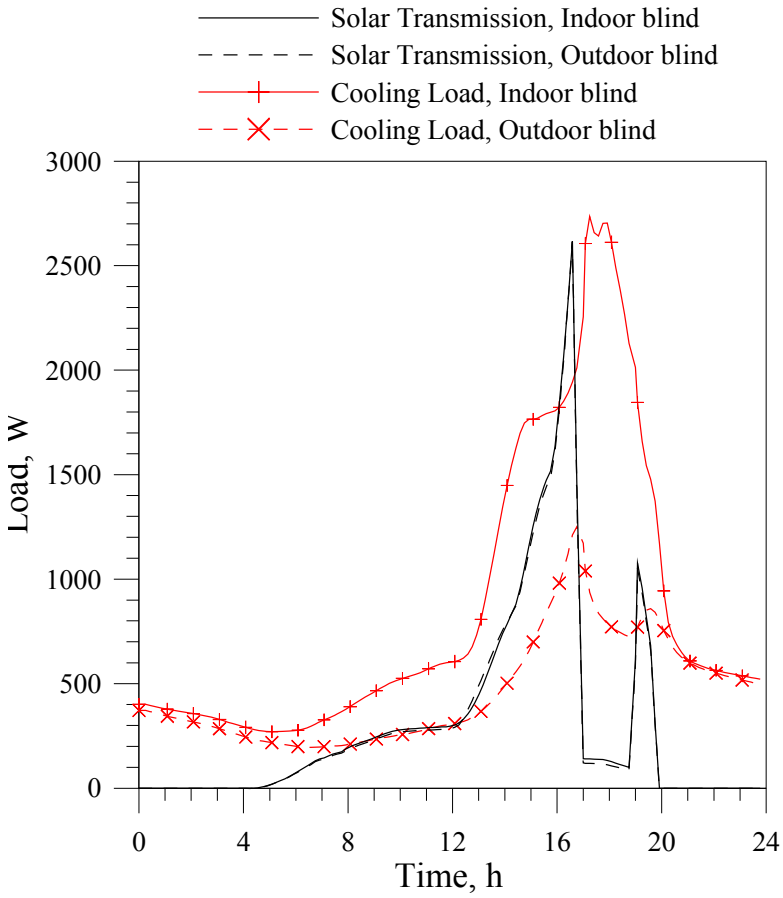

Figure 5.20: Hourly solar transmission and cooling load for outdoor and indoor slat blind with simple control scheme. Simulation results for Toronto, July 7 CWEC data.

Chapter 6

Conclusions and Recommendations

The successful implementation of the AGSL shading models into ESP-r in the form of the Complex Fenestration Construction has been demonstrated. The Complex Fenestration Construction was developed with emphasis on glazing/shading system generality to allow for specification of any combination of shading/glazing layers. In conjunction with the glazing/shading layer editor, GSLedit, developed concurrently at UW, the generation of input files for CFC types relies on the straightforward characterization of the fenestration system input parameters.

The results of the comparison tests for glazing modeling using Transparent Multi-layer Constructions (TMCs) and Complex Fenestration Constructions (CFCs) in ESP-r showed very good agreement. Thus, a by product of the work is an alternate facility for modeling glazings in ESP-r, taking advantage of the GSLedit program which can be used to select various glazing layers based on an extensive database, as well as fill gases and mixtures.

The slat-type blind solar and thermal models developed at UW's Advanced Glazing Systems Laboratory were validated during previous studies. Comparison of slat-type blind models between EnergyPlus 2.0 and the CFC type in ESP-r has shown encouraging results, further giving confidence to the models and implementation strategy in ESP-r. Further testing and comparison to simulated results is recommended. A good start is to conduct simulations in ESP-r by replicating the test cell conditions of previous work at the Swiss Federal Laboratories for Materials Testing and Research (EMPA) used for experimental validation of slat-type blinds and other shading devices. Additional research and empirical testing is also recommended to assess the applicability of the indoor blind convection model used in the CFC type.

The dynamic control of slat blinds on a time-step basis was shown as a proof of concept of the capability of the CFC models, however, control algorithms were not developed in this work. In

its current state, the CFC type can readily be used to model glazings with or without a slat-type blind in any combination, but control can only be imposed by modifying the source code.

In order to gain acceptance amongst the users of ESP-r, the CFC models must be extended to include dynamic control strategies of slat-type blinds as well as the treatment of other shading layers such as drapes, roller blinds and screens. In addition, coupling the CFC type with daylighting models within ESP-r would enable the accurate simulation of luminance control strategies. Lastly, an extension of the current diffuse insolation model to treat the sky and ground components separately would improve the prediction of the solar model somewhat.

With these enhancements, it is anticipated that such a comprehensive tool will be of significant value to building design practitioners, promoting the straightforward analysis of shading attachments in buildings designed for sustainability and energy efficiency.

References

ASHRAE (2001) ASHRAE Handbook – Fundamentals.

Alamdari, F., Hammond, G.P. (1983) 'Improved data correlations for buoyancy-driven convection in rooms', *Building Services Engineering Research and Technology* 4(3), pp. 106-112.

Beausoleil-Morrison I. and Strachan P. (1999) 'On the Significance of Modeling Internal Surface Convection in Dynamic Whole-Building Simulation Programs', *ASHRAE Transactions* 105 (2).

Beausoleil-Morrison, I. (2000) 'The adaptive coupling of heat and air flow modelling within dynamic whole-building simulation', Glasgow, University of Strathclyde, PhD thesis.

Clarke, J.A. (2001) *Energy Simulation in Building Design* , *2nd Edition*, Oxford, Butterworth-Heinemann.

Chantrasrisalai, C., Fisher, D.E. (2004), 'Comparative Analysis of One-Dimensional Slat-Type Blind Models', *Proceedings of the SimBuild 2004 Conference*, Boulder, Colorado. IBPSA-USA.

Collins, M.R. (2004) 'Convective heat transfer coefficients from an internal window surface and adjacent sunlit Venetian blind', *Energy and Buildings* 36, pp. 309-318.

Collins, M.R., Wright, J.L. (2006) 'Calculating Center-Glass Performance Indices of Windows with a Diathermanous Layer', *ASHRAE Transactions*, Vol. 112, Pt. 2. pp. 22-29.

Collins, M.R., Tasnim, S.H., and Wright, J.L. (2008) 'Determination of Convective Heat Transfer for Glazing Systems with Between-the-Glass Louvered Shades', *International Journal of Heat and Mass Transfer*, Vol. 51, pp. 2742-2751.

Collins, M.R. (2008), Personal correspondence, October 24.

Crawley, D.B., Hand, J.W., Kummert, M., Griffith, B.T. (2005), 'Contrasting the Capabilities of Building Energy Performance Simulation Programs', A Joint Report by DOE (U.S. Department of Energy), Washington, DC, USA; Univeristy of Strathclyde, Glasgow, Scotland; University of Wisconsin, Madison, Wisconsin, USA; National Renewable Energy Laboratory, Golden, Colorado, USA.

Duffie, J.A., Beckman, W.A. (1980), *Solar Engineering of Thermal Processes*, New York, John Wiley.

EN 410 (1998), Glass in buildings - Determination of luminous and solar characteristics of glazing, EN Standard.

EN 673 (1997), Glass in buildings - Determination of thermal transmittance (U-value) - Calculation method, EN Standard.

EN 13363 -2 E (2004) Solar protection devices combined with glazing - Calculation of total solar energy transmittance and light transmittance - Part 2: Detailed calculation method, EN Standard.

EN ISO 10077-1 (2000) Thermal performance of windows, doors and shutters - Calculation of thermal transmittance - Part 1: Simplified method, EN/ISO Standard.

EnergyPlus 2.2.0 (2008), Building Energy Simulation Code, DOE (U.S. Department of Energy), **<**http://apps1.eere.energy.gov/buildings/energyplus>

EnergyPlus Engineering Reference (2008) DOE (U.S. Department of Energy).

ESP-r v11.5 (2008), Building Energy Simulation Code, University of Strathclyde, Glasgow, Available from: <http://www.esru.strath.ac.uk>

Finlayson, E.U., Arasteh, D.K., Huizenga, C., Rubin, M.D., and Reilly, M.S. (1993) 'WINDOW 4.0: documentation of calculation procedures', Lawrence Berkley Laboratory Report LBL-33946, University of California Report UC-350.

Furler, R.A. (1991) 'Angular dependence of optical properties of homogeneous glasses', *ASHRAE Transactions,* Vol. 97(2).

Gebhart, B. (1959) 'A New Method for Calculating Radiant Exchanges', *ASHRAE Transactions*, Vol. 65, pp. 321-332.

Hellstrom, B., Kvist, H., Hakansson, H., Bulow-Hube, H. (2007) 'Description of ParaSol v3.0 and comparison with measurements', *Energy and Buildings* 39, pp. 279-283.

Hollands, K.G.T., Wright, J.L., Granqvist, C.G. (2001) *Solar Energy – The State of the Art – ISES Position Papers,* James & James Ltd., Ch. 2 (Glazings and Coatings), pp. 29-107.

Hollands, K.G.T. (2004) *Thermal Radiation Fundamentals*, New York, Begell House, Inc., Ch. 16.

Huang, N.Y.T., Wright, J.L., Collins, M.R. (2006) 'Thermal Resistance of a Window with an Enclosed Venetian Blind: Guarded Heater Plate Measurements', *ASHRAE Transactions*, Vol. 112, Pt. 2. pp. 13-21.

ISO 15099 (2003) Thermal Performances of Windows, Doors, and Shading Devices—Detailed Calculations, ISO Standard.

ISO 6946 (1996) Building components and building elements - Thermal resistance and thermal transmittance - Calculation method, ISO Standard.

Karlsson, J., Rubin, M., Roos, A. (2001) 'Evaluation of predictive models for the angle-dependent total solar energy transmittance of glazing materials', *Solar Energy,* Vo. 71(1), pp. 23-31.

Kotey, N.A., Collins, M.R., Wright, J.L., and Jiang, T. (2008) 'A Simplified Method For Calculating The Effective Solar Optical Properties Of A Venetian Blind Layer For Building Energy Simulation', *ASME Journal of Solar Energy Engineering*, In review.

Kotey, N.A., Wright, J.L., Barnaby, C.S. Collins, M.R. (2009) 'Solar Gain Through Windows with Shading Devices: Simulation Versus Measurement', *ASHRAE Transactions*, Vol. 115, Pt. 2, In Review.

LBNL (2008) International Glazing Database (IGDB), <http://windows.lbl.gov/materials/igdb/>

Lomanowski, B.A., Wright, J.L. (2007) 'Heat Transfer Analysis of Windows with Venetian Blinds: A Comparative Study', *Proceedings of the 32nd Conference of the Solar Energy Society of Canada (SESCI) and 2nd Conference of the Solar Building Research Network (SBRN)*, Calgary, Alberta.

Loutzenhiser, P.G., Manz, H., Strachan, P.A., Felsmann, C., Frank, T., Maxwell, G.M., Oelhafen, P. (2006) 'An empirical validation of solar gain models found in building energy simulation programs', *HVAC&R Research* 12, pp.1097–1116.

Loutzenhiser, P.G., Manz, H., Felsmann, C., Strachan, P.A., Maxwell, G.M. (2007) 'An empirical validation of modeling solar gain through a glazing unit with external and internal shading screens', *Applied Thermal Engineering* 27, pp.528–538.

Loutzenhiser, P.G., Manz, H., Carl, S., Simmler, H., Maxwell, G.M. (2008) 'Empirical validations of solar gain models for a glazing unit with exterior and interior blind assemblies', *Energy and Buildings* 40, pp.330–340.

Lstiburek, J.W. (2008) 'Energy Flow Across Enclosures', *ASHRAE Journal*, Vol. 50, September.

Manz, H., Loutzenhiser, P., Frank, T., Strachan, P.A., Bundi, R., Maxwell, G.M. (2006) 'Series of experiments for empirical validation of solar gain modeling in building energy simulation codes—experimental setup, test cell characterization, specifications and uncertainty analysis', *Building and Environment* 41, pp. 1784–1797.

McQuiston, F., Parker, J., Spitler, J. (2005) *Heating, Ventilating, and Air Conditioning, 6th Edition*, John Wiley & Sons, Inc.

Milburn, D. (1994) 'Measurement of Solar Transmittance of Advanced Glazing Materials', Ph.D. Thesis, Department of Mechanical Engineering. Waterloo, ON: University of Waterloo.

Mitchell, R., Kohler, C., Klems, J., Rubin, M., Arasteh, D., Huizenga, C., Yu, T., Curcija, D., (2008) 'WINDOW 6.2/THERM 6.2 Research Version User Manual', Program Description LBNL-941.

Naylor, D., Shahid, H., Harrison, S.J., Oosthuizen, P.H. (2006) 'A simplified method for modeling the effect of blinds on window thermal performance', *International Journal of Energy Research*, Vol. 30, pp. 471-488.

NFRC (2001), NFRC 100:2001 Procedure for Determining Fenestration Product U-factors, National Fenestration Research Council, Technical Document.

Oosthuizen, P.H., Sun, L., Harrison, S.J., Naylor, D., Collins, M. (2005) 'The Effect of Coverings on Heat Transfer from a Window to a Room', *Heat Transfer Engineering*, Vol. 26(5), pp. 57-65.

Parasol v4.1 (2008) <http://www.parasol.se>

Parmelee, G. V., Aubele, W. W. (1952) 'The shading of sunlit glass: an analysis of the effect of uniformly spaced flat opaque slats', *ASHVE Transactions*, Vol. 58, pp. 377-398.

Perez, R. Ineichen, P., Seals, R., Michalsky, J., Stewart, R. (1990) 'Modeling daylight availability and irradiance components from direct and global irradiance', *Solar Energy* 44, pp.271–289.

Pfrommer, P., Lomas, K.J., Kupke, C. (1996) 'Solar Radiation Transport through Slat-Type Blinds: a New Model and its Application for Thermal Simulation of Buildings', *Solar Energy*, Vol. 57, No. 2, pp. 77-91.

Plus Energy House in Thening, Austria (2001)
<http://www.iea-shc.org/task28/publications /Austria_Thening.pdf>

Riverdale Net Zero Home (2008) <http://www.riverdalenetzero.ca>

Rosenfeld, J.L.J., Platzer, W.J., Van Dijk, H., and Maccari, A. (2000) 'Modeling the Optical and Thermal Properties of Complex Glazing: Overview of Recent Developments', *Solar Energy*, Vol. 69 Supplement, No. 1-6, pp.1-13.

Simmler, H., Fischer, U., and Winkelmann, F. (1996) 'Solar-Thermal Window Blind Model for DOE-2', Lawrence Berkeley National Laboratory, Simulation Research Group internal report, (unpublished).

Shahid, H., Naylor, D. (2005) 'Energy performance assessment of a window with a horizontal Venetian blind', *Energy and Buildings*, Vol.37, pp. 836-843.

Shewen, E., Hollands, K.G.T., Raithby, G.D. (1996) 'Heat Transfer by Natural Convection Across a Vertical Cavity of Large Aspect Ratio', *Journal of Heat Transfer*, Vol. 118, pp. 993-995.

TARCOG (2006) 'Mathematical models for calculation of thermal performance of glazing systems with or without shading devices', Technical Report, Carli. Inc.

Walton, G. N. (1983) Thermal Analysis Research Program Reference Manual, NBSSIR 83-2655, National Bureau of Standards.

WINDOW 6.2 and THERM 6.2 (2008)
<http://windows.lbl.gov/software/window/6/index.html>

WIS 3.0.1 (2006) <http://www.windat.org/wis/html/index.html>

Wright, J.L. (2008) 'Calculating Centre-Glass Performance Indices of Glazing Systems with Shading Devices', *ASHRAE Transactions*, Vol. 114, Pt. 2

Wright, J.L. (1998) 'Calculating Center-Glass Performance Indices of Windows', *ASHRAE Transactions,* Vol. 1004, 1B, SF-98-12-4, pp. 1230-1241.

Wright, J.L. (1995), 'Summary and Comparison of Methods to Calculate Solar Heat Gain', *ASHRAE Transactions,* Vol. 101, 2, CH95-8-2, pp. 1-17.

Wright, J.L., Kotey, N.A. (2006) 'Solar Absorption by Each Element in a Glazing/Shading Layer Array', *ASHRAE Transactions*, Vol. 112, Pt. 2. pp. 3-12.

Wright, J.L., Collins, M.R., Kotey, N.A., Barnaby, C.S. (2009) 'Improving Cooling Load Calculations for Fenestration with Shading Devices', ASHRAE Report 1311-RP.

Wright, J.L., McGowan, A. (1999) 'Calculating the Solar Heat Gain of Window Frames', *ASHRAE Transactions*, Vol. 105, pp. 1011-1021.

Yahoda, D.S., Wright, J.L. (2005) 'Methods for Calculating the Effective Solar-Optical Properties of a Venetian Blind Layer', *ASHRAE Transactions*, Vol. 111, Pt. 1, pp. 572-586.

Appendix A:
Convection Heat Transfer Coefficients at Surfaces Exposed to the Environment[1]

Figure A.1 shows the three-resistor network used to model convective heat transfer at surfaces exposed to the environment. The freestream air temperature is T_{air}, the temperature of the shading attachment is T_{shade} and the temperature of the exposed window surface is T_{glass}. It is necessary to evaluate the three heat transfer coefficients associated with the three resistors. More discussion of this network can be found in (Wright 2008), particularly discussion of jump resistors (e.g., $R_{jump}=(Ah_{g-a})^{-1}$).

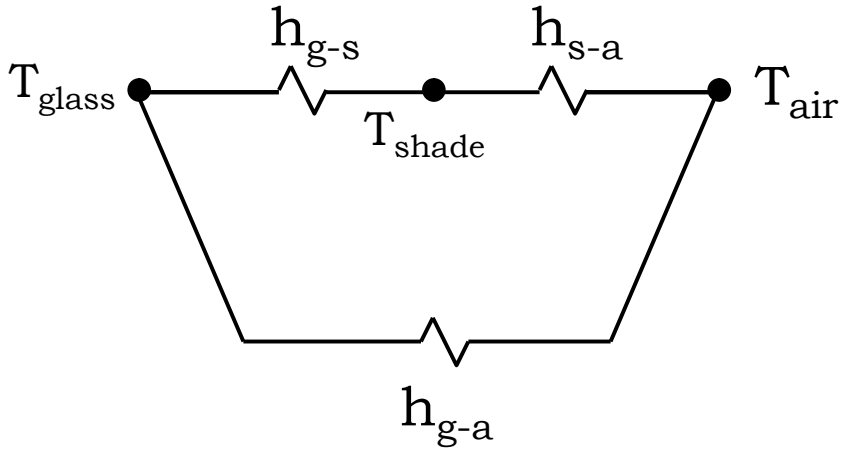

Figure A.1: Three-resistor network used to model convective heat transfer at surfaces exposed to the environment.

The value of h_{g-s} is estimated by assuming that the airflow between the glass and shade is laminar and for the most part parallel to the glass surface.

[1] Contents reproduced with author's permission from (Wright, Collins, Kotey and Barnaby 2008).

$$h_{g\text{-}s} = \frac{k_{air}}{b} \qquad \text{(A.1)}$$

where k_{air} is the thermal conductivity of air and b is the spacing between the glass and shading layers. In most instances, when the shading attachment is spaced well away from the window (b is large), $h_{g\text{-}s}$ will be small and its influence will be unimportant.

To retain generality the other two heat transfer coefficients are evaluated by starting with a reference convective heat transfer coefficient, h_c, that is supplied by the user (i.e., the calling routine of the building simulation program). The value of h_c can be specified to represent, for example, natural convection ($h_c \approx 3.5 \frac{W}{m^2K}$) or forced convection ($h_c \approx 20 \frac{W}{m^2K}$).

Next, the heat transfer coefficients for layer surfaces exposed to the air can be estimated by imposing known limits for extreme values of the spacing, b. When b is large the convective heat transfer at one layer will not be influenced by the presence of the other layer so $h_{g\text{-}a} = h_c$ and $h_{s\text{-}a} = 2\,h_c$. When b approaches zero it can be seen that the shading layer prevents the air from gaining access to the glass, $h_{g\text{-}a} = 0$, and only one side of the shading layer is exposed, $h_{s\text{-}a} = h_c$. A decaying exponential function was used to apply a smooth transition between the known limits, with respect to spacing, while noting that the influence of b should disappear as b becomes large. This transition was scaled by assuming that the boundary layers at the glass and shading layer surfaces will not interfere with each other once b exceeds $0.1\ m$ (4 inches). See Equations A.2 and A.3 as well as Figure A.2.

$$h_{g\text{-}a} = h_c\left(1 - \exp\left(-4.6\frac{b}{0.1}\right)\right) \quad [b \text{ in meters}] \qquad \text{(A.2)}$$

$$h_{s\text{-}a} = h_c\left(2 - \exp\left(-4.6\frac{b}{0.1}\right)\right) \quad [b \text{ in meters}] \qquad \text{(A.3)}$$

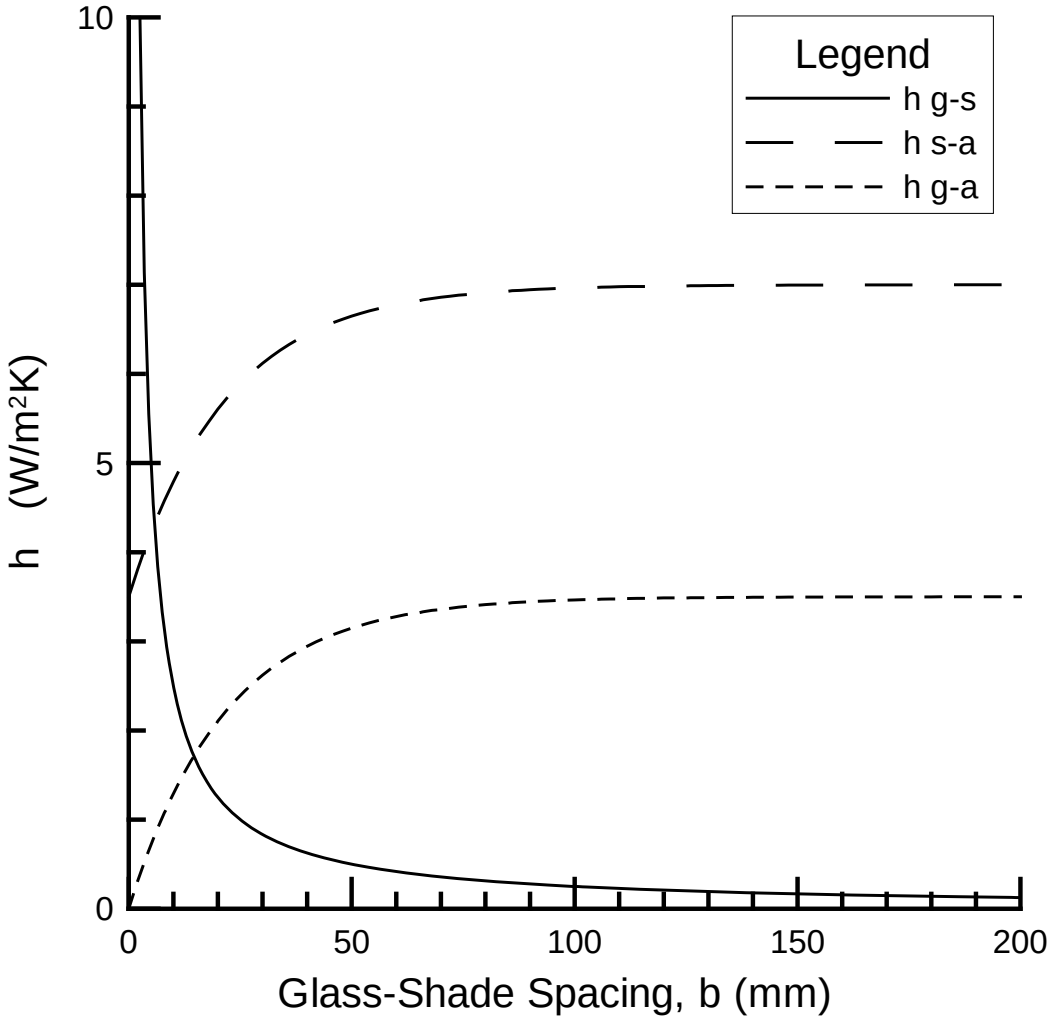

Figure A.2: Convective heat transfer coefficients as functions of window/shading layer spacing, b, with $h_c \approx 3.5 \frac{W}{m^2 K}$.

One additional adjustment is made for horizontal venetian blinds. It has been noted, on the basis of numerical simulation and interferometry (Collins 2008), that buoyancy will pump an appreciable amount of air through the shading layer when the slats are at any angle other than fully open (slat angle = $\varphi = 0$) or fully closed. Therefore, a factor is calculated as a function of slat angle and applied to augment $h_{s\text{-}a}$ by as much as 20%. See Equation A.4.

$$h_{s\text{-}a} = h_c \left(2 - \exp\left(-4.6 \frac{b}{0.1} \right) \right) \cdot \left(1 + 0.2 \left| \sin(2\varphi) \right| \right) \quad \text{[b in meters]} \qquad \text{(A.4)}$$

The maximum value of this factor, 20%, was established by a hand calculation comparing convective heat transfer from a single sloped slat to heat transfer from a large, vertical surface - both in still air.

Equations A.1 through A.3 are also applied for unsealed shading layers placed on the outdoor side of the window. In this case, it is likely that h_c will be specified to represent forced convection.

Note that Equations A.1 through A.4 are applied in the CFC models by interpreting the gap spacing, b, as an effective gap spacing when a venetian blind is adjacent to the gap. In this case the convective heat transfer coefficients are evaluated as if the venetian blind slats were shortened by 30%. The gap spacing and effective gap spacing are both determined as a function of slat angle and are updated as needed. This model for effective gap spacing (Huang, Wright and Collins 2006) was developed for the case of a venetian blind located in a glazing cavity and is applied in the CFC model for venetian blinds attached at the exposed window surface because much of the reasoning related to fill gas or air flow patterns is assumed to apply in both cases. The use of effective gap spacing will have very little influence except for the situation where a venetian blind is placed very close to the glass.

It is also worth noting that each of the resistors shown in Figure A.1 exists in parallel with a resistor that applies to radiant heat transfer. For the case of natural convection the radiant mode of heat transfer will be dominant, largely because of the very high probability that the emissivity of each component will be high.

Appendix B:
Off-Normal Solar Property Adjustment for Glazing Layers[2]

The known value of transmittance at normal incidence, $\tau(\theta = 0)$, is converted to the off-normal transmittance, $\tau(\theta)$, using the ratio R_τ.

$$\tau(\theta) = R_\tau \cdot \tau(\theta = 0) \qquad \text{(B.1)}$$

Similarly the known values of front and back surface reflectance at normal incidence, $\rho_f(\theta = 0)$ and $\rho_b(\theta = 0)$, are converted to off-normal reflectance values, $\rho_f(\theta)$ and $.\rho_b(\theta)$. Omitting the f and b subscripts for convenience,

$$1 - \rho(\theta) = R_\rho \cdot (1 - \rho(\theta = 0)) \qquad \text{(B.2)}$$

The CFC models estimate the off-normal solar properties of an uncoated glazing layer by duplicating the off-normal characteristics of a piece of uncoated glass. This reference glass has a refractive index of n=1.526 and its extinction coefficient-thickness product is KL=0.0771. These properties correspond to a 3 mm thick layer of common window glass, solar transmittance $\tau_{f,bb}(\theta = 0) = \tau_{b,bb}(\theta = 0) \approx 0.85$. Similarly, the off-normal solar properties of a coated glazing layer are estimated by duplicating the off-normal characteristics of a piece of bronze glass. This reference glass has a refractive index of n=1.7 and its extinction coefficient-thickness product is KL=0.302. These properties correspond to a 3 mm thick layer of bronze glass, solar transmittance $\tau_{f,bb}(\theta = 0) = \tau_{b,bb}(\theta = 0) \approx 0.645$.

[2] Reproduced with modifications pertaining to CFC models with author's permission from (Wright, Collins and Barnaby 2008).

The optical properties of uncoated glazing layers, and therefore R_τ and R_ρ, can be calculated from theory using a combination of Fresnel equations, Snell's Law and the Stokes equations. Details can be found in most solar-engineering text books (e.g., Duffie and Beckman 1980).

When a beam of radiation encounters an interface between air and a different material some of the energy is reflected.

$$R_M = \frac{\tan^2(\theta - \theta')}{\tan^2(\theta + \theta')} \qquad \text{(B.3)}$$

$$R_E = \frac{\sin^2(\theta - \theta')}{\sin^2(\theta + \theta')} \qquad \text{(B.4)}$$

where R_M and R_E are the interface reflectivities with respect to the magnetic and electric polarization components of the incident radiation and

$$\sin(\theta) = n \cdot \sin(\theta') \qquad \text{(B.5)}$$

The off-normal transmittance of the uncoated glazing layer is obtained by assuming the incident solar radiation to be randomly polarized.

$$\tau(\theta) = (\tau_M(\theta) + \tau_E(\theta))/2 \qquad \text{(B.6)}$$

where

$$\tau_M(\theta) = \frac{A(1 - R_M)^2}{1 - R_M^2 A^2} \qquad \tau_E(\theta) = \frac{A(1 - R_E)^2}{1 - R_E^2 A^2} \qquad \text{(B.7)}$$

and

$$A = \exp\left(\frac{KL}{\cos(\theta')}\right) \qquad \text{(B.8)}$$

Finally,

$$R_\tau = \frac{\tau(\theta)}{\tau(\theta = 0)} \qquad \text{(B.9)}$$

Note that at normal incidence, $\theta = \theta' = 0$, R_M and R_E are equal.

$$R = R_M = R_E = \left(\frac{n-1}{n+1}\right)^2 \qquad \text{(B.10)}$$

A similar calculation is used to determine the ratio of off-normal versus normal reflectance of the reference glass.

$$R_\rho = \frac{1-\rho(\theta)}{1-\rho(\theta = 0)} \qquad \text{(B.11)}$$

R_τ and R_ρ are plotted versus θ in Figure B.1.

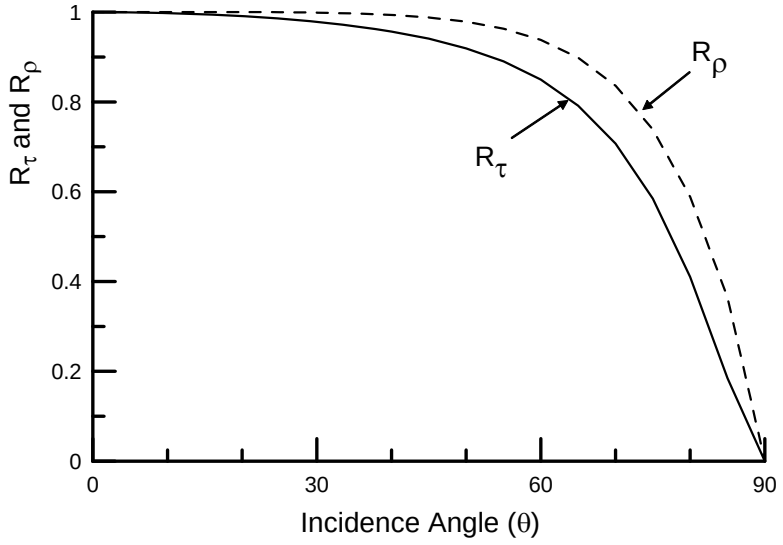

Figure B.1: Ratios R_τ and R_ρ used to characterize off-normal solar properties of glazing layers, n=1.526, KL=0.33.

Appendix C:
Formulation of the Exchange Factor Method

The exchange factor method is used to determine the longwave radiative heat transfer between each pair of surfaces comprising the CFC glazing/shading system. This is made possible by evaluating a set of exchange factors that, like shape/view factors, account for direct radiation exchange, but unlike shape/view factors, also account for all inter-reflections within the enclosure. Thus, given two surfaces, i and j, the exchange factor $F_{i \to j}$ represents the fraction of the radiant energy emitted by surface i that reaches surface j directly and by all possible reflections within the enclosure.

The exchange of longwave radiation in a system of parallel glazing layers is straightforward as the glazing layers are opaque to longwave radiation. The situation is more complicated if a diathermanous layer is present within the multi-layer array. Now non-adjacent layers are in thermal communication with each other through the diathermanous layer. If a diathermanous layer, such as a slat-type blind, is present on the outdoor or indoor sides, the longwave radiation exchange is extended beyond the glazing/shading layer array to the outdoor surroundings and indoor zone surfaces, respectively.

The exchange factor method is an extension of the procedure outlined in (Wright 2008). This earlier work applies to a system of layers that includes a representative outdoor layer, an array of glazing/shading layers and an indoor layer that represents the room. The system does not consider individual interior zone surfaces, rather, the interior surfaces are treated collectively as an additional parallel surface in the multi-layer system. This equivalent internal surface is treated as black with an equivalent mean radiant temperature. Maintaining the nodal scheme in ESP-r requires that each internal surface be considered individually in order to apply the nodal source terms that account for longwave radiative exchange between internal surfaces and CFC layers. The method by Wright (2008) is extended to account for this individual treatment of internal zone surfaces. The following example illustrates the modified procedure as applied to a simple sub-system that includes an interior zone surface. This procedure can be applied to a system of any

number of interior surfaces with any number of diathermanous layers in the CFC multi-layer system.

Consider the system of layers shown in Figure C.1. This system is comprised of an indoor glazing layer (1), an indoor diathermanous blind layer (2) and a room surface (k). The enclosure is thus composed of four surfaces {(b,1), (f,2),(b,2),and(k)}. The CFC layer surface areas, $A_{b,1}$, $A_{f,2}$ and $A_{b,2}$ are equal and can be set to the area of the CFC surface, A_{cfc}. The indoor zone surface has an area A_k. A system of equations can be written to describe the radiosity J for each surface, comprising the emitted, reflected and transmitted components of longwave radiative energy.

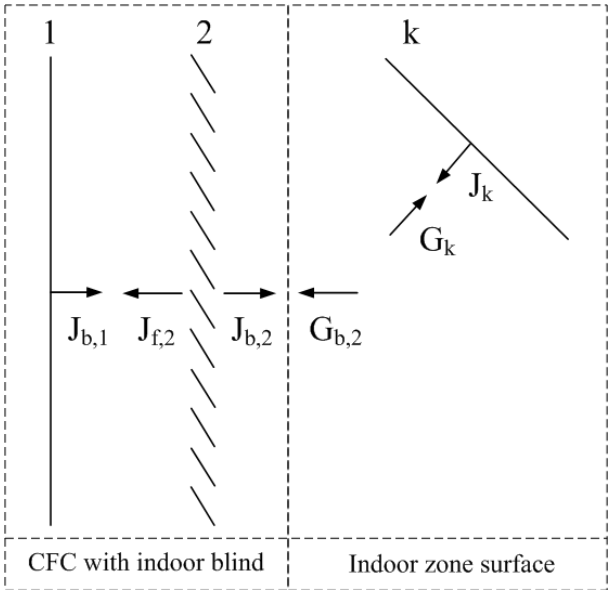

Figure C.1: Surface radiosities and irradiances for four surface enclosure with diathermanous layer.

$$J_{b,1} = E_{b,1} + \rho_{b,1} J_{f,2} \tag{C.1}$$

$$\begin{aligned} J_{f,2} &= E_{f,2} + \rho_{f,2} J_{b,1} + \tau_2 G_{b,2} \\ &= E_{f,2} + \rho_{f,2} J_{b,1} + \tau_2 F_{b,2\to k} J_k \end{aligned} \tag{C.2}$$

$$\begin{aligned} J_{b,2} &= E_{b,2} + \rho_{b,2} G_{b,2} + \tau_2 J_{b,1} \\ &= E_{b,2} + \rho_{b,2} F_{b,2\to k} J_k + \tau_2 J_{b,1} \end{aligned} \tag{C.3}$$

$$J_k = E_k + \rho_k G_k = E_k + \rho_k F_{k\to b,2} J_{b,2} \tag{C.4}$$

The variables $E_{b,1}$, $E_{f,2}$, $E_{b,2}$ and E_k represent a source of radiant flux for each surface, respectively. The shape/view factors, $F_{b,2\to k}$ and $F_{k\to b,2}$ that represent the fraction of direct radiation exchange between layer 2 and surface k are supplied by ESP-r. In an actual enclosure with multiple room surfaces, the irradiance on surface (b,2), $G_{b,2}$ is the summation of the shape factor and radiosity product from each room surface, such that $G_{b,2} = \sum_{i=1}^{n} F_{b,2\to i} J_i$. Similarly, the irradiance on any room surface is then $G_k = \sum_{i=1}^{n} F_{k\to i} J_i$.

Equations C.1 to C.4 represent a system of four equations and four unknown radiosities. This system can be solved through matrix inversion for a matrix representation given by Ax=B where

$$A = \begin{bmatrix} 1 & -\rho_{b,1} & 0 & 0 \\ -\rho_{f,2} & 1 & 0 & -\tau_2 F_{b,2\to k} \\ -\tau_2 & 0 & 1 & -\rho_{b,2} F_{b,2\to k} \\ 0 & 0 & -\rho_k F_{k\to b,2} & 1 \end{bmatrix} \qquad \text{(C.5)}$$

x is a column matrix whose transpose is

$$x^t = \left[J_{b,1}, J_{f,2}, J_{b,2}, J_k \right] \qquad \text{(C.6)}$$

and B is a column vector whose transpose is

$$B^t = \left[E_{b,1}, E_{f,2}, E_{b,2}, E_k \right] \qquad \text{(C.7)}$$

As described in (Wright 2008), setting the values of $E_{b,1}$, $E_{f,2}$, $E_{b,2}$, and E_k to the corresponding emissive powers will yield radiosities that can be used to calculate the net radiant flux between any two surfaces. The solution of net radiant fluxes cannot establish the absorbed flux at a surface j as a result of the emission from surface i only. In order to solve for indoor zone surface fluxes arising from longwave radiative exchange with a CFC surface ONLY, the determination of exchange factors is needed. This is achieved by using the values of $E_{b,1}$, $E_{f,2}$, $E_{b,2}$, and E_k to create unit source fluxes, one surface at a time. For example, to determine the exchange factor from surface (b,1) to the remaining surfaces, the value of $E_{b,1}$ is set to unity and $E_{f,2}$, $E_{b,2}$

and E_k are set to zero. The inverse matrix solution yields radiosities which are now given superscripts to denote the surface of origin of the unit source of radiation. The net longwave radiation heat transfer rate between surface i and j can now be established.

$$q_{i-j} = \left[\begin{array}{l}\text{the fraction of radiant energy}\\ \text{emitted by surface i that reaches}\\ \text{surface j via both direct radiation}\\ \text{and by all possible reflections}\end{array}\right] - \left[\begin{array}{l}\text{the fraction of radiant energy emitted}\\ \text{by surface j that reaches surface i via}\\ \text{both direct radiation and by all possible}\\ \text{reflections}\end{array}\right]$$

For example, the net heat transfer rate between layers 1 and 2 is

$$\begin{aligned} q_{1-2} &= \varepsilon_{b,1}\sigma T_1^4 A_{b,1}\left(\frac{J_{b,1}^{(b,1)}A_{f,2}}{E_{b,1}A_{b,1}}\right)\alpha_{f,2} - \varepsilon_{f,2}\sigma T_2^4 A_{f,2}\left(\frac{J_{f,2}^{(f,2)}A_{b,1}}{E_{f,2}A_{f,2}}\right)\alpha_{b,1} \\ &+ \varepsilon_{b,1}\sigma T_1^4 A_{b,1}\left(\frac{G_{b,2}^{(b,1)}A_{b,2}}{E_{b,1}A_{b,1}}\right)\alpha_{b,2} - \varepsilon_{b,2}\sigma T_2^4 A_{b,2}\left(\frac{J_{f,2}^{(b,2)}A_{b,1}}{E_{b,2}A_{b,2}}\right)\alpha_{b,1} \end{aligned} \qquad \text{(C.8)}$$

By replacing the bracketed terms in equation C.8 with the corresponding exchange factors (e.g., $\left(\frac{J_{b,1}^{(b,1)}A_{f,2}}{E_{b,1}A_{b,1}}\right) = F_{b,1\to f,2}$), equation C.8 becomes

$$\begin{aligned} q_{1-2} &= \varepsilon_{b,1}\sigma T_1^4 F_{b,1\to f,2}A_{b,1}\alpha_{f,2} - \varepsilon_{f,2}\sigma T_2^4 F_{f,2\to b,1}A_{f,2}\alpha_{b,1} \\ &+ \varepsilon_{b,1}\sigma T_1^4 F_{b,1\to b,2}A_{b,1}\alpha_{b,2} - \varepsilon_{b,2}\sigma T_2^4 F_{b,2\to b,1}A_{b,2}\alpha_{b,1} \end{aligned} \qquad \text{(C.9)}$$

Assuming that all temperatures in the system span a small enough range, Kirchoff's Law can be applied so that the total emissivity and total absorptivity can be equated in the longwave band such that $\varepsilon_{b,1} = \alpha_{b,1}$, $\varepsilon_{f,2} = \alpha_{f,2}$ and $\varepsilon_{b,2} = \alpha_{b,2}$. Based on the reciprocity relationship proven by Gebhert (1959), it can be shown that $F_{b,1\to f,2}A_{b,1} = F_{f,2\to b,1}A_{f,2}$ and $F_{b,1\to b,2}A_{b,1} = F_{b,2\to b,1}A_{b,2}$. But since $A_{b,1} = A_{f,2} = A_{b,2} = A_{cfc}$ the reciprocity relation for CFC layers simply

yields $F_{b,1\to f,2} = F_{f,2\to b,1}$, and $F_{b,1\to b,2} = F_{b,2\to b,1}$. This is true only if the areas of the two surfaces are equal. Finally, the net heat transfer between layers 1 and 2 becomes

$$q_{1-2} = \varepsilon_{b,1}\varepsilon_{f,2}F_{b,1\to f,2}A_{cfc}\sigma(T_1^4 - T_2^4) + \varepsilon_{b,1}\varepsilon_{b,2}F_{b,1\to b,2}A_{cfc}\sigma(T_1^4 - T_2^4) \qquad (C.10)$$

Similarly, the net heat transfer between layer 1 and surface k is

$$q_{1-k} = \varepsilon_{b,1}\varepsilon_{k}F_{b,1\to k}A_{cfc}\sigma(T_1^4 - T_k^4) \qquad (C.11)$$

and the net heat transfer between layer 2 and surface k is

$$q_{2-k} = \varepsilon_{f,2}\varepsilon_{k}F_{f,2\to k}A_{cfc}\sigma(T_2^4 - T_k^4) + \varepsilon_{b,2}\varepsilon_{k}F_{b,2\to k}A_{cfc}\sigma(T_2^4 - T_k^4) \qquad (C.12)$$

Appendix D:

ESP-r Solar Processing Flow Chart

D.1 Subroutine “MZSOLR”

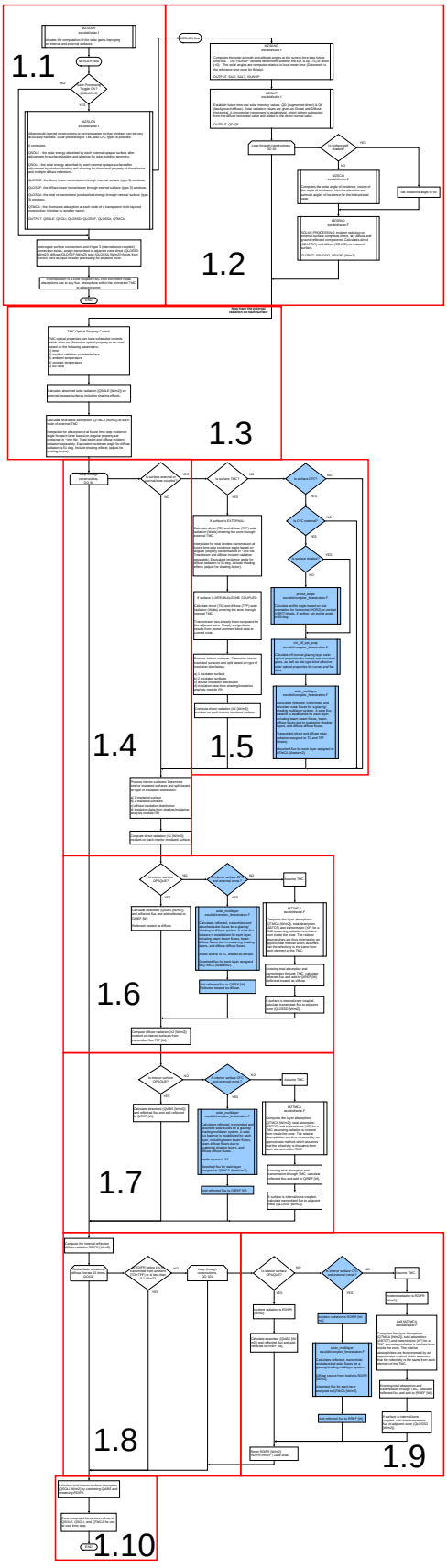

ESP-r routines unaltered

New routines for CFC

ESP-r routines with CFC modifications

1.1

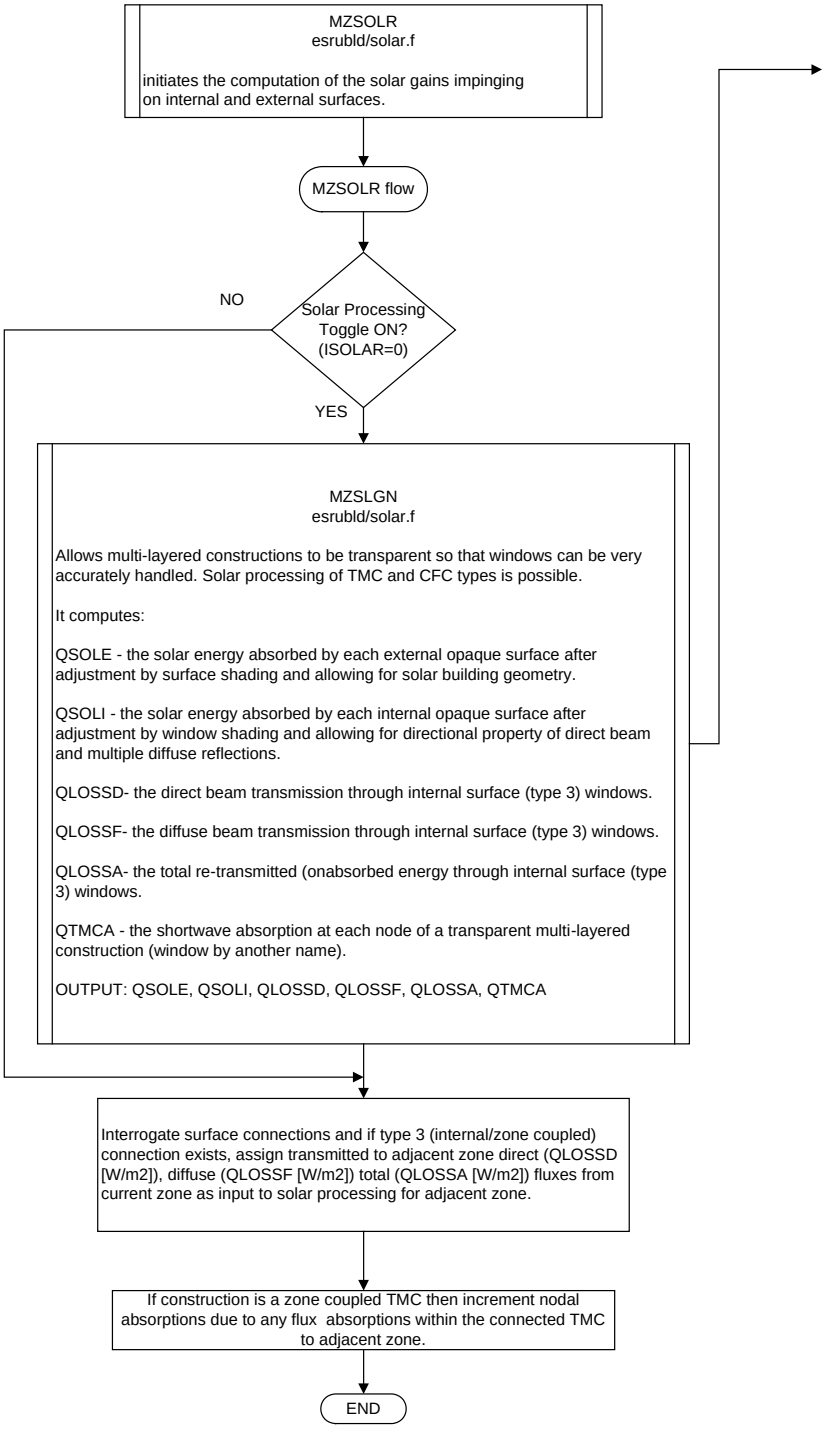
MZSOLR
esrubld/solar.f
initiates the computation of the solar gains impinging on internal and external surfaces.
MZSOLR flow
Solar Processing Toggle ON? (ISOLAR=0)
NO
YES
MZSLGN
esrubld/solar.f
Allows multi-layered constructions to be transparent so that windows can be very accurately handled. Solar processing of TMC and CFC types is possible.
It computes:
QSOLE - the solar energy absorbed by each external opaque surface after adjustment by surface shading and allowing for solar building geometry.
QSOLI - the solar energy absorbed by each internal opaque surface after adjustment by window shading and allowing for directional property of direct beam and multiple diffuse reflections.
QLOSSD- the direct beam transmission through internal surface (type 3) windows.
QLOSSF- the diffuse beam transmission through internal surface (type 3) windows.
QLOSSA- the total re-transmitted (onabsorbed energy through internal surface (type 3) windows.
QTMCA - the shortwave absorption at each node of a transparent multi-layered construction (window by another name).
OUTPUT: QSOLE, QSOLI, QLOSSD, QLOSSF, QLOSSA, QTMCA
Interrogate surface connections and if type 3 (internal/zone coupled) connection exists, assign transmitted to adjacent zone direct (QLOSSD [W/m2]), diffuse (QLOSSF [W/m2]) total (QLOSSA [W/m2]) fluxes from current zone as input to solar processing for adjacent zone.
If construction is a zone coupled TMC then increment nodal absorptions due to any flux absorptions within the connected TMC to adjacent zone.
END

1.2

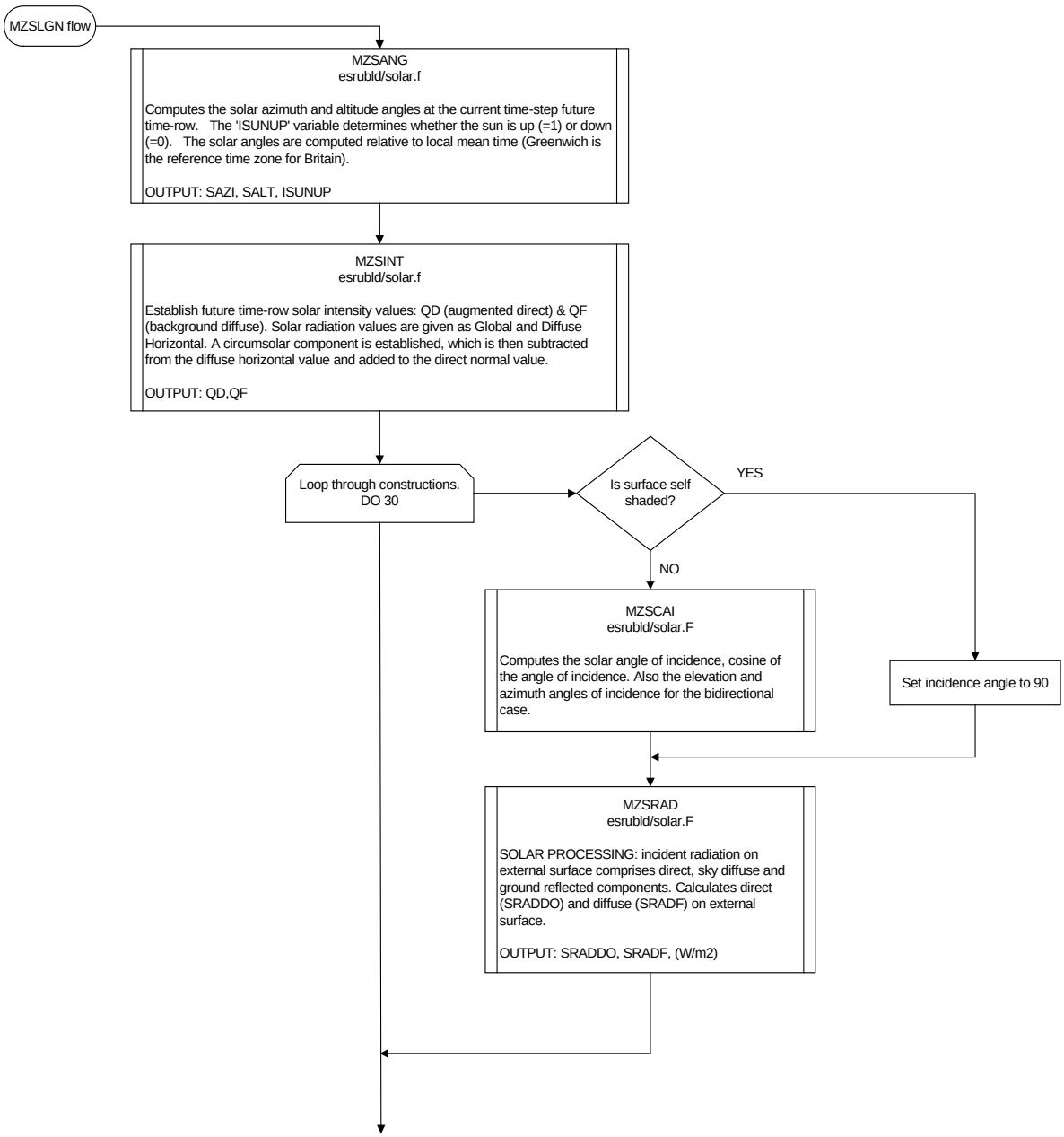
MZSLGN flow
MZSANG
esrubld/solar.f
Computes the solar azimuth and altitude angles at the current time-step future time-row. The 'ISUNUP' variable determines whether the sun is up (=1) or down (=0). The solar angles are computed relative to local mean time (Greenwich is the reference time zone for Britain).
OUTPUT: SAZI, SALT, ISUNUP
MZSINT
esrubld/solar.f
Establish future time-row solar intensity values: QD (augmented direct) & QF (background diffuse). Solar radiation values are given as Global and Diffuse Horizontal. A circumsolar component is established, which is then subtracted from the diffuse horizontal value and added to the direct normal value.
OUTPUT: QD,QF
Loop through constructions.
DO 30
Is surface self shaded?
YES
NO
MZSCAI
esrubld/solar.F
Computes the solar angle of incidence, cosine of the angle of incidence. Also the elevation and azimuth angles of incidence for the bidirectional case.
Set incidence angle to 90
MZSRAD
esrubld/solar.F
SOLAR PROCESSING: incident radiation on external surface comprises direct, sky diffuse and ground reflected components. Calculates direct (SRADDO) and diffuse (SRADF) on external surface.
OUTPUT: SRADDO, SRADF, (W/m2)

1.3

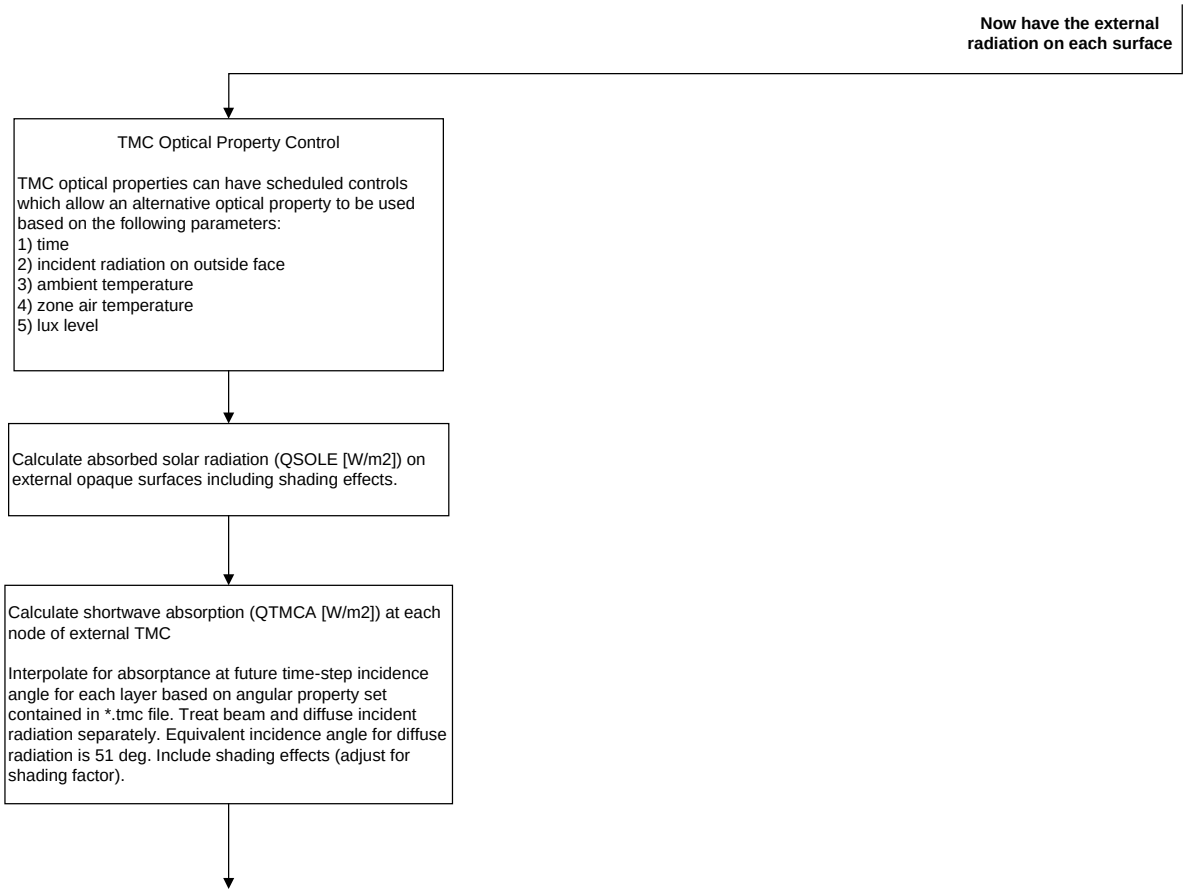
Now have the external radiation on each surface
TMC Optical Property Control
TMC optical properties can have scheduled controls which allow an alternative optical property to be used based on the following parameters:
1) time
2) incident radiation on outside face
3) ambient temperature
4) zone air temperature
5) lux level
Calculate absorbed solar radiation (QSOLE [W/m2]) on external opaque surfaces including shading effects.
Calculate shortwave absorption (QTMCA [W/m2]) at each node of external TMC
Interpolate for absorptance at future time-step incidence angle for each layer based on angular property set contained in *.tmc file. Treat beam and diffuse incident radiation separately. Equivalent incidence angle for diffuse radiation is 51 deg. Include shading effects (adjust for shading factor).

1.4

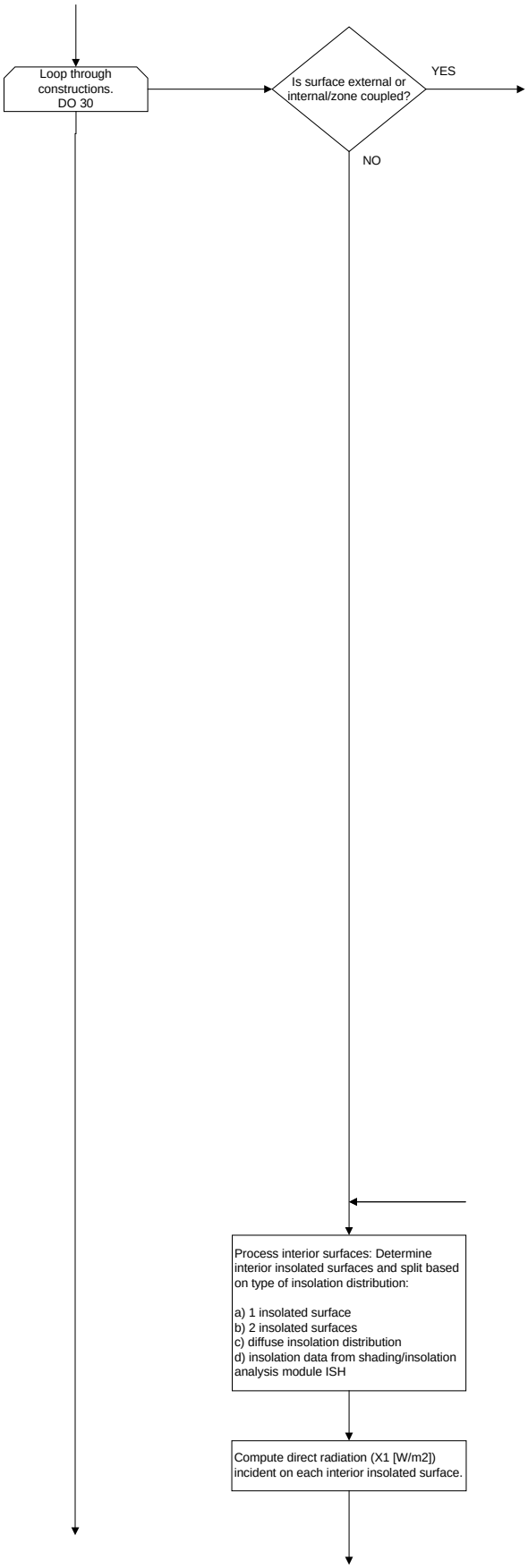
Loop through constructions. DO 30
Is surface external or internal/zone coupled?
YES
NO
Process interior surfaces: Determine interior insolated surfaces and split based on type of insolation distribution:
a) 1 insolated surface
b) 2 insolated surfaces
c) diffuse insolation distribution
d) insolation data from shading/insolation analysis module ISH
Compute direct radiation (X1 [W/m2]) incident on each interior insolated surface.

1.5

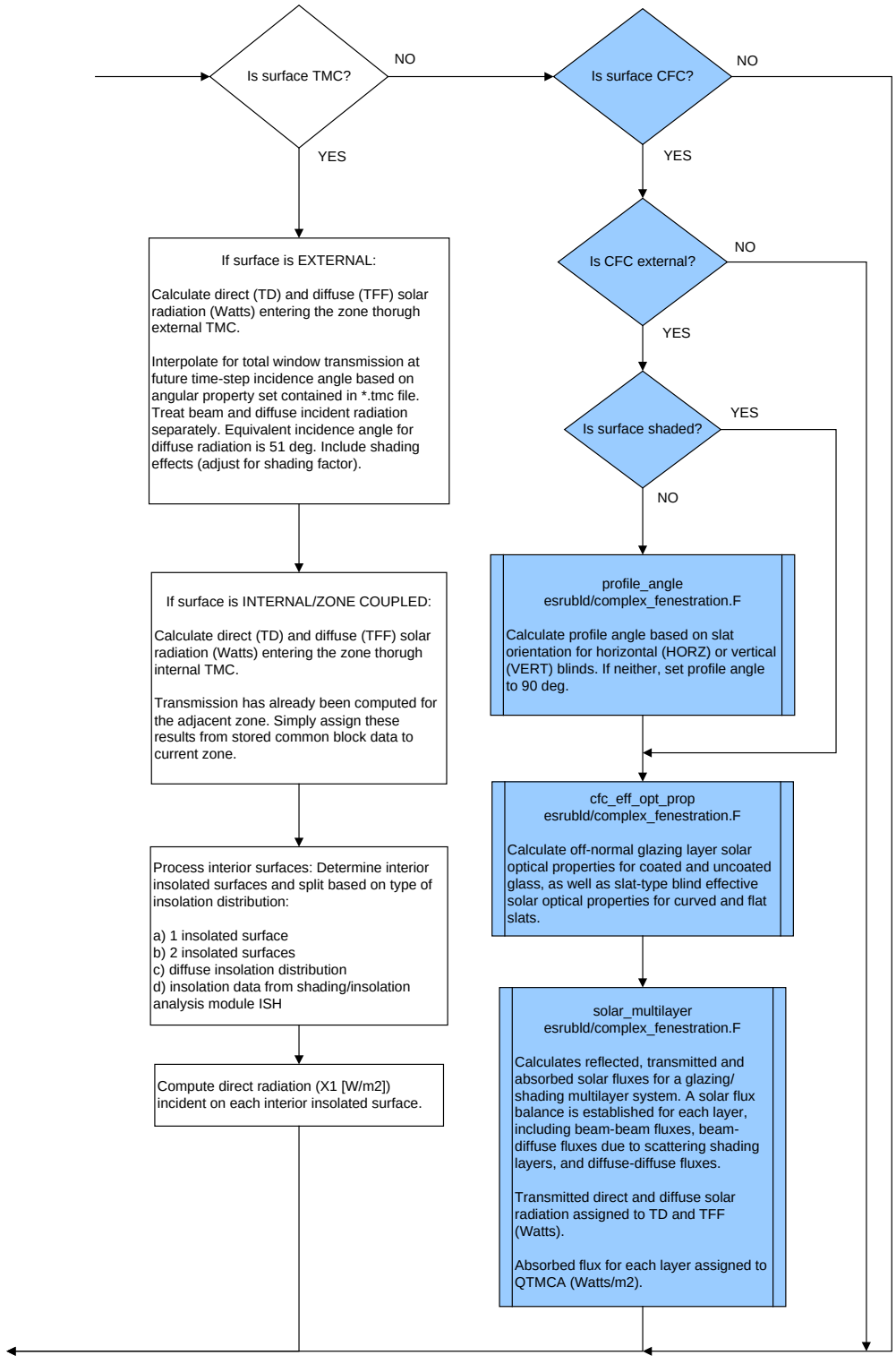
Is surface TMC?
NO
YES
Is surface CFC?
NO
YES
Is CFC external?
NO
YES
Is surface shaded?
YES
NO
If surface is EXTERNAL:
Calculate direct (TD) and diffuse (TFF) solar radiation (Watts) entering the zone thorugh external TMC.
Interpolate for total window transmission at future time-step incidence angle based on angular property set contained in *.tmc file. Treat beam and diffuse incident radiation separately. Equivalent incidence angle for diffuse radiation is 51 deg. Include shading effects (adjust for shading factor).
If surface is INTERNAL/ZONE COUPLED:
Calculate direct (TD) and diffuse (TFF) solar radiation (Watts) entering the zone thorugh internal TMC.
Transmission has already been computed for the adjacent zone. Simply assign these results from stored common block data to current zone.
Process interior surfaces: Determine interior insolated surfaces and split based on type of insolation distribution:
a) 1 insolated surface
b) 2 insolated surfaces
c) diffuse insolation distribution
d) insolation data from shading/insolation analysis module ISH
Compute direct radiation (X1 [W/m2]) incident on each interior insolated surface.
profile_angle
esrubld/complex_fenestration.F
Calculate profile angle based on slat orientation for horizontal (HORZ) or vertical (VERT) blinds. If neither, set profile angle to 90 deg.
cfc_eff_opt_prop
esrubld/complex_fenestration.F
Calculate off-normal glazing layer solar optical properties for coated and uncoated glass, as well as slat-type blind effective solar optical properties for curved and flat slats.
solar_multilayer
esrubld/complex_fenestration.F
Calculates reflected, transmitted and absorbed solar fluxes for a glazing/ shading multilayer system. A solar flux balance is established for each layer, including beam-beam fluxes, beam-diffuse fluxes due to scattering shading layers, and diffuse-diffuse fluxes.
Transmitted direct and diffuse solar radiation assigned to TD and TFF (Watts).
Absorbed flux for each layer assigned to QTMCA (Watts/m2).

1.6

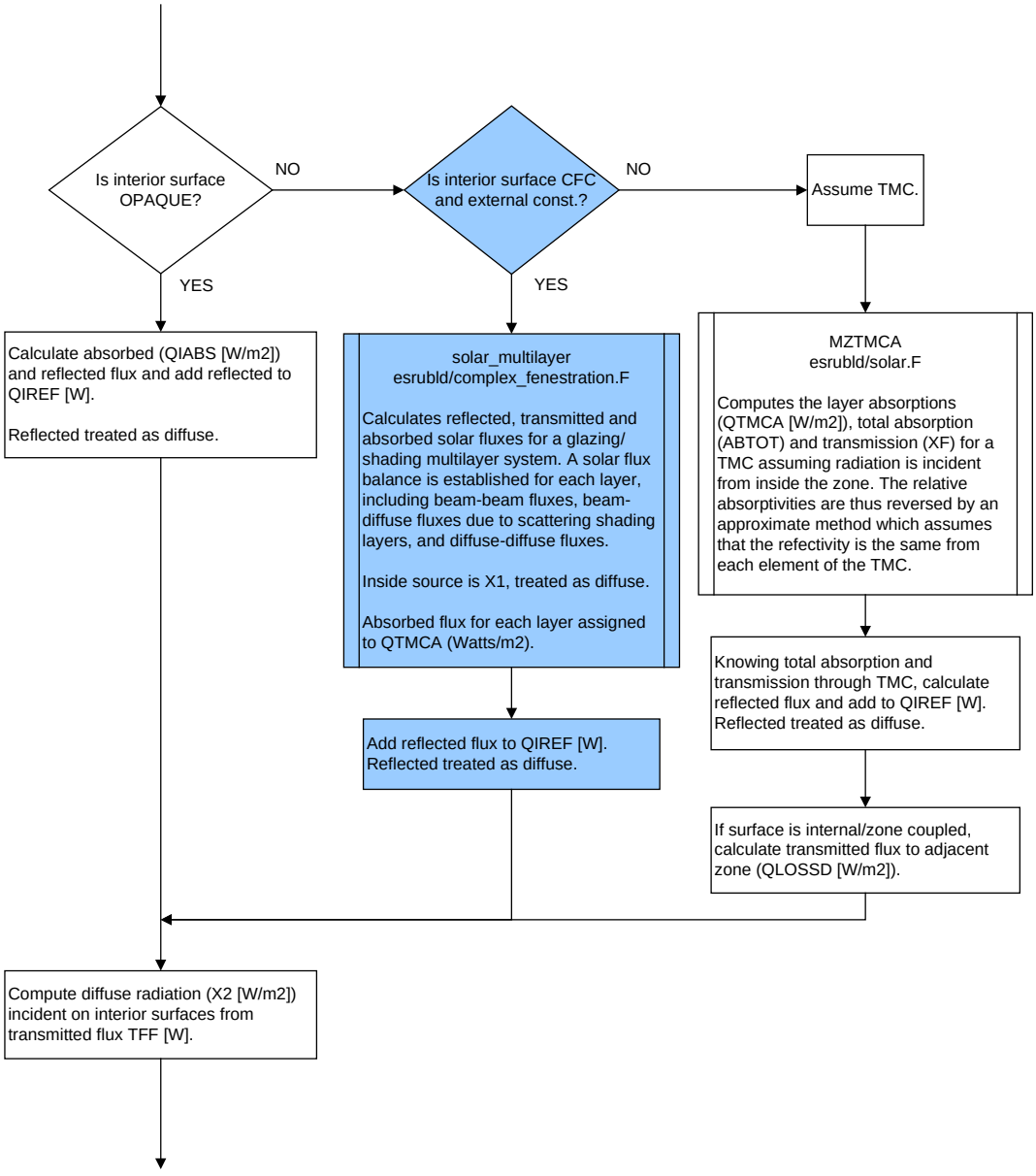
Is interior surface OPAQUE?
NO
Is interior surface CFC and external const.?
NO
Assume TMC.
YES
YES
Calculate absorbed (QIABS [W/m2]) and reflected flux and add reflected to QIREF [W].
Reflected treated as diffuse.
solar_multilayer
esrubld/complex_fenestration.F
Calculates reflected, transmitted and absorbed solar fluxes for a glazing/ shading multilayer system. A solar flux balance is established for each layer, including beam-beam fluxes, beam-diffuse fluxes due to scattering shading layers, and diffuse-diffuse fluxes.
Inside source is X1, treated as diffuse.
Absorbed flux for each layer assigned to QTMCA (Watts/m2).
MZTMCA
esrubld/solar.F
Computes the layer absorptions (QTMCA [W/m2]), total absorption (ABTOT) and transmission (XF) for a TMC assuming radiation is incident from inside the zone. The relative absorptivities are thus reversed by an approximate method which assumes that the refectivity is the same from each element of the TMC.
Knowing total absorption and transmission through TMC, calculate reflected flux and add to QIREF [W]. Reflected treated as diffuse.
Add reflected flux to QIREF [W]. Reflected treated as diffuse.
If surface is internal/zone coupled, calculate transmitted flux to adjacent zone (QLOSSD [W/m2]).
Compute diffuse radiation (X2 [W/m2]) incident on interior surfaces from transmitted flux TFF [W].

1.7

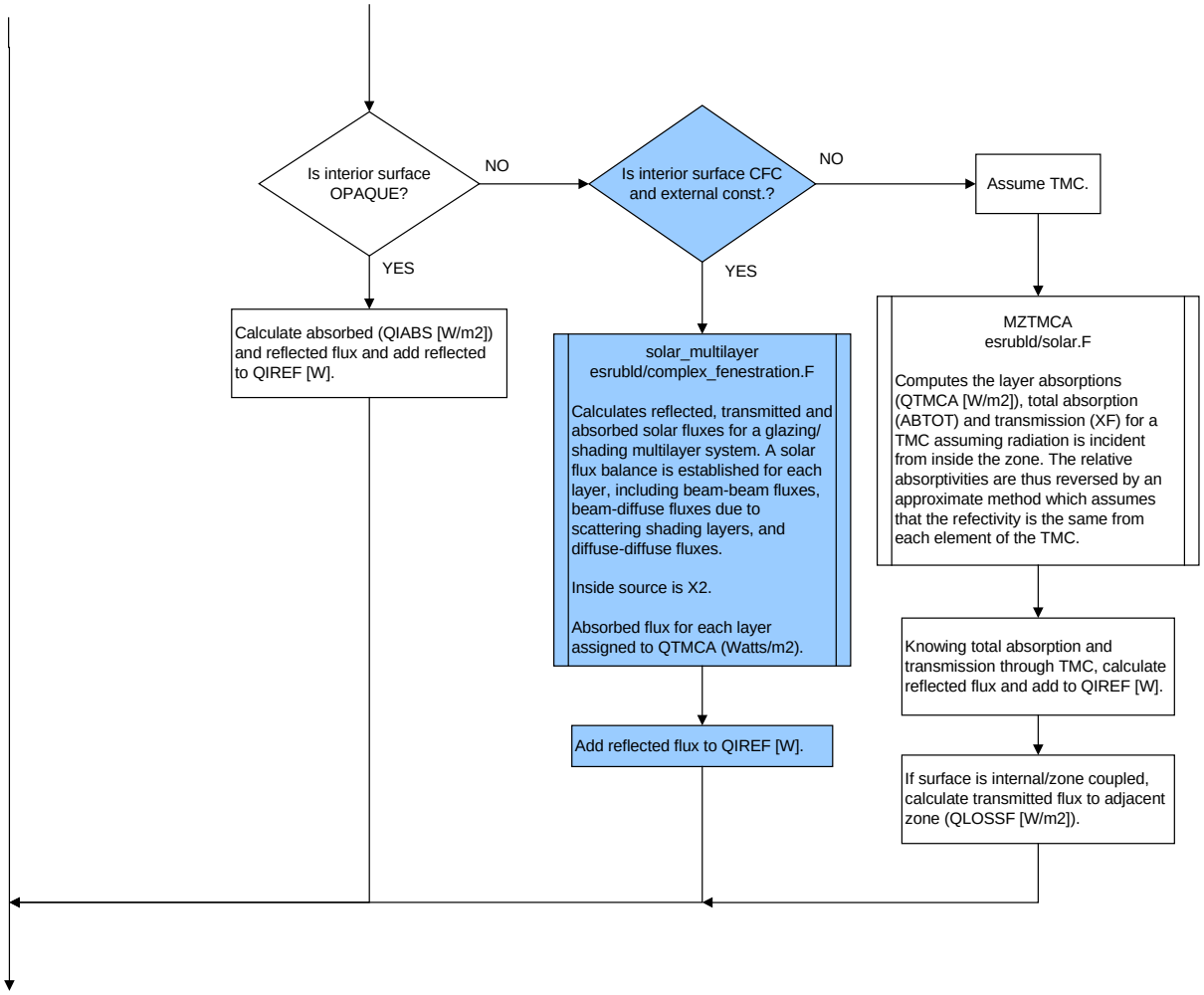
Is interior surface OPAQUE?
NO
Is interior surface CFC and external const.?
NO
Assume TMC.
YES
YES
Calculate absorbed (QIABS [W/m2]) and reflected flux and add reflected to QIREF [W].
solar_multilayer
esrubld/complex_fenestration.F
Calculates reflected, transmitted and absorbed solar fluxes for a glazing/ shading multilayer system. A solar flux balance is established for each layer, including beam-beam fluxes, beam-diffuse fluxes due to scattering shading layers, and diffuse-diffuse fluxes.
Inside source is X2.
Absorbed flux for each layer assigned to QTMCA (Watts/m2).
MZTMCA
esrubld/solar.F
Computes the layer absorptions (QTMCA [W/m2]), total absorption (ABTOT) and transmission (XF) for a TMC assuming radiation is incident from inside the zone. The relative absorptivities are thus reversed by an approximate method which assumes that the refectivity is the same from each element of the TMC.
Knowing total absorption and transmission through TMC, calculate reflected flux and add to QIREF [W].
Add reflected flux to QIREF [W].
If surface is internal/zone coupled, calculate transmitted flux to adjacent zone (QLOSSF [W/m2]).

1.8

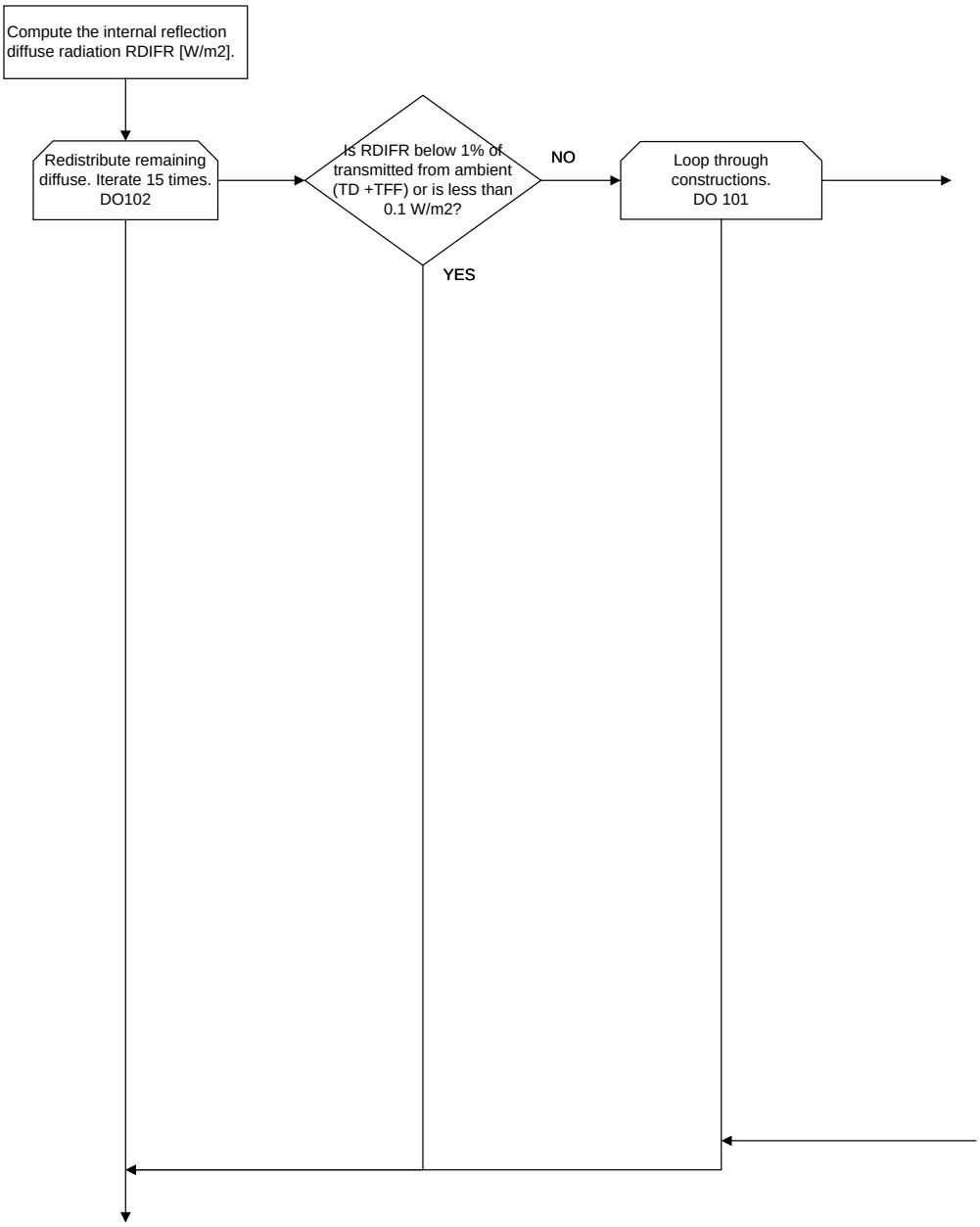
Compute the internal reflection diffuse radiation RDIFR [W/m2].
Redistribute remaining diffuse. Iterate 15 times. DO102
Is RDIFR below 1% of transmitted from ambient (TD +TFF) or is less than 0.1 W/m2?
NO
YES
Loop through constructions. DO 101

1.9

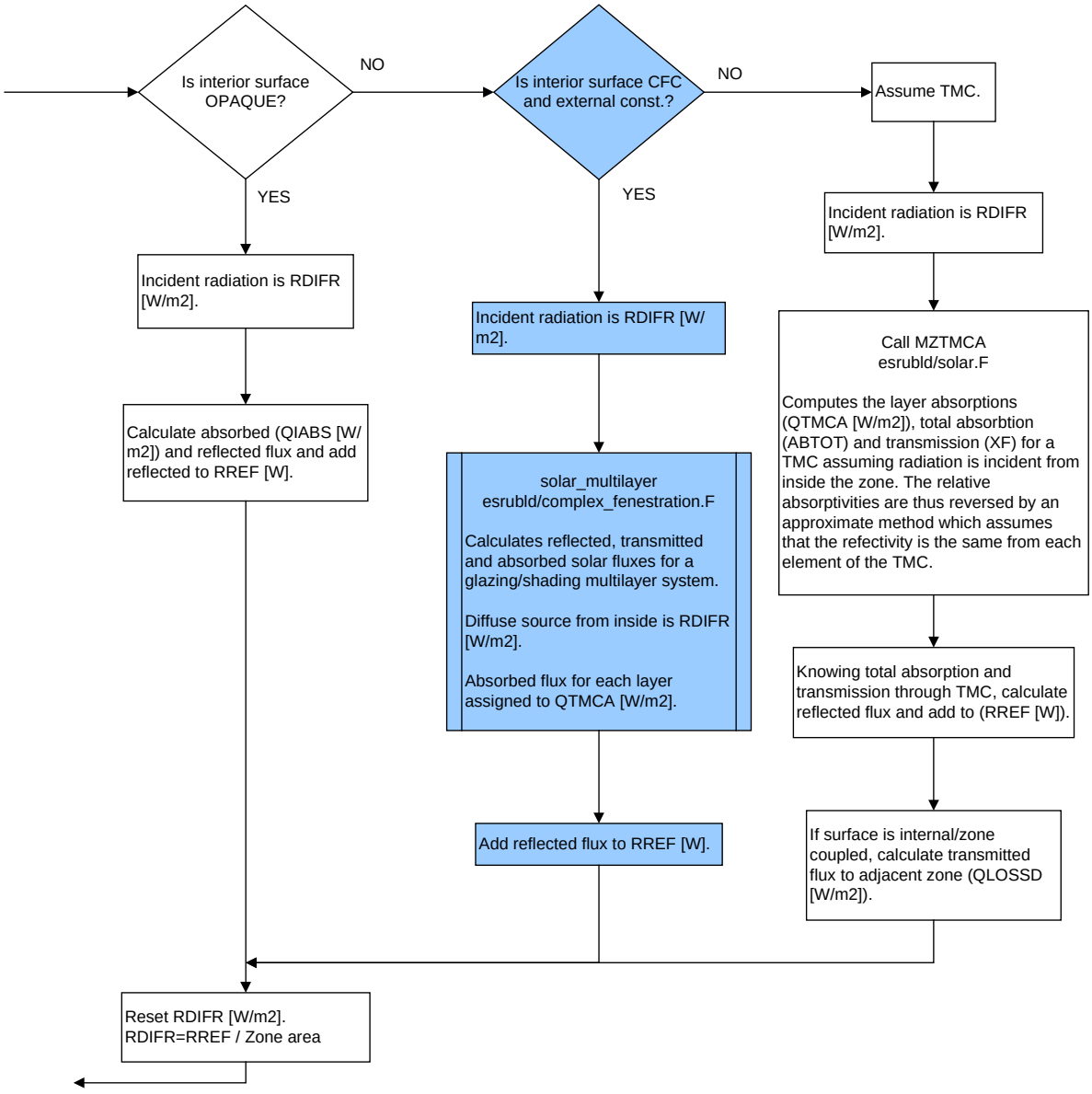
Is interior surface OPAQUE?
NO
Is interior surface CFC and external const.?
NO
Assume TMC.
YES
YES
Incident radiation is RDIFR [W/m2].
Incident radiation is RDIFR [W/m2].
Incident radiation is RDIFR [W/m2].
Calculate absorbed (QIABS [W/m2]) and reflected flux and add reflected to RREF [W].
solar_multilayer esrubld/complex_fenestration.F
Calculates reflected, transmitted and absorbed solar fluxes for a glazing/shading multilayer system.
Diffuse source from inside is RDIFR [W/m2].
Absorbed flux for each layer assigned to QTMCA [W/m2].
Call MZTMCA esrubld/solar.F
Computes the layer absorptions (QTMCA [W/m2]), total absorbtion (ABTOT) and transmission (XF) for a TMC assuming radiation is incident from inside the zone. The relative absorptivities are thus reversed by an approximate method which assumes that the refectivity is the same from each element of the TMC.
Knowing total absorption and transmission through TMC, calculate reflected flux and add to (RREF [W]).
Add reflected flux to RREF [W].
If surface is internal/zone coupled, calculate transmitted flux to adjacent zone (QLOSSD [W/m2]).
Reset RDIFR [W/m2].
RDIFR=RREF / Zone area

1.10

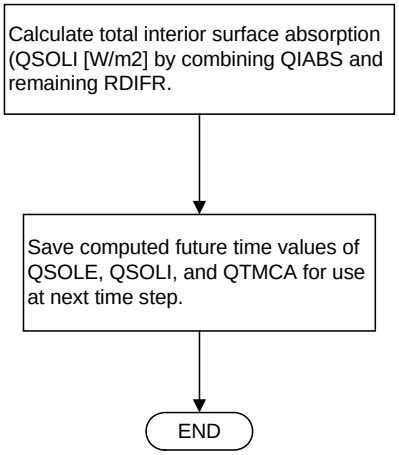
Calculate total interior surface absorption (QSOLI [W/m2] by combining QIABS and remaining RDIFR.
Save computed future time values of QSOLE, QSOLI, and QTMCA for use at next time step.
END

D.2 Subroutine “cfc_eff_opt_prop”

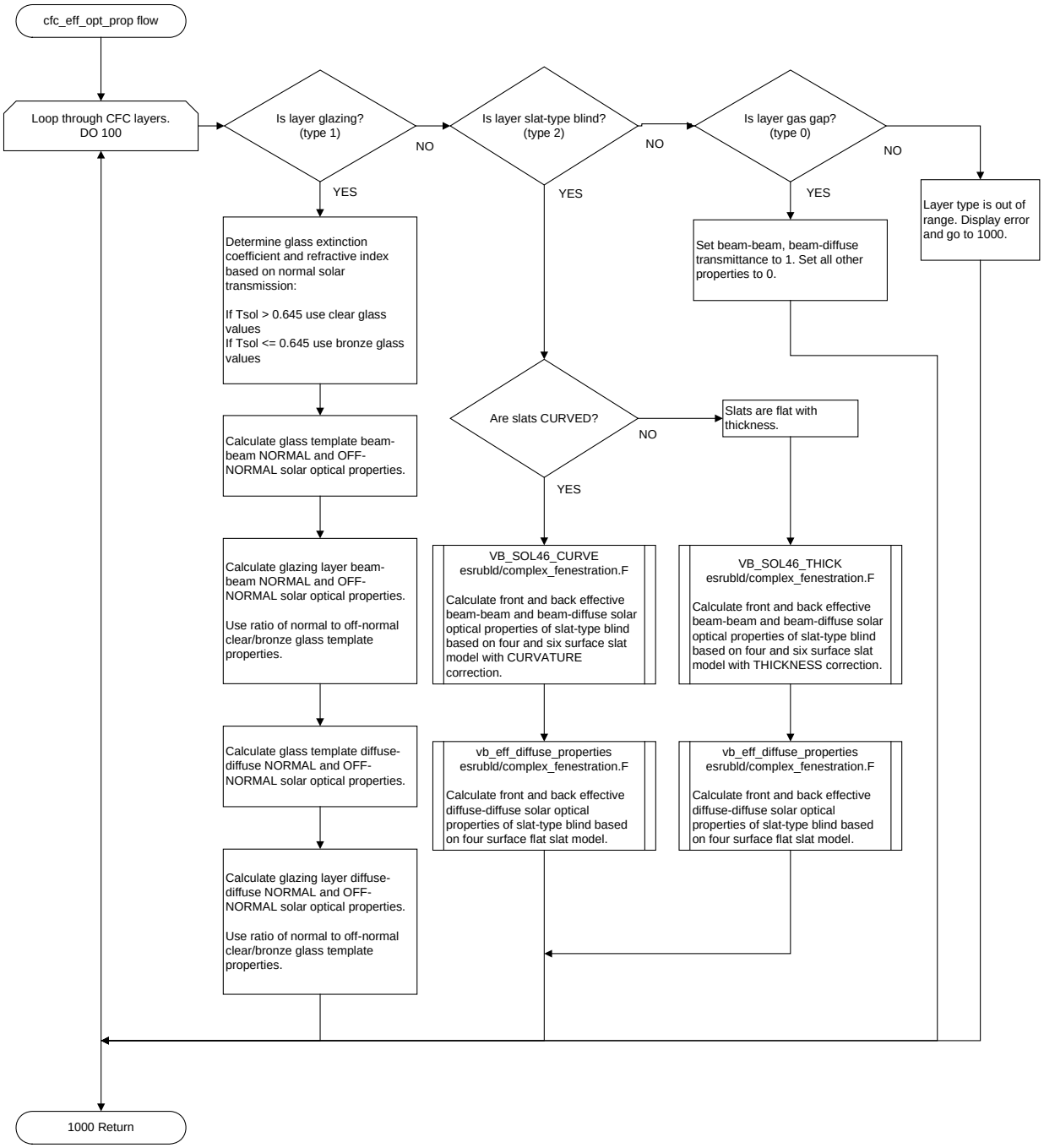

D.3 Subroutine “solar_multilayer”

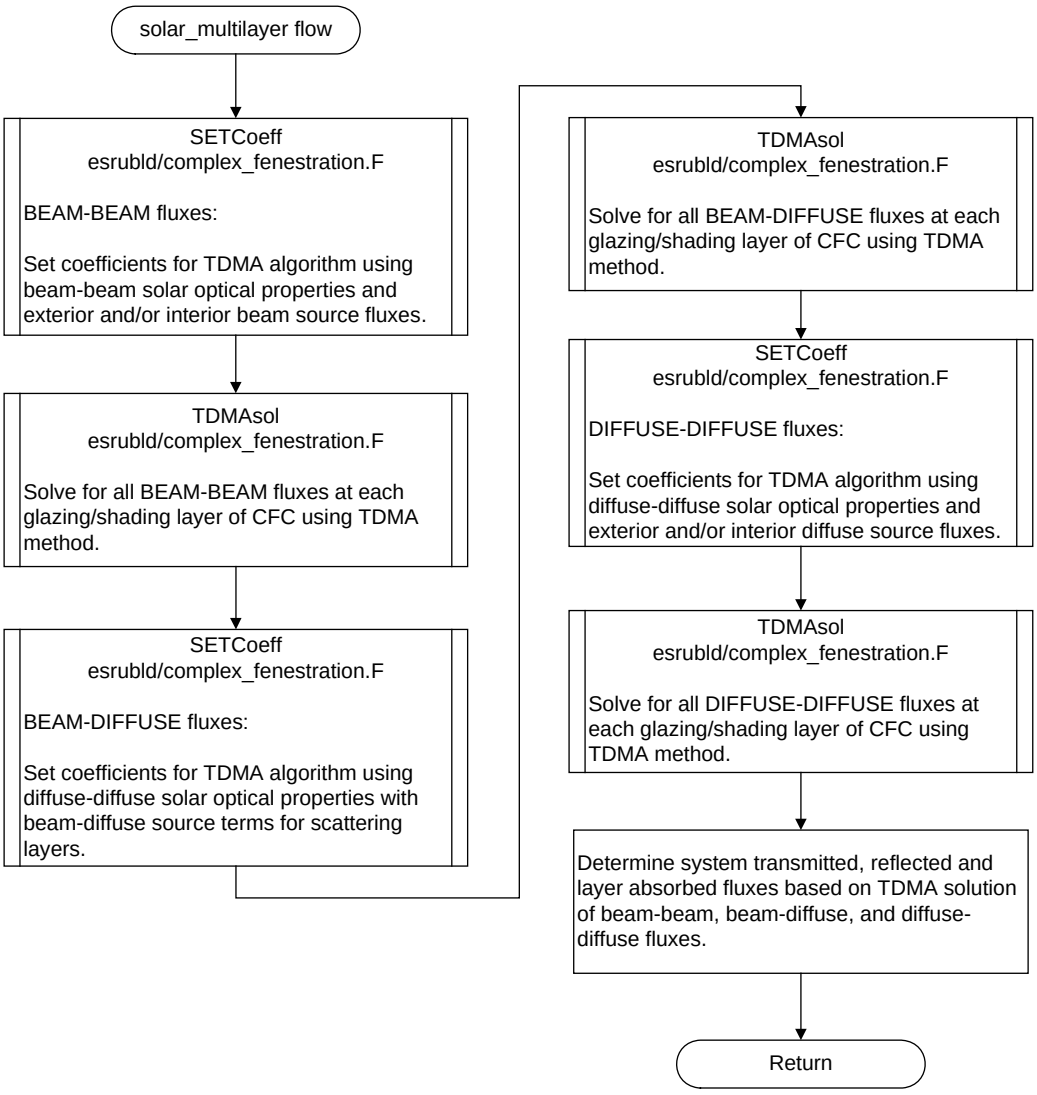

Appendix E:
ESP-r Thermal Simulation Flow Chart

E.1 Program “bps”

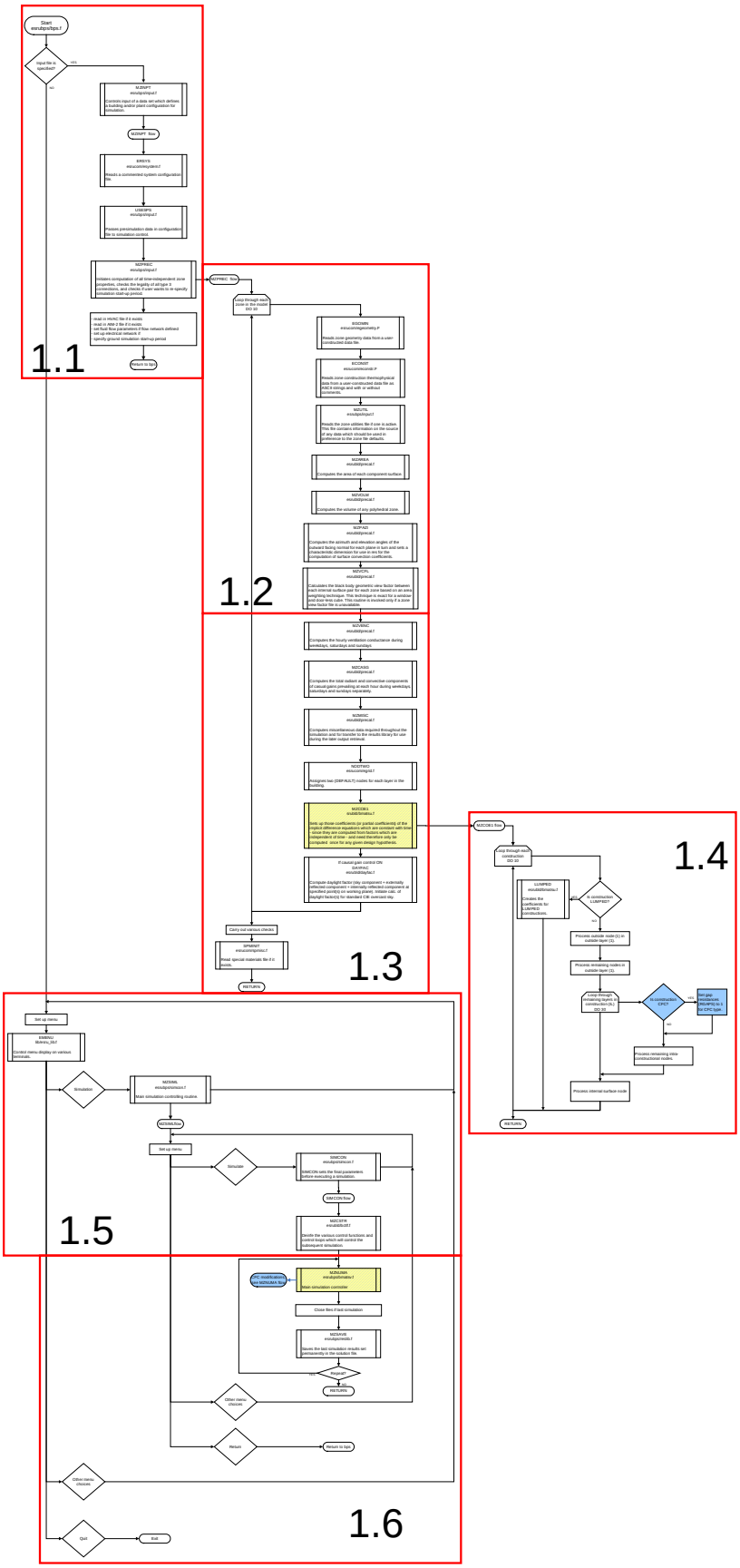

ESP-r routines unaltered

New routines for CFC

ESP-r routines with CFC modifications

1.1

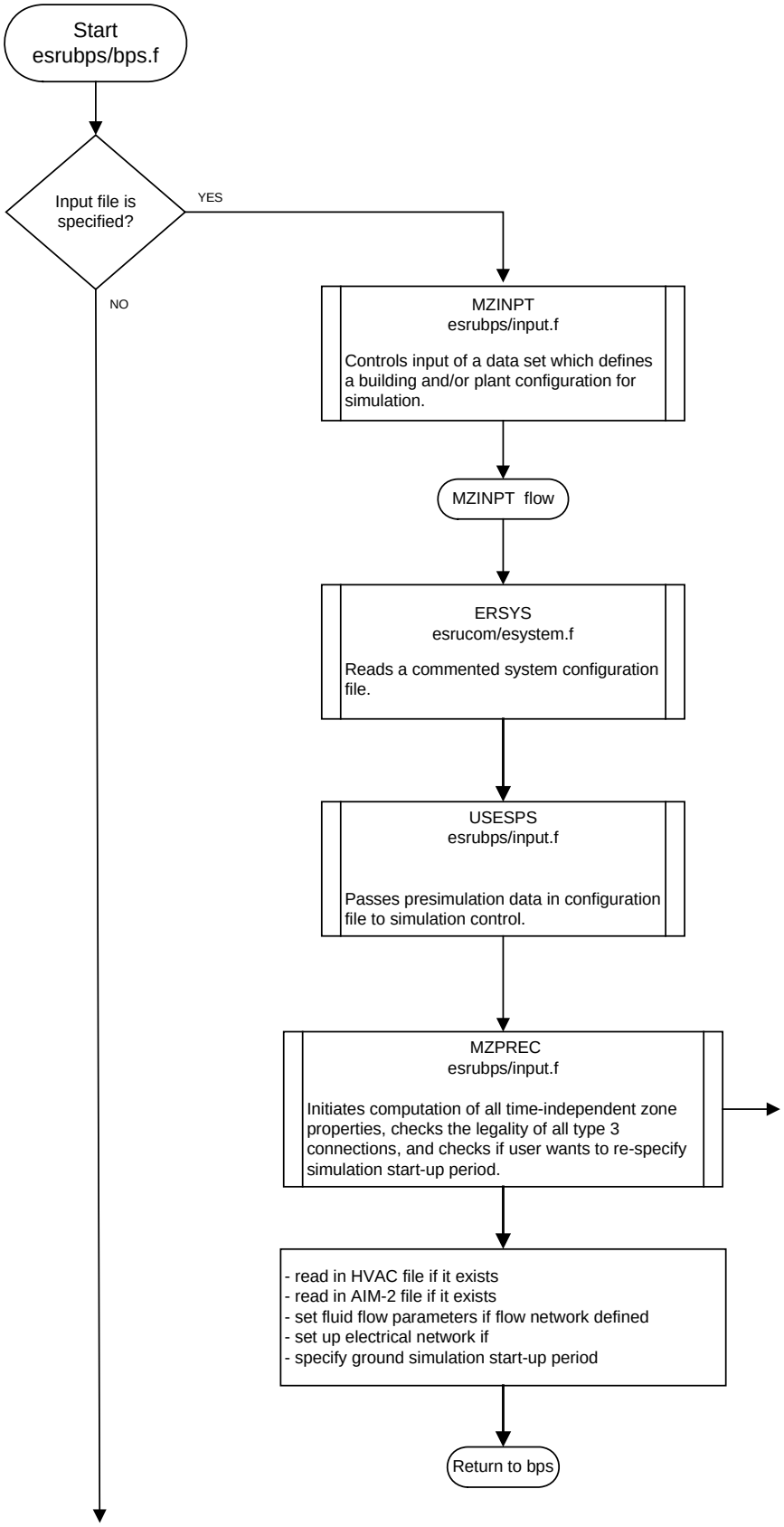
Start
esrubps/bps.f
Input file is specified?
YES
NO
MZINPT
esrubps/input.f
Controls input of a data set which defines a building and/or plant configuration for simulation.
MZINPT flow
ERSYS
esrucom/esystem.f
Reads a commented system configuration file.
USESPS
esrubps/input.f
Passes presimulation data in configuration file to simulation control.
MZPREC
esrubps/input.f
Initiates computation of all time-independent zone properties, checks the legality of all type 3 connections, and checks if user wants to re-specify simulation start-up period.
- read in HVAC file if it exists
- read in AIM-2 file if it exists
- set fluid flow parameters if flow network defined
- set up electrical network if
- specify ground simulation start-up period
Return to bps

1.2

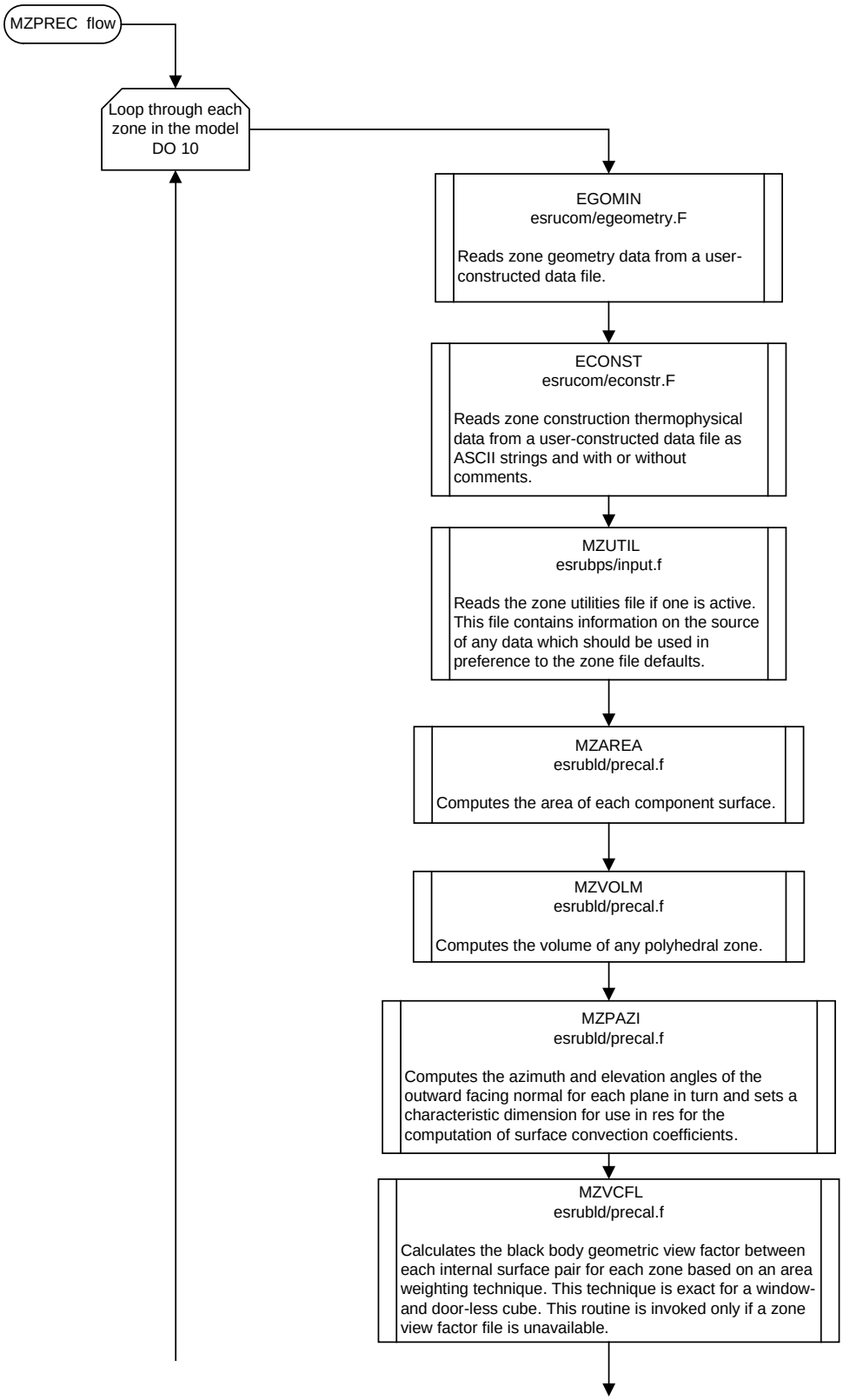
MZPREC flow
Loop through each zone in the model DO 10
EGOMIN
esrucom/egeometry.F
Reads zone geometry data from a user-constructed data file.
ECONST
esrucom/econstr.F
Reads zone construction thermophysical data from a user-constructed data file as ASCII strings and with or without comments.
MZUTIL
esrubps/input.f
Reads the zone utilities file if one is active. This file contains information on the source of any data which should be used in preference to the zone file defaults.
MZAREA
esrubld/precal.f
Computes the area of each component surface.
MZVOLM
esrubld/precal.f
Computes the volume of any polyhedral zone.
MZPAZI
esrubld/precal.f
Computes the azimuth and elevation angles of the outward facing normal for each plane in turn and sets a characteristic dimension for use in res for the computation of surface convection coefficients.
MZVCFL
esrubld/precal.f
Calculates the black body geometric view factor between each internal surface pair for each zone based on an area weighting technique. This technique is exact for a window- and door-less cube. This routine is invoked only if a zone view factor file is unavailable.

1.3

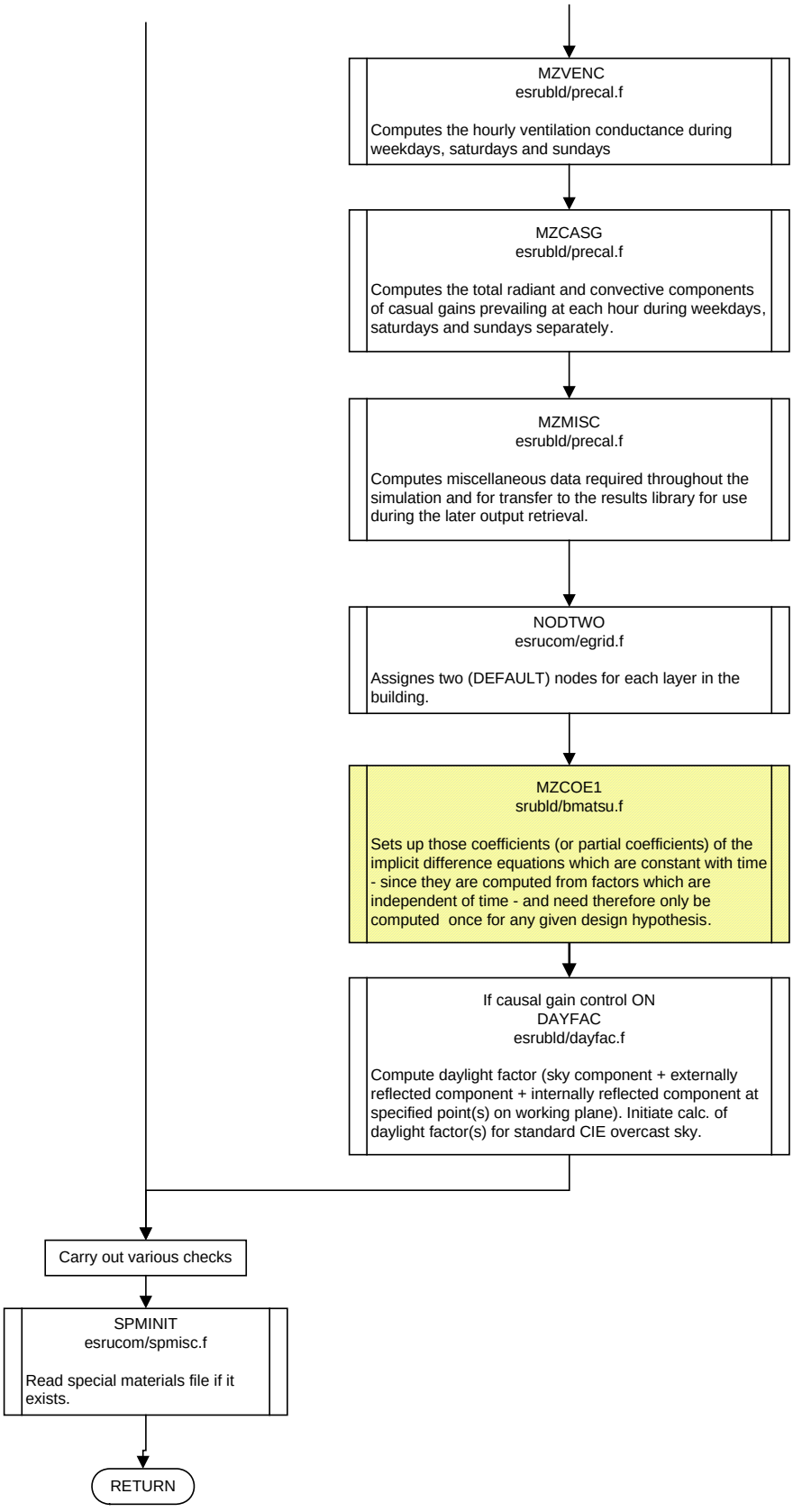
MZVENC
esrubld/precal.f
Computes the hourly ventilation conductance during weekdays, saturdays and sundays
MZCASG
esrubld/precal.f
Computes the total radiant and convective components of casual gains prevailing at each hour during weekdays, saturdays and sundays separately.
MZMISC
esrubld/precal.f
Computes miscellaneous data required throughout the simulation and for transfer to the results library for use during the later output retrieval.
NODTWO
esrucom/egrid.f
Assignes two (DEFAULT) nodes for each layer in the building.
MZCOE1
srubld/bmatsu.f
Sets up those coefficients (or partial coefficients) of the implicit difference equations which are constant with time - since they are computed from factors which are independent of time - and need therefore only be computed once for any given design hypothesis.
If causal gain control ON
DAYFAC
esrubld/dayfac.f
Compute daylight factor (sky component + externally reflected component + internally reflected component at specified point(s) on working plane). Initiate calc. of daylight factor(s) for standard CIE overcast sky.
Carry out various checks
SPMINIT
esrucom/spmisc.f
Read special materials file if it exists.
RETURN

1.4

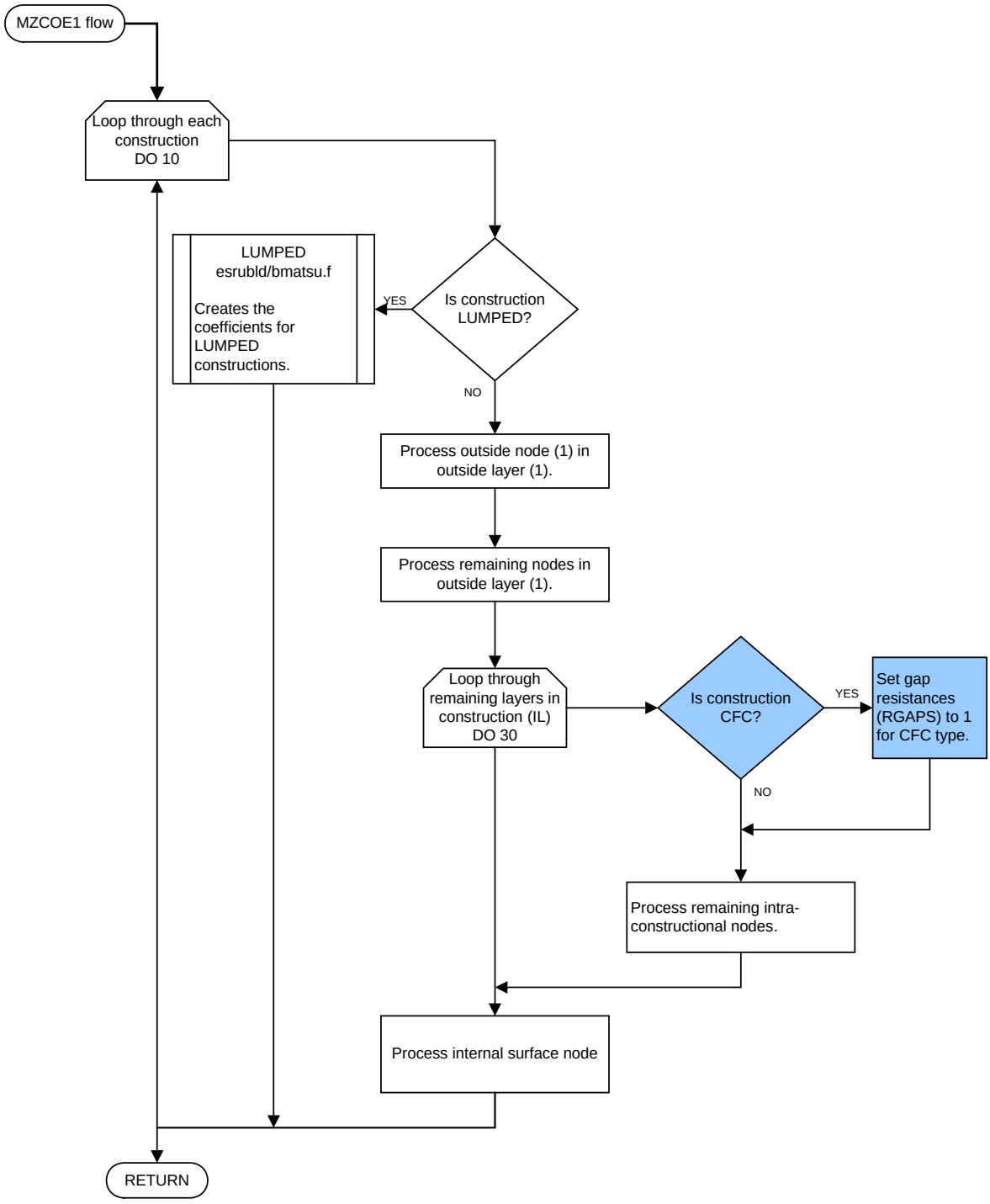
MZCOE1 flow
Loop through each construction DO 10
Is construction LUMPED?
YES
LUMPED esrubld/bmatsu.f
Creates the coefficients for LUMPED constructions.
NO
Process outside node (1) in outside layer (1).
Process remaining nodes in outside layer (1).
Loop through remaining layers in construction (IL) DO 30
Is construction CFC?
YES
Set gap resistances (RGAPS) to 1 for CFC type.
NO
Process remaining intra-constructional nodes.
Process internal surface node
RETURN

1.5

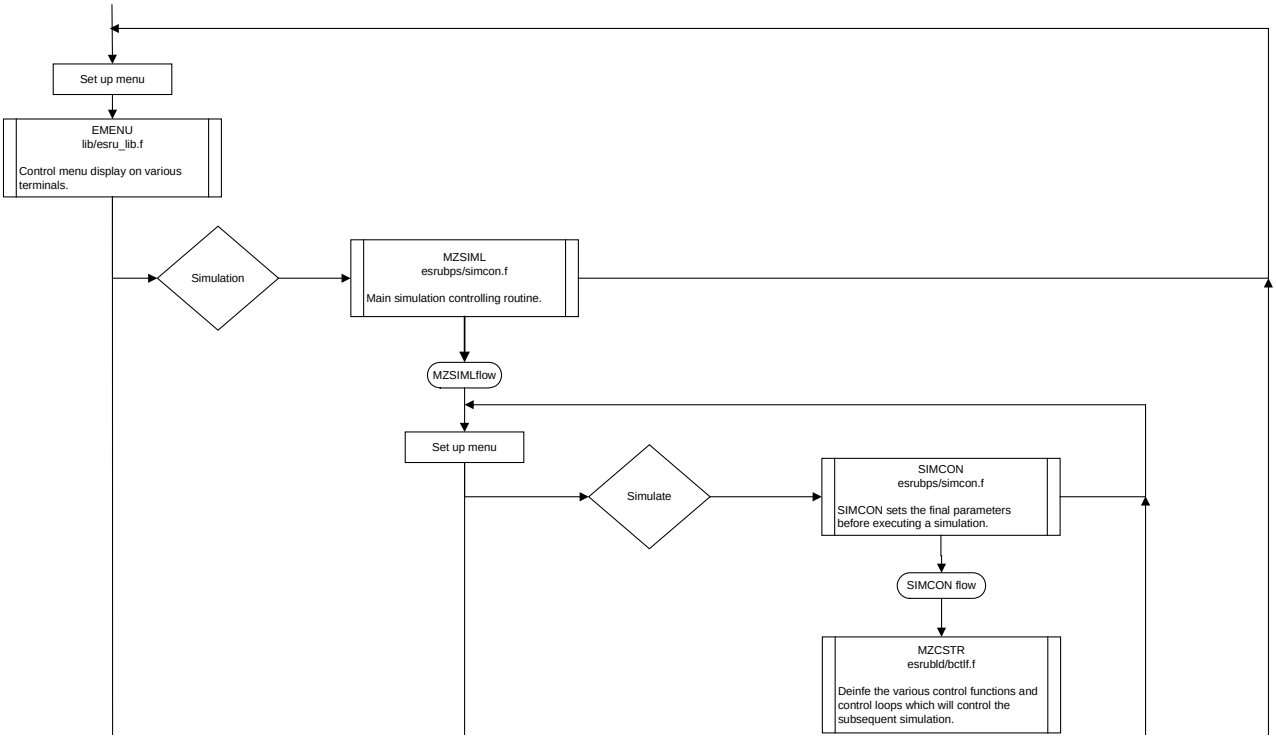
Set up menu
EMENU
lib/esru_lib.f
Control menu display on various terminals.
Simulation
MZSIML
esrubps/simcon.f
Main simulation controlling routine.
MZSIMLflow
Set up menu
Simulate
SIMCON
esrubps/simcon.f
SIMCON sets the final parameters before executing a simulation.
SIMCON flow
MZCSTR
esrubld/bctlf.f
Deinfe the various control functions and control loops which will control the subsequent simulation.

1.6

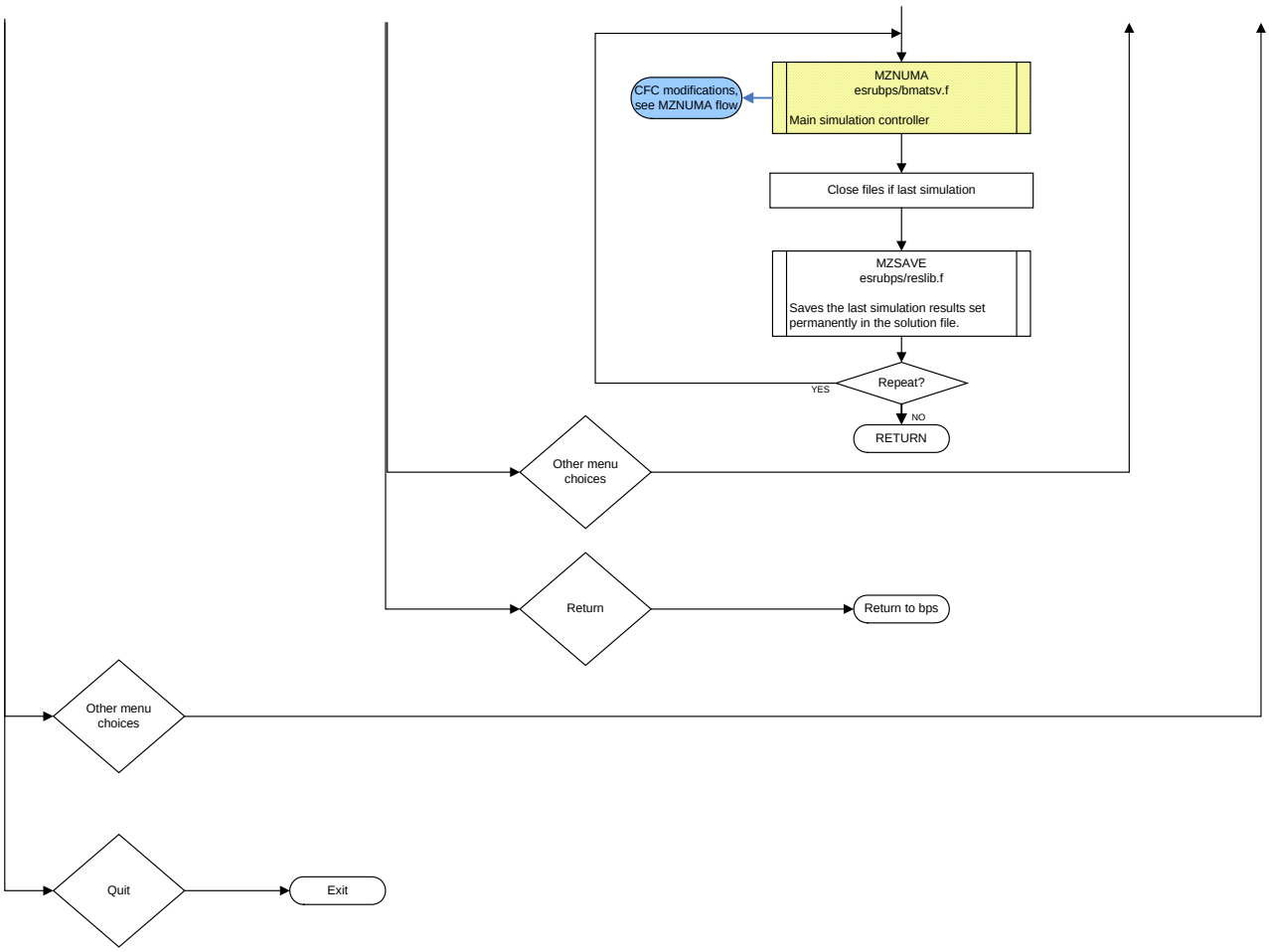
MZNUMA
esrubps/bmatsv.f
Main simulation controller
CFC modifications, see MZNUMA flow
Close files if last simulation
MZSAVE
esrubps/reslib.f
Saves the last simulation results set permanently in the solution file.
Repeat?
YES
NO
RETURN
Other menu choices
Return
Return to bps
Other menu choices
Quit
Exit

E.2 Subroutine “MZNUMA”

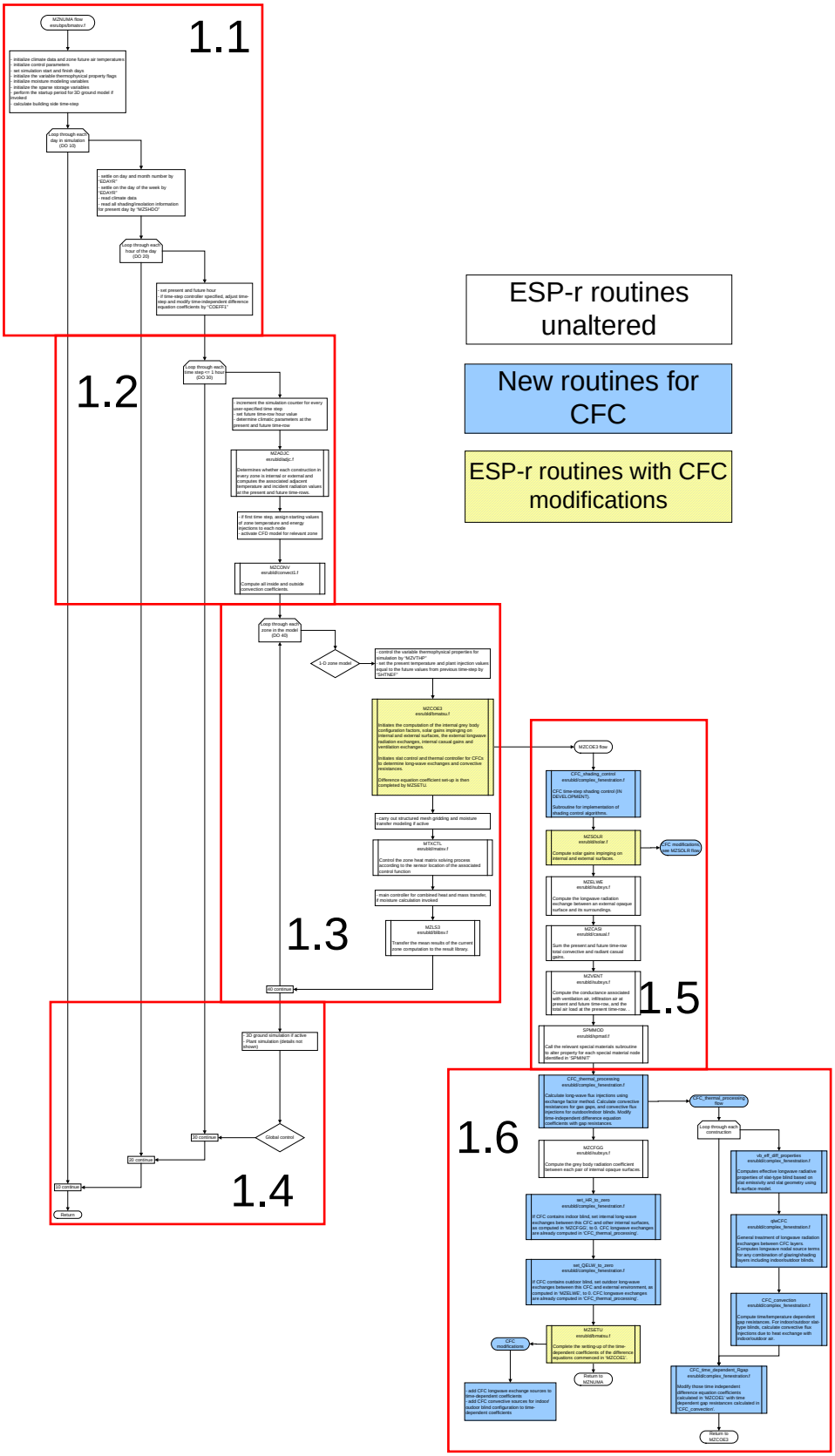

1.1

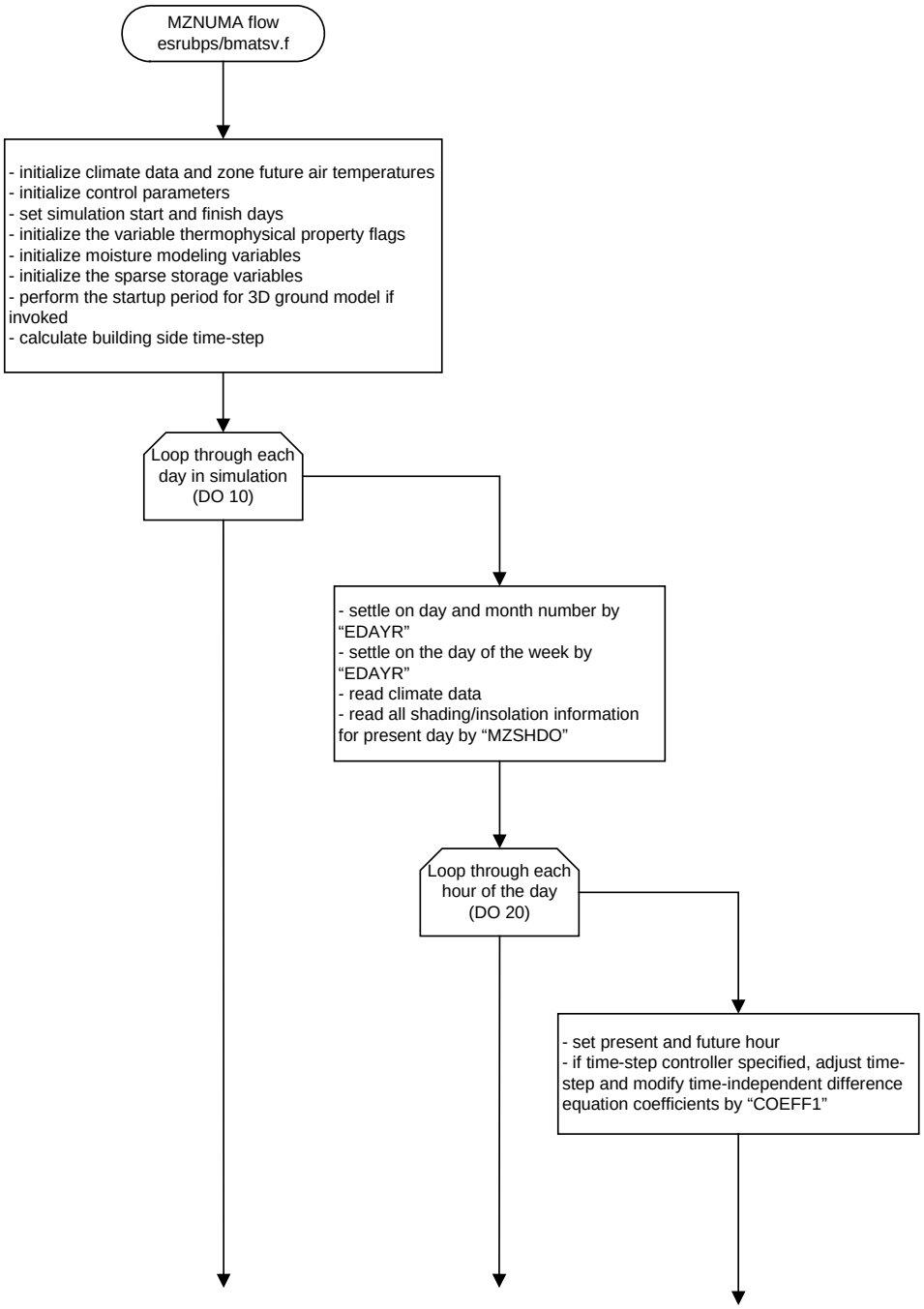
MZNUMA flow
esrubps/bmatsv.f
- initialize climate data and zone future air temperatures
- initialize control parameters
- set simulation start and finish days
- initialize the variable thermophysical property flags
- initialize moisture modeling variables
- initialize the sparse storage variables
- perform the startup period for 3D ground model if invoked
- calculate building side time-step
Loop through each day in simulation (DO 10)
- settle on day and month number by "EDAYR"
- settle on the day of the week by "EDAYR"
- read climate data
- read all shading/insolation information for present day by "MZSHDO"
Loop through each hour of the day (DO 20)
- set present and future hour
- if time-step controller specified, adjust time-step and modify time-independent difference equation coefficients by "COEFF1"

1.2

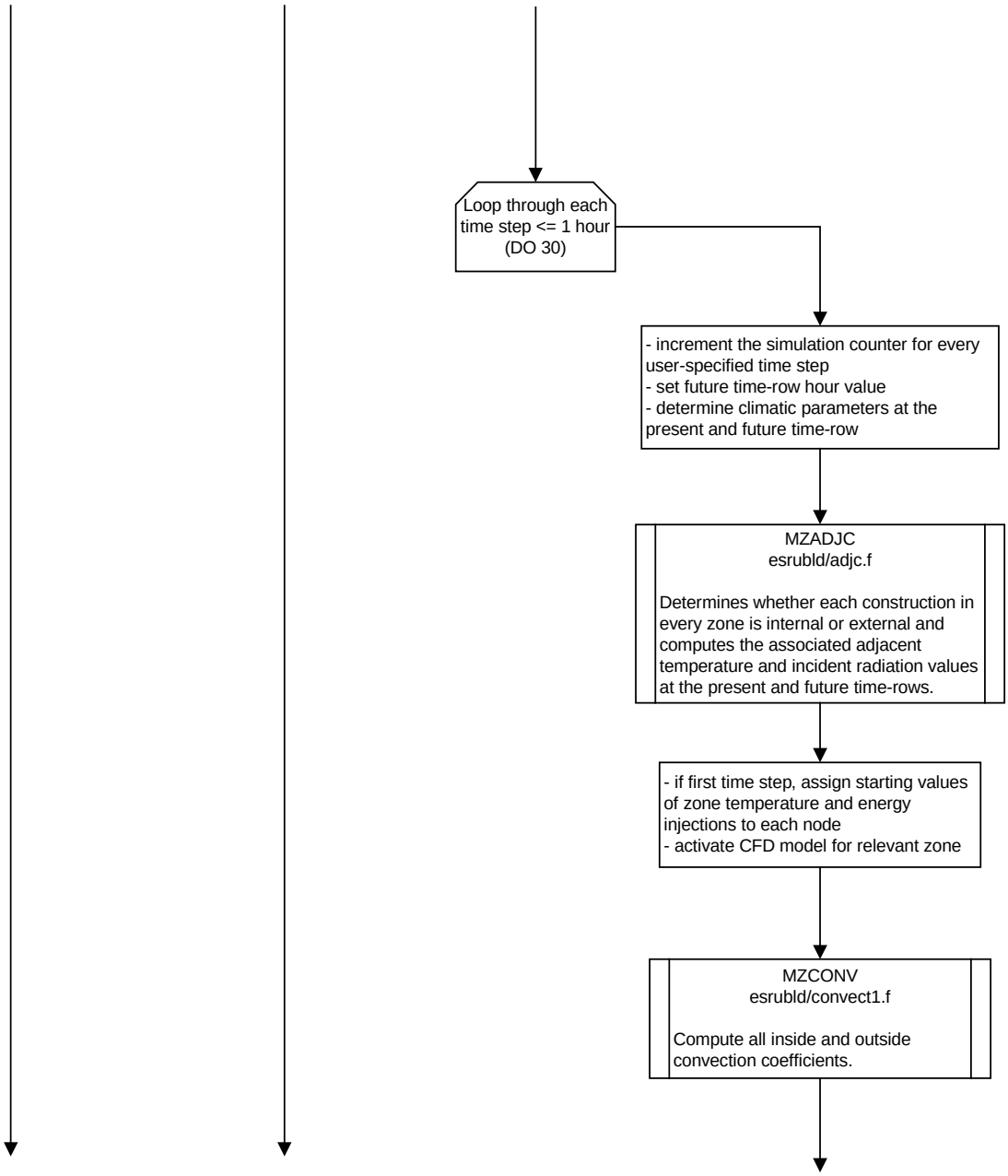
Loop through each time step <= 1 hour (DO 30)
- increment the simulation counter for every user-specified time step
- set future time-row hour value
- determine climatic parameters at the present and future time-row
MZADJC
esrubld/adjc.f
Determines whether each construction in every zone is internal or external and computes the associated adjacent temperature and incident radiation values at the present and future time-rows.
- if first time step, assign starting values of zone temperature and energy injections to each node
- activate CFD model for relevant zone
MZCONV
esrubld/convect1.f
Compute all inside and outside convection coefficients.

1.3

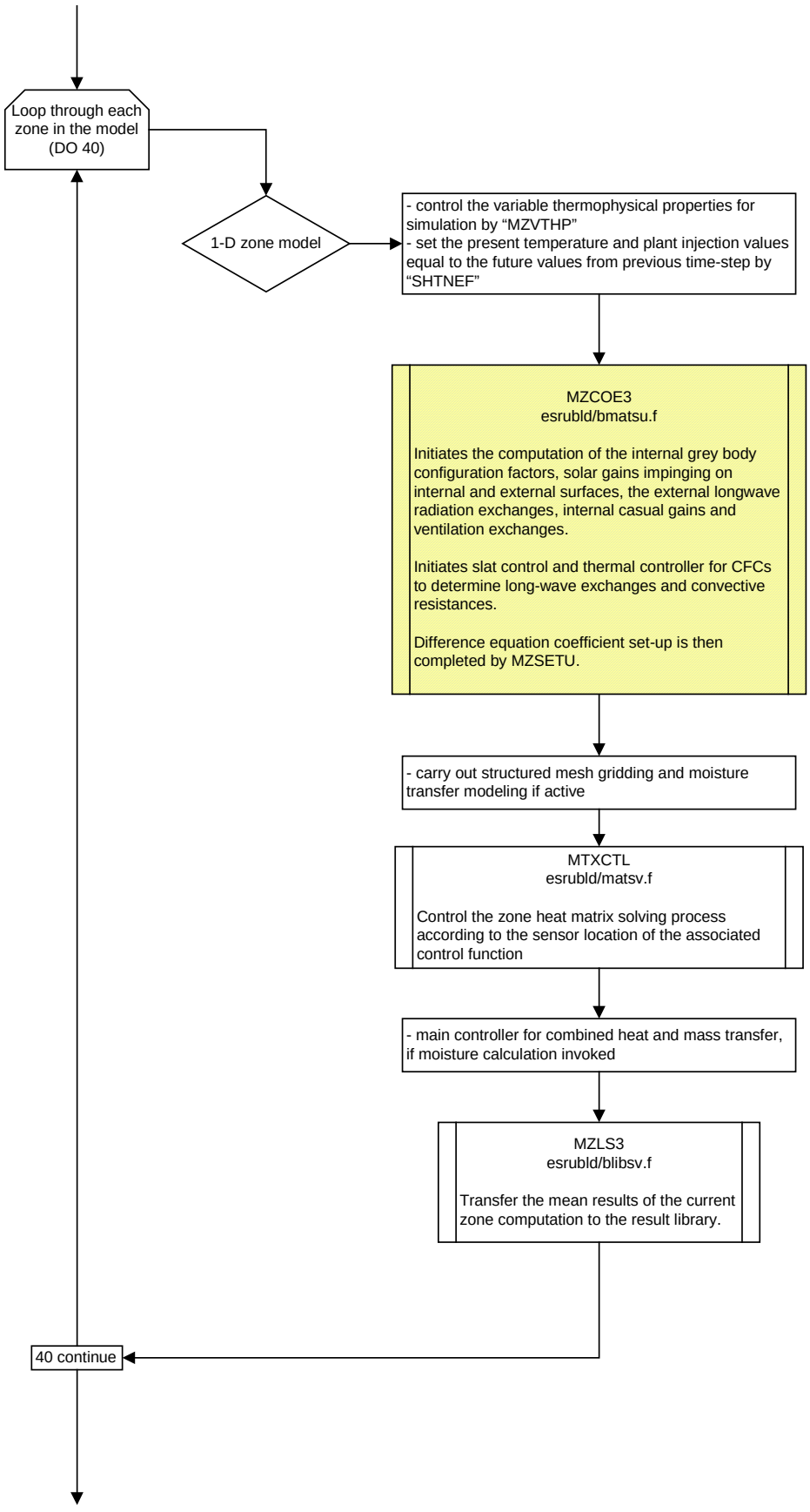
Loop through each zone in the model (DO 40)
1-D zone model
- control the variable thermophysical properties for simulation by “MZVTHP”
- set the present temperature and plant injection values equal to the future values from previous time-step by “SHTNEF”
MZCOE3
esrubld/bmatsu.f
Initiates the computation of the internal grey body configuration factors, solar gains impinging on internal and external surfaces, the external longwave radiation exchanges, internal casual gains and ventilation exchanges.
Initiates slat control and thermal controller for CFCs to determine long-wave exchanges and convective resistances.
Difference equation coefficient set-up is then completed by MZSETU.
- carry out structured mesh gridding and moisture transfer modeling if active
MTXCTL
esrubld/matsv.f
Control the zone heat matrix solving process according to the sensor location of the associated control function
- main controller for combined heat and mass transfer, if moisture calculation invoked
MZLS3
esrubld/blibsv.f
Transfer the mean results of the current zone computation to the result library.
40 continue

1.4

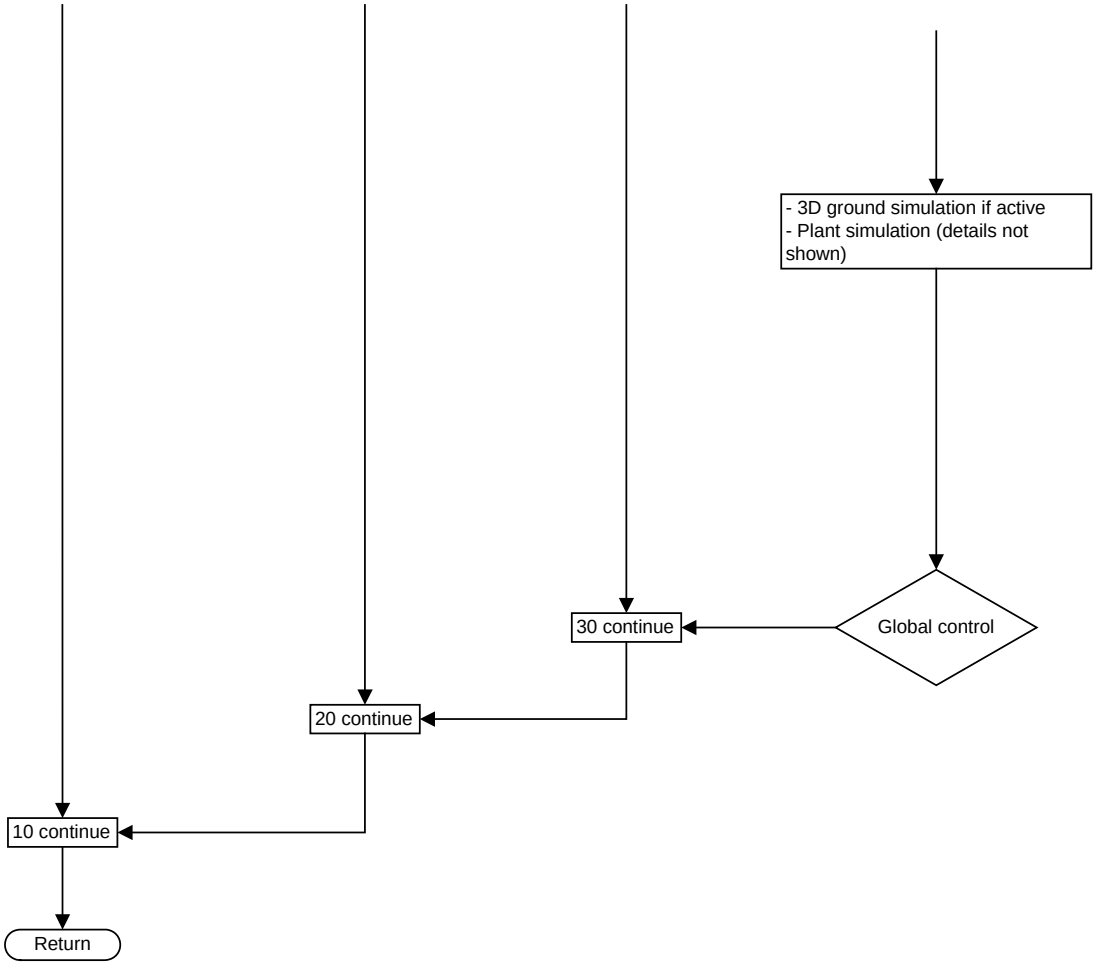
- 3D ground simulation if active
- Plant simulation (details not shown)
Global control
30 continue
20 continue
10 continue
Return

1.5

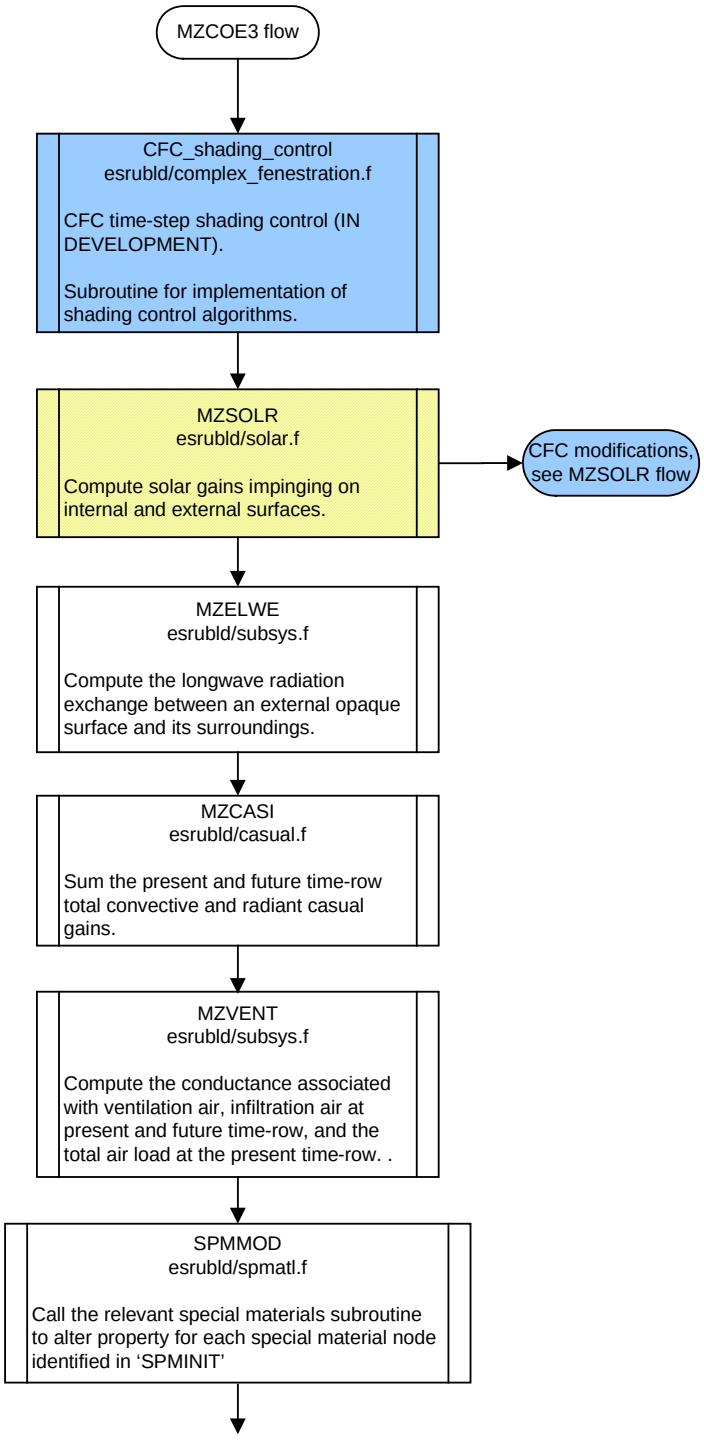
MZCOE3 flow
CFC_shading_control
esrubld/complex_fenestration.f
CFC time-step shading control (IN DEVELOPMENT).
Subroutine for implementation of shading control algorithms.
MZSOLR
esrubld/solar.f
Compute solar gains impinging on internal and external surfaces.
CFC modifications, see MZSOLR flow
MZELWE
esrubld/subsys.f
Compute the longwave radiation exchange between an external opaque surface and its surroundings.
MZCASI
esrubld/casual.f
Sum the present and future time-row total convective and radiant casual gains.
MZVENT
esrubld/subsys.f
Compute the conductance associated with ventilation air, infiltration air at present and future time-row, and the total air load at the present time-row. .
SPMMOD
esrubld/spmatl.f
Call the relevant special materials subroutine to alter property for each special material node identified in 'SPMINIT'

1.6

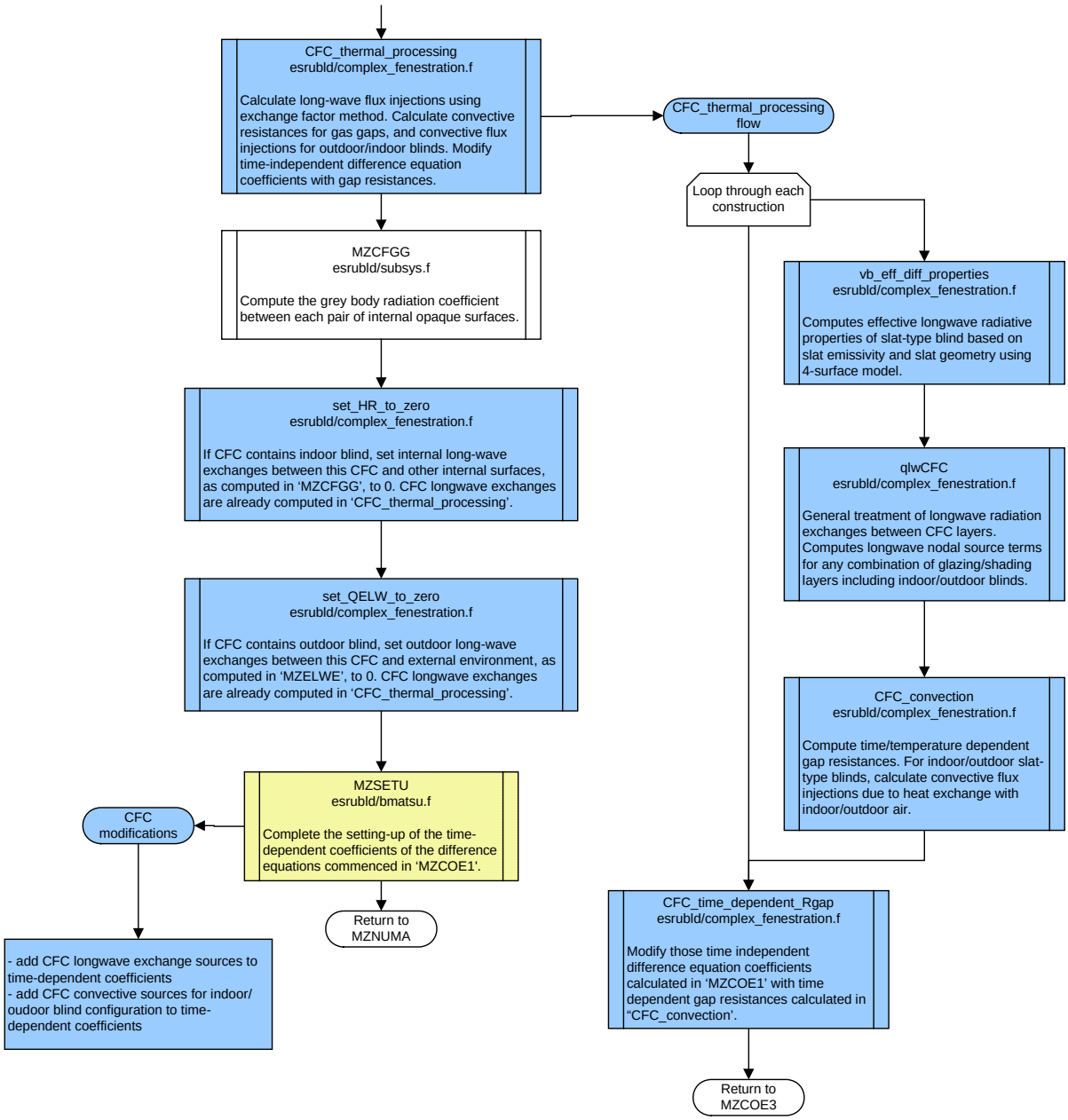
CFC_thermal_processing
esrubld/complex_fenestration.f
Calculate long-wave flux injections using exchange factor method. Calculate convective resistances for gas gaps, and convective flux injections for outdoor/indoor blinds. Modify time-independent difference equation coefficients with gap resistances.
CFC_thermal_processing flow
Loop through each construction
MZCFGG
esrubld/subsys.f
Compute the grey body radiation coefficient between each pair of internal opaque surfaces.
vb_eff_diff_properties
esrubld/complex_fenestration.f
Computes effective longwave radiative properties of slat-type blind based on slat emissivity and slat geometry using 4-surface model.
set_HR_to_zero
esrubld/complex_fenestration.f
If CFC contains indoor blind, set internal long-wave exchanges between this CFC and other internal surfaces, as computed in 'MZCFGG', to 0. CFC longwave exchanges are already computed in 'CFC_thermal_processing'.
qlwCFC
esrubld/complex_fenestration.f
General treatment of longwave radiation exchanges between CFC layers. Computes longwave nodal source terms for any combination of glazing/shading layers including indoor/outdoor blinds.
set_QELW_to_zero
esrubld/complex_fenestration.f
If CFC contains outdoor blind, set outdoor long-wave exchanges between this CFC and external environment, as computed in 'MZELWE', to 0. CFC longwave exchanges are already computed in 'CFC_thermal_processing'.
CFC_convection
esrubld/complex_fenestration.f
Compute time/temperature dependent gap resistances. For indoor/outdoor slat-type blinds, calculate convective flux injections due to heat exchange with indoor/outdoor air.
MZSETU
esrubld/bmatsu.f
Complete the setting-up of the time-dependent coefficients of the difference equations commenced in 'MZCOE1'.
CFC modifications
Return to MZNUMA
- add CFC longwave exchange sources to time-dependent coefficients
- add CFC convective sources for indoor/ oudoor blind configuration to time-dependent coefficients
CFC_time_dependent_Rgap
esrubld/complex_fenestration.f
Modify those time independent difference equation coefficients calculated in 'MZCOE1' with time dependent gap resistances calculated in "CFC_convection'.
Return to MZCOE3

E.3 Subroutine “qlwCFC”

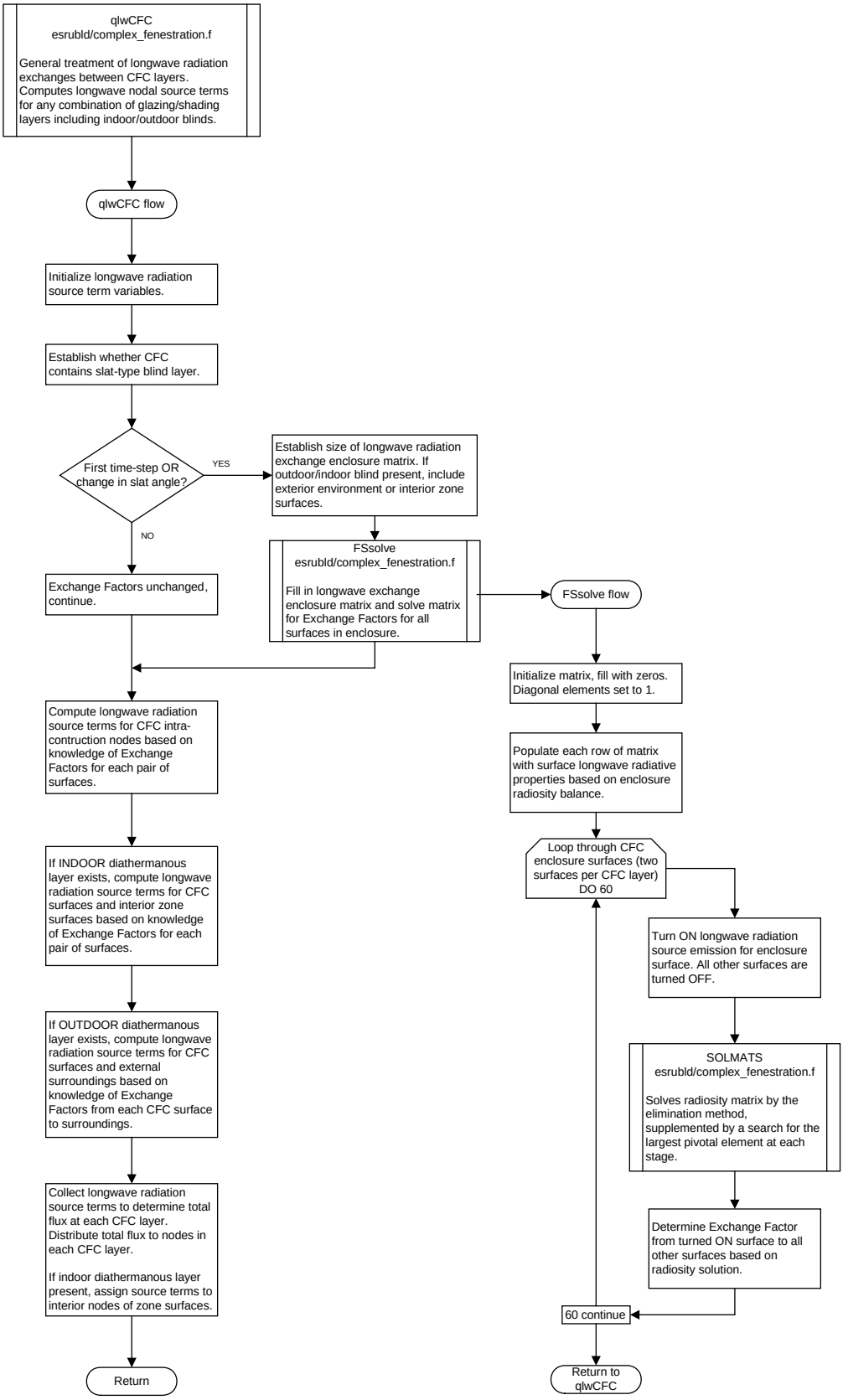

E.4 Subroutine “CFC_convection”

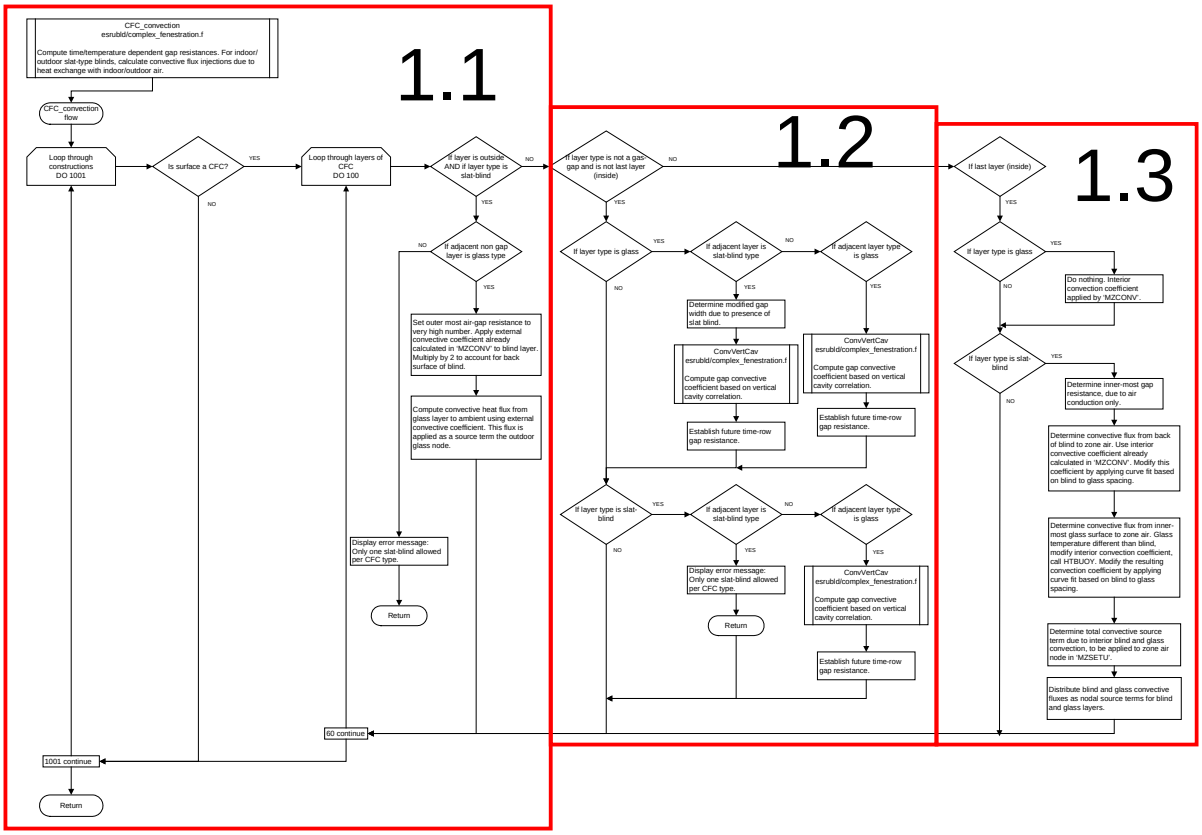

1.1

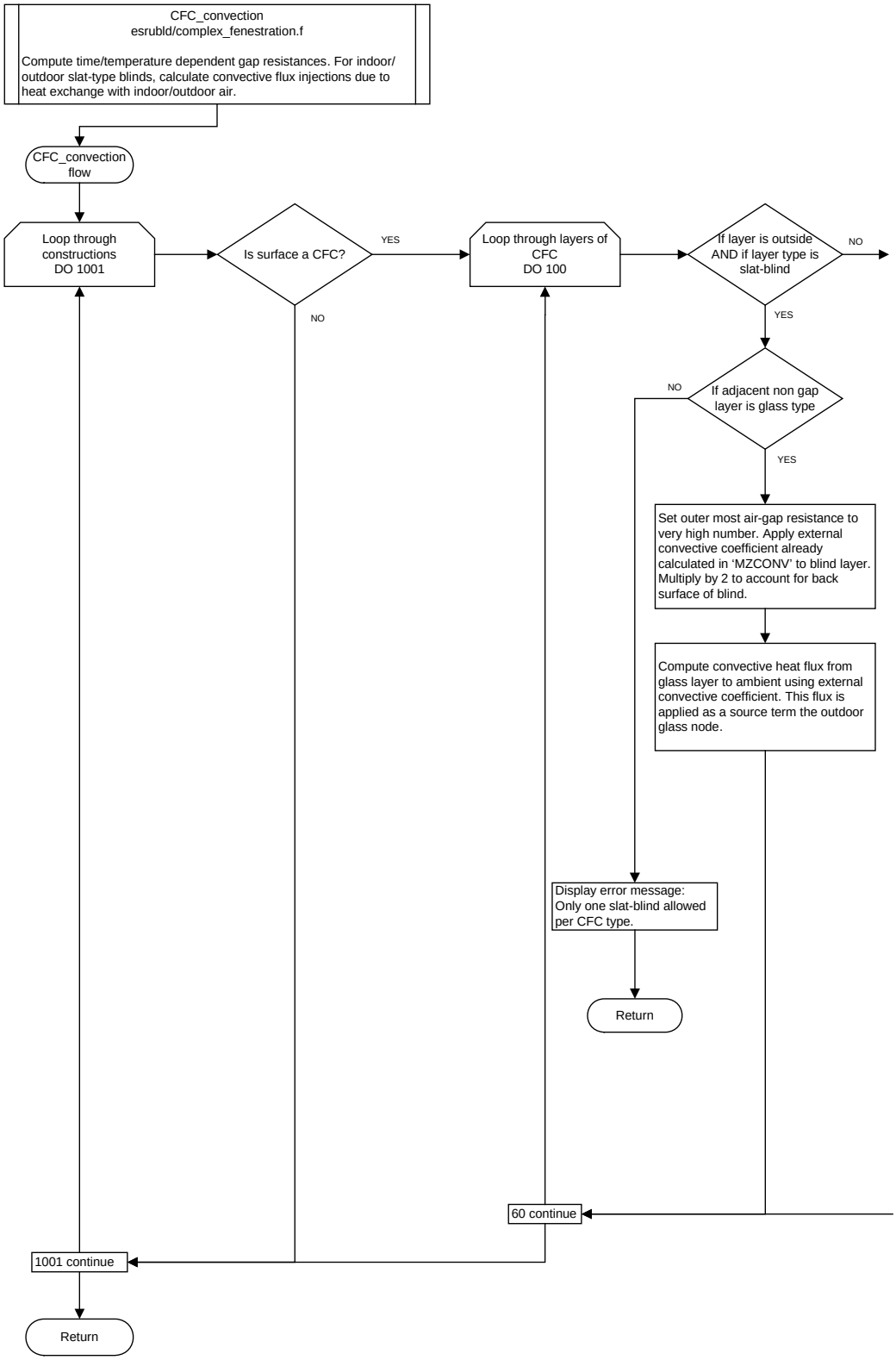
CFC_convection
esrubld/complex_fenestration.f
Compute time/temperature dependent gap resistances. For indoor/ outdoor slat-type blinds, calculate convective flux injections due to heat exchange with indoor/outdoor air.
CFC_convection flow
Loop through constructions DO 1001
Is surface a CFC?
YES
NO
Loop through layers of CFC DO 100
If layer is outside AND if layer type is slat-blind
NO
YES
If adjacent non gap layer is glass type
NO
YES
Set outer most air-gap resistance to very high number. Apply external convective coefficient already calculated in 'MZCONV' to blind layer. Multiply by 2 to account for back surface of blind.
Compute convective heat flux from glass layer to ambient using external convective coefficient. This flux is applied as a source term the outdoor glass node.
Display error message: Only one slat-blind allowed per CFC type.
Return
60 continue
1001 continue
Return

1.2

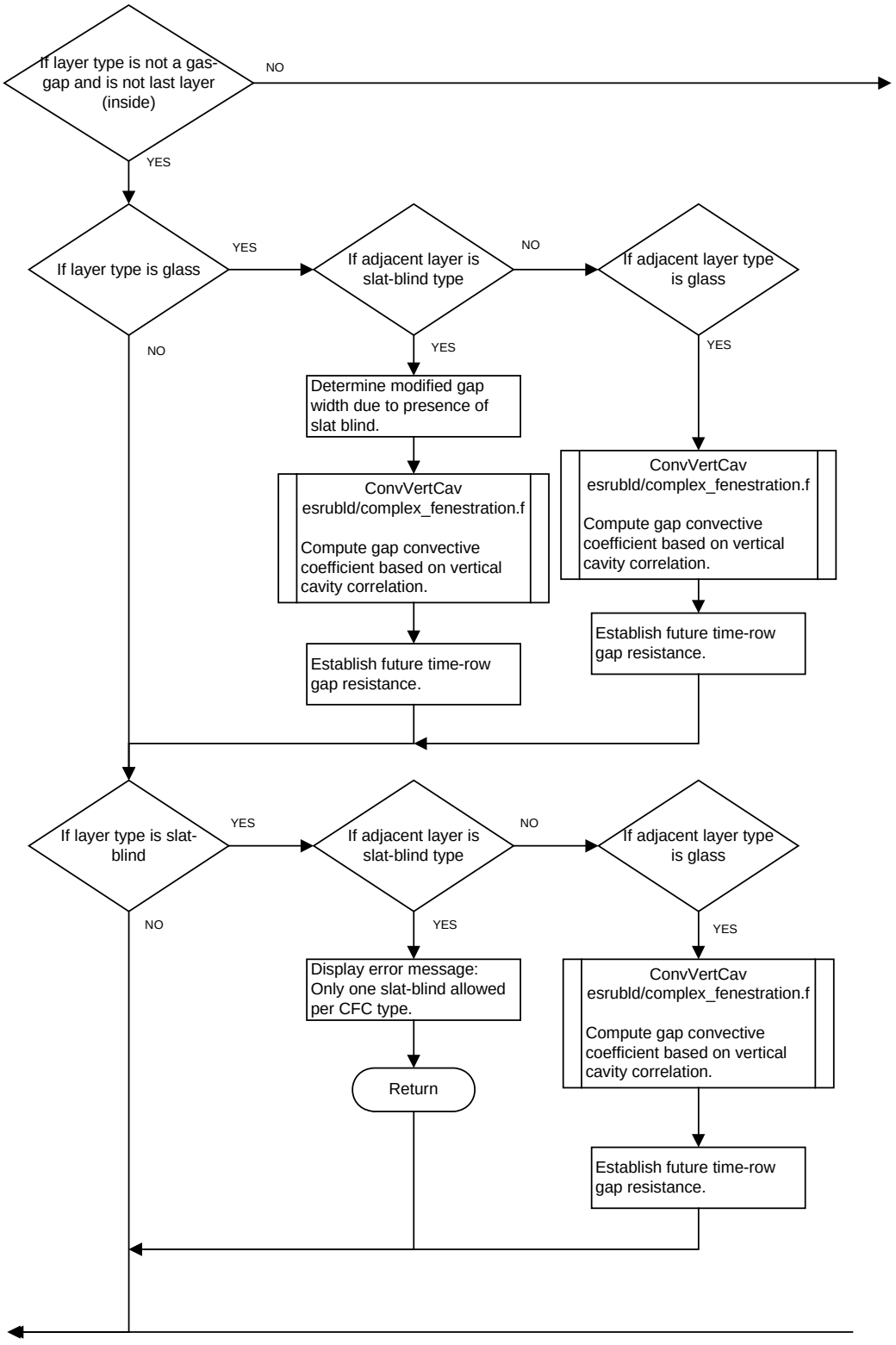
If layer type is not a gas-gap and is not last layer (inside)
NO
YES
If layer type is glass
YES
If adjacent layer is slat-blind type
NO
If adjacent layer type is glass
NO
YES
YES
Determine modified gap width due to presence of slat blind.
ConvVertCav esrubld/complex_fenestration.f
Compute gap convective coefficient based on vertical cavity correlation.
ConvVertCav esrubld/complex_fenestration.f
Compute gap convective coefficient based on vertical cavity correlation.
Establish future time-row gap resistance.
Establish future time-row gap resistance.
If layer type is slat-blind
YES
If adjacent layer is slat-blind type
NO
If adjacent layer type is glass
NO
YES
YES
Display error message: Only one slat-blind allowed per CFC type.
Return
ConvVertCav esrubld/complex_fenestration.f
Compute gap convective coefficient based on vertical cavity correlation.
Establish future time-row gap resistance.

1.3

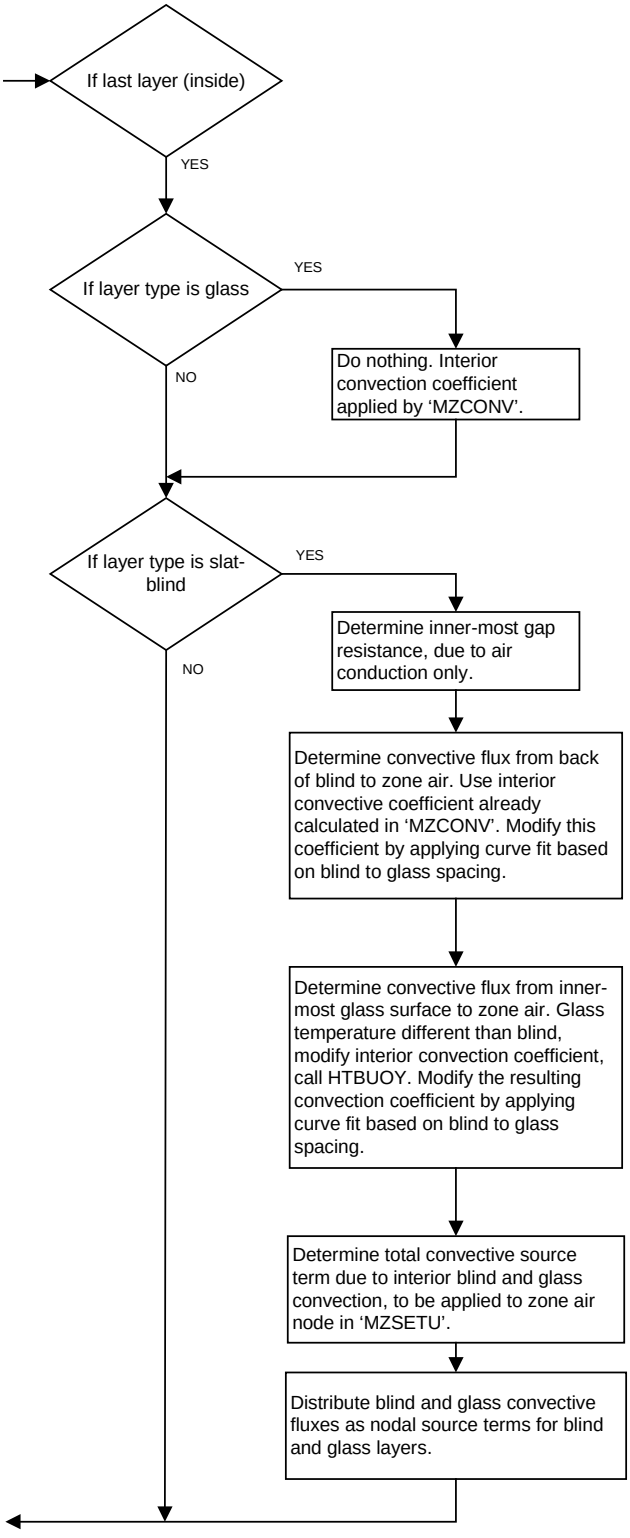
If last layer (inside)
YES
If layer type is glass
YES
Do nothing. Interior convection coefficient applied by 'MZCONV'.
NO
If layer type is slat-blind
YES
Determine inner-most gap resistance, due to air conduction only.
NO
Determine convective flux from back of blind to zone air. Use interior convective coefficient already calculated in 'MZCONV'. Modify this coefficient by applying curve fit based on blind to glass spacing.
Determine convective flux from inner-most glass surface to zone air. Glass temperature different than blind, modify interior convection coefficient, call HTBUOY. Modify the resulting convection coefficient by applying curve fit based on blind to glass spacing.
Determine total convective source term due to interior blind and glass convection, to be applied to zone air node in 'MZSETU'.
Distribute blind and glass convective fluxes as nodal source terms for blind and glass layers.

Appendix F: CFC User's Reference

F.1 Overview

The Complex Fenestration Construction (CFC) allows for a more accurate treatment of modeling windows with shading devices in ESP-r. The nodal structure of a CFC composition is equivalent to transparent multilayer constructions (TMC) and opaque multilayer constructions (MLC), however, new solar models have been implemented to solve for glazing/shading system solar optical properties at each time-step, as well as new thermal models to solve for the convective and radiant exchanges in glazing/shading layer combinations. The models process the solar, convective and radiant properties of the glazing/shading system at each time-step, making it possible to model automated operable shading devices with control resolution at the time-step level. Thermal resistances of sealed cavities between glazing/shading layers are calculated at each time-step for various fill gases and mixtures. In addition to modeling glazing/shading layer combinations, the CFC type also provides an alternate method of treating glazings without relying on third party software to characterize the solar optics and cavity resistances. An overview of the underlying CFC models and a summary of CFC capabilities is given in Chapter 4.

Thus far, the current implementation of CFCs in ESP-r does not support dynamic shading control. Slat angle control algorithms may be added to the source code via the subroutine "CFC_shading_control" in esrubld\complex_fenestration.F.

General Modeling Procedure

A CFC is composed of glazing and/or shading layers separated by gas gaps. Currently, the only shading types supported are operable slat-type blinds (e.g., venetian blinds). The specification of layer composition is general such that the shading layer may be placed in any position with respect to the multi-layer array. Only external, vertical surfaces may be attributed with a CFC composition.

The general procedure for using the CFC type in ESP-r simulations is as follows:

1) Create a CFC composition in the constructions database.

2) Create an import file (*.GSL) with solar optical, longwave radiative and fill gas properties and shading layer geometry using Glazing Shading Layer Editor, GSLedit.
3) Attribute the CFC composition to the model surfaces and import the corresponding *.GSL file to create an ESP-r CFC inpute file (*.cfc) for each zone containing CFC surfaces.

F.2 Create a CFC composition in constructions database

Complex Fenestration Constructions are created in the same way as transparent or opaque multilayer constructions, with some additional considerations that are explained in the following illustrative examples.

Example 2.1: Double glazing with indoor slat blind

Step 1: Create an entry in the materials database for the shade layer. The relevant properties for the shading layer are conductivity, density, and specific heat. All others may be left as the default values.

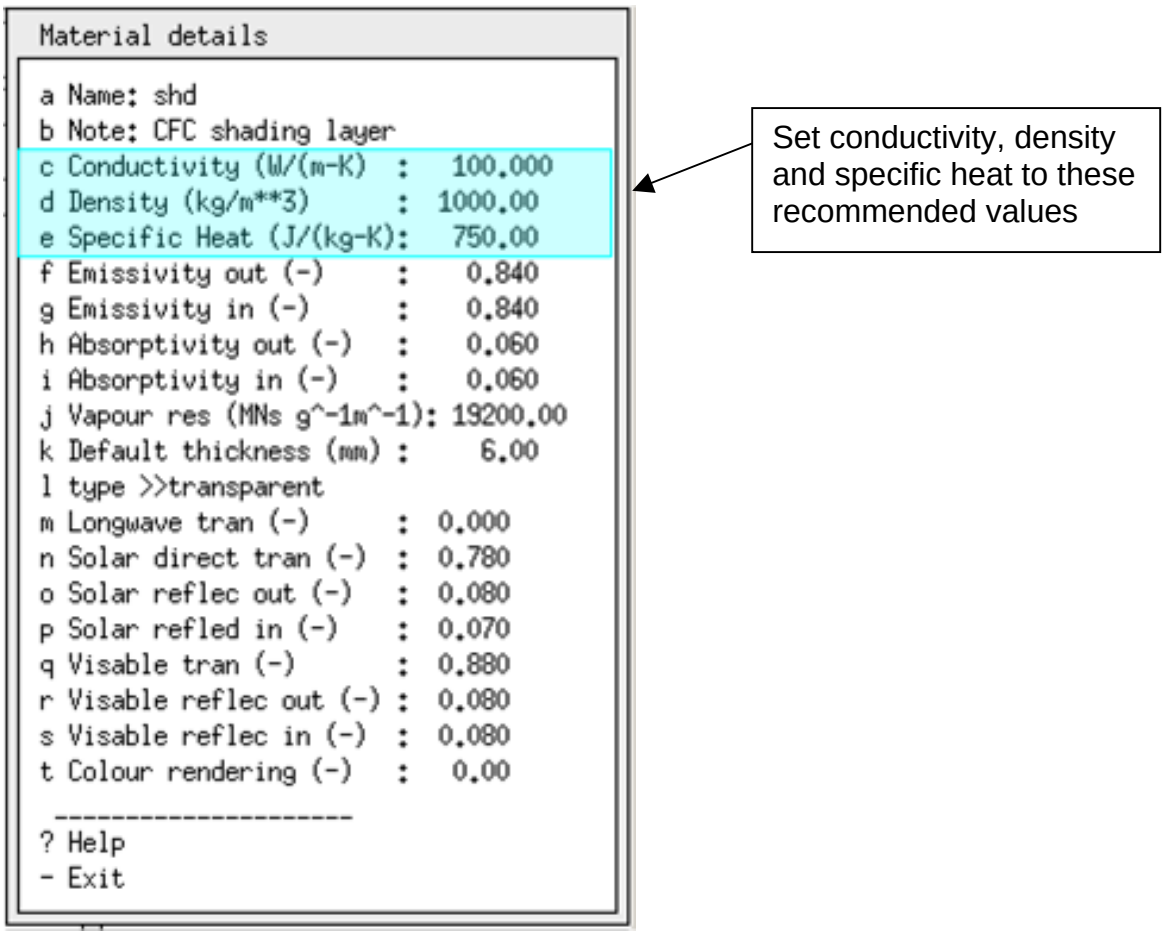

Figure F.1: Create material for shade layer.

Step 2: Assemble the CFC layers in the constructions database.

- Choose "Complex Fenestration Construction" under "General type". Under "Optical Properties", the note "Use GSLedit" will appear. This informs the user that for CFC types, the optical properties are specified using the GSL Editor, as discussed in section F.3.

Note 1: Although an air gap has been specified with default gap resistance, this layer is just a place holder and will be replaced with a fill gas as selected in GSLedit. The correct gap thickness must be specified.

Note 2: Layer 4 represents the air gap between glass and shade layers, which is naturally ventilated to the interior air. The thickness of this air gap represents the distance from the glass to the tips of the slats when slats are in the horizontal position.

Note 3: The thickness of the shading layer does not represent any actual shade layer dimension. It is only relevant to the shading layer thermal capacity. The thickness of 15 mm, in combination with the density and specific heat specified in Step 1 gives an equivalent thermal capacity of a 6 mm plate glass layer. This amount of thermal capacity is recommended to ensure solver stability.

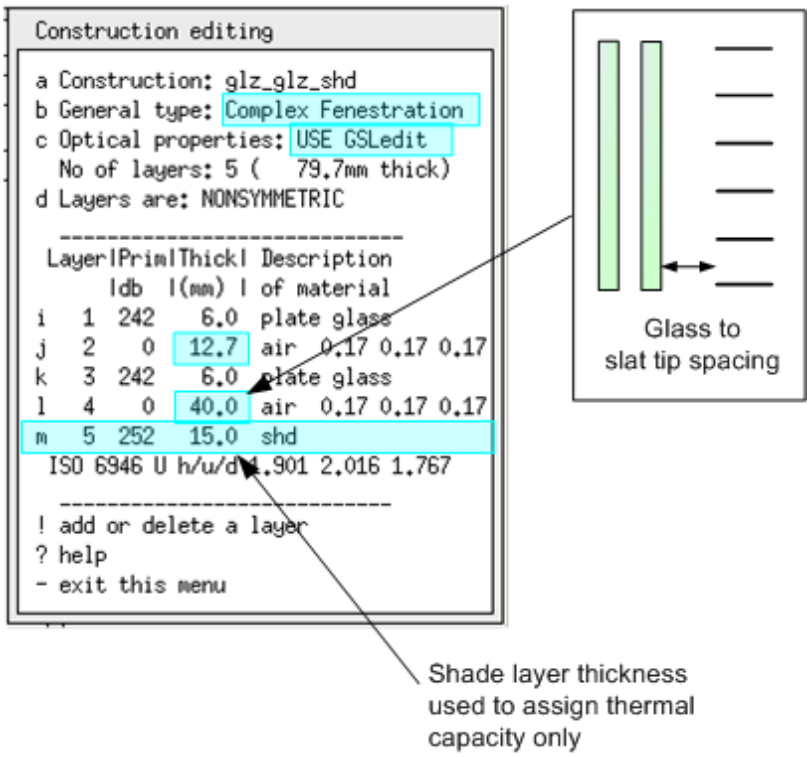

Figure F.2: Construction layers for double glazing with indoor slat blind.

Example 2.2: Double glazing with between-glass slat blind

Step 1: Same as in Example 2.1.

Step 2: Same as in Example 2.1 except for placement of shading layer. Figure F.3 illustrates the convention for shade layer to glass spacing when the shade layer is placed between two glass panes. Again, the thickness of the shading layer specified is not relevant to the shade layer geometry.

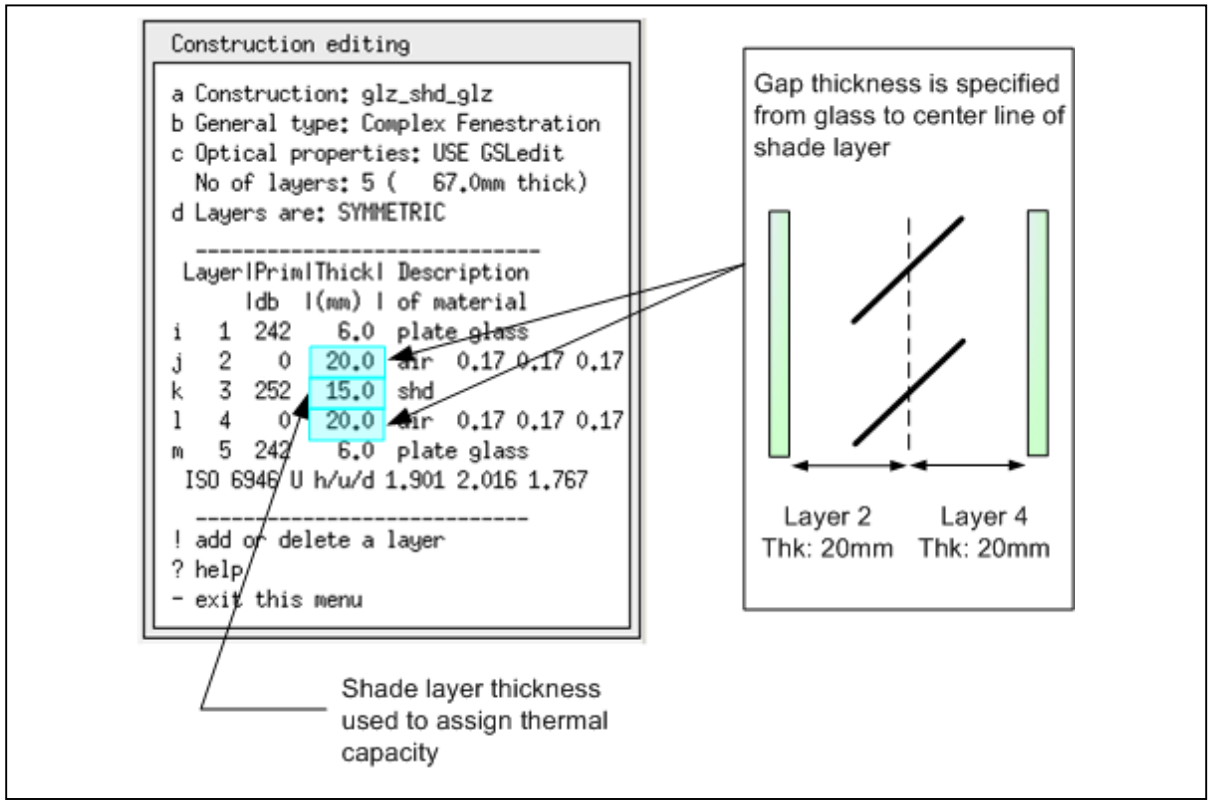

Figure F.3: Construction layers for double glazing with between-glass slat blind.

Example 2.3: Double glazing with outdoor slat blind

Step 1: Same as in Example 2.1.

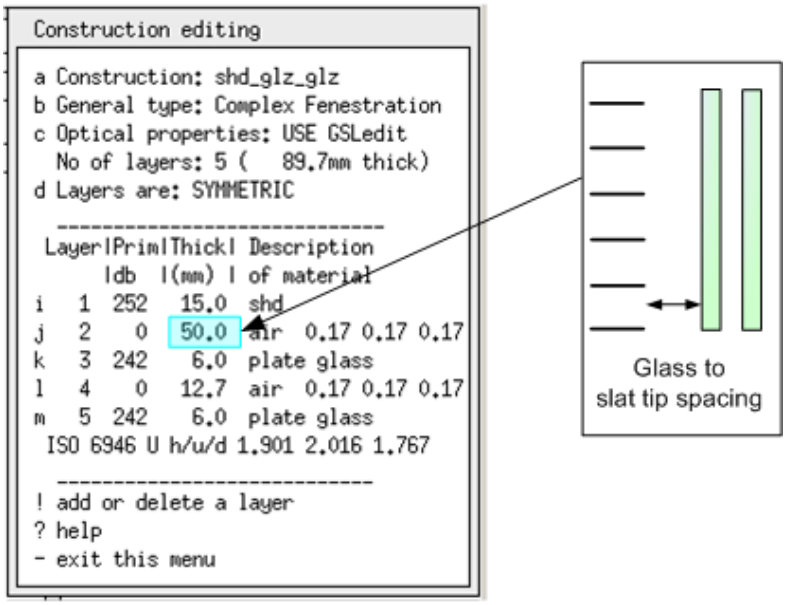

Figure F.4: Construction layers for double glazing with outdoor slat blind.

Step 2: Same as in Example 2.1.

F.3 Create *.GSL file using the Glazing Shading Layer Editor (GSLedit)

For each of the constructions created in Section E.2, an input property file must be created in GSLedit.

Step 1: Assemble glazing/shading layers to match the CFC layers in the constructions database of ESP-r.

- Open GSLedit, click "New" and select the number of layers in the system.

The number of layers will not correspond to the number of layers in ESP-r's construction database as the gap layers are not counted. For example, for a double glazing with shade, ESP-r counts five layers, but GSLedit counts 3.

- Left click on each layer and gap to assemble the layer properties.
- Select a glazing or shade from the databases. The glazing databases are based on the International Glazing Database (IGD) (LBNL 2008).
- Select a fill gas or fill gas mixture and spacing for gap layers. If the shading layer is on the outdoor or indoor side, select vented outdoors/indoors.
- Right click on any glazing/shading layer or gap to display the layer solar optical and longwave properties and the fill gas properties.

Note 1: Currently only glazing and venetian blind layers are allowed. If another type of shading layer is selected, the data will not be imported into ESP-r.

Note 2: Additional entries to the databases can be made by editing the database text files located in the \GSLbeta\GLZfiles directory. Changes to the current entries can also be made here.

Note 3: Make sure that the glazing and shading layer position and gap thicknesses match the CFC layer composition in ESP-r.

Step 2: Save the system for ESP-r output file format.

- Click "Setup", clilck "Output File Format" and choose "ESP-r".
- Click "Save" and choose a descriptive name for the file, e.g., "clear_clear_blind".
- A *.GSL file will be saved to \GSLbeta\GSLsystems directory.

Step 4: Copy the *.GSL file to the \zones directory of the ESP-r model.

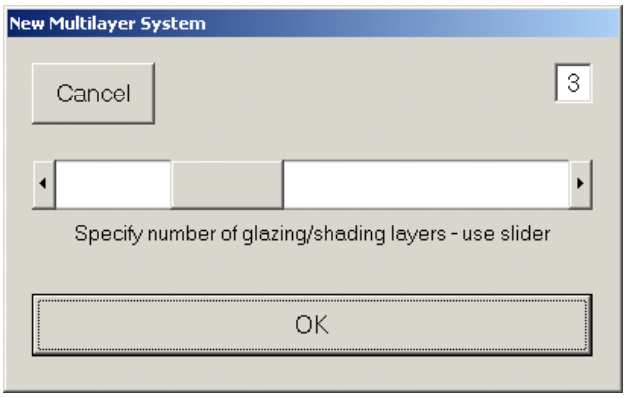

Figure F.5: Number of layers in GSLedit does not include gap layers.

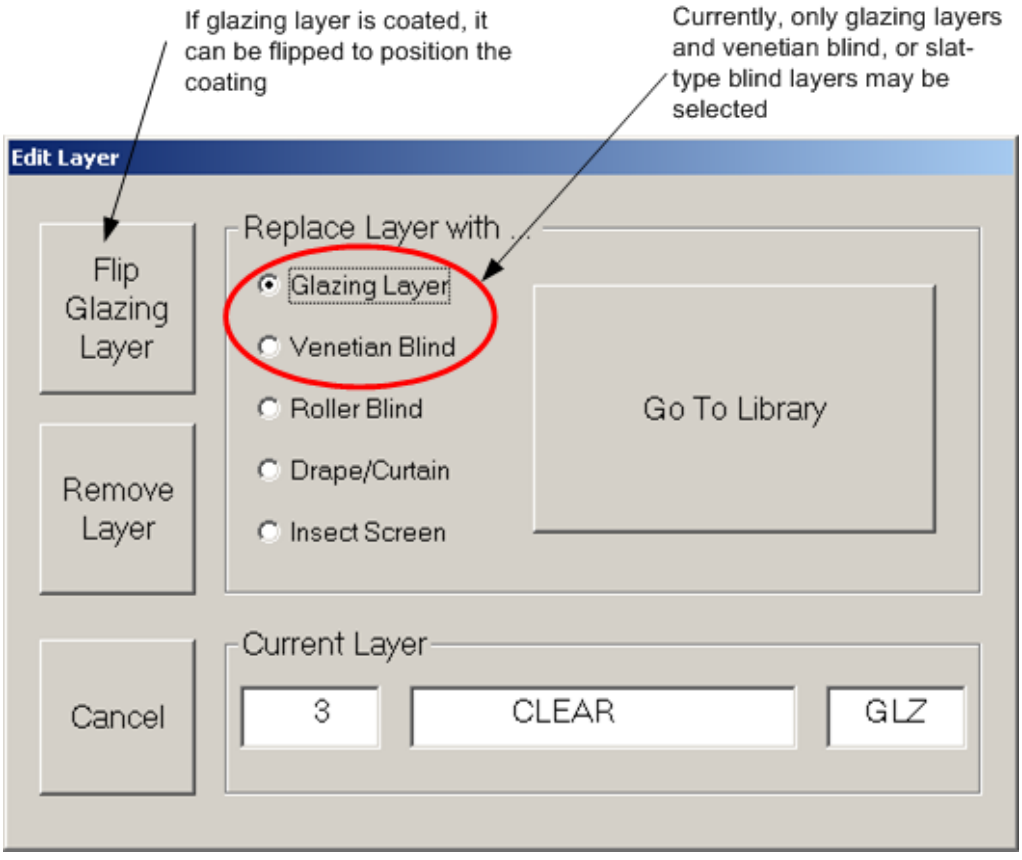

Figure F.6: Layer type selection.

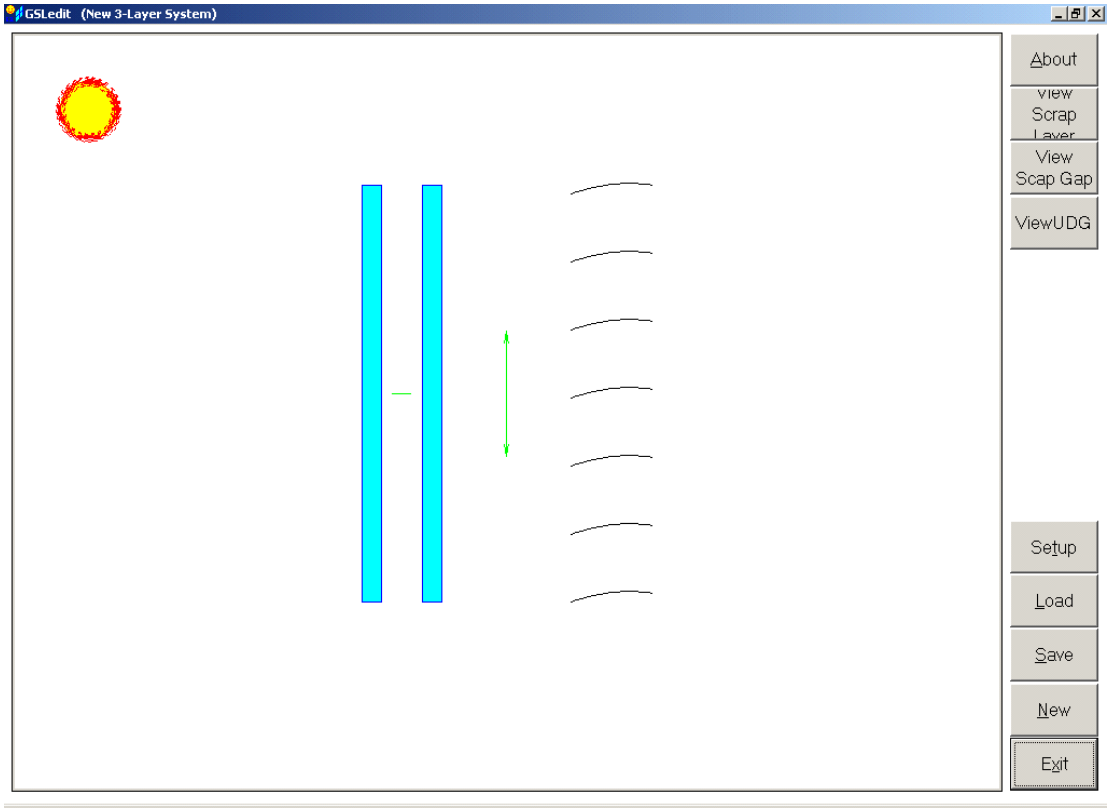

Figure F.7: Main window of GSLedit. Left click on layer or gap to change properties. Right click on layer or gap to display selected properties.

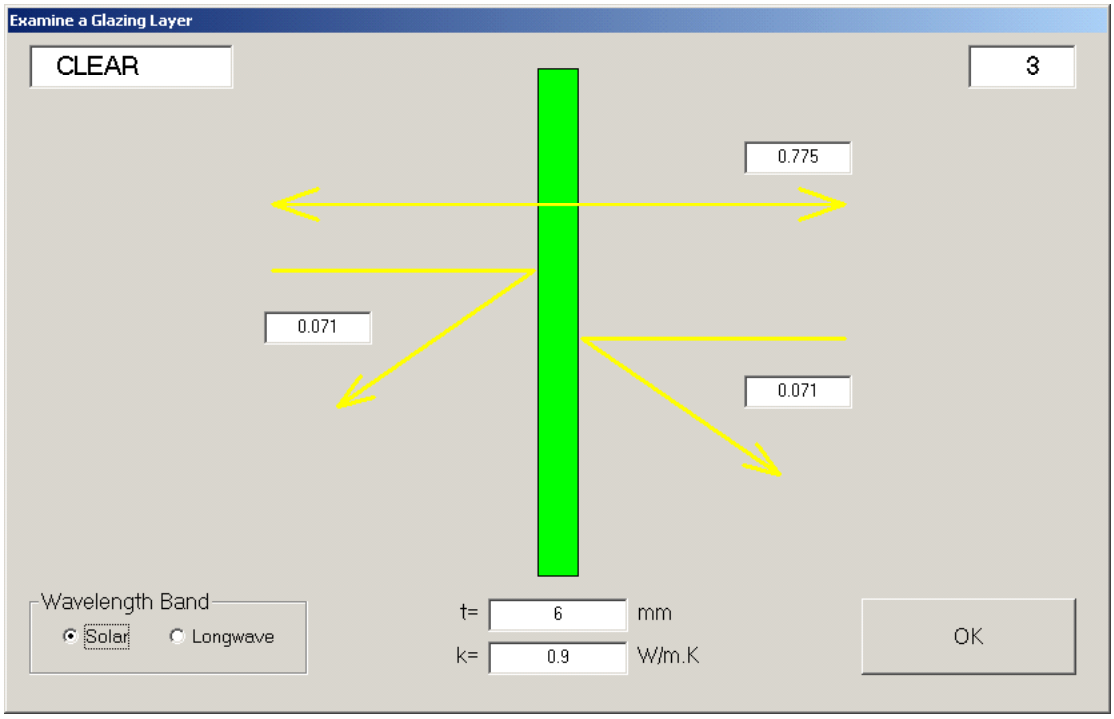

Figure F.8: Solar and longwave property display window of glazing layer.

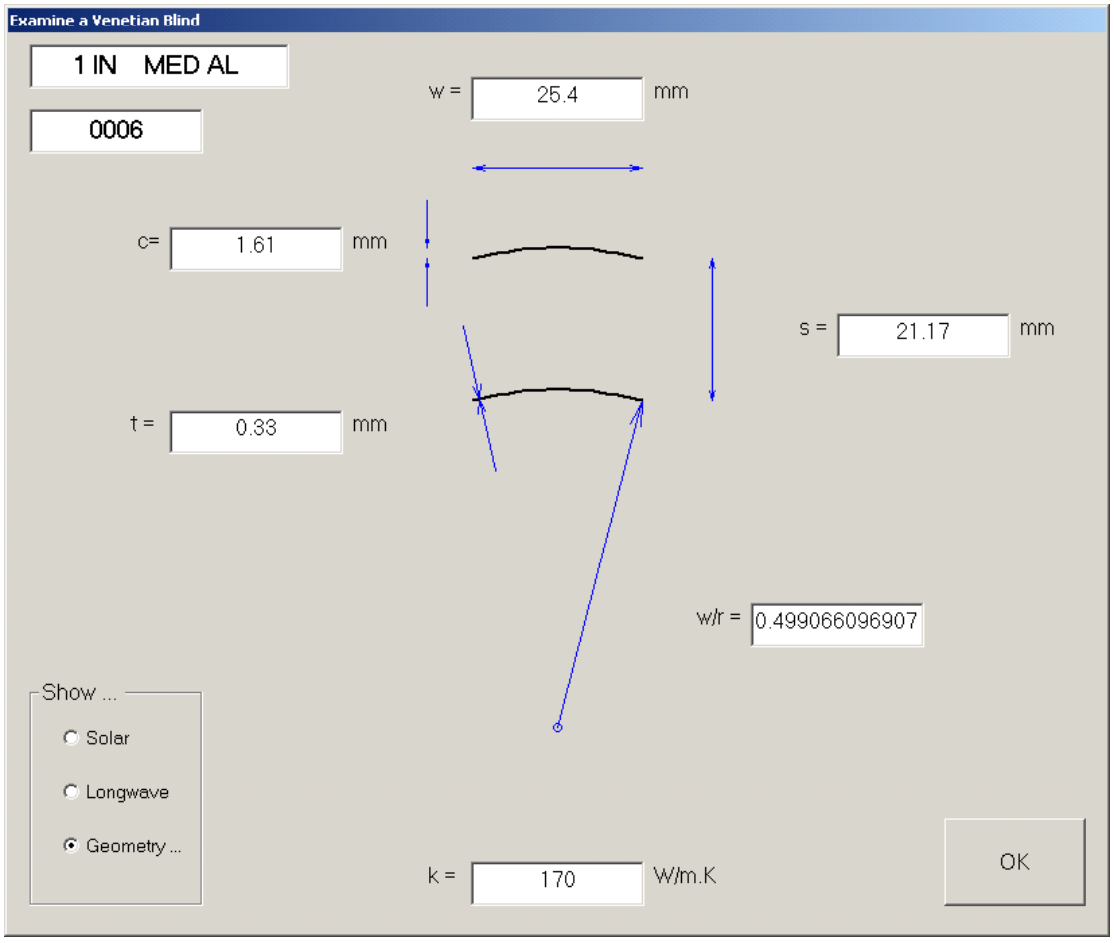

Figure F.9: Property display window of venetian blind layer.

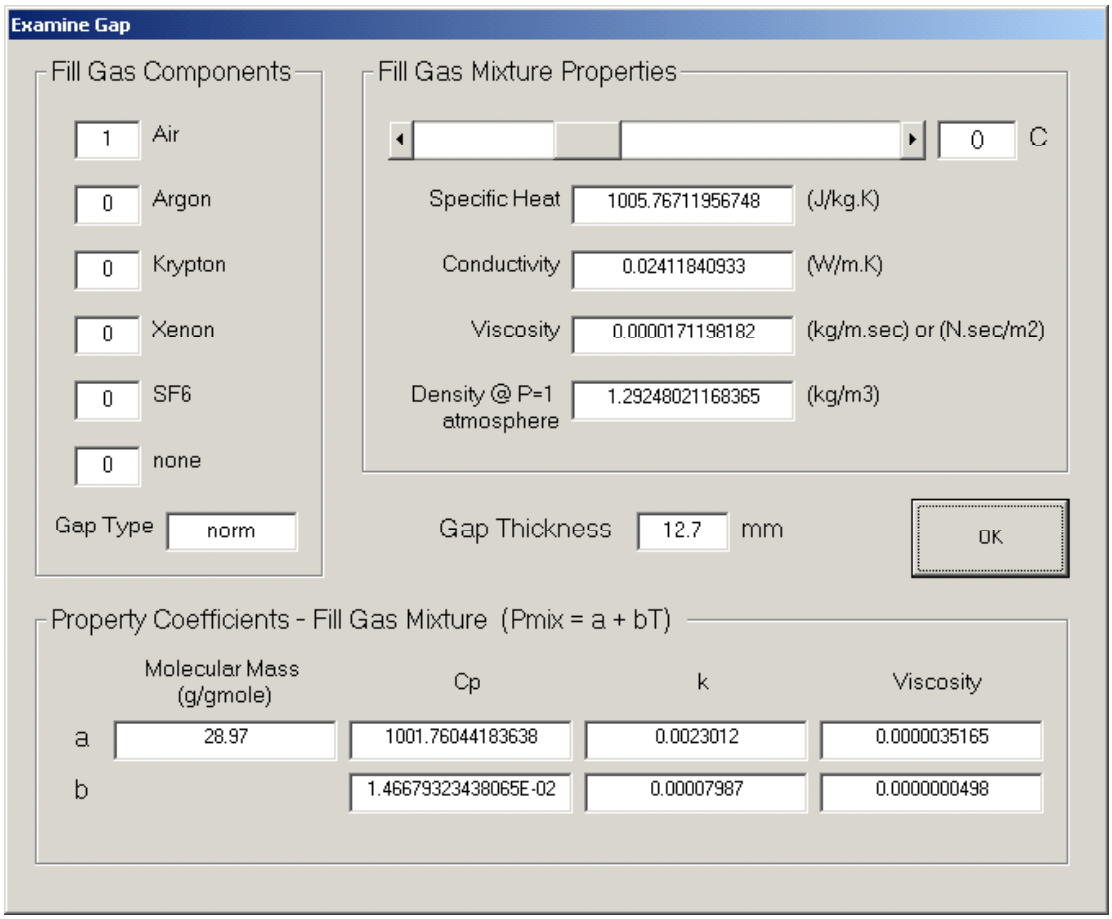

Figure F.10: Fill gas property display window.

F.4 Addition of CFCs to the ESP-r Model

Once the CFC has been constructed in ESP-r's constructions database, and the accompanying *.GSL file has been created and copied to the \zones directory of the model, the CFC can now be added to the simulation model.

This process is illustrated in the following example in which the model has been created with two windows that have been initially attributed with a double glazing TMC composition. The example replaces the double glazing TMC with two different CFCs that were constructed in section F.2 and compares the differences in solar transmission and cooling load given a 24 h simulation period for a summer day in Toronto, Canada.

Example – Room with large south and west glazings

This is a simple model with basic cooling control, no plant, constant ventilation rate and an internal gains schedule. The goal is to replace the "south_glz" and "west_glz" surfaces with Complex Fenestration Constructions and see the impact on the cooling load and solar transmission results.

Step 1: Replace TMC "dbl_glz" construction for surfaces "south_glz" and "west_glz" with CFC composition "shd_glz_glz".

- Navigate to "composition" > "geometry and attribution" > "surface attributes".
- Click "* attribute many", select "composition", select the desired CFC composition from the constructions library.
- Select surfaces "south_glz" and "west_glz".
- Click "Yes" to update the zone construction files.
- Enter the zone *.cfc file name. The *.cfc file is the ESP-r input file for CFCs which holds the glazing/shading system properties.

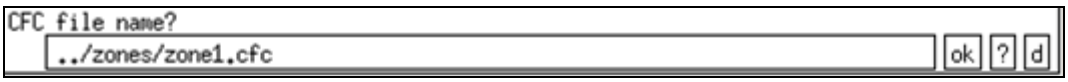

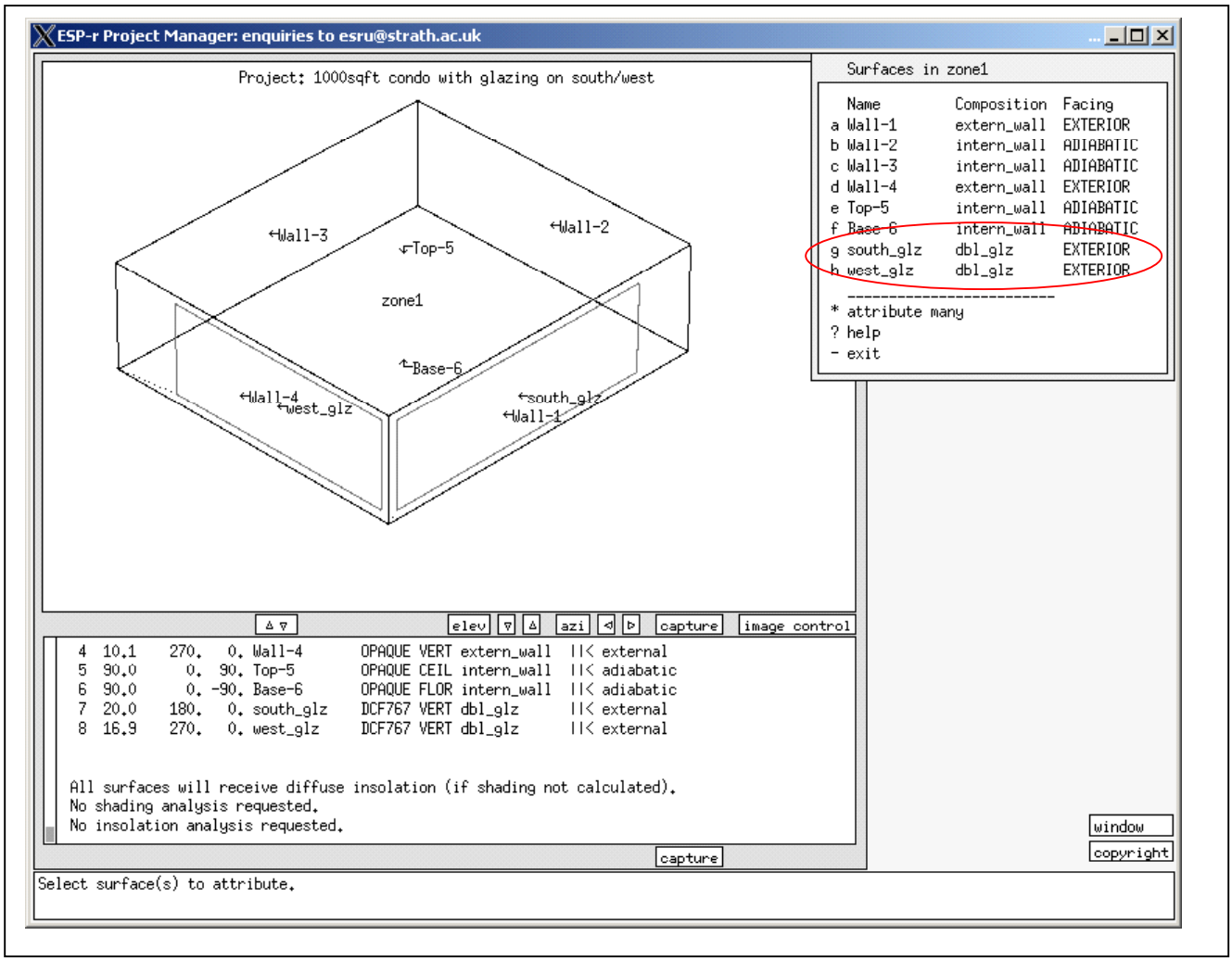

Figure F.11: Geometry, composition and boundary conditions of example model.

- Click "Import GSLedit files"

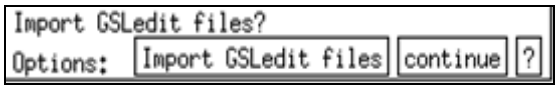

- Enter the Number of CFC types.

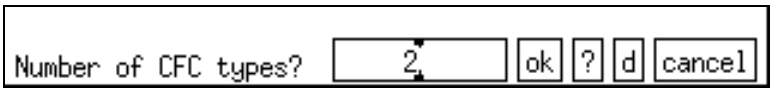

Note 1: A CFC type refers to the different CFC compositions and different slat orientations of the shading layer. Multiple types can exist for the same composition, but with different slat angles. For example, if "south_glz" and "west_glz" are the same composition but different slat angles, two CFC types are required for the zone:

Type 1: double glazing with outdoor venetian blind – slat angle 45 deg
Type 2: double glazing with outdoor venetian blind – slat angle 0 deg

If the composition of "south_glz" is different from "west_glz", two CFC types for the zone are necessary.

If the composition AND the slat angles are the same for both constructions, only one type is necessary.

- Assign the CFC type to each CFC surface.

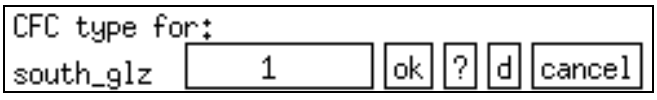

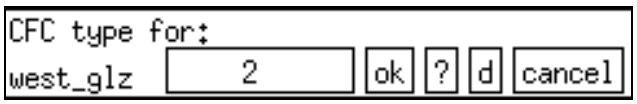

- Assign *.GSL file name for CFC type 1

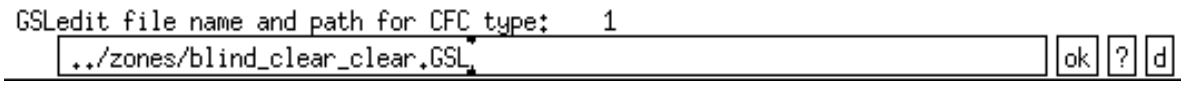

- Specify slat orientation.

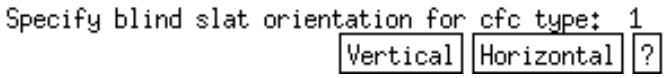

- Specify initial slat angle.

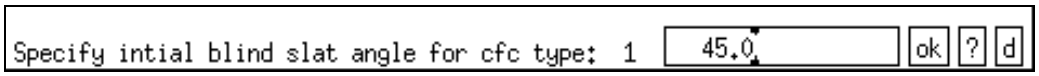

If the data from the *.GSL file was imported successfully to the *.cfc file the following message will display:

- Assign *.GSL file name for CFC type 2 (in this case same as type 1), specify orientation and slat angle for type 2 (same procedure as above).

The *.cfc file now contains all necessary data to carry out the simulation. The program will prompt the user to "Import GSLedit files" every time a change is made to the model construction or geometry. Once the files have been imported once, this prompt can be skipped by clicking on "continue".

Note 2: The slat angle convention used in CFCs is shown in Figure F.12

Note 3: The importing process can be repeated without changing the geometry attribution by navigating to the "zone constructions" window and clicking on "> save construction data". The user will then be prompted to import the GSLedit files.

Step 2: Carry out simulation.

- The time-step must be reduced to ensure stability and convergence of the solution. A recommended setting is 6 time-steps per hour.

Simulation Results

Figure F.13 shows the solar transmission and cooling load results carried out for a 24 h simulation period for a summer day in Toronto. The results show the initial case where a TMC double glazing composition was assigned to "south_glz" and "west_glz" surfaces, compared with the CFC case in which the two surfaces were replaced with the "shd_glz_glz" CFC composition. The "south_glz" surface slat angle was set to 45º whereas the "west_glz" slat angle was set to 0º. The cooling load and solar transmission are seen to peak in the afternoon hours since the west-facing slats are set in the horizontal position, resulting in high solar transmittance.

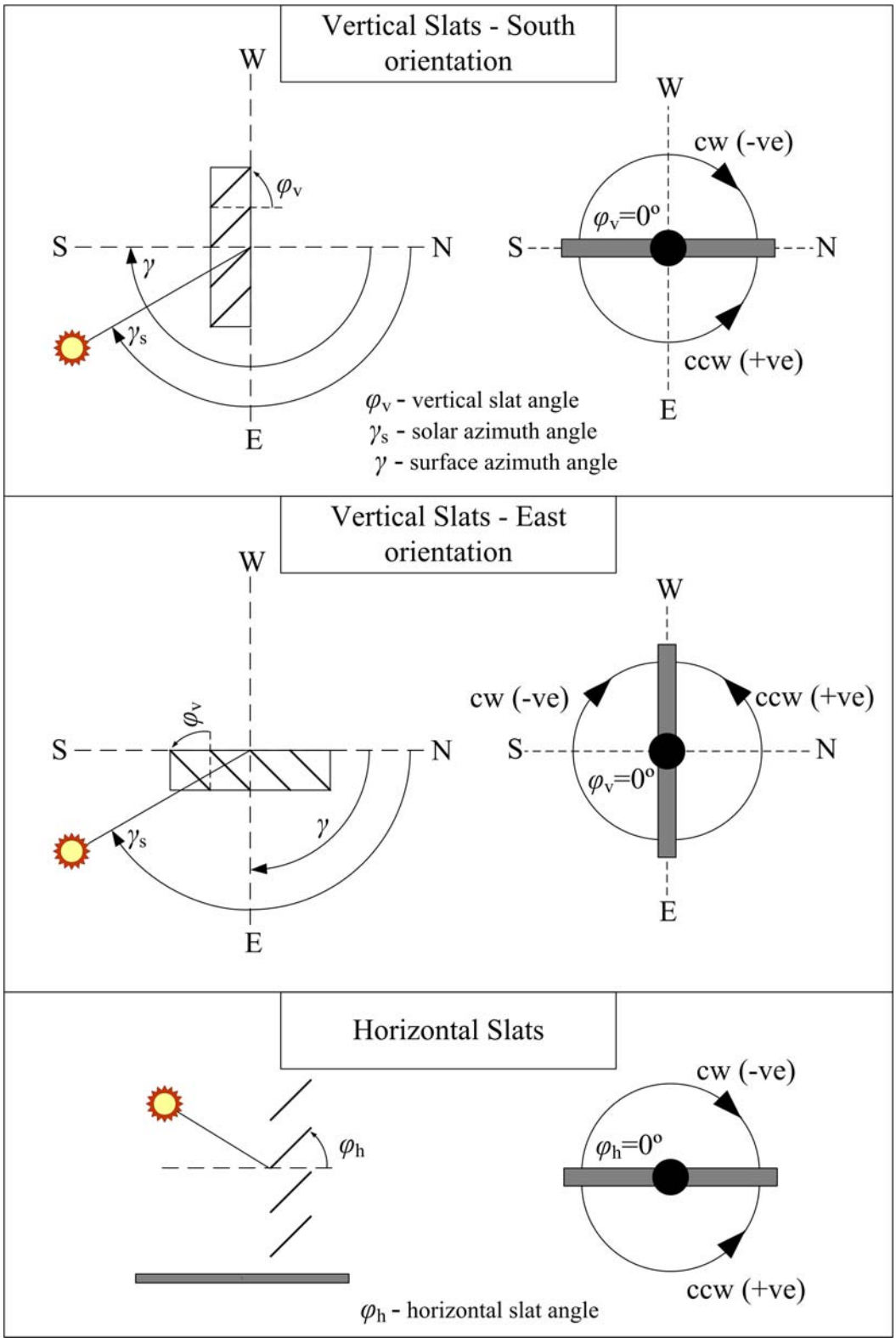

Figure F.12: Slat angle convention for vertical and horizontal slat blinds.

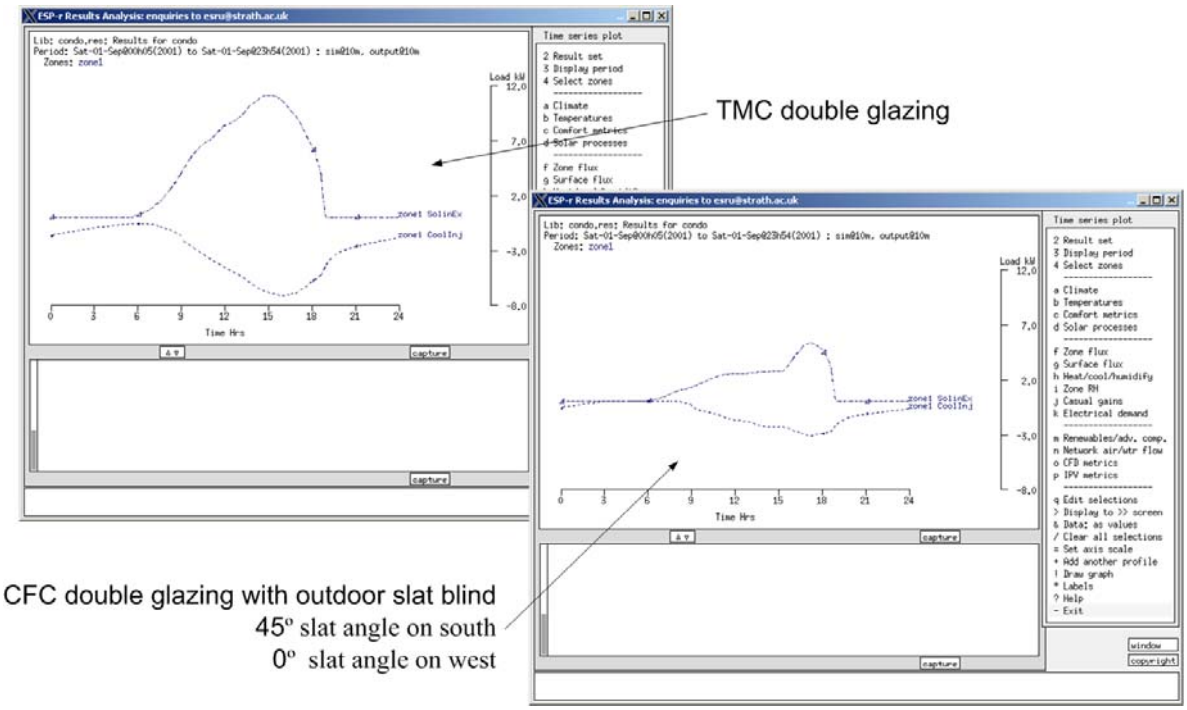

Figure F.13: Example simulation results.

F. 5 CFC input file data model

Each model zone is assigned a *.cfc input file much like other ESP-r input files (e.g., *.tmc, *.con). The *.cfc input file below is taken from the example of Section F.4. There are two CFC types in this example. The composition of the two types is the same but the slat angles differ. Although not recommended, each zone *.cfc file may be modified manually, bypassing the process of importing *.GSL files.

```
# complex fenestration construction properties of zone1 defined in #../zones/zone1.cfc
   8   # surfaces
# CFC index for each surface
0,0,0,0,0,0,1,2
   5   # layers in cfc type:  1
# For each layer: normal solar optical properties - R_fr, R_bk, Tran.
   0.500   0.500   0.000   # venetian blind
   0.000   0.000   0.000   # gas gap
   0.071   0.071   0.775   # glazing
   0.000   0.000   0.000   # gas gap
   0.071   0.071   0.775   # glazing
# For each layer: normal visible optical properties - R_fr, R_bk, Tran.
   0.500   0.500   0.000   # venetian blind
   0.000   0.000   0.000   # gas gap
   0.080   0.080   0.881   # glazing
   0.000   0.000   0.000   # gas gap
   0.080   0.080   0.881   # glazing
# For each layer: normal longwave radiative properties - R_fr, R_bk, Tran.
   0.150   0.150   0.000   # venetian blind
   0.000   0.000   0.000   # gas gap
   0.160   0.160   0.000   # glazing
   0.000   0.000   0.000   # gas gap
   0.160   0.160   0.000   # glazing
   5   # layers in cfc type:  2
# For each layer: normal solar optical properties - R_fr, R_bk, Tran.
   0.500   0.500   0.000   # venetian blind
   0.000   0.000   0.000   # gas gap
   0.071   0.071   0.775   # glazing
   0.000   0.000   0.000   # gas gap
   0.071   0.071   0.775   # glazing
# For each layer: normal visible optical properties - R_fr, R_bk, Tran.
   0.070   0.070   0.600   # venetian blind
   0.000   0.000   0.000   # gas gap
   0.080   0.080   0.881   # glazing
   0.000   0.000   0.000   # gas gap
   0.080   0.080   0.881   # glazing
# For each layer: normal longwave radiative properties - R_fr, R_bk, Tran.
   0.150   0.150   0.000   # venetian blind
   0.000   0.000   0.000   # gas gap
   0.160   0.160   0.000   # glazing
   0.000   0.000   0.000   # gas gap
   0.160   0.160   0.000   # glazing
```

CFC type index

CFC Type 1 solar, visible and longwave radiative properties for each CFC layer:

For Glazing:
R_fr: front reflectance
R_bk: back reflectance
Tran: transmittance

For Venetian Blind:
R_fr: slat top reflectance
R_bk: slat bot. Reflectance
Tran: slat transmittance

CFC Type 2 solar, visible and longwave radiative properties for each CFC layer

```
# layer type index for cfc type:  1
2,0,1,0,1
# Gas mixture properties for cfc type:  1
# gas layer   2
 0.290E+02        # molecular mass of gas mixture (g/gmole)
 0.230E-02  0.799E-04        # a and b coeffs.- gas conductivity (W/m.K)
 0.352E-05  0.498E-07        # a and b coeffs.- gas viscosity (N.s/m2)
 0.100E+04  0.147E-01        # a and b coeffs.- specific heat (J/kg.K)
# gas layer   4
 0.290E+02        # molecular mass of gas mixture (g/gmole)
 0.230E-02  0.799E-04        # a and b coeffs.- gas conductivity (W/m.K)
 0.352E-05  0.498E-07        # a and b coeffs.- gas viscosity (N.s/m2)
 0.100E+04  0.147E-01        # a and b coeffs.- specific heat (J/kg.K)
# venetian blind attributes for cfc type:  1
# slat: width(mm); spacing(mm); angle(deg); orientation(HORZ/VERT);
# crown (mm); w/r ratio; slat thickness (mm)
  25.400  21.170   0.000  HORZ    1.610   0.499   0.330
# layer type index for cfc type:  2
2,0,1,0,1
# Gas mixture properties for cfc type:  2
# gas layer   2
 0.290E+02        # molecular mass of gas mixture (g/gmole)
 0.230E-02  0.799E-04        # a and b coeffs.- gas conductivity (W/m.K)
 0.352E-05  0.498E-07        # a and b coeffs.- gas viscosity (N.s/m2)
 0.100E+04  0.147E-01        # a and b coeffs.- specific heat (J/kg.K)
# gas layer   4
 0.290E+02        # molecular mass of gas mixture (g/gmole)
 0.230E-02  0.799E-04        # a and b coeffs.- gas conductivity (W/m.K)
 0.352E-05  0.498E-07        # a and b coeffs.- gas viscosity (N.s/m2)
 0.100E+04  0.147E-01        # a and b coeffs.- specific heat (J/kg.K)
# venetian blind attributes for cfc type:  2
# slat: width(mm); spacing(mm); angle(deg); orientation(HORZ/VERT);
# crown (mm); w/r ratio; slat thickness (mm)
  25.400  21.170  45.000  HORZ    1.610   0.499   0.330
```

Layer types:
0 - gas gap
1 - glazing
2 - venetian blind

CFC Type 1 fill gas/mixture properties for each layer

See Figure F.10

CFC Type 1 slat geometry

CFC Type 2 fill gas/mixture properties for each layer

CFC Type 2 slat geometry